Universidade Federal de Minas Gerais
Escola de Engenharia
Programa de Pós-Graduação em Engenharia Elétrica

Petrus Emmanuel Oliveira Gomes Brant Abreu

IDENTIFICATION AND COMPENSATOR DESIGN USING NARX MODELS

Belo Horizonte
2021

Petrus Emmanuel Oliveira Gomes Brant Abreu

IDENTIFICATION AND COMPENSATOR DESIGN USING NARX MODELS

Thesis presented to the Graduate Program in Electrical Engineering of the Universidade Federal de Minas Gerais as a partial requirement to obtain the degree of Doctor in Electrical Engineering.

Advisor: Prof. Luis Antonio Aguirre, Dr.
Co-Advisor: Prof. Bruno Otávio Soares Teixeira, Dr.

Belo Horizonte
2021

A162i

Abreu, Petrus Emmanuel Oliveira Gomes Brant.
Identification and compensator design using NARX models [recurso eletrônico] / Petrus Emmanuel Oliveira Gomes Brant Abreu. - 2021.
1 recurso online (153 f. : il., color.) : pdf.

Orientador: Luis Antonio Aguirre.
Coorientador: Bruno Otávio Soares Teixeira.

Tese (doutorado) - Universidade Federal de Minas Gerais, Escola de Engenharia.

Bibliografia: f. 135-153.

Exigências do sistema: Adobe Acrobat Reader.

1. Engenharia elétrica - Teses. 2. Histerese- Teses. 3. Identificação de sistemas – Teses. I. Aguirre, Luis Antonio. II. Teixeira, Bruno Otávio Soares. III. Universidade Federal de Minas Gerais. Escola de Engenharia. IV. Título.

CDU: 621.3(043)

Ficha catalográfica elaborada pela Bibliotecária Letícia Alves Vieira - CRB-6/2337
Biblioteca Prof. Mário Werneck - Escola de Engenharia da UFMG

UNIVERSIDADE FEDERAL DE MINAS GERAIS
ESCOLA DE ENGENHARIA
Programa de Pós-Graduação em Engenharia Elétrica

ATA DA 386ª DEFESA DE TESE DE DOUTORADO
DO PROGRAMA DE PÓS-GRADUAÇÃO EM ENGENHARIA ELÉTRICA

ATA DE DEFESA DE TESE DE DOUTORADO do aluno **Petrus Emmanuel Oliveira Gomes Brant Abreu** - registro de matrícula de número 2017711998. Às 13:00 horas do dia 14 do mês de dezembro de 2021, reuniu-se virtualmente via Zoom a Comissão Examinadora da TESE DE DOUTORADO para julgar, em exame final, o trabalho intitulado **"Identification and Compensator Design Using NARX Models"** da Área de Concentração em Sinais e Sistemas. O Prof. Luis Antonio Aguirre, orientador do aluno, abriu a sessão apresentando os membros da Comissão e, dando continuidade aos trabalhos, informou aos presentes que, de acordo com o Regulamento do Programa no seu Art. 8.16, será considerado APROVADO na defesa da Tese de Doutorado o candidato que obtiver a aprovação unânime dos membros da Comissão Examinadora. Em seguida deu início à apresentação do trabalho pelo Candidato. Ao final da apresentação seguiu-se a arguição do candidato pelos examinadores. Logo após o término da arguição a Comissão Examinadora se reuniu, sem a presença do Candidato e do público, e elegeu o Prof ...Luis Antonio Aguirre.... para presidir a fase de avaliação do trabalho, constituída de deliberação individual de APROVAÇÃO ou de REPROVAÇÃO e expedição do resultado final. As deliberações individuais de cada membro da Comissão Examinadora foram as seguintes:

Membro da Comissão Examinadora	Instituição de Origem	Deliberação	Assinatura
Prof. Dr. Luis Antonio Aguirre - Orientador	DELT (UFMG)	aprovado	
Prof. Dr. Bruno Otávio Soares Teixeira - Coorientador	DELT (UFMG)	aprovado	BRUNO OTAVIO SOARES TEIXEIRA:01358300607 Assinado de forma digital por BRUNO OTAVIO SOARES TEIXEIRA:01358300607 Dados: 2021.12.16 14:09:52 -03'00'
Prof. Dr. Luiz Carlos Sandoval Góes	Engenharia Mecânica (ITA)	aprovado	
Prof. Dr. Claudio Garcia	Telecomunicações e Controle (USP-Poli)	aprovado	
Prof. Dr. Samir Ângelo Milani Martins	Departamento de Engenharia Elétrica (UFSJ)	aprovado	
Prof. Dr. Luciano Antonio Frezzatto Santos	DELT (UFMG)	aprovado	

Tendo como base as deliberações dos membros da Comissão Examinadora a Tese de Doutorado foi aprovada. O resultado final de aprovação foi comunicado publicamente ao Candidato pelo Presidente da Comissão, ressaltando que a obtenção do Grau de Doutor em ENGENHARIA ELÉTRICA fica condicionada à entrega do TEXTO FINAL da Tese de Doutorado. O Candidato terá um prazo máximo de 30 (trinta) dias, a partir desta data, para fazer as CORREÇÕES DE FORMA e entregar o texto final da Tese de Doutorado na secretaria do PPGEE/UFMG. As correções de forma exigidas pelos membros da Comissão Examinadora deverão ser registradas em um exemplar do texto da Tese de Doutorado, cuja verificação ficará sob a responsabilidade do Presidente da Banca Examinadora. Nada mais havendo a tratar o Presidente encerrou a reunião e lavrou a presente ATA, que será assinada pelo Presidente da Comissão Examinadora. Belo Horizonte, 14 de dezembro de 2021.

ASSINATURA DO PRESIDENTE DA COMISSÃO EXAMINADORA

Agradecimentos

Agradeço primeiramente a Deus por tudo que ele tem me concedido. A cada etapa, um novo aprendizado de vida.

Agradeço aos meus pais, Pascalle e Cássio, por todo apoio e carinho. Assim como, aos meus avôs, tios e irmão, obrigado pelas motivações e apoios dados nos momentos de dificuldades.

Ao meu orientador, Luis Aguirre, pela confiança, assistência, paciência e ensinamentos durante o desenvolvimento deste trabalho. Também ao meu co-orientador Bruno Teixeira, pelo auxilio nesta caminhada de aprendizado. Foi uma honra trabalhar com vocês!

Ao Claudio, pelo acolhimento e assistência no Laboratório LCPI da Universidade de São Paulo. Assim como, ao Victor, pelo auxilio e parceria durante este intercâmbio.

Aos amigos do Laboratório CPH: Antônio, Arthur, Ercílio, Felipe, João, Leandro e Leo, obrigado por tornarem o ambiente de trabalho agradável e pela parceria. Em especial, ao Lucas, pela amizade e contribuições de grande valor.

Aos meus amigos do Laboratório MACSIN: Ana, Rodrigo, Victor e Wendy, obrigado pelo companheirismo e apoio dado na etapa do mestrado. Em especial, ao Marcus, obrigado pela constante troca de ideias e amizade.

Aos meus amigos do Laboratório MACRO: Arturo, Brenner, Juan José e Rafael, obrigado pela troca de conhecimentos e por tornarem as madrugadas estudando na UFMG mais agradáveis. Em especial, ao Daniel, obrigado pela amizade de longa data e pelo encorajamento.

Agradeço todo apoio financeiro proveniente do Conselho Nacional de Desenvolvimento Científico e Tecnológico, CNPq.

Abstract

Gray-box identification techniques provide a promising way to build mathematical models that can be tailored to reproduce specific features of real systems and that have a suitable structure for their use in control or compensation schemes. In this thesis, some of the main concepts, definitions, and tools originally formulated in the black-box context to build Nonlinear polynomial AutoRegressive models with eXogenous inputs (NARX) and their necessary extensions to deal with the gray-box scenario are addressed. A more general NARX representation that fits the gray-box scenario is formalized when it is assumed that the auxiliary information can be converted as a new class of regressors that can optionally be included in the model. Some guidelines on how to determine a promising class of regressors from data are explored. Aiming at work on issues that have important implications for both the science and industry, the use of gray-box NARX models is studied for modeling and compensation of dynamic systems with hysteresis, a nonlinear behavior present in several applications. For a more consistent representation of this nonlinear behavior, some constraints on the structure and a specific one on the parameters of NARX polynomial models are proposed to be considered during the identification procedure. Such identified models are then able to describe not only the dynamic behavior, but also the static response which, despite being a very important feature for hysteretic systems, has been generally neglected in the literature. In addition, a more general framework is developed to explain how hysteresis occurs in such models. In the context of compensation, three approaches to design compensators are formulated for general dynamic systems and also for hysteretic systems. In short, the proposed approaches provide different ways to identify NARX models or rewrite the identified ones as a function of the compensation input signal and then use this function/compensator to calculate their values iteratively. Numerical and experimental examples are given throughout the text to enrich some discussions. Results obtained with a simulated piezoelectric actuator and an experimental pneumatic control valve demonstrate the efficiency of the identification and compensation proposals. Also, it has been found that the compensators based on gray-box techniques outperform those based on models identified through black-box techniques, and that any of the three proposed approaches significantly reduce the tracking error compared to the uncompensated system.

Keywords: Gray-box identification; Compensation of nonlinearities; NARX polynomial models; Hysteresis.

Resumo

Técnicas de identificação caixa-cinza fornecem uma maneira promissora de construir modelos matemáticos que podem ser ajustados para reproduzir características específicas de sistemas reais e que têm uma estrutura adequada para seu uso em esquemas de controle ou compensação. Nesta tese, alguns dos principais conceitos, definições e ferramentas originalmente formuladas no contexto caixa-preta, para construir modelos NARX polinomiais (do inglês, *Nonlinear polynomial AutoRegressive models with eXogenous inputs*), e suas extensões necessárias para lidar com o cenário caixa-cinza são abordadas. Uma representação NARX mais geral que se ajusta ao cenário caixa-cinza é formalizada ao se assumir que as informações auxiliares podem ser convertidas como uma nova classe de regressores que podem ser opcionalmente incluídos no modelo. Algumas diretrizes sobre como determinar uma classe promissora de regressores a partir de dados são exploradas. Visando trabalhar com questões que tenham implicações importantes tanto para a ciência quanto para a indústria, estuda-se a utilização de modelos NARX caixa-cinza para modelagem e compensação de sistemas dinâmicos com histerese, comportamento não linear presente em diversas aplicações. Para uma representação mais consistente deste comportamento não linear, algumas restrições na estrutura e uma específica nos parâmetros dos modelos NARX polinomiais são propostas para serem consideradas durante o procedimento de identificação. Esses modelos identificados são então capazes de descrever não apenas o comportamento dinâmico, mas também a resposta estática que, apesar de ser uma característica muito importante para os sistemas histeréticos, geralmente tem sido negligenciada na literatura. Além disso, uma estrutura mais geral é desenvolvida para explicar como a histerese ocorre em tais modelos. No contexto de compensação, três abordagens para projetar compensadores são formuladas para sistemas dinâmicos em geral e também para sistemas histeréticos. Resumidamente, as abordagens propostas fornecem diferentes maneiras de identificar modelos NARX ou reescrever os identificados em função do sinal de entrada de compensação e então utiliza-se essa função/compensador para calcular seus valores de forma iterativa. Exemplos numéricos e experimentais são fornecidos ao longo do texto para enriquecer algumas discussões. Para demonstrar a eficácia das propostas de identificação e compensação, resultados simulados e experimentais são obtidos, respectivamente, com um atuador piezoelétrico e uma válvula de controle pneumática. Além disso, verificou-se que os compensadores baseados em técnicas caixa-cinza superam aqueles baseados em modelos identificados por meio de técnicas caixa-preta e que qualquer uma das abordagens propostas reduz significativamente o erro de rastreamento em comparação com o sistema não compensado.

Palavras-chave: Identificação caixa-cinza; Compensação de não linearidades; Modelos NARX polinomiais; Histerese.

List of Figures

List of Tables

List of Symbols

$\mathbb{R}$	the set of real numbers
$\mathbb{N}$	the set of natural numbers
a	italic lowercase letters denote scalars
$\boldsymbol{a}$	boldface italic lowercase letters denote vectors
A	italic uppercase letters denote matrices
$\mathcal{S}$	dynamical system to be identified
$\mathcal{M}$	model built to estimate output signal of system $\mathcal{S}$
$\check{\mathcal{M}}$	model built to estimate input signal of system $\mathcal{S}$
$\mathcal{C}$	compensator
k	discrete-time index
t	continuous-time index
ℓ	maximum degree of nonlinearity
u_k, y_k	input and output signal
$\bar{u}, \bar{y}$	steady-state values of u_k and y_k
$\tilde{y}$	output resulting from quasi-static analysis
$\phi_{i,k}$	a class of additional regressors defined as functions of lagged values of u_k and y_k
n_u, n_y	maximum input and output lags
n_{ϕ_i}	maximum lag for the i-th function included $\phi_{i,k}$
n_θ	dimension of the parameter vector $\hat{\boldsymbol{\theta}}$
τ_d	pure time delay
τ_u, τ_y	arbitrary input and output delays
τ_s	number of time steps that y_k should be delayed with respect to u_k
Σ_y	sum of parameters of all linear output regressors
r_k, m_k	reference and compensation signal
T_s	sampling time
$\check{\bullet}$	indicates a variable or function of the inverse model $\check{\mathcal{M}}$
$\hat{\bullet}$	estimate of $\bullet$
$\dot{\bullet}$	time derivative of $\bullet$
$(\bullet)^T$	denotes the transpose of $\bullet$
$(\bullet)^{-1}$	denotes the inverse of $\bullet$
$\lvert\bullet\rvert$	absolute value of $\bullet$
sign($\bullet$)	sign function of $\bullet$
max($\bullet$), min($\bullet$)	maximum and minimum values of $\bullet$

List of Acronyms

AIC	Akaike's Information Criterion
ARX	AutoRegressive model with eXogenous inputs
CLS	Constrained Least Squares
ERR	Error Reduction Ratio
ELS	Extended Least Squares
FF	Forgetting Factor
FIR	Finite Impulse Response
KP	Krasnosel'skii-Pokroviskii
MAPE	Mean Absolute Percentage Error
NARX	Nonlinear AutoRegressive model with eXogenous inputs
NSAVI	Normalized Sum of the Absolute Variation of the Input
PRBS	Pseudo Random Binary Signal
PRVS	Pseudo Random Variable Steps
PRFS	Pseudo Random Filtered Signal
pH	Potential of hydrogen
PID	Proportional-Integral-Derivative
RLS	Recursive Least Squares
LMIs	Linear Matrix Inequalities
LS	Least Squares

Contents

Chapter 1

Introduction

1.1 Context and Motivation

Mathematical modeling of dynamical systems concerns the area of knowledge that deals with techniques developed to mathematically describe, even if roughly, the behavior present in real systems. In general, the techniques used for this purpose can be grouped into two frameworks, one based on the *laws* and *first principles* that govern the investigated dynamical system and the other one based on *empirical data* collected from such a system where little or no prior knowledge is necessary. The former leads to mathematical models where all terms and parameters have physical meaning. However, the common lack of full understanding of some phenomena that characterize real systems and the fact that such models are built to describe the behavior of a specific system, which limits their application to other systems, makes this modeling approach not always efficient or feasible to be used. Besides, often such models also have their application somewhat limited in model-based control or compensation design due to their structural complexity (Peng and Chen, 2013; Hassani et al., 2014). In the latter, mathematical models are built from data, which is generally an easier way compared to the one based on first principles and allows choosing a more suitable structure to be used in control or compensation schemes. Such techniques are part of a mature field known as *system identification* (Ljung, 1999; Isermann and Münchhof, 2011; Billings, 2013).

The system identification field deals with building mathematical models typically from *black-box* or *gray-box* perspectives. When it comes to black-box modeling, it must be assumed that the only available source of information about the dynamic behavior is the input and output data collected from the investigated system, while gray-box techniques also use *auxiliary information* about the system (Aguirre, 2019). Auxiliary/additional information refers to some kind of prior knowledge commonly based on physical insights about the dynamic behavior of the system, which will be incorporated into the model during the identification procedure (Eskinat et al., 1993). The inclusion of such information in the model aims to improve its predictive performance or make it suitable for some particular purpose, since specific features and/or an adequate structure that allows the use of the identified model in control or compensation schemes are not ensured by black-box techniques (Sjöberg et al., 1995). Some ways to achieve this refer to the use of constraints on the structure

and/or parameters, adoption of algorithms for recursive parameter updating and/or the inclusion of a certain class of regressors that are able to extract information underlying the data that has a known relevant feature, such as specific nonlinearity, time-invariant or time-varying behavior, among other.

Most experimental systems have some level of nonlinear and time-varying behavior, which are commonly related to physical and chemical phenomena, as well as caused by aging or component wear (Bequette, 1991). Some examples include processes associated with wind turbines (Gebraad et al., 2013), pneumatic control valves (Choudhury et al., 2008), robotic manipulators (Koo, 1995), and potential of hydrogen (pH) (Stebel and Czeczot, 2009). Despite the nonlinear features, in most cases, works in the literature address ways to get linear time-invariant models to predict the system behavior at a specific operation region, which provide only a localized representation. However, for cases where the system has highly nonlinear dynamic behaviors and when its operating point may change over a large region, such a system cannot be well approximated using linear models. In this sense, some nonlinear systems are often classified in the literature as systems with *hard* or *severe nonlinearities* due to their dominant nonlinear characteristics, generally non-differentiable and unknown, which tend to present considerable challenges for identification and control purposes (Tao and Kokotovic, 1995; Choudhury et al., 2008; Visone, 2008; Billings, 2013; Biagiola et al., 2016; Pop et al., 2018). Thus, due to the nonlinear nature of these systems, traditional identification techniques aimed at building linear models and well established approaches for the design of conventional linear controllers (e.g. in the frequency domain) are generally inefficient (Schoukens and Pintelon, 1991; Hatipoglu and Ozguner, 1998; Coelho and dos Santos Coelho, 2016). Recent works have addressed several tools to identify and control these types of systems, encouraging further research to solve open problems (Tao and Lewis, 2001; Hassani et al., 2014; Aguirre, 2015; Gomez, 2015; Hermansson and Syafiie, 2015; Al Janaideh et al., 2016b; Bhadra et al., 2019a; Karami et al., 2021).

Dynamical systems that present some type of severe nonlinearity have attracted great interest due to the presence of these nonlinear behaviors in many applications and devices. As mentioned before, such nonlinearities are commonly related to phenomena of ferromagnetism, plasticity, friction, and chemical reactions, among others (Bequette, 1991; Visintin, 1994). Some examples include mechanical, electronic, biomedical and pH neutralization processes, as well as sensors and actuators such as pneumatic control valves and piezoelectric actuators (Choudhury et al., 2008; Stebel and Czeczot, 2009; Peng and Chen, 2013; Rakotondrabe, 2013). Because these systems and equipment are widely found in various industrial sectors, where their inadequate operation tends to directly impact economic, environmental and even safety issues, their control is an essential step. Such relevance has led several research groups to deal with different approaches for the design of model-based controllers (Hong et al., 1996; Ikhouane and Rodellar, 2007; Abdullah et al., 2012; Esbrook et al., 2013; Chaoui and Gualous, 2016; Abreu et al., 2018b; Bhadra et al., 2019a; Larico and Garcia, 2019; Lacerda Júnior et al.,

2019). An alternative that has also drawn attention in the literature refers to the design of model-based compensators in order to mitigate the nonlinear effects of the system prior to feedback control design, so that the system becomes more linear and, consequently, more amenable for control (Visone, 2008; Al Janaideh et al., 2011; Qin et al., 2013; Chaoui and Gualous, 2016; Yi et al., 2019). In short, compensation approaches aim to design a compensation input that attenuates the nonlinearity, allowing for more accurate control and tracking, which typically starts with a suitable dynamic model that has a simple structure and that represents the most fundamental aspects of the system. In this context, the use of Nonlinear polynomial AutoRegressive models with eXogenous inputs (NARX) presents some advantages due to their ability to represent a wide class of nonlinear behaviors (Leontaritis and Billings, 1985a,b) and their structural flexibility which, when combined with gray-box identification techniques (Aguirre, 2019), are promising for their use in control or compensation schemes. In addition, it has been argued that it is viable to enforce constraints on the model structure in order to make it suitable for designing compensators (Pearson, 1999).

Among the severe nonlinearities widely investigated in the literature, one can mention those related to friction (Romano and Garcia, 2011; Baeza and Garcia, 2018), dead-zone (Aguirre, 2014), dead-band (Choudhury et al., 2008), hysteresis (Morris, 2011) and those related to pH neutralization (Bhadra et al., 2019b). This doctoral thesis focuses on the study of hysteresis, which is a nonlinear behavior present in several applications and, therefore, has important implications for both the scientific field and the industrial sector. Specifically, it deals with the problem of hysteresis identification and nonlinearity compensation in dynamical systems using NARX polynomial models.

In the literature, some works have associated the occurrence of hysteresis with the existence of several fixed points whenever such systems are subject to constant (Morris, 2011) or time-varying (Martins and Aguirre, 2016) input signals. For the case where the input signal is time-varying, a characteristic loop behavior exhibited in the input-output plane has been adopted as the hallmark of such systems. As a consequence, many works in the literature have been dedicated to building and evaluating models with respect to their ability to reproduce the hysteresis loop and the temporal response of such systems when subjected to time-varying input signals (Ni et al., 1998; Smyth et al., 2002; Hu and Ben Mrad, 2003; Oh and Bernstein, 2005; Al Janaideh et al., 2008b; Zakerzadeh et al., 2011; Domínguez-González et al., 2014; Zhang et al., 2017a). However, we have not found any critical analysis addressing *whether* or *how* the hysteretic behavior affects the *steady-state* of such systems, i.e. when the input signal is/becomes constant. This work explores this question and proposes a new framework to explain how hysteresis occurs in NARX models. In addition, based on gray-box techniques, the use of some constraints during the identification procedure is proposed to ensure that the identified NARX models are able to describe both dynamical and static features of hysteresis, which is not even tested by most works in the literature, e.g. see (Leva and Piroddi, 2002; Parlitz et al., 2004; Worden et al., 2007;

Deng and Tan, 2009; Worden and Barthorpe, 2012; Martins and Aguirre, 2016; Zhang et al., 2017a; Lacerda Júnior et al., 2019).

As for the *compensation of hysteresis*, there are some works in the literature that use specific models based on first principles, such as Bouc-Wen (Rakotondrabe, 2011) and the Prandtl-Ishlinskii operator (Gu et al., 2012; Rakotondrabe, 2013). However not every hysteretic system can be represented by such models. Besides, there are many challenges related to the estimation of the parameters of such nonlinear-in-the-parameter models. Also, their structural complexity represents an additional difficulty in the design of compensators. On the other hand, NARX polynomial models are both quite general and can present simple structure. However, the literature on the use of NARX models in the compensation of hysteresis is still scarce (Dong and Tan, 2014; Lacerda Júnior et al., 2019). One of the very few papers that is concerned with obtaining structurally simple NARX models that are particularly suitable for model-based control is (Leva and Piroddi, 2002). Although the authors identify a compact model for a hysteretic system, they have not used the identified model in any control or compensation scheme. It is also important to note that the methodology proposed by them does not guarantee that the identified models are suitable for designing compensators. This can be verified by manipulating such a compact model in (Leva and Piroddi, 2002) to obtain a compensator following the strategies provided in the present work. As a result, it can be seen that the compensator obtained would have a singularity when the velocity variable is equal to zero. A similar problem would happen in (Lacerda Júnior et al., 2019). The lack of NARX-based methods for hysteresis design can arguably be explained by the modeling problems that could not be solved in the context of black-box techniques. With such hurdles out of the way, simple model-based techniques can be now developed. This doctoral thesis also proposes, based on gray-box models, three systematic procedures to ensure that the identified NARX models are suitable for designing compensators. The compensation procedures are formulated to handle general dynamical systems as well as hysteretic systems modeled by NARX models.

1.2 Contributions of this Work

The main goal of this thesis is to investigate the identification of hysteresis and the compensation of nonlinearities in dynamical systems using NARX models identified from data, aiming to propose systematic approaches to build models that are accurate and also suitable for model-based compensation. The contributions of this work are summarized below.

- Detailed review on hysteresis modeling. In this literature search, some classical phenomenological models of hysteresis are briefly discussed, while a more in-depth analysis based on black-box and gray-box modeling of NARX polynomial models to predict hysteretic systems is made. As the main concepts, definitions

and tools for building NARX models are formulated in the black-box context, all the necessary extensions to deal with the gray-box scenario have been developed. In this sense, a NARX representation that fits the gray-box scenario is formalized when it is assumed that the auxiliary information can be converted as a class of additional regressors $\phi_{i,k}$ in the model; see Remark 2.1. A critical review is developed considering the pros and cons that some works that use NARX models present to describe some features of hysteresis. The review ends by analyzing some more subtle properties of hysteretic systems and provides interesting guidelines for building gray-box NARX models with the ability to reproduce these properties.

- Development of a detailed mathematical formulation to generate an excitation input signal suitable for the identification of nonlinear dynamical systems; see Section 2.3.2. In this proposal, the input signal is a sequence of steps here called *Pseudo Random Variable Steps* (PRVS). Based on some preliminary experiments carried out on the system, the design procedure is able to consider dynamic dependencies related to the increasing or decreasing input signal value and its magnitude, which commonly affects the output of some nonlinear systems. Also, to deal with nonlinear systems that demand more subtle excitation signals, such as hysteretic systems that have a strong dependence on the rate of change of the input signal, a mathematical formulation that generates an excitation input signal with smoother transitions is revisited (Tavares, 2020; Tavares et al., 2021). This input signal is here called *Pseudo Random Filtered Signal* (PRFS), which was developed in collaboration with Lucas Amaral Tavares.

- Regarding the identification of hysteretic systems, the proposition of some constraints on the structure and a specific one on the parameters of NARX models are made to guarantee a *continuum of steady-state solutions* (Definition 2.5), which is an important feature for hysteresis. As a consequence, the identified models that comply with such constraints are able to describe not only the dynamic behavior of hysteresis, but also its static behavior, providing more consistent models when compared to those that do not. In addition, following a quasi-static analysis, a schematic framework is put forward to explain how the hysteresis loop results from an interplay of attracting and repelling regions in the input-output plane.

- Formulation of three systematic approaches to design compensators for general dynamical systems, and also for hysteretic systems, represented by NARX polynomial models. The first one provides a compensator by rewriting the identified model as an algebraic polynomial whose unknown variable is the compensation input signal and then calculating the roots of this polynomial iteratively. As this type of compensator might produce more than one root per iteration, an algorithm is proposed to determine which one should be used as the compensation input at each instant of time. The second approach consists of some structural

specifications that are enforced during the identification procedure in such a way that the compensation input can be isolated when the identified model is rewritten as a compensator. In the third approach, the compensation law is directly identified from the data. These were developed with the collaboration of Lucas Amaral Tavares. Numerical and experimental results are shown for both identification and compensation proposals. It has been found that the compensators based on gray-box models outperform those that use models identified following black-box techniques.

1.3 List of Publications

The following scientific manuscripts were published, or are under preparation for submission, during the course of this work.

Journal papers:

- (Abreu et al., 2020) **Petrus E. O. G. B. Abreu**, Lucas A. Tavares, Bruno O. S. Teixeira and Luis A. Aguirre. Identification and nonlinearity compensation of hysteresis using NARX models. *Nonlinear Dynamics*, 102(1):285–301.
- (Tavares et al., 2022) Lucas A. Tavares, **Petrus E. O. G. B. Abreu** and Luis A. Aguirre. Nonlinearity compensation based on identified NARX polynomial models. *Nonlinear Dynamics*, 107(1):709–725.
- (Abreu et al., 2022) **Petrus E. O. G. B. Abreu**, Henrique C. Castro, Bruno H. G. Barbosa and Luis A. Aguirre. Identification and control of nonlinear systems: concepts and tools. (*In progress*).

Conference papers:

- (Abreu et al., 2021) **Petrus E. O. G. B. Abreu**, Victor D. R. Dreke, Luis A. Aguirre and Claudio Garcia. Enabling invariant models to describe time-varying dynamics: a case study. *In Proc. of Third IFAC Conference on Modelling, Identification and Control of Nonlinear Systems* (MICNON2021), Tokyo, Japan.
- (Tavares et al., 2021) Lucas A. Tavares, **Petrus E. O. G. B. Abreu** and Luis A. Aguirre. Input design and recommendations for the identification of hysteretic NARX models. *In Proc. of XV Simpósio Brasileiro de Automação Inteligente* (SBAI2021), Rio Grande, Brasil.
- (Tavares et al., 2019) Lucas A. Tavares, **Petrus E. O. G. B. Abreu** and Luis A. Aguirre. Estimação de parâmeros de modelos Bouc-Wen via algoritmos evolutivos para compensação de histerese. *In Proc. of XIV Simpósio Brasileiro de Automação Inteligente* (SBAI2019), Ouro Preto, Brasil.

- (Abreu et al., 2018b) **Petrus E. O. G. B. Abreu**, Bruno O. S. Teixeira and Luis A. Aguirre. Projeto de Controlador Backstepping para Sistemas de Posicionamento Acionados por um Atuador Piezoelétrico. *In Proc. of XXII Congresso Brasileiro de Automática* (CBA2018), João Pessoa, Brasil.

- (Abreu et al., 2018a) **Petrus E. O. G. B. Abreu**, Fernando O. Souza, Bruno O. S. Teixeira and Luis A. Aguirre. Projeto de Controlador PID via LMIs para Sistemas de Posicionamento Sujeitos a Histerese e Retardo de Tempo. *In Proc. of XXII Congresso Brasileiro de Automática* (CBA2018), João Pessoa, Brasil.

1.4 Thesis Outline

This manuscript is organized as follows. Chapter 2 presents a brief review on some of the main phenomenological models of hysteresis and provides an in-depth analysis of NARX models covering the main concepts, definitions, and tools originally formulated in the black-box context and necessary extensions to deal with the gray-box scenario. Besides, a critical review of some works that use NARX polynomial models to describe hysteretic systems, as well as some interesting properties inherent in such systems that have not yet been explored using these polynomial models and alternative ways to achieve them in a gray-box context, are also addressed.

Chapter 3 reviews approaches commonly used in the literature for the control and compensation of hysteretic systems and points out some remaining challenges and limitations found in these approaches.

Based on the theoretical foundation and a critical look at the literature previously presented, Chapter 4 deals with the main proposals of this work. In terms of hysteresis modeling, some constraints on the structure and parameters of NARX models are proposed to ensure that the identified models are able to describe both dynamic and static features of hysteresis. In addition, a more general framework is developed to explain how hysteresis occurs in such models. For the compensation context, three approaches are proposed to ensure that NARX models identified for general dynamical systems, and also for hysteretic systems, are suitable for the design of compensators.

Chapter 5 concerns a simulated piezoelectric actuator and an experimental pneumatic control valve that are used to illustrate the efficiency of the identification and compensation proposals.

Finally, Chapter 6 presents the final considerations and some proposals for future work.

Chapter 2

A Review on Modeling of Hysteretic Systems

2.1 Introduction

Hysteresis is a nonlinear behavior that is present in several systems and devices. It is commonly related to phenomena such as ferromagnetism, plasticity, and friction, among others (Visintin, 1994). Some examples include mechanical, electronic and biomedical systems, as well as sensors and actuators such as magneto-rheological dampers, piezoelectric actuators and pneumatic control valves (Choudhury et al., 2008; Rakotondrabe, 2013; Peng and Chen, 2013). An intrinsic feature of such systems is the memory effect, meaning that the output depends on the history of the corresponding input.

In addition to the memory effect, the literature provides different definitions and conditions to distinguish such systems and characterize the hysteretic behavior. In some cases, the occurrence of hysteresis has been associated with the existence of several fixed points whenever these systems are subject to constant (Morris, 2011) or time-varying (Martins and Aguirre, 2016) input signals. Additionally, hysteresis has also been defined as a hard nonlinearity that depends on the magnitude and rate of the input signal. If not properly taken into account during controller design, these aspects may pose performance limitations, such as the occurrence of undesirable oscillations, tracking inaccuracy, and even instability (Tao and Kokotovic, 1995; Rakotondrabe, 2013). Hence, a common goal is to attenuate the hysteretic behavior of the system (Visone, 2008; Chaoui and Gualous, 2016; Yi et al., 2019) prior to feedback control design.

In many approaches, the compensation of hysteresis starts with obtaining a suitable model. In the literature, several hysteresis models have been proposed based on phenomenological, black-box, and gray-box modeling approaches. In order to address these issues, this chapter reviews the modeling of hysteretic systems, while control and compensation schemes are discussed in Chapter 3.

It is worth mentioning that, as the most important phenomenological hysteresis models are already well established in the literature, only a brief contextualization of such models is presented. In this case, the reader will be referred to some fundamental and comprehensive works. Conversely, there are very few works regarding black-

box and gray-box modeling of NARX polynomial models for the representation of hysteresis. For these modeling approaches, a critical review mainly addressing some gaps related to gray-box identification techniques, as well as the advances found in the literature that use such models for hysteretic systems, is provided.

This chapter is organized as follows. Section 2.2 briefly reviews the phenomenological models, where special attention is given to the Bouc-Wen model and the Prandtl-Ishlinskii operator. Section 2.3 provides an in-depth analysis of NARX models, with definitions and formulations originally raised in the black-box context, where some are extended to the gray-box scenario.

2.2 Phenomenological Models

In the realm of *models based on first principles*, important contributions have been made based on differential equations and operators (Hassani et al., 2014), such as the Bouc-Wen model (Wen, 1976), the Duhem model (Oh and Bernstein, 2005), the Preisach model (Ge and Jouaneh, 1996) and the Prandtl-Ishlinskii operator (Brokate and Sprekels, 1996). These models have been widely used to represent hysteresis behavior due to their ability to describe a variety of hysteresis loops that resemble the properties of a wide class of real nonlinear hysteretic systems (Smyth et al., 2002). Besides, such models are known to be challenging for system identification techniques (Quaranta et al., 2020). In some cases, as for the Bouc-Wen model that has a well known structure, the challenge stems from the problem of estimating its parameters, which appear nonlinearly in the equation. This has led many works in the literature to focus on how to estimate the parameters of such a model, which often requires sophisticated optimization algorithms (Kyprianou et al., 2001; Worden and Hensman, 2012; Carboni et al., 2018). Apart from the computational effort required in the identification of phenomenological models, their application in the design of compensators is somewhat limited due to their structural complexity (Peng and Chen, 2013; Hassani et al., 2014).

In order to give a glance over two of these well known phenomenological models, a brief review is made in what follows for the Bouc-Wen and Prandtl-Ishlinskii models.

2.2.1 Bouc-Wen Model

The first works that addressed the hysteresis phenomenon, through a functional, were developed by Robert Bouc (Bouc, 1971). In this approach, the hysteresis phenomenon is described by the following equation:

$$\dot{\mathcal{F}}(t) = \mathrm{g}\Big(x(t), \mathcal{F}(t), \mathrm{sign}(\dot{x}(t))\Big)\dot{x}(t), \tag{2.1}$$

where $\mathrm{g}(\cdot)$ is a nonlinear mapping, $x(t)$ is a displacement, $\mathcal{F}(t)$ represents a resultant

force, and $\text{sign}(\dot{x}(t))$ is the sign function (Definition 2.1) of the displacement time derivative.

Definition 2.1. [Sign function (Popiołek, 1990)]. $\text{sign}(\cdot) : \mathbb{R} \to \mathbb{R}$ *is a function that extracts the sign of a real number* x*, defined as:*

$$\text{sign}(x) = \begin{cases} 1, & \text{if } x > 0; \\ -1, & \text{if } x < 0; \\ 0, & \text{if } x = 0. \end{cases} \tag{2.2}$$

According to Sain et al. (1998), Bouc proposed the functional (2.1) in order to obtain a model to describe the relationship between the forced vibrations of a hysteretic system under periodic excitation. This type of relationship might be illustrated as shown in Figure 2.1, in which the relationship between an output force $\mathcal{F}$ and an input displacement x is presented.

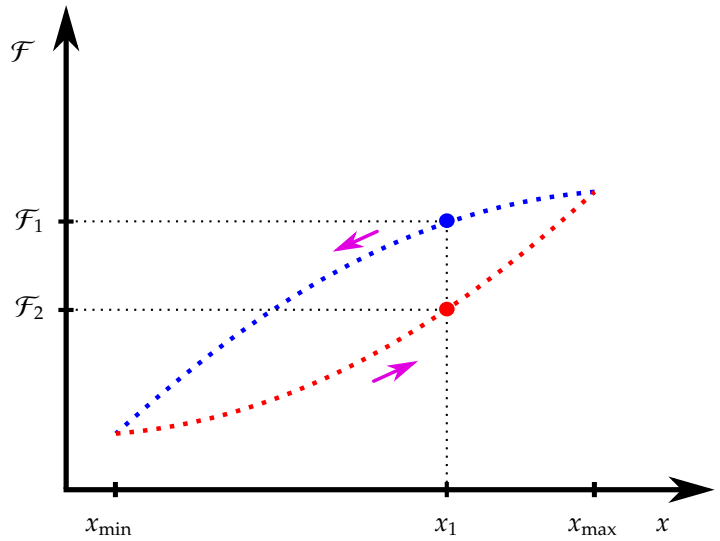

Figure 2.1: Schematic representation of the input-output relationship for a hysteresis functional. For an input value x_1, there are two output values $\mathcal{F}_1$ (•) and $\mathcal{F}_2$ (•), which depend on the input rate. (·····) refers to the hysteresis loop, while (→) indicates its orientation and in which the periodic input x varies.

As can be seen in Figure 2.1, the force $\mathcal{F}$ is not a function of displacement x, since there are two force values $\mathcal{F}_1$ and $\mathcal{F}_2$ associated with a single displacement value x_1. In addition, it is noticeable that, except for the extremum values of the input x, each force value depends on the history of the corresponding input. Such dependence is related to the memory effect, which is one of the features commonly used in the literature to characterize hysteretic systems (Visintin, 1994). Additionally, Bouc (1971) worked with the assumption that the shape of the hysteresis loop in Figure 2.1 remains the same for any input frequency, which refers to the *rate-independent property* present in such systems and will be further discussed in Section 2.3.7.3.

The class of dynamical systems studied by Bouc (1971) can be represented as:

$$\ddot{x}(t) + \mathcal{F}(t) = p(t), \tag{2.3}$$

where $p(t)$ refers to system input. Models (2.1) and (2.3) describe a hysteretic oscillator. In order to obtain an analytical solution for (2.1) that preserve some hysteresis properties (Ikhouane and Rodellar, 2007), Bouc (1971) proposed a variant of the Stieltjes integral for the output $\mathcal{F}$, such that (2.1) and (2.3) could be rewritten as:

$$\ddot{x}(t) + \mu^2 x(t) + \sum_{i_\mathrm{h}=1}^{N_\mathrm{h}} h_{i_\mathrm{h}}(t) = p(t), \tag{2.4}$$

$$\dot{h}_{i_\mathrm{h}}(t) + \beta_{i_\mathrm{h}} |\dot{x}(t)| h_{i_\mathrm{h}}(t) - A_{i_\mathrm{h}} \dot{x}(t) = 0, \qquad i_\mathrm{h} = 1, \cdots, N_{i_\mathrm{h}}, \tag{2.5}$$

for which h_{i_h} corresponds to the hysteretic behavior of the N_{i_h} restoring forces acting on the system, whose constant coefficients μ, β_{i_h} and A_{i_h} must be estimated. Models (2.4) and (2.5) are known as the Bouc model.

In order to improve the predictive capacity of the Bouc hysteresis model so that a greater variety of hysteresis loops can be represented, Wen (1976) extended model (2.5) based on laws of physics, giving rise to the so-called Bouc-Wen model expressed as:

$$\dot{h}(t) = A\dot{x}(t) - \beta |\dot{x}(t)| |h(t)|^{n-1} h(t) - \gamma \dot{x}(t) |h(t)|^n, \tag{2.6}$$

such that $h(t)$ determines the hysteresis output, $x(t)$ is the model input. The scale and general shape of the hysteresis loop are determine by A, β and γ, while its smoothness is adjusted by n (Wang and Zhu, 2011). This model is widely used in the literature to model devices with hysteresis, such as piezoelectric actuators, magneto-rheological dampers, among others (Domínguez-González et al., 2014; Ahmad, 2018).

Example 2.1. Bouc-Wen model and its Hysteresis Loop.

In order to illustrate how the parameters of the Bouc-Wen model (2.6) can significantly influence the shape of the hysteresis loop, the following two test scenarios are adopted. In the first one, it is shown how different values of n might affect the hysteresis loop, while the other parameters are kept constant at a given value; see Figure 2.2(a). In the second test scenario, the case where the value of parameters n and A is fixed, and different values of β and γ are considered; see Figure 2.2(b). A more in-depth analysis of the parameters of the Bouc-Wen model and their influence on the hysteresis loop can be found in (Ismail et al., 2009; Charalampakis, 2010).

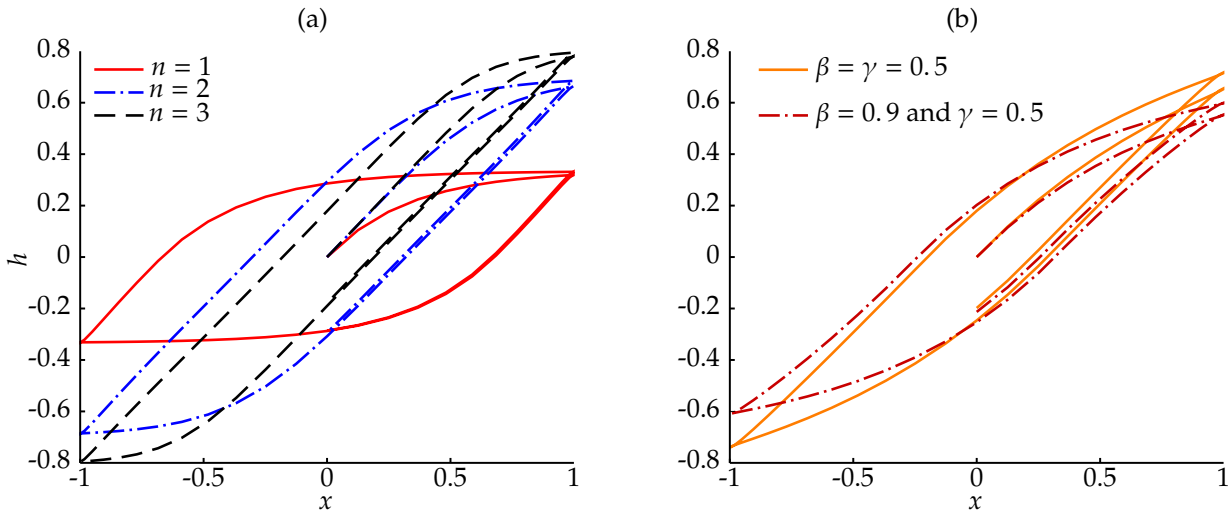

Figure 2.2: Illustration of different hysteresis loops of the Bouc-Wen model (2.6). (a) the effect of n on hysteresis loop for A=1, β=1, γ=2 and n={1, 2, 3}, while in (b) the hysteresis loops for n=1 and A=1 with β=γ=0.5 and β=0.9 and γ=0.5. The input signal is $x(t)$= sin(2πft) with f = 1 Hz.

△

As can be seen in Figure 2.2, the parameter estimation step of the Bouc-Wen model is strictly related to its efficiency in predicting the hysteresis phenomenon present in real systems. Thus, to deal with this problem, many works have used and proposed different methods to estimate the parameters of this model, such as those based on evolutionary algorithms, least squares, and adaptive methods, among others (Ha et al., 2005; Hassani et al., 2014; Wei et al., 2014; Tavares et al., 2019).

A detailed investigation of some properties of the Bouc-Wen model and issues related to the modeling and control of dynamical systems that include this type of hysteresis is presented in (Ikhouane and Rodellar, 2007; Ismail et al., 2009).

2.2.2 Prandtl-Ishlinskii Operator

Among the phenomenological models used to represent hysteretic systems are those based on differential equations, such as the Bouc-Wen model reviewed in Section 2.2.1, as well as models based on operators (Zakerzadeh et al., 2011). This latter type of model has attracted great interest since the early 1970s, when Mark Alexandrovich Krasnosel'skii and co-workers proposed the mathematical formulation of hysteresis operators (Visintin, 1994).

One of the most popular operator-based models used to characterize hysteresis behavior is the Preisach model (Hu and Ben Mrad, 2003). From this model, two operator-based models can be derived, the Krasnosel'skii-Pokroviskii (KP) model and the Prandtl-Ishlinskii model. In terms of predictive performance, the KP model appears as a good alternative compared to the Preisach, since discontinuity issues are overcome by it, but it still has a high structural complexity that makes its analytical inversion

unfeasible and that hinders its use in real-time applications (Banks et al., 1997; Hassani et al., 2014). On the other hand, the Prandtl-Ishlinskii model has a simple mathematical structure and its inverse can be calculated analytically. Therefore, such features make this model more effective for real-time applications when compared to the Preisach and KP models (Gu et al., 2012).

The Prandtl-Ishlinskii model is defined as the sum of several weighted elementary operators, also called *play operators* (Kuhnen, 2003). Each of these operators is parameterized by a radius, or threshold, denoted as r_{aj}. Thus, the j-th play operator $P_{r_{aj}}$ for a continuous input $u(t)$ is illustrated in Figure 2.3 and defined by the following equation:

$$\begin{aligned} v_{r_{aj}}(t) &= \max\Big(\min(u(t)+r_{aj},\, v_{r_{aj}}(t^-)),\, u(t)-r_{aj}\Big) \\ &\triangleq P_{r_{aj}}\Big(u(t);\, v_{r_{aj}}(t^-)\Big), \end{aligned} \tag{2.7}$$

for which $v_{r_{aj}}(t)$ and $v_{r_{aj}}(t^-)$ are, respectively, the current and previous state of the play operator.

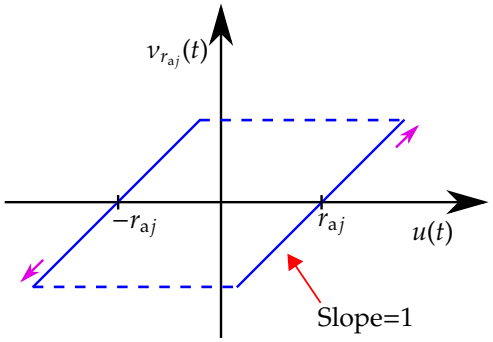

Figure 2.3: Play operator. $u(t)$ is the input signal, and $v_{r_{aj}}(t)$ represents the state values of the j-th operator.

For each play operator, there are two possible modes in which its state can be found at time t, as can be seen in Figure 2.3 and observed in (2.7). One of these modes corresponds to the linear region, i.e. where the state varies linearly subject or not to a translation, such that $v_{r_{aj}}(t) = u(t) \pm r_{aj}$, which is illustrated by blue continuous lines in Figure 2.3. The second mode is called the play region, where the state is constant, given by $v_{r_{aj}}(t) = v_{r_{aj}}(t^-)$ and indicated by dashed lines in Figure 2.3 (Esbrook et al., 2014).

Considering that the hysteresis behavior might be represented by a Prandtl-Ishlinskii operator composed of n_r play operators $P_{r_{aj}}$ (2.7), its output $H(\cdot)$ is given by:

$$v(t) = H\Big(u(t);\, \boldsymbol{\nu}_{r_a}(t^-)\Big) = \sum_{j=1}^{n_r} \theta_j P_{r_{aj}}\Big(u(t);\, v_{r_{aj}}(t^-)\Big), \tag{2.8}$$

where $\boldsymbol{\nu}_{r_a}(t) \triangleq [v_{r_{a1}}(t)\; v_{r_{a2}}(t)\; \cdots\; v_{r_{an_r}}(t)]^T$ is the vector composed of the state variables $v_{r_{aj}}(t)$, of the n_r play operators, at the current time t, and $\boldsymbol{\nu}_{r_a}(t^-) \triangleq [v_{r_{a1}}(t^-)\; v_{r_{a2}}(t^-)\; \cdots\; v_{r_{an_r}}(t^-)]^T$

is the vector of state variables at the instant immediately preceding the current time. Each weight θ_j is assumed to be bounded, non-negative and greater than zero, while the radii $r_{\mathrm{a}j}$ satisfy the following condition: $0 = r_{\mathrm{a}1} < r_{\mathrm{a}2} < \cdots < r_{\mathrm{a}n_r} < \infty$ (Esbrook et al., 2014).

In order to rewrite (2.8) in a compact form, one can define $\mathcal{P} \triangleq [P_{r_{\mathrm{a}1}}\ P_{r_{\mathrm{a}2}}\ \cdots\ P_{r_{\mathrm{a}n_\mathrm{r}}}]^T$, which represents the temporal evolution of states $\boldsymbol{\nu}_{r_\mathrm{a}}(t)$ of (2.8) with respect to input $u(t)$, such that:

$$\boldsymbol{\nu}_{r_\mathrm{a}}(t) = \mathcal{P}\Big(u(t);\, \boldsymbol{\nu}_{r_\mathrm{a}}(t^-)\Big). \tag{2.9}$$

Furthermore, $\boldsymbol{\theta} \triangleq [\theta_1\ \theta_2\ \cdots\ \theta_{n_\mathrm{r}}]^T$ and $\boldsymbol{r}_\mathrm{a} \triangleq [r_{\mathrm{a}1}\ r_{\mathrm{a}2}\ \cdots\ r_{\mathrm{a}n_\mathrm{r}}]^T$. Thus, one can represent the output of the Prandtl-Ishlinskii operator (2.8) as:

$$v(t) = H\Big(u(t);\, \boldsymbol{\nu}_{r_\mathrm{a}}(t^-)\Big) = \boldsymbol{\theta}^T \boldsymbol{\nu}_{r_\mathrm{a}}(t). \tag{2.10}$$

Example 2.2. Prandtl-Ishlinskii Operator and its Hysteresis Loop.

For illustrative purposes, consider that the Prandtl-Ishlinskii operator (2.10) is composed of three play operators (2.8), i.e. $n_\mathrm{r} = 3$, with radii given by $\boldsymbol{r}_\mathrm{a} = [0\ \ 0.8\ \ 1.7]^T$ and weighted by $\boldsymbol{\theta} = [5.88\ \ 1.58\ \ 0.47]^T$ (Abreu et al., 2018a). The input-output relation of each play operator and the resulting hysteresis loop are shown in Figures 2.4(a) and 2.4(b), respectively.

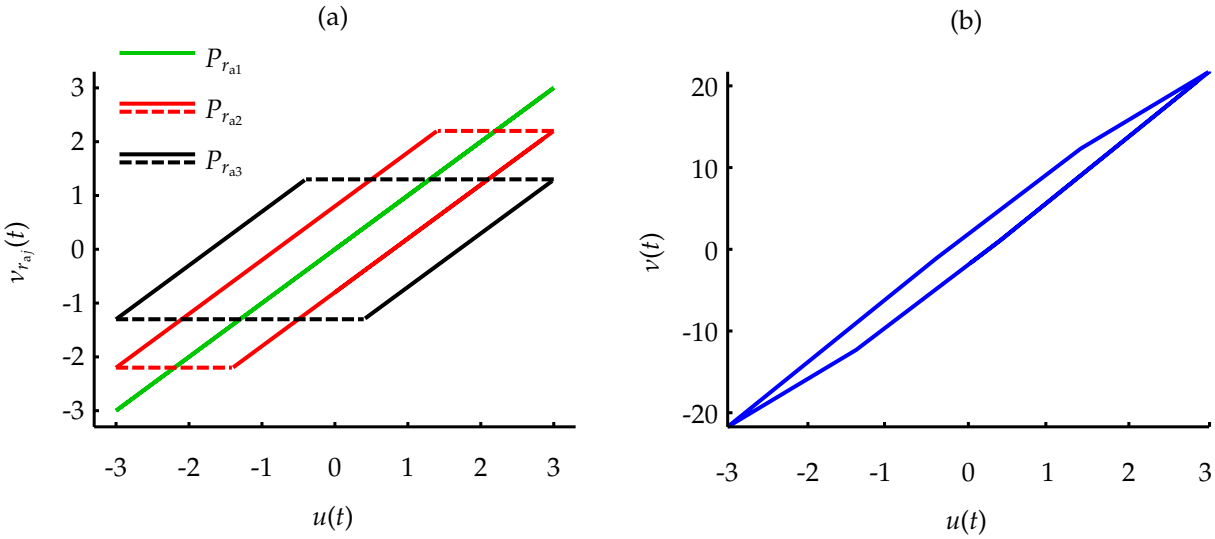

Figure 2.4: Illustration of an operator (2.10). (a) output of the operators $P_{r_{\mathrm{a}1}}$, $P_{r_{\mathrm{a}2}}$ and $P_{r_{\mathrm{a}3}}$, and in (b) the hysteresis loop of the operator (2.10). The input signal is $u(t)$=3 sin($2\pi ft$) with $f = 1$ Hz.

△

More details on Prandtl-Ishlinskii models can be found in the following references (Visintin, 1994; Brokate and Sprekels, 1996).

2.3 NARX Model

In a more general field of modeling nonlinear systems, the Nonlinear Autoregressive with eXogenous inputs (NARX) representation is considered a convenient choice due to its ability to predict a wide class of nonlinear behaviors (Leontaritis and Billings, 1985a,b). According to Billings (2013), although initially introduced as a kind of mathematical representation, the name NARX became known as a framework for the identification of nonlinear systems, whose main goal is to build models that are quite general and that present simple structures. Therefore, the NARX philosophy concerns not only obtaining models that closely fit the behavior of the investigated systems, but that can also be used to help understanding the nonlinear dynamics inherent in such systems, since the structural simplicity of their models would make possible a more in-depth analysis of the fundamental dynamical properties (Aguirre and Billings, 1995b; Aguirre and Mendes, 1996; Pearson, 1999). Indeed, such a philosophy is commonly associated with some procedure for choosing the terms to be included in the model, so that the candidate regressors are ranked and included one by one, according to their importance, until reaching a desired predictive performance.

The classic concepts for building NARX models are grounded on *black-box modeling*, for which it is assumed that *all* relevant information about dynamic behavior is present *only* in the input and output signals collected from the investigated system. Therefore, it should be emphasized that black-box models do not rely on prior knowledge about the system (Sjöberg et al., 1995; Chan et al., 2015; Ayala et al., 2015; Fu et al., 2016). Thus, relevant features that should be present in a model to reproduce more subtle aspects of the system dynamics, as well as its use for a model-based control or compensation context that, in general, rely on an appropriate model structure, are not ensured by black-box techniques. To circumvent this issue, the use of *gray-box techniques* to build models that can be tailored to reproduce specific relevant features, that are accurate and that have a suitable structure for their use in control or compensation schemes, has become a promising way (Aguirre, 2019).

As for the use of gray-box modeling, it is first pointed out that there are very few works in the literature and that the term gray-box is applied in a variety of ways. For instance, some of them range from those in which the auxiliary information is the model structure itself, i.e. the estimation of parameters for well established models (Parlitz et al., 2004; Worden et al., 2007), to those that the *only* auxiliary information is the fact that the data set is collected from a system that has a known relevant feature (Leva and Piroddi, 2002; Aguirre, 2014), such as specific nonlinearity, time-invariant or time-varying behavior, among other features. The latter way is a more comprehensive gray-box approach, since the methods adopted to incorporate in a model the ability to mimic a relevant feature are based on the physical insights about the dynamic behavior of the real system. This provides advantages in the applicability of this approach, which can be extended and that is simpler than the adoption of physically-inspired

model structures to handle different types of systems. A common route raised by such methods is to use physical insights to suggest specific functions of the measured data, to be included as new candidate regressors during identification, and/or constraints to be imposed during the parameter estimation step (Billings and Chen, 1989; Aguirre et al., 2004; Martins and Aguirre, 2016). Although such a gray-box approach can be effective, a systematic representation and guidelines of *how* to extract useful information from data and incorporate it into a NARX model remain an open subject for research in the identification of nonlinear systems. In light of this problem, some preliminary aspects that ground the formulation of NARX models in the black-box context, as well as their extension to the gray-box scenario, are stated in Section 2.3.1.

The classic concepts behind the NARX philosophy for nonlinear system identification are briefly reviewed and discussed from Section 2.3.2 to Section 2.3.6, which address some of the main steps used to build such models. It is noteworthy that the main tools related to the black-box and gray-box techniques tend to remain, except for their adaptation to suit the representation adopted for the gray-box models, and for cases where more refined algorithms are required. Both occurrences have been addressed in these sections, as needed. In addition, it is important to keep in mind that the main focus of this chapter is to deal with the modeling of hysteresis nonlinearity in dynamical systems. Therefore, although such a review is presented in a more comprehensive manner, the main discussions throughout the text involve the literature on hysteresis, but are not limited to it.

In the context of hysteretic systems, the use of NARX models that are especially dedicated to the description of such systems and/or that can be effectively used to design compensators that mitigate their hysteresis nonlinearity is an open and recent branch of research, whose results are still scarce in the literature (Deng and Tan, 2009; Dong and Tan, 2014; Martins and Aguirre, 2016; Lacerda Júnior et al., 2019). Based on this research field, some works that use them for hysteretic systems are also reviewed, adopting a critical posture, in Section 2.3.7. Such a review intends, mainly, to present a concise analysis and discussion addressing chronologically the advances found in the literature, as well as discuss their pros and cons to mimic some features of hysteretic systems. Finally, Section 2.3.8 points out some alternative ways and guidelines for building models with the ability to reproduce some more subtle aspects of hysteresis, which refer to interesting topics to be pursued in the future.

2.3.1 Preliminaries

A black-box NARX representation is given by (Leontaritis and Billings, 1985a,b):

$$y_k = F\Big(y_{k-1}, \cdots, y_{k-n_y}, u_{k-\tau_d}, \cdots, u_{k-n_u}\Big), \tag{2.11}$$

where $y_k \in \mathbb{R}$ is the output at instant $k \in \mathbb{N}$, and $u_k \in \mathbb{R}$ is the input signal, which are obtained by measuring the continuous data $y(t)$ and $u(t)$ at sampling intervals T_s,

respectively, and $\tau_d \in \mathbb{N}^+$ is the pure time delay. Moreover, n_y and n_u are the maximum lags for the output and input, respectively, and $F(\cdot)$ is a nonlinear function of the lagged outputs and inputs.

Among the numerous model classes that can be obtained by restricting the function $F(\cdot)$ are: polynomial, rational models, and neural networks (Billings, 2013). As a consequence of this choice, in addition to different model structures and identification techniques, each model type has its pros and cons to represent the behavior of a dynamical system. An interesting work that provides an in-depth analysis and some useful guidelines linking different discrete-time model structures with some of the important qualitative behaviors that these can produce was done by Pearson (1999). This type of study is rarely found in the literature and it brings a valuable perspective on choosing an appropriate class of models to describe systems that have specific dynamic features. Based on NARX representation (2.11), Pearson (1999) emphasized that such models stand out due to their ability to produce a wide variety of qualitative behaviors that can be obtained by a simple description of the system. Some of the qualitative behaviors that NARX models, especially in polynomial form, may exhibit are: input amplitude-dependent stability, super and subharmonic generation, asymmetric responses to symmetric input changes, and output multiplicity. Most of them are cited by works in the literature as features commonly found in hysteretic systems (Deng and Tan, 2009; Wei et al., 2014; Martins and Aguirre, 2016; Fujii et al., 2018). Furthermore, other more exotic behaviors such as chaos, bifurcation, and a variety of real systems have been described using NARX models in (Billings, 2013) and the references therein.

In terms of data fitting, NARX neural networks are an excellent choice due to their property of universal approximators, which leads to models with good performance for predicting nonlinear systems (Ayala et al., 2015; Chan et al., 2015; Fu et al., 2016). However, such models tend to have a larger number of parameters and complex functions that hinder their analysis and manipulation and, therefore, make their use unfeasible to help understand and relate their terms to the dynamic behaviors of the investigated system. On the other hand, the use of NARX polynomial models has been argued to be an appealing way, since it may be possible to achieve good performance and generality through models with about six terms (Aguirre et al., 2002; Martins and Aguirre, 2016; Lacerda Júnior et al., 2019). In addition, such polynomial models also have some advantages related to structural flexibility and the fact that they are linear-in-the-parameters, which makes them easy to be implemented and enables the use of algorithms from the least squares family for parameter estimation (Ljung, 1999; Isermann and Münchhof, 2011). It has been argued that for a model with these features it is feasible to enforce some constraints on its structure and parameters, in order to make it suitable for model-based control or compensation, as well as to predict more subtle dynamics (Pearson, 1999; Leva and Piroddi, 2002; Aguirre, 2019). Moreover, as such models are linear-in-the-parameters, the problem of getting trapped in local minima is avoided during estimation, which commonly occurs with models based on

neural networks. From now on, NARX polynomial models will be considered as the model class. Just out of curiosity, a theoretical justification for using them to represent nonlinear systems has been presented in (Chen and Billings, 1989).

As one of our intentions here is to address ways, commonly used in the literature, to incorporate in a model the ability to describe more subtle dynamic aspects, we start with the description of the *adopted gray-box representation*, which is given by:

$$y_k = F^{\ell}\Big(y_{k-1}, \cdots, y_{k-n_y}, u_{k-\tau_d}, \cdots, u_{k-n_u}, \phi_{i,k-1}, \cdots, \phi_{i,k-n_{\phi_i}}\Big), \tag{2.12}$$

where n_{ϕ_i} is the maximum lag considered for the i-th specific function that can optionally be included as a candidate regressor in the model, represented by $\phi_{i,k}$, $F^{\ell}(\cdot)$ is a polynomial function of the regressor variables up to degree $\ell \in \mathbb{N}^+$, and the other variables are the same as defined in (2.11). The additional term $\phi_{i,k}$ is commonly defined as a function of lagged values of y_k and u_k, as done in (Billings and Chen, 1989; Leva and Piroddi, 2002; Martins and Aguirre, 2016). It should be remembered that, as aforementioned, some works in the literature are based on the use of (2.12) to improve the predictive power of the identified models and/or by means of appropriate parameter estimation tools, which are addressed in Section 2.3.5.

Remark 2.1. It should be clear that simply including a class of regressors $\phi_{i,k}$ in a model does not make it a gray-box model. In fact, gray-box techniques are grounded on building models using some prior knowledge about the investigated system, i.e. *auxiliary information*, so that such knowledge can be incorporated into the model in order to improve its predictive performance or make it suitable for some specific purpose. As previously explained, some ways to achieve this refer to the use of constraints on the structure and/or parameters, adoption of algorithms for recursively updating parameters, and/or inclusion of certain regressors $\phi_{i,k}$ that provide relevant information about the system. Therefore, since it is assumed that $\phi_{i,k}$ is chosen based on prior knowledge about the system to be identified, (2.12) is a gray-box representation.

The reason for explicitly including a certain class of regressors $\phi_{i,k}$ during the identification procedure is based on the fact that, if the pool of candidate regressors that is used is not large enough or does not provide relevant information about the dynamic features of interest, then the procedure will be unable to identify the appropriate model (Billings, 2013). Therefore, a careful look at the *dynamic details* present in the measured output of the investigated system, such as its high correlation or strong dependence on system signals in a complex manner, becomes a powerful tool. For instance, in order to identify hysteretic systems, which have hard nonlinearities that depend on the rate of the input signal, the addition of the first difference of the input, e.g. $\phi_{i,k} = u_k - u_{k-1}$, as a candidate regressor has been adopted and discussed in the literature (Khalid et al., 2014; Martins and Aguirre, 2016). This additional regressor has provided a good estimate of the input rate inherent in such systems and thus improving the predictive power of the identified model, being this a *way used to extract that information from the data*. A point

to be considered is that this regressor could casually appear in the identified model if, during the structure selection procedure (Section 2.3.4), each term was chosen separately, e.g. u_k and u_{k-1}. However, the estimated parameters would have to be *exactly reciprocal* in order to have the effect of $\theta_i\phi_{i,k} = \theta_i(u_k - u_{k-1})$, which is extremely unlike in the context of black-box modeling. Therefore, although this information is buried in the collected data, the probability of identifying a *parsimonious* hysteretic model with such regressor is almost zero unless the first difference is explicitly incorporated into the set of candidate regressors. Likewise, this fact is even more evident for cases where more complicated functions are desired, such as absolute value, sine and sign functions (Billings and Chen, 1989; Leva and Piroddi, 2002).

Remark 2.2. Note that *parsimony* is a criterion inherent in the NARX philosophy, whose core idea is not in a gross approximation of the system behavior, but rather to find a model structure as simple as possible that contains only the most significant terms (Billings, 2013). Thus, such a criterion also aims to avoid the use of excessive terms in the model, which would lead to problems ranging from those related to numerical to those that induce additional spurious dynamic behaviors. These are commonly referred to as *overfitting* or *overparametrization* (Aguirre and Billings, 1995a).

Indeed, the goal is to choose functions $\phi_{i,k}$ that allow the models to predict systems whose nonlinearities cannot be well approximated using only regressors based on monomials of lagged input and output values. Thus, a relevant question arises: *How to determine, or which are, such functions?* For this purpose, two ways that can be explored are presented below.

Example 2.3. Ways to Extract Information.

In order to illustrate some possible ways of determining promising functions $\phi_{i,k}$ that might provide relevant information about the dynamic features of interest and, thus, extract such information from the collected data, two examples are presented below. The first one aims to deal with the hysteresis, seeking insights through the analysis of the terms that make up a well known phenomenological model, for which we chose the Bouc-Wen model; see Section 2.2.1. The second example refers to an idea recently raised to describe a kind of *time*-varying dynamics of a system by means of a specific function of its output signal, which is based on a mathematical interpretation proposed to capture this behavior. Such functions can be used as candidate regressors of model (2.12).

A) Hysteresis

Consider that a discrete counterpart of the Bouc-Wen model (2.6) can be approximated by:

$$\frac{y_{kT_s} - y_{[k-1]T_s}}{T_s} = A\frac{u_{kT_s} - u_{[k-1]T_s}}{T_s} - \beta\left|\frac{u_{kT_s} - u_{[k-1]T_s}}{T_s}\right|y_{[k-1]T_s} - \gamma\frac{u_{kT_s} - u_{[k-1]T_s}}{T_s}\left|y_{[k-1]T_s}\right|, \quad (2.13)$$

for small values of T_s and, for convenience, using y_k and u_k here, respectively, as the model output and input (Ahmad, 2018). For the intended analysis, one can assume T_s=1, so that (2.13) can be rewritten as:

$$y_k = y_{k-1} + A[u_k - u_{k-1}] - \beta\left|u_k - u_{k-1}\right|y_{k-1} - \gamma[u_k - u_{k-1}]\left|y_{k-1}\right|. \tag{2.14}$$

A basic property of the absolute value function is stated below.

Property 2.1. [(Popiołek, 1990)]. *The absolute value $|\cdot|$ of a real number x can be expressed as the product of this real number and its sign function (Defintion 2.1), such that:*

$$\left|x\right| = x \cdot \text{sign}(x).$$

From Property 2.1, model (2.14) is recast as:

$$y_k = y_{k-1} + A\underbrace{[u_k - u_{k-1}]}_{\phi_{1,k}} - \beta[u_k - u_{k-1}]\underbrace{\text{sign}(u_k - u_{k-1})}_{\phi_{2,k}}y_{k-1} - \gamma[u_k - u_{k-1}]\underbrace{\text{sign}(y_{k-1})}_{\phi_{3,k}}y_{k-1}. \tag{2.15}$$

Since model (2.15) is a discrete version of a phenomenological model, its structure provides some interesting suggestions for functions of the input and output signals that might be used as candidate regressors of model (2.12). Specifically, note that we highlight the three main terms $\phi_{i,k}$ found. As mentioned above, for hysteretic systems, the term $\phi_{1,k}$ in (2.15) can easily be defined taking into account the insights of the interrelationship between their characteristic behavior related to the strong dependence on the rate of the input signal, which is widely discussed in the literature, and a mathematical operator that may provide such a feature. Conversely, terms $\phi_{2,k}$ and $\phi_{3,k}$ indicate more complex functions that probably could not be defined based on a simple analysis of the behavior of these systems. In (Martins and Aguirre, 2016), the use of term $\phi_{2,k}$ as a regressor of polynomial models led to a sufficient condition that enables them to reproduce a hysteresis loop, thus indicating the improvement achieved when such term is used. More details of this work are revisited in Section 2.3.7. Based on the term $\phi_{3,k}$, we did not find studies in the literature dealing with its use. For this reason, some initial tests were performed here to predict a simulated Bouc-Wen model, however, the results obtained do not indicate an improvement in the predictive performance of the models identified using $\phi_{3,k}$ as one of the candidate regressors. In a very short view, such tests consisted of considering $\phi_{1,k}$, $\phi_{2,k}$ and $\phi_{3,k}$ as possible additional candidate regressors during the identification procedure and then evaluating the predictive performance of the identified models. It was observed that, in some cases, $\phi_{3,k}$ was not even selected to compose the final model and that, when selected, the improvement in the prediction was not significant. The tools used to select the model structure during these tests were the error reduction ratio together with the Akaike's information criterion, which are detailed in Section 2.3.4. Therefore, in principle, the use of $\phi_{3,k}$ can be disregarded, despite the need for a more careful investigation.

As a matter of interest, a NARX model (2.12) was identified for an experimental electronic circuit with hysteresis, in which the sign of the first difference of the output, i.e. sign($y_k - y_{k-1}$), was included as one of the regressors (Lacerda Júnior et al., 2019). However, the authors do not mention a reason for its use or why it should be included as a candidate regressor, which also needs further investigation.

It is noteworthy that this type of approach to extract information can be extended to other systems whose phenomenological models are known, so that the functions found can be used as candidate regressors in the identification using model (2.12).

B) A Kind of *Time*-Varying Behavior

Here, the approach presented is based on a thorough examination of the collected data set, without depending on the knowledge of a phenomenological model, as a way of detecting behaviors that are hidden in it. Recently in (Abreu et al., 2021), this approach was used to detect relevant behaviors of a potential of hydrogen (pH) neutralization process from experimental data, for which a class of regressors $\phi_{i,k}$ was proposed to improve the ability of the identified NARX models to describe varying behavior in such processes – such varying behavior may not necessarily be time-dependent. To illustrate this, consider Figure 2.5.

From the temporal responses in Figure 2.5(a), it is possible to notice that the measured output signal has a subtle behavior with respect to its rate of change over time, which is clearer in the enlarged figure. Such varying behavior becomes more evident when compared with the estimated output of the black-box model, which was identified using only the input and output signals of the pH process. For instance, in the range of $220 - 290\,k$, the decay rate of the measured output can be approximated by an exponential, while the decay rate of the estimated output by a constant. In addition, note that the input signal in this range has a constant value, which suggests that the core information of interest is within the measured output signal.

In order to extract useful information about this varying behavior, which might be related to nonlinear and/or time-varying dynamics commonly found in pH processes (Marques, 2015), Abreu et al. (2021) propose the use of the time derivative of the output signal, which can be approximated as:

$$\dot{y}(t) \approx \frac{y_{kT_s} - y_{[k-1]T_s}}{T_s} = \phi_{1,k}. \tag{2.16}$$

In Figure 2.5(b), the first difference of the output signal (2.16) for the black-box model and the process is shown. As can be seen, the calculation of (2.16) for the measured output signal provides relevant information about the varying behavior, while for the estimated output it indicates that the black-box model is not able to predict such behavior, as expected. Therefore, the authors proposed the use of delayed values of the first difference of the measured output signal (2.16) as a candidate regressor during the

identification procedure, so that the identified models can incorporate this information, improving their predictive power. More details can be found in (Abreu et al., 2021).

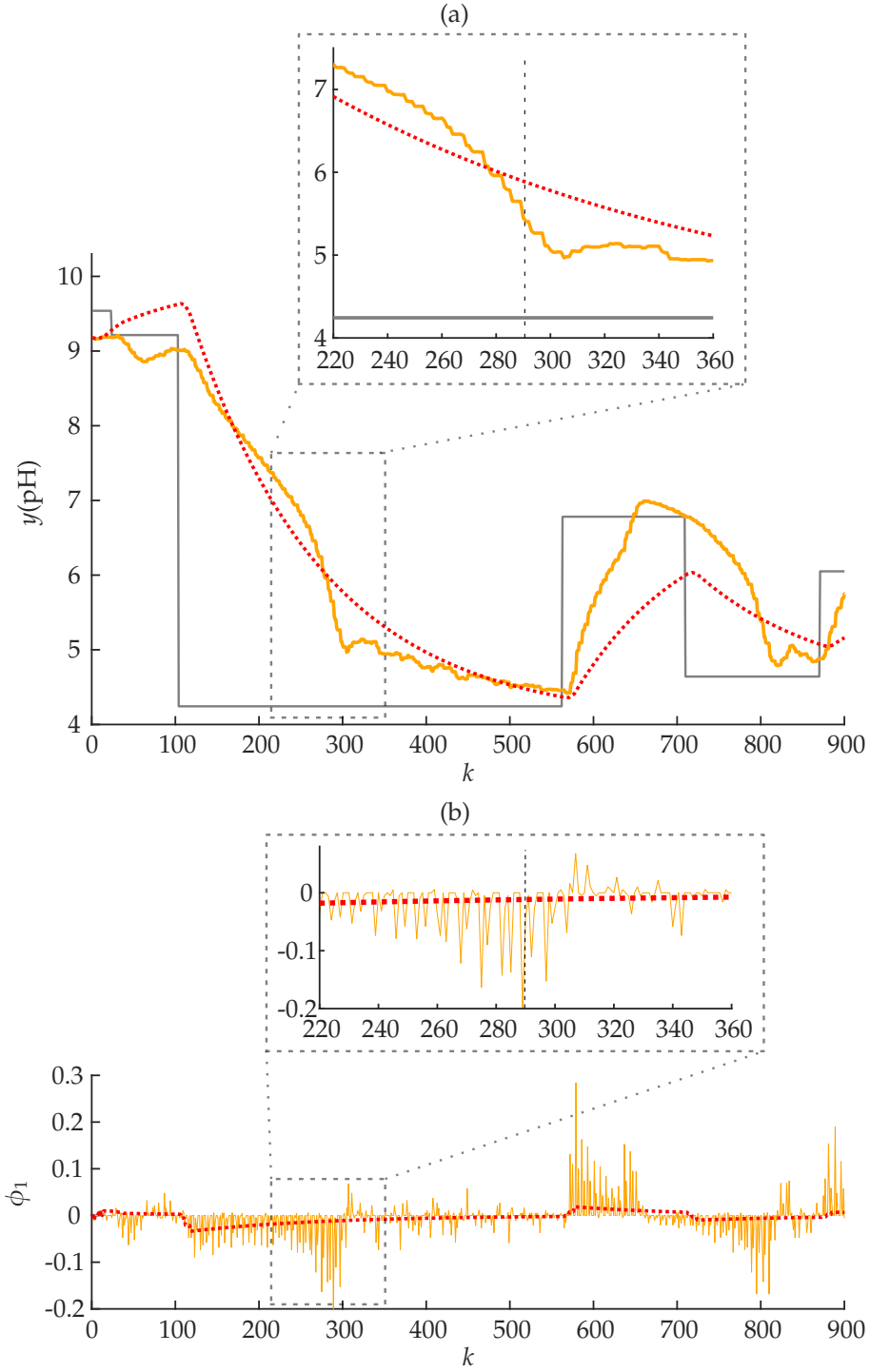

Figure 2.5: An excerpt of the collected data, with the sampling time of T_s=1 s, and the predictive results obtained for the pH neutralization process studied in (Abreu et al., 2021). (a) estimates of the pH process, and (b) the first difference of the output. (–) refers to the input, (–) the measured output, and (···) the estimated output – see Eq. (9) in (Abreu et al., 2021) – using constant parameters.

Note that the approach described in this example tends to be more general than the one described in the previous one, since it assumes that all information is within the collected data set and can be discovered with a thorough examination. However, this task may not be as easy as it seems, since it depends on a critical look at all the dynamic details, and then extract/represent this information through a mathematical operator. △

Given the initial definitions and assumptions provided above, some of the main steps and concepts of NARX philosophy for nonlinear system identification are presented in what follows.

2.3.2 Dynamic Tests

As the identification procedure aims to build models from a set of data collected from an investigated system, a fundamental first step refers to the design of dynamic tests that excite the characteristics of interest. Therefore, issues related to the range of amplitude and frequency to be excited, as well as the type of signal used for this purpose, need to be determined a priori. An important aspect to be pursued in this context is the use of a *persistently exciting input signal* (Ljung, 1999; Billings, 2013). In terms of nonlinear identification, such a signal is commonly described to be able to excite a certain frequency range and reach a variety of operating points within the amplitude range of the investigated system (Schoukens and Ljung, 2019).

Another interesting point that deserves attention is that a sampling time T_s should be defined so that the collected data preserve the fundamental features of the system during the dynamic tests. This subject is important mainly due to the trade-off between low and high values of T_s, which can affect the reconstruction of information and the identification of nonlinear systems (Shannon, 1949; Billings and Aguirre, 1995). In short, for excessively large T_s, the relevant dynamic information in the set of data collected from the system will be lost and, thus, its use becomes inappropriate for reconstruction and identification. On the other hand, for very small T_s, the data may become highly correlated, which affects the performance of the algorithms used (Aguirre, 1994; Billings, 2013). Billings and Aguirre (1995) presented a procedure based on linear and nonlinear correlation functions of the data, which can be used to choose an appropriate value of T_s for the identification of nonlinear systems. Based on it, two ways are commonly adopted. The first one refers to an ideal scenario, for which it is possible to repeat the experiments, now using the appropriate value found for the sampling time. However, there are several situations in which repeating or even doing an experiment (e.g. for the use of historical data) becomes unfeasible due to factors related to time, high costs, safety, among others. The second way, widely used in the literature, aims to convert this sampling time into a *decimation factor* so that the original data can be decimated to provide a properly sampled data set.

For the specific case of hysteretic systems, an interesting question related to how the discretization method and the choice of the sampling time affect the parameter estimation of a polynomial model was investigated in (Lacerda Júnior et al., 2017). From the results of this study, the authors came to the conclusion that the use of any decimation factor in hysteretic data leads to less accurate models compared to the case in which their parameters are estimated without decimating such data. Therefore, since the value chosen for the sampling time is directly related to the quality of the identified model and the use of decimation factors leads to the loss of relevant dynamic characteristics in the data collected from hysteretic systems, such a task must be performed with caution. It is suggested that, whenever possible, preliminary experiments should be carried out to guide the choice of the most appropriate sampling time and, thus, to avoid the application of decimation in hysteretic data.

Regarding the design of a persistent input signal for identification purposes, there are some descriptions and mathematical formulations provided in the literature to achieve it. In the context of linear identification, a *Pseudo Random Binary Signal* (PRBS) is commonly used to excite the dynamic features of the system due to the fact that it is easy to generate, covers a wide frequency range, and excites only two amplitudes values to capture the linear behavior around a desired operating point. The mathematical formulation used to implement this signal can be found in (Ljung, 1999; Keesman, 2011). However, it has been argued that, in general, such an excitation signal is inappropriate when it comes to identifying nonlinear systems, since it may not bring out the nonlinear behaviors that arise when different operating points over the full amplitude range are traversed (Leontaritis and Billings, 1987; Nelles, 2001; Shariff et al., 2013). Thus, an alternative solution usually described for this problem is to extend the PRBS, so that different amplitude values can be explored. Although this type of solution has been widely used by works in the literature, it is hard to find a detailed description of how to design it, e.g. the input was generated to maintain and change its value following some probability distribution (Hernández and Arkun, 1993; Bomberger and Seborg, 1998; Retes and Aguirre, 2019). Therefore, in what follows, we present a detailed formulation for the design of this type of excitation signal, in which it is possible to consider more complicated dependencies inherent to some dynamical systems.

In order to illustrate the procedure proposed for designing this excitation input, which is referred to in this work as *Pseudo Random Variable Steps* (PRVS), consider the schematic representation in Figure 2.6. The input is a sequence of steps, with amplitudes within the range $u_{\min} \leq u_k \leq u_{\max}$, $\forall k$. Assuming that preliminary experiments can be carried out on the system, then, one must initially determine the amplitude values ($u_{s_{\mathring{l}}} \in \mathbb{R}^+$ for $\mathring{l} = 1, 2, \cdots, n_s$) for each step signal that will be applied to the system. It is suggested that these n_s values are proportionally distributed within the amplitude range of the investigated system and satisfy the following condition: $0 < u_{s1} < u_{s2} < \cdots < u_{sn_s} \leq (u_{\max} - u_{\min})$; see Figure 2.6(a). The objective with the choice of n_s different amplitude values is to take into account the nonlinear dynamic behaviors that might be

noticed in the system output. Also, another dynamic behavior that might commonly affect the output of some nonlinear systems refers to its dependence on how the input signal changes its value over time, i.e. for cases in which the input signal is an *increasing step* or is a *decreasing step*; see Figure 2.6(a). In this sense, it is assumed that each of these step signals $u_{s\mathring{\imath}}$ are applied as an increasing step and a decreasing step, so that their corresponding outputs can be used to properly adjust the setup coefficients $k^{up}_{min,\mathring{\imath}}$ and $k^{up}_{max,\mathring{\imath}}$, and $k^{d}_{min,\mathring{\imath}}$ and $k^{d}_{max,\mathring{\imath}}$, respectively. It is worth mentioning that $k^{(\bullet)}_{min,\mathring{\imath}} \in \mathbb{N}^+$ refers to a minimum number of samples that the excitation input might be kept constant at a given value, while $k^{(\bullet)}_{max,\mathring{\imath}} \in \mathbb{N}^+$ refers to its maximum number of samples. Thus, based on temporal responses collected from the investigated system for each step signal $u_{s\mathring{\imath}}$, the corresponding pair $k^{(\bullet)}_{min,\mathring{\imath}}$ and $k^{(\bullet)}_{max,\mathring{\imath}}$ should be chosen so that the resulting excitation input signal will be kept constant until the system provides some response and that it will not be kept constant long enough to reach the steady-state response, respectively.

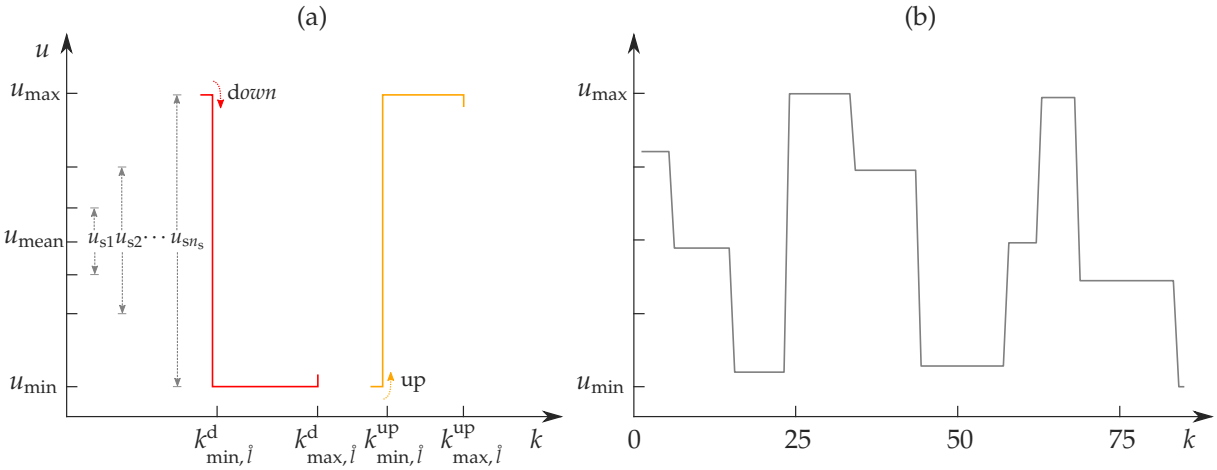

Figure 2.6: Schematic representation for the design of a PRVS excitation signal. (a) the main setup coefficients to be determined, and (b) a resulting excitation signal.

In the sequel, after determining the values of the setup coefficients, it is necessary to define how to assign a certain degree of randomness to changes in the amplitude values and in the number of samples for which the excitation input will be kept constant. This type of feature aims to make pseudo random signals more appropriate for nonlinear identification purposes, i.e. providing a persistently exciting signal (Billings, 2013). First, in this work, we consider that the excitation input signal to be generated can be represented as a vector $\boldsymbol{u} \in \mathbb{R}^N$, which is compose of a total of $N \in \mathbb{N}^+$ samples. From this, it is assumed that all possible input signal values are uniformly distributed within the full amplitude range, being denoted by a continuous uniform random variable $\mathring{A}$ whose values are equally likely. Its shorthand notation is $\mathring{A} \sim \mathcal{U}(0, u_{max}-u_{min})$, which means that $\mathring{A}$ is *distributed according to* a continuous uniform distribution $\mathcal{U}(0, u_{max}-u_{min})$ with lower and upper limits of amplitude values defined here as 0 and $(u_{max} - u_{min})$, respectively. Also, we assume that $\mathring{a}_{\mathring{\jmath}} \in \mathbb{R}$ is a possible

value, i.e. a realization, obtained by performing the $\mathring{j}$-th numerical trial (or experiment) of $\mathring{A}$ (Kay, 2006). In a similar vein, it is considered that the number of samples, for which each value $\mathring{a}_{\mathring{j}}$ is kept constant, is determined by the $\mathring{j}$-th realization of a discrete uniform random variable $\mathring{K}_{\mathring{l}}^{(\bullet)}$ as $\mathring{\kappa}_{\mathring{l},\mathring{j}}^{(\bullet)} \in \mathbb{N}^{+}$. Thus, its shorthand notation is defined as $\mathring{K}_{\mathring{l}}^{(\bullet)} \sim \mathcal{U}\{k_{\min,\mathring{l}}^{(\bullet)}, k_{\max,\mathring{l}}^{(\bullet)}\}$, where $\mathcal{U}\{k_{\min,\mathring{l}}^{(\bullet)}, k_{\max,\mathring{l}}^{(\bullet)}\}$ represents a discrete uniform distribution with lower and upper limits $k_{\min,\mathring{l}}^{(\bullet)}$ and $k_{\max,\mathring{l}}^{(\bullet)}$, respectively. It should be noted that $\mathring{\kappa}_{\mathring{l},\mathring{j}}^{(\bullet)}$ consists of an integer value that is a realization of $\mathring{K}_{\mathring{l}}^{(\bullet)}$, whose lower and upper limits are dependent on the behavior of the input signal as an increasing or a decreasing step and its magnitude, which are obtained using the preliminary experiments, as previously explained. Therefore, in order to properly compose the PRVS signal vector $\boldsymbol{u}$ to be generated with N samples according to the procedure described above, the following algorithm can be defined:

$$\mathring{\Delta}_{\mathring{j}} = \mathring{a}_{\mathring{j}} - \mathring{a}_{\mathring{j}-1}, \tag{2.17}$$

$$\mathring{l} = \begin{cases} 1, & \text{for} \quad |\mathring{\Delta}_{\mathring{j}}| \leq u_{\mathrm{s}\,1}; \\ 2, & \text{for} \quad u_{\mathrm{s}\,1} < |\mathring{\Delta}_{\mathring{j}}| \leq u_{\mathrm{s}\,2}; \\ \vdots & \quad \vdots \\ n_{\mathrm{s}}, & \text{for} \quad u_{\mathrm{s}\,[n_{\mathrm{s}}-1]} < |\mathring{\Delta}_{\mathring{j}}| \leq u_{\mathrm{s}\,n_{\mathrm{s}}}. \end{cases} \tag{2.18}$$

$$\mathring{N}_{\mathring{j}} = \begin{cases} \mathring{\kappa}_{\mathring{l},\mathring{j}}^{\mathrm{up}}, & \text{for} \;\; \mathring{\Delta}_{\mathring{j}} > 0; \\ \mathring{\kappa}_{\mathring{l},\mathring{j}}^{\mathrm{d}}, & \text{for} \;\; \mathring{\Delta}_{\mathring{j}} < 0. \end{cases} \tag{2.19}$$

$$\mathring{\boldsymbol{s}}_{\mathring{j}} = \mathring{a}_{\mathring{j}}\mathbf{1}, \quad \text{for} \;\; \mathbf{1} \triangleq [1 \;\; 1 \;\; \cdots \;\; 1]^{T} \;\; \text{being a} \;\; \mathring{N}_{\mathring{j}} \times 1 \;\; \text{vector}; \tag{2.20}$$

which must be done iteratively (for $\mathring{j} = 1, 2, \cdots, \mathring{j}_{f}^{*}$) until an excitation input signal

$$\boldsymbol{u} \triangleq \left[\mathring{\boldsymbol{s}}_1; \; \mathring{\boldsymbol{s}}_2; \; \cdots; \; \mathring{\boldsymbol{s}}_{\mathring{j}_{f}^{*}}\right] \in \mathbb{R}^{N} \tag{2.21}$$

is generated, such that $N = \mathring{N}_1 + \mathring{N}_2 + \cdots + \mathring{N}_{\mathring{j}_{f}^{*}}$. The initial value $\mathring{a}_0$ in (2.17) can be taken as a realization of $\mathring{A}$. For the last iteration $\mathring{j}_{f}^{*}$, which initially has an unknown value, the corresponding number of samples $\mathring{N}_{\mathring{j}_{f}^{*}}$ obtained with (2.19) can be adjusted, when necessary, so that $\mathring{N}_{\mathring{j}_{f}^{*}} = N - \mathring{N}_1 - \mathring{N}_2 - \cdots - \mathring{N}_{\mathring{j}_{f}^{*}-1}$ is satisfied and, thus, generates the input signal (2.21); see Figure 2.6(b). This procedure is briefly illustrate in Example 2.4.

Example 2.4. Design of a PRVS Excitation Signal.

In order to identify nonlinear models to predict an experimental pH neutralization process, Abreu et al. (2021) used the procedure presented here to generate a suitable PRVS input signal. Based on the titration curve presented in Figure 2.7(a), which provides insights into the nonlinearity inherent in this process (McMillan and Cameron, 2004), the operation region $u_{\min} \leq u_k \leq u_{\max}$ is defined and also the amplitude values $u_{s\,\mathring{l}}$ for each step signal to be used in the preliminary experiments. It should be noted that the setup coefficients included in Figure2.7(a) are merely illustrative, but help to give an idea of how to choose them; compare to Figure 2.6(a). The temporal responses collected from the pH process for the input signal as an increasing step and a decreasing step with amplitude u_{s5}=5 and the corresponding value chosen for the coefficients $k^{(\bullet)}_{\min,5}$ and $k^{(\bullet)}_{\max,5}$ are shown in Figures 2.7(b) and 2.7(c), respectively.

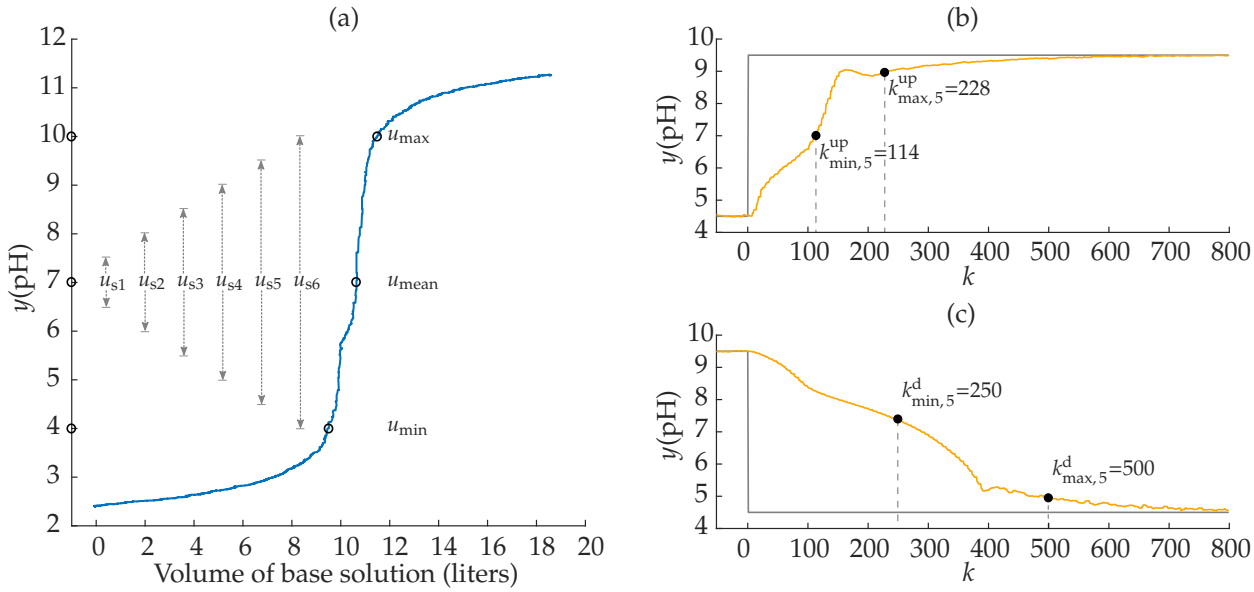

Figure 2.7: Preliminary experiments carried out for the design of the PRVS excitation signal used in (Abreu et al., 2021) to identify a pH neutralization process. (a) the titration curve with amplitudes values $u_{s\,\mathring{l}}$ used in the experiments, and temporal responses for the step input signal with amplitude $u_{s5} = 5$ as step up and down in (b) and (c), respectively. (−) refers to the input, and (−) the measured output.

It should be remembered that, as mentioned before, the literature provides only some guidance on how to determine the minimum and maximum number of samples, i.e. $k^{(\bullet)}_{\min,\mathring{l}}$ and $k^{(\bullet)}_{\max,\mathring{l}}$, for which the excitation input might be kept constant at a given amplitude value. Therefore, for the pH process under study, it was defined that the minimum $k^{(\bullet)}_{\min,\mathring{l}}$ must be determined as *the time required for the process output to reach approximately* 45% *of its covered value range*, in the preliminary experiments, and the maximum as $k^{(\bullet)}_{\max,\mathring{l}} = 2k^{(\bullet)}_{\min,\mathring{l}}$; as illustrated in Figures 2.7(b) and 2.7(c). The values obtained for each setup coefficient are summarized in Table 2.1.

Table 2.1: Setup coefficients chosen to design a PRVS signal for the pH process.

Input Signal	**Number of Samples**	**Amplitude Values -** $u_{s\mathring{l}}$					
		u_{s1}=1	u_{s2}=2	u_{s3}=3	u_{s4}=4	u_{s5}=5	u_{s6}=6
Increasing step	$k^{up}_{min,\mathring{l}}$	54	64	74	94	114	134
	$k^{up}_{max,\mathring{l}}$	108	128	148	188	228	268
Decreasing step	$k^{d}_{min,\mathring{l}}$	60	110	150	180	250	280
	$k^{d}_{max,\mathring{l}}$	120	220	300	360	500	560

Based on the coefficients determined in Table 2.1 and using the proposed algorithm (2.17)–(2.21), Abreu et al. (2021) obtained the excitation input signal $\boldsymbol{u}$ and the corresponding process output shown in Figure 2.8.

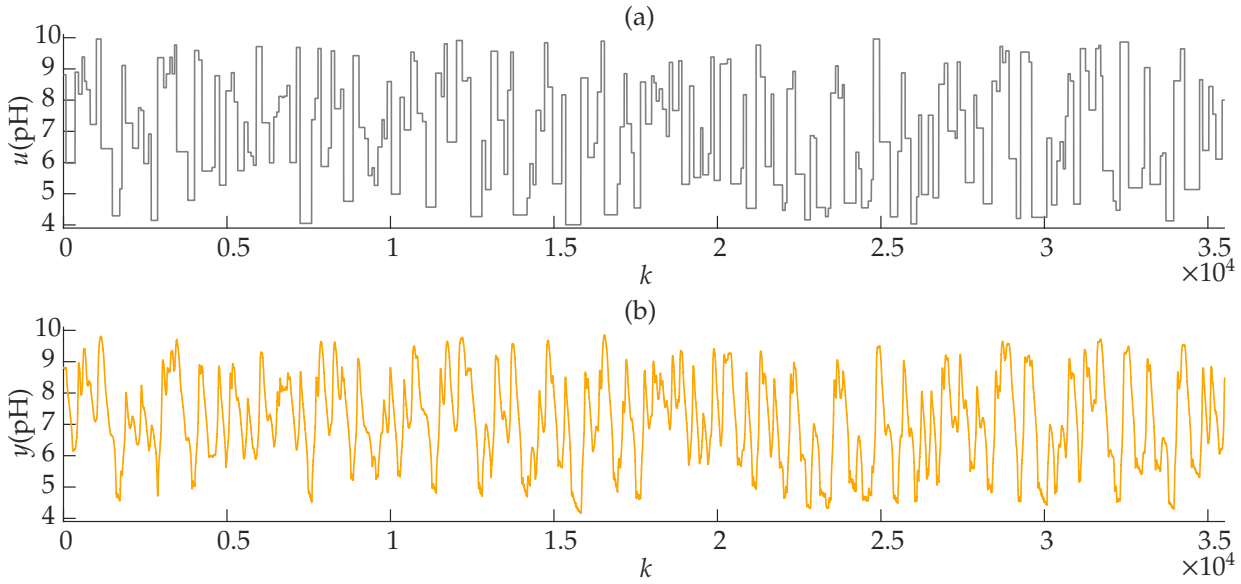

Figure 2.8: Data collected, with T_s=1 s, from the pH neutralization process studied in (Abreu et al., 2021). (a) PRVS excitation input signal, and (b) measured output.

△

Although this type of input signal, i.e. sequence of steps, is commonly used to identify nonlinear systems, there are some systems that demand more subtle excitation signals. For instance, to identify hysteretic systems, whose nonlinearity is dominant at low-frequency and has a strong dependence on the rate of change of the input signal, the use of smoother signals tends to be more appropriate to preserve these characteristics in the collected data (Ikhouane and Rodellar, 2007; Cao et al., 2013; Khalid et al., 2014). Therefore, in order to design smoother and persistently exciting input signals, Tavares (2020) proposed a concise mathematical formulation that allows the user to select the frequencies and operating points of interest to be covered, so that such information is

preserved in the identification data. In this work, this type of excitation input signal is referred to as a *Pseudo Random Filtered Signal* (PRFS). To address the formulation raised in (Tavares, 2020) to generate this input signal, its procedure is briefly revisited below.

A schematic representation is given in Figure 2.9 to provide an overview of the framework used and the main coefficients involved in the design of a PRFS.

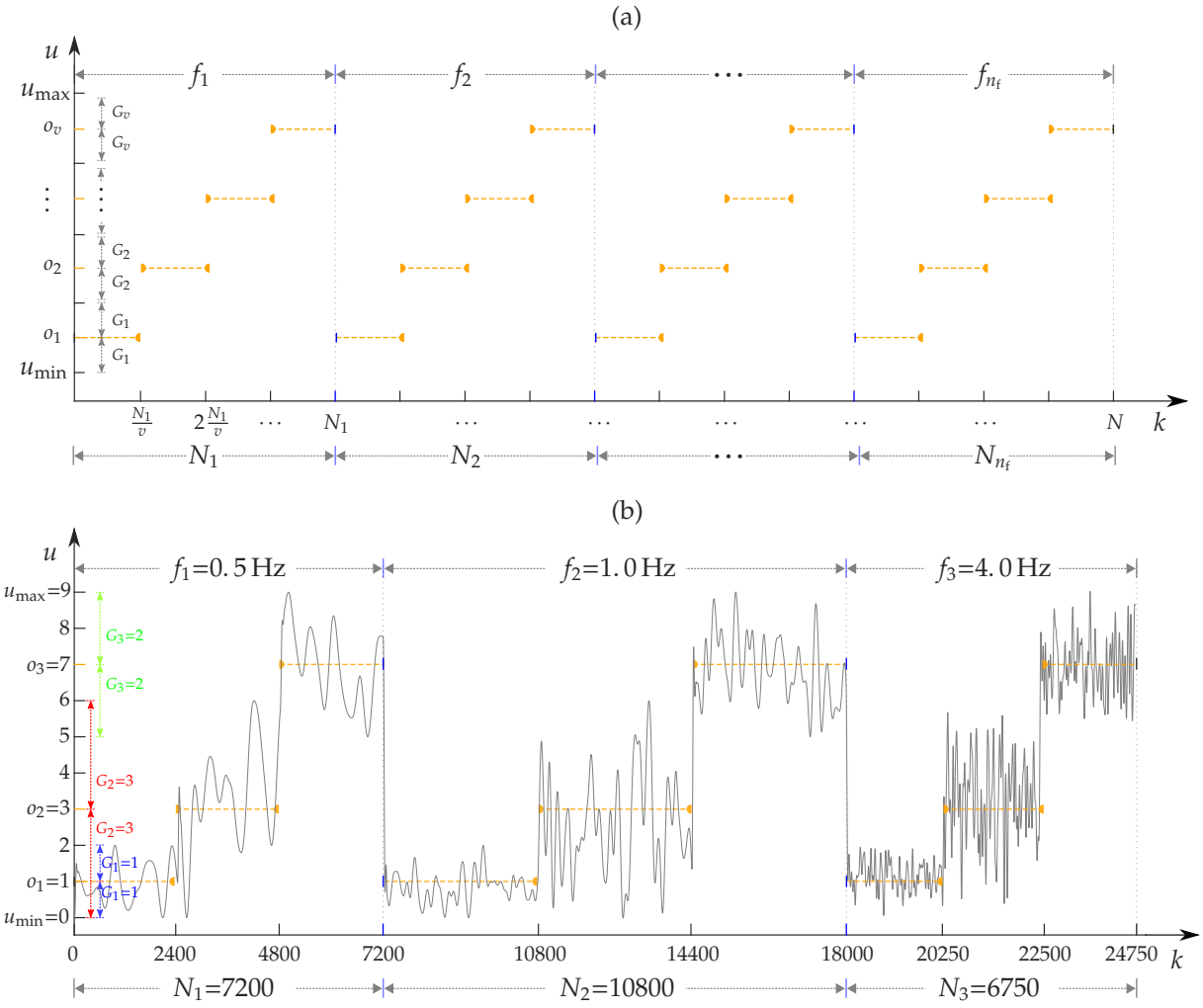

Figure 2.9: Schematic representation for the design of an excitation input as a PRFS. (a) the main setup coefficients to be determined, and (b) a resulting excitation signal.

As the goal here is to generate signals that, besides being persistently exciting, have smoother value changes, the first decisions to be made refer to the range of frequencies and operating points to be covered, as well as how to assign randomness to changes in the amplitude values. Therefore, the user must determine the frequencies ($f_{\mathring{\imath}} \in \mathbb{R}^+$ for $\mathring{\imath} = 1, 2, \cdots, n_f$) of interest to be contained in the excitation signal $\boldsymbol{u} \in \mathbb{R}^N$. For this purpose, fifth-order low-pass Butterworth filters, $\mathcal{B}_{\mathring{\imath}}(q)$, are designed with a respective cutoff frequency $f_{\mathring{\imath}}$. Such filters are then applied to a vector $\mathring{\boldsymbol{b}}_{\mathring{\imath}} \triangleq [\mathring{b}_1 \;\; \mathring{b}_2 \;\; \cdots \;\; \mathring{b}_{N_{\mathring{\imath}}}]^T \in \mathbb{R}^{N_{\mathring{\imath}}}$ composed of $N_{\mathring{\imath}} \in \mathbb{N}^+$ realizations extracted from a normal random variable $\mathring{B}$ that

provides the degree of randomness to reach a variety of input signal values within the full amplitude range. Its shorthand notation is $\mathring{B} \sim \mathcal{N}(0,1)$, where $\mathcal{N}(0,1)$ represents a standard normal distribution with mean 0 and variance 1. Each of these filtered random value vectors is represented by:

$$^{\mathrm{f}}\mathring{\boldsymbol{b}}_{\mathring{\imath}} = \mathcal{B}_{\mathring{\imath}}(q)\mathring{\boldsymbol{b}}_{\mathring{\imath}} \triangleq \left[^{\mathrm{f}}\mathring{b}_1 \;\; ^{\mathrm{f}}\mathring{b}_2 \;\; \cdots \;\; ^{\mathrm{f}}\mathring{b}_{N_{\mathring{\imath}}}\right]^T \in \mathbb{R}^{N_{\mathring{\imath}}}, \tag{2.22}$$

which, for convenience, is conditioned to have its maximum and minimum values as 1 and -1, respectively, as follows:

$$^{\mathrm{f}}\mathring{\boldsymbol{b}}_{\mathring{\imath}} = 2\left[\frac{^{\mathrm{f}}\mathring{\boldsymbol{b}}_{\mathring{\imath}} - \min(^{\mathrm{f}}\mathring{\boldsymbol{b}}_{\mathring{\imath}})}{\max(^{\mathrm{f}}\mathring{\boldsymbol{b}}_{\mathring{\imath}}) - \min(^{\mathrm{f}}\mathring{\boldsymbol{b}}_{\mathring{\imath}})}\right] - 1. \tag{2.23}$$

It should be noted that once the excitation signal $\boldsymbol{u}$ to be generated has N samples, the $N_{\mathring{\imath}}$ samples that make up each of the vectors $^{\mathrm{f}}\mathring{\boldsymbol{b}}_{\mathring{\imath}}$ must be chosen so that $N{=}N_1{+}N_2{+}\cdots{+}N_{n_{\mathrm{f}}}$ is satisfied. In addition, in order to ensure that specific operating points are covered, one can determine those of interest as being $o_{\mathring{\imath}} \in \mathbb{R}$ for $\mathring{\imath} = 1, 2, \cdots, v$. The maximum amplitude to be explored around each of these points $o_{\mathring{\imath}}$ is defined as $G_{\mathring{\imath}} \in \mathbb{R}^+$. Therefore, once the desired frequencies and operating points have been defined, it is assumed that for each of the frequencies $f_{\mathring{\imath}}$, all v operating points are covered with the same number of samples and, thus, $N_{\mathring{\imath}}$ must be defined as a multiple of the number of operating points. An illustrative representation of these setup coefficients is shown in Figure 2.9.

After that, in order to properly compose the excitation input vector $\boldsymbol{u}$ according to the procedure described above to generate one PRFS, the following signal can be computed:

$$\boldsymbol{s}_{\mathring{\imath}} = \begin{cases} G_1\mathring{\boldsymbol{b}}^*_{\mathring{\imath},1} + o_1, & \text{with } \mathring{\boldsymbol{b}}^*_{\mathring{\imath},1} \triangleq \left[^{\mathrm{f}}\mathring{b}_1 \;\; ^{\mathrm{f}}\mathring{b}_2 \;\; \cdots \;\; ^{\mathrm{f}}\mathring{b}_{\frac{N_{\mathring{\imath}}}{v}}\right]^T; \\ G_2\mathring{\boldsymbol{b}}^*_{\mathring{\imath},2} + o_2, & \text{with } \mathring{\boldsymbol{b}}^*_{\mathring{\imath},2} \triangleq \left[^{\mathrm{f}}\mathring{b}_{\frac{N_{\mathring{\imath}}}{v}+1} \;\; ^{\mathrm{f}}\mathring{b}_{\frac{N_{\mathring{\imath}}}{v}+2} \;\; \cdots \;\; ^{\mathrm{f}}\mathring{b}_{2\frac{N_{\mathring{\imath}}}{v}}\right]^T; \\ \vdots \qquad\qquad & \qquad\qquad \vdots \\ G_v\mathring{\boldsymbol{b}}^*_{\mathring{\imath},v} + o_v, & \text{with } \mathring{\boldsymbol{b}}^*_{\mathring{\imath},v} \triangleq \left[^{\mathrm{f}}\mathring{b}_{[v-1]\frac{N_{\mathring{\imath}}}{v}+1} \;\; ^{\mathrm{f}}\mathring{b}_{[v-1]\frac{N_{\mathring{\imath}}}{v}+2} \;\; \cdots \;\; ^{\mathrm{f}}\mathring{b}_{N_{\mathring{\imath}}}\right]^T; \end{cases} \tag{2.24}$$

thus yielding a vector $\boldsymbol{s}_{\mathring{\imath}} \in \mathbb{R}^{N_{\mathring{\imath}}}$. Note that, as aforementioned, for each operating point $o_{\mathring{\imath}}$ the $N_{\mathring{\imath}}$ filtered realizations of $\mathring{B}$, which make up the vector $^{\mathrm{f}}\mathring{\boldsymbol{b}}_{\mathring{\imath}}$ (2.23), are equally divided and represented as values of a vector $\mathring{\boldsymbol{b}}^*_{\mathring{\imath},\mathring{\imath}}$ in (2.24), i.e. $^{\mathrm{f}}\mathring{\boldsymbol{b}}_{\mathring{\imath}} = \left[\mathring{\boldsymbol{b}}^*_{\mathring{\imath},1}; \mathring{\boldsymbol{b}}^*_{\mathring{\imath},2}; \cdots; \mathring{\boldsymbol{b}}^*_{\mathring{\imath},v}\right]$. So, calculating (2.24) for $\mathring{\imath} = 1, 2, \cdots, n_{\mathrm{f}}$, we have the excitation input given by:

$$\boldsymbol{u} \triangleq \left[\boldsymbol{s}_1; \boldsymbol{s}_2; \cdots; \boldsymbol{s}_{n_{\mathrm{f}}}\right] \in \mathbb{R}^N. \tag{2.25}$$

As the concatenation of signals $\boldsymbol{s}_{\mathring{\imath}}$ to compose $\boldsymbol{u}$ might produce higher frequencies that are not desired, an additional filtering is performed in (2.25), i.e. $\boldsymbol{u}{=}\mathcal{B}_{\mathring{\imath}}(q)\boldsymbol{u}$, for which we

suggest using a filter with at least twice the highest frequency value $f_{\hat{i}}$. Considering the algorithm (2.22)–(2.25), an illustrative excitation input signal is shown in Figure 2.9(b), for which the following setup coefficients were used: $n_{\mathrm{f}} = 3$, $f_1 = 0.5\,\mathrm{Hz}$, $f_2 = 1.0\,\mathrm{Hz}$, $f_1 = 4.0\,\mathrm{Hz}$, $v = 3$, $o_1 = 1$, $o_2 = 3$, $o_3 = 7$, $G_1 = 1$, $G_2 = 3$, $G_3 = 2$, $N = 24750$, $N_1 = 7200$, $N_2 = 10800$, and $N_3 = 6750$. This type of excitation input signal, i.e. PRFS, will be used in Chapter 5 to identify hysteretic systems.

2.3.3 NARX Clustering Representation

An interesting way to represent a NARX polynomial model (2.12) is to express it as the summation of terms, i.e. regressors, with degrees of nonlinearity in the range $[1 \;\; \ell]$. Each $(p + m + q_i)$-th order term can contain a p-th order factor in $y_{k-\tau_J}$, an m-th order factor in $u_{k-\tau_J}$, and a q_i-th order factor in $\phi_{i,k-\tau_J}$, which refers to the i-th regressor included to compose the gray-box model (Remark 2.1), and is multiplied by a constant parameter $c_{p,m,q_i}(\tau_1,\cdots,\tau_{p+m+q_i})$, with $\tau_J \in \mathbb{N}^+$ being an arbitrary delay. So rewriting (2.12) in this way, we have (Peyton-Jones and Billings, 1989):

$$y_k = \sum_{q_i=0}^{\ell} \sum_{m=0}^{\ell-q_i} \sum_{p=0}^{\ell-m-q_i} \sum_{\tau_1,\tau_m,\tau_{q_i}}^{n_y,n_u,n_{\phi_i}} c_{p,m,q_i}(\tau_1,\cdots,\tau_{p+m+q_i}) \prod_{J=1}^{p} y_{k-\tau_J} \prod_{J=1}^{m} u_{k-\tau_{p+J}} \prod_{J=1}^{q_i} \phi_{i,k-\tau_{p+m+J}}, \tag{2.26}$$

where

$$\sum_{\tau_1,\tau_m,\tau_{q_i}}^{n_y,n_u,n_{\phi_i}} \equiv \sum_{\tau_1=1}^{n_y} \cdots \sum_{\tau_p=1}^{n_y} \sum_{\tau_{p+1}=\tau_{\mathrm{d}}}^{n_u} \cdots \sum_{\tau_{p+m}=\tau_{\mathrm{d}}}^{n_u} \sum_{\tau_{p+m+1}=1}^{n_{\phi_i}} \cdots \sum_{\tau_{p+m+q_i}=1}^{n_{\phi_i}},$$

and the upper limit is n_y if the summation refers to factors in $y_{k-\tau_J}$, n_u for factors in $u_{k-\tau_J}$ or n_{ϕ_i} for factors in $\phi_{i,k-\tau_J}$. It is worth mentioning that if it is desired to deal with a black-box NARX polynomial model, for which no additional regressors $\phi_{i,k}$ should be considered, the summation symbol and terms related to $\phi_{i,k}$ in (2.26) can simply be excluded. Conversely, it is important to keep in mind that, although the representation (2.26) takes into account the i-th regressor included in model (2.12), when more than one additional regressor is adopted, a small modification is required to represent it properly. Such modification consists of including the corresponding number of sum operators that is in accordance with the number of included regressors. For instance, considering a gray-box NARX model (2.12) with two additional regressors $\phi_{1,k}$ and $\phi_{2,k}$, the first part of the representation (2.26) becomes $y_k = \sum_{q_2=0}^{\ell} \sum_{q_1=0}^{\ell-q_2} \sum_{m=0}^{\ell-q_1-q_2} \sum_{p=0}^{\ell-m-q_1-q_2} \cdots$, which corresponds to the necessary modification.

Remark 2.3. As the parameters of model (2.26) are estimated from data sampled at sampling intervals T_{s}, it would be appropriate to represent them as $c_{p,m,q_i}(T_{\mathrm{s}},\tau_1,\cdots,\tau_{p+m+q_i})$. However, for simplicity, the argument T_{s} is dropped (Billings, 2013).

Example 2.5. NARX Expanded as a Summation of Terms.

For illustrative purposes, the NARX model (2.26) is expanded taken ℓ=2, yielding:

$$\begin{aligned} y_k \quad &= c_{0,0,0} + \sum_{\tau_1=1}^{n_y} c_{1,0,0}(\tau_1) y_{k-\tau_1} + \sum_{\tau_1=\tau_\mathrm{d}}^{n_u} c_{0,1,0}(\tau_1) u_{k-\tau_1} + \sum_{\tau_1=1}^{n_{\phi_i}} c_{0,0,1}(\tau_1) \phi_{i,k-\tau_1} \\ &+ \sum_{\tau_1=1}^{n_y} \sum_{\tau_2=1}^{n_y} c_{2,0,0}(\tau_1,\tau_2) y_{k-\tau_1} y_{k-\tau_2} + \sum_{\tau_1=\tau_\mathrm{d}}^{n_u} \sum_{\tau_2=\tau_\mathrm{d}}^{n_u} c_{0,2,0}(\tau_1,\tau_2) u_{k-\tau_1} u_{k-\tau_2} \\ &+ \sum_{\tau_1=1}^{n_{\phi_i}} \sum_{\tau_2=1}^{n_{\phi_i}} c_{0,0,2}(\tau_1,\tau_2) \phi_{i,k-\tau_1} \phi_{i,k-\tau_2} + \sum_{\tau_1=1}^{n_y} \sum_{\tau_2=\tau_\mathrm{d}}^{n_u} c_{1,1,0}(\tau_1,\tau_2) y_{k-\tau_1} u_{k-\tau_2} \\ &+ \sum_{\tau_1=1}^{n_y} \sum_{\tau_2=1}^{n_{\phi_i}} c_{1,0,1}(\tau_1,\tau_2) y_{k-\tau_1} \phi_{i,k-\tau_2} + \sum_{\tau_1=\tau_\mathrm{d}}^{n_u} \sum_{\tau_2=1}^{n_{\phi_i}} c_{0,1,1}(\tau_1,\tau_2) u_{k-\tau_1} \phi_{i,k-\tau_2}. \end{aligned} \tag{2.27}$$

△

Based on the NARX model formulated as (2.26), Aguirre and Billings (1995b) defined the concepts of *term clusters* and *cluster coefficients* in the context of system identification. Such concepts aim not to look at each regressor that makes up a NARX model as in (2.27), but rather in a compact form, as members of a class that share similar characteristics. The similarity adopted was related to the degree of nonlinearity of the regressors, since it is intuitively known that those belonging to this same type of class or term cluster explain the same type of nonlinear behavior, regardless of their lag. Thus, having grouped the regressors of the investigated model in an appropriate term cluster, its corresponding cluster coefficient is defined as the summation of the parameters of all the regressors that are contained in such a cluster (Aguirre and Billings, 1995b). To formalize these concepts, the authors started from the premise that the sampling time T_s is small enough such that:

$$\begin{cases} y_{k-1} \approx y_{k-2} \approx \cdots \approx y_{k-n_y}, \\ u_{k-\tau_\mathrm{d}} \approx u_{k-\tau_\mathrm{d}-1} \approx \cdots \approx u_{k-n_u}, \\ \phi_{i,k-1} \approx \phi_{i,k-2} \approx \cdots \approx \phi_{i,k-n_{\phi_i}}, \end{cases} \tag{2.28}$$

and, thus, (2.26) can be rewritten as:

$$y_k \approx \sum_{q_i=0}^{\ell} \sum_{m=0}^{\ell-q_i} \sum_{p=0}^{\ell-m-q_i} \left[\sum_{\tau_1,\tau_m,\tau_{q_i}}^{n_y,n_u,n_{\phi_i}} c_{p,m,q_i}(\tau_1,\cdots,\tau_{p+m+q_i}) \right] y_{k-1}^{p} u_{k-\tau_\mathrm{d}}^{m} \phi_{i,k-1}^{q_i}. \tag{2.29}$$

Definition 2.2. [Term clusters and cluster coefficients (Aguirre and Billings, 1995b)]. *The constants* $\sum_{\tau_1,\tau_m,\tau_{q_i}}^{n_y,n_u,n_{\phi_i}} c_{p,m,q_i}(\tau_1,\cdots,\tau_{p+m+q_i})$ *in (2.29) are the coefficients of the term clusters* $\Omega_{y^p u^m \phi_i^{q_i}}$, *which contain the set of all terms, or regressors, of the form* $y_{k-\tau_y}^{p} u_{k-\tau_u}^{m} \phi_{i,k-\tau_{\phi_i}}^{q_i}$ *for* $m + p + q_i \leq \ell$, *where* τ_y, τ_u *and* τ_{ϕ_i} *are any time lags. Such coefficients are called cluster coefficients and are represented as* $\Sigma_{y^p u^m \phi_i^{q_i}}$, *which refers to the sum of the coefficients of all terms that make up the cluster* $\Omega_{y^p u^m \phi_i^{q_i}}$.

Remark 2.4. As will be seen, Definition 2.2 has a close and important relationship with the steady-state, which is a particular case of the classical premise adopted in (2.28) to achieve (2.29) (Aguirre and Billings, 1995b; Aguirre and Mendes, 1996). Nevertheless, we chose to keep this classical formulation because it allows us to deal even with those regressors that vanish at steady-state, such as $\phi_{1,k} = u_k - u_{k-1}$ which is commonly used to describe hysteretic systems (Example 2.3). Note that if steady-state was assumed during formulation, terms like this $\phi_{1,k}$ would be eliminated from (2.29) and hence from Definition 2.2.

The following example illustrates the application of Definition 2.2.

Example 2.6. NARX Clustering Representation.
Consider the following NARX model:

$$y_k{=}\theta_1 y_{k-1}{+}\theta_2 u_{k-2}{+}\theta_3\phi_{1,k-1}{+}\theta_4 y_{k-2}u_{k-4}{+}\theta_5 y_{k-1}y_{k-2}{+}\theta_6 y_{k-1}u_{k-1} + \theta_7 u_{k-1}\phi_{1,k-2}, \quad (2.30)$$

where $\phi_{1,k}{=}u_k{-}u_{k-1}$ and $\tau_d{=}1$. In order to describe such a model in the form of (2.26), we have: $\theta_1{=}c_{1,0,0}(1)$, $\theta_2{=}c_{0,1,0}(2)$, $\theta_3{=}c_{0,0,1}(1)$, $\theta_4{=}c_{1,1,0}(2,4)$, $\theta_5{=}c_{2,0,0}(1,2)$, $\theta_6{=}c_{1,1,0}(1,1)$ and $\theta_7{=}c_{0,1,1}(1,2)$. From Definition 2.2, the term clusters and cluster coefficients of model (2.30) are, respectively, represented by: Ω_y with coefficient $\Sigma_y{=}\theta_1$, Ω_u with $\Sigma_u{=}\theta_2$, Ω_{ϕ_1} with $\Sigma_{\phi_1}{=}\theta_3$, Ω_{yu} with $\Sigma_{yu}{=}\theta_4{+}\theta_6$, Ω_{y^2} with coefficient $\Sigma_{y^2}{=}\theta_5$ and $\Omega_{u\phi_1}$ with $\Sigma_{u\phi_1}{=}\theta_7$. Hence, model (2.30) in clustering representation (2.29) can be expressed as:

$$y_k{\approx}\Sigma_y y_{k-1} + \Sigma_u u_{k-1} + \Sigma_{\phi_1}\phi_{1,k-1} + \Sigma_{yu} y_{k-1}u_{k-1} + \Sigma_{y^2} y_{k-1}^2 + \Sigma_{u\phi_1} u_{k-1}\phi_{1,k-1}.$$

△

In (Aguirre and Mendes, 1996), a more detailed investigation showed that the term clusters and cluster coefficients (Definition 2.2) can be exactly defined when it comes to the steady-state analysis of NARX polynomial models, since the approximation (2.28) must be taken as an equality, such that: $y_k = \bar{y}, \forall k$, $u_k = \bar{u}, \forall k$ and $\phi_{i,k} = \bar{\phi}_i, \forall k$. In addition, it was presented how these concepts are useful to characterize the number, location and stability of fixed points. The definition of fixed points is given below.

Definition 2.3. [Fixed points (Aguirre and Mendes, 1996)]. *The steady-state analysis of model (2.12) is computed by taking $y_k{=}\bar{y}, \forall k$, $u_k{=}\bar{u}, \forall k$ and $\phi_{i,k}{=}\bar{\phi}_i, \forall k$, yielding $\bar{y}{=}\bar{F}^{\ell}(\bar{y},\bar{u},\bar{\phi}_i)$, whose solution(s) $\bar{y}$ for a given constant value of input $\bar{u}$ and $\bar{\phi}_i$ is defined as the fixed point(s), or equilibria, of model (2.12).*

It is important to point out that the extensions in the formulations and definitions presented throughout this work are directly linked to the inclusion of candidate regressor $\phi_{i,k}$. Therefore, it should be clear that the main difference between these and those originally proposed in the black-box context refers to the need for proper mathematical manipulation of the predefined regressor $\phi_{i,k}$, which will be some function of lagged values of y_k and u_k, during the intended analysis.

Remark 2.5. For steady-state analysis, in (2.29), y_k and y_{k-1} are replaced by $\bar{y}$, u_{k-1} by $\bar{u}$, and $\phi_{i,k-1}$ by $\bar{\phi}_i$, respectively. Also, the symbol "$\approx$" is replaced by "=". The solution of model (2.29), adopting these modifications, will yield the fixed points, or equilibria, of model (2.12) for a given $\bar{u}$ and $\bar{\phi}_i$.

The number of solutions for which the model remains invariant, given $\bar{u}$ and $\bar{\phi}_i$, depends on the maximum degree of output regressors in the model. The condition that each solution must satisfy to be *locally stable* is defined below.

Definition 2.4. [Stability of Fixed points (Aguirre and Mendes, 1996)]. *The local stability of the fixed points (Definition 2.3) is verified by evaluating the eigenvalues of the Jacobian matrix of model (2.12) at each fixed point. Its Jacobian matrix is determined as:*

$$D = \begin{bmatrix} 0 & 1 & 0 & \cdots & 0 \\ 0 & 0 & 1 & \cdots & 0 \\ \vdots & \vdots & \vdots & \cdots & \vdots \\ 0 & 0 & 0 & \cdots & 1 \\ \frac{\partial F^\ell}{\partial y_{k-n_y}} & \frac{\partial F^\ell}{\partial y_{k-n_y+1}} & \frac{\partial F^\ell}{\partial y_{k-n_y+2}} & \cdots & \frac{\partial F^\ell}{\partial y_{k-1}} \end{bmatrix}, \tag{2.31}$$

and the condition to be evaluated is:

$$\left|\text{eig}(D)_{y_k=\bar{y},\, u_k=\bar{u},\, \phi_{i,k}=\bar{\phi}_i}\right| < 1, \tag{2.32}$$

where eig$(\cdot)$ *indicates the eigenvalues and its subscript emphasizes the analysis at each fixed point $\bar{y}$ for a given $\bar{u}$ and $\bar{\phi}_i$. Thus, roughly, if all eigenvalues of (2.31) satisfy condition (2.32), the fixed point is stable, otherwise it is unstable. It is worth mentioning that, for the sake of simplicity, many of the works in the literature have shortened the notation of (2.31) and (2.32) as:*

$$\left|\text{eig}\left(\frac{\partial F^\ell\left(\boldsymbol{y},\bar{u},\bar{\phi}_i\right)}{\partial \boldsymbol{y}}\right)\right| < 1, \tag{2.33}$$

where $\boldsymbol{y} = [y_{k-1}\ \ldots\ y_{k-n_y}]^T$, and with $F^\ell(\cdot)$ being the right side of model (2.12).

Example 2.7. NARX Clustering Representation at Steady-State.

For the model in Example 2.6, it was seen that:

$$y_k \approx \Sigma_y y_{k-1} + \Sigma_u u_{k-1} + \Sigma_{\phi_1}\phi_{1,k-1} + \Sigma_{yu} y_{k-1}u_{k-1} + \Sigma_{y^2} y_{k-1}^2 + \Sigma_{u\phi_1} u_{k-1}\phi_{1,k-1},$$

which, from Remark 2.5, can be rewritten as:

$$\Sigma_{y^2}\bar{y}^2 + [\Sigma_{yu}\bar{u} + \Sigma_y - 1]\bar{y} + \Sigma_u\bar{u} = 0. \tag{2.34}$$

Note that, as for steady-state analysis $u_k{=}\bar{u}, \forall k$, then $\phi_{1,k}{=}u_k{-}u_{k-1} = 0, \forall k$ and, consequently, the term clusters that possess $\phi_{1,k}$ as a regressor vanish, i.e. $\Omega_{\phi_1} = \Omega_{u\phi_1} = \emptyset$ in (2.34).

Since (2.34) is a quadratic polynomial, there are two fixed points (Definition 2.3), which are given by the following analytical expressions:

$$\begin{cases} \bar{y}_1 = \dfrac{1-\Sigma_y-\Sigma_{yu}\bar{u}+\sqrt{[\Sigma_{yu}\bar{u}+\Sigma_y-1]^2-4\Sigma_{y^2}\Sigma_u\bar{u}}}{2\Sigma_{y^2}}, & (2.35) \\ \bar{y}_2 = \dfrac{1-\Sigma_y-\Sigma_{yu}\bar{u}-\sqrt{[\Sigma_{yu}\bar{u}+\Sigma_y-1]^2-4\Sigma_{y^2}\Sigma_u\bar{u}}}{2\Sigma_{y^2}}. & (2.36) \end{cases}$$

For the stability analysis of fixed points (2.35) and (2.36), as stated in Definition 2.4, the following conditions are obtained for the eigenvalues of the Jacobian matrix of model (2.30):

$$\begin{cases} -1 < \left(\dfrac{d_1+\sqrt{d_1^2+4d_2}}{2}\right)_{y_k=\bar{y},\,u_k=\bar{u}} < 1, \\ -1 < \left(\dfrac{d_1-\sqrt{d_1^2+4d_2}}{2}\right)_{y_k=\bar{y},\,u_k=\bar{u}} < 1, \end{cases} \tag{2.37}$$

where $d_1 = \frac{\partial F^\ell}{\partial y_{k-1}} = \theta_1 + \theta_5 y_{k-2} + \theta_6 u_{k-1}$ and $d_2 = \frac{\partial F^\ell}{\partial y_{k-2}} = \theta_4 u_{k-4} + \theta_5 y_{k-1}$. Therefore, if both conditions in (2.37) are satisfied for the fixed point (2.35) or (2.36) and for a given constant input value $\bar{u}$, then such a fixed point is asymptotically stable. △

In terms of hysteretic systems, a small but important difference related to the number of solutions that characterize such nonlinear systems is briefly mentioned here and will be investigated more carefully in Chapter 4. For this type of nonlinearity, some works have been directed to answer the following fundamental and primary question: *What is hysteresis?* (Bernstein, 2007; Morris, 2011). Based on their statements raised, a common feature expected in hysteretic models is the fact that any solution obtained with a constant input is an equilibrium and, therefore, such models have a *continuum of steady-state solutions*, whose definition is given below which assumes that F^ℓ in (2.12) is smooth and that it has two additional candidate regressors $\phi_{1,k}$=$u_k - u_{k-1}$ and $\phi_{2,k}$=sign($\phi_{1,k}$).

Definition 2.5. [Continuum of steady-state solutions (Morris, 2011)]. *Let u_k=$\bar{u}$, $\forall k$, be any constant input of model (2.12). Hence, $\phi_{1,k}$=$u_k - u_{k-1}$=0 and $\phi_{2,k}$=sign($\phi_{1,k}$)=0, $\forall k$, thus yielding y_k=$F^\ell(y_{k-1},\cdots,y_{k-n_y},\bar{u})$, where y_k is the output at instant k given $\bar{u}$. If in steady-state, for each constant $\bar{u}$, y_k converges* and remains *at some constant value $\bar{y}$, then the model (2.12) has a continuum of steady-state solutions.*

It should be remembered that the reason for using $\phi_{1,k}$=$u_k - u_{k-1}$ and $\phi_{2,k}$=sign($\phi_{1,k}$) as additional candidate regressors of model (2.12), to describe hysteretic systems, was briefly discussed in Example 2.3 **A)**. More details about it can be found in Section 2.3.7.

2.3.4 Model Structure Selection

One of the most important steps in identifying nonlinear systems corresponds to the selection of the model structure. In the literature, there are some works that address the difficult task of selecting a suitable structure for a given application (Billings et al., 1989; Aguirre and Billings, 1995b; Aguirre and Mendes, 1996; Piroddi and Spinelli, 2003; Baldacchino et al., 2013; Shi and Wu, 2013; Falsone et al., 2015). In the case of polynomial models, some interesting relationships between their structure and dynamic properties have been presented. In particular, it has been argued that the choice of an inadequate structure does not allow obtaining a representative model, even if the identification data set to be used to estimate the model parameters is changed.

The complexity of determining which terms should make up the polynomial model (2.12) grows exponentially with the increase of the degree of nonlinearity ℓ and the maximum delays n_y of the output, n_u of the input, and n_{ϕ_i} of the additional regressor. In order to calculate the maximum number of candidate terms, the following expression is provided (Korenberg et al., 1988):

$$n_\theta = M + 1, \tag{2.38}$$

where n_θ is the number of terms in the model and

$$M = \sum_{\imath=1}^{\ell} n_\imath,$$

with

$$n_\imath = \frac{n_{\imath-1}(n_y + n_u + n_{\phi_i} + \imath - 1)}{\imath}, \quad n_0 = 1.$$

As one might note, even for relatively low *meta-parameters* values (i.e. ℓ, n_y, n_u and n_{ϕ_i}), the number of candidate terms (2.38) tends to be too high, giving rise to an excessive amount of possible combinations of terms that could be impractical to solve by brute force (Korenberg et al., 1988; Aguirre, 1994). Furthermore, as the NARX philosophy aims to identify parsimonious models, the use of all, or excessive, n_θ candidate terms to compose the final model generally leads to inadequate models and should be avoided; see Remark 2.2. Therefore, in order to deal with the structure selection problem, several works in the literature have been dedicated to providing effective procedures that help to reduce the number of candidate terms or that determine which terms should be included in the model to improve its predictive capacity (Aguirre, 1997; Piroddi, 2008; Martins et al., 2013; Falsone et al., 2015; Retes and Aguirre, 2019; Araújo et al., 2019). In

what follows, some interesting tools commonly used for structure selection of NARX polynomial models are briefly reviewed.

First of all, we draw attention to the fact that such a polynomial model (2.12) is linear-in-the-parameters and, therefore, can be expressed in linear regression form as:

$$y_k = \boldsymbol{\psi}_{k-1}^T \hat{\boldsymbol{\theta}} + \xi_k = \sum_{l=1}^{n_\theta} \hat{\theta}_l \psi_{l,k-1} + \xi_k, \tag{2.39}$$

for which $\boldsymbol{\psi}_{k-1} \in \mathbb{R}^{n_\theta}$ contains linear and nonlinear combinations of output $y_{k-1},\ldots,y_{k-n_y}$, input $u_{k-\tau_d},\ldots,u_{k-n_u}$ and additional terms $\phi_{i,k-1},\ldots,\phi_{i,k-n_{\phi_i}}$, which are weighted by the estimated parameter vector $\hat{\boldsymbol{\theta}} \in \mathbb{R}^{n_\theta}$, $\xi_k \in \mathbb{R}$ is the residual[1], and T indicates the transpose. Moreover, $\psi_{l,k-1}$ and $\hat{\theta}_l$ represent the l-th regressor and its corresponding parameter, which are elements of vector $\boldsymbol{\psi}_{k-1}$ and $\hat{\boldsymbol{\theta}}$, respectively. It should be mentioned that representation (2.39) corresponds to the starting point for the parameter estimation step, which is discussed in Section 2.3.5.

In terms of structure selection, a widely used criterion is based on a mono-objective optimization problem that aims to provide the order in which each of the n_θ (2.38) candidate regressors should be inserted in the model (2.12) to be identified, so that the one-step-ahead prediction error is minimized, called the *Error Reduction Ratio* (ERR) (Korenberg et al., 1988; Chen et al., 1989). The basic principle behind this criterion is that model (2.39) can be represented in its orthogonal form, which has allowed to evaluate the contribution of each candidate regressor independently and, thus, helping to select the relevant terms to be included in a polynomial model. Therefore, consider model (2.39) rewritten as:

$$y_k = \sum_{l=1}^{n_\theta} \hat{g}_l w_{l,k-1} + \xi_k, \tag{2.40}$$

where $\hat{g}_l$ refers to the parameters that weight their corresponding regressors $w_{l,k-1}$, which are orthogonal to the identification data set. This orthogonal representation can be achieved, for example, with the Householder transformation (Householder, 1958).

As the regressors in (2.40) are orthogonal to each other over the data set composed of N samples, the property that $\boldsymbol{w}_{l_1}^T \boldsymbol{w}_{l_2} = 0, \forall l_1 \neq l_2$, is satisfied throughout this data set, for which $\boldsymbol{w}_l \triangleq [w_{l,1}\ w_{l,2}\ \cdots\ w_{l,N}]^T \in \mathbb{R}^N$ is the measurement vector of the l-th regressor w_l. Thus, multiplying (2.40) by itself and taking the time average over the data, yields:

$$\frac{1}{N}\boldsymbol{y}^T\boldsymbol{y} = \frac{1}{N}\sum_{l=1}^{n_\theta} \hat{g}_l^2 \boldsymbol{w}_l^T \boldsymbol{w}_l + \frac{1}{N}\boldsymbol{\xi}^T\boldsymbol{\xi}, \tag{2.41}$$

where $\boldsymbol{y} \triangleq [y_1\ y_2\ \cdots\ y_N]^T \in \mathbb{R}^N$ is the vector of output measurements, and $\boldsymbol{\xi} \triangleq [\xi_1\ \xi_2\ \cdots\ \xi_N]^T \in \mathbb{R}^N$ is the residual vector. Based on (2.41), it is possible to notice that

[1]The residual over the identification data set is defined as the difference between the data and the one-step-ahead prediction, i.e. $\xi_k = y_k - \boldsymbol{\psi}_{k-1}^T \hat{\boldsymbol{\theta}}$.

the output variance $\frac{\boldsymbol{y}^T\boldsymbol{y}}{N}$ can be explained by the variance $\frac{\sum_{l=1}^{n_\theta}\hat{g}_l^2\boldsymbol{w}_l^T\boldsymbol{w}_l}{N}$ of the orthogonal regressors, while $\frac{\boldsymbol{\xi}^T\boldsymbol{\xi}}{N}$ corresponds to its unexplained part. Therefore, the contribution that each regressor provides to explain the output variance can be calculated independently as $\frac{\hat{g}_l^2\boldsymbol{w}_l^T\boldsymbol{w}_l}{N}$. Thus, in order to quantify the contribution of the l-th regressor as a fraction of the output variance, ERR is defined as:

$$[\text{ERR}]_l = \frac{\hat{g}_l^2\boldsymbol{w}_l^T\boldsymbol{w}_l}{\boldsymbol{y}^T\boldsymbol{y}}. \tag{2.42}$$

The parameters of such an orthogonal model (2.40) can be calculated as (Billings, 2013):

$$\hat{g}_l = \frac{\boldsymbol{w}_l^T\boldsymbol{y}}{\boldsymbol{w}_l^T\boldsymbol{w}_l}. \tag{2.43}$$

Therefore, (2.42) can be used to rank and select candidate regressors hierarchically according to their contribution to reduce the residual variance. Other techniques that help to classify candidate regressors, based on some optimization problem, to be included in the model according to their importance can be found in (Mendes and Billings, 2001; Piroddi and Spinelli, 2003; Martins et al., 2013; Araújo et al., 2019).

Although the ERR criterion is able to order the candidate regressors hierarchically, there is still a need for an additional procedure that helps determining the number of regressors to be included in the model. For this purpose, the so-called *information criteria*, which consist of statistical cost functions to be optimized, have been shown to be an interesting way to guide the choice of the size of the final model. A concise description and discussion of the use of some well known information criteria, in a nonlinear context, can be found in (Aguirre, 1994; Mendes and Billings, 2001) and the references therein. One of the most popular is the *Akaike's Information Criterion* (AIC), which is defined by the following cost function (Akaike, 1974):

$$\text{AIC}(n_\theta) = N\ln[\sigma_\xi^2(n_\theta)] + 2n_\theta, \tag{2.44}$$

where $\sigma_\xi^2(n_\theta)$ is the variance of the residuals associated with model (2.12) composed of n_θ terms. The AIC aims to assess the trade-off between the model complexity, which is related to the number of terms included to compose it as $2n_\theta$, and its ability to reduce the variance of the residuals as $N\ln[\sigma_\xi^2(n_\theta)]$. Thus, as the number of terms is increased in the model, e.g. considering the order determined with ERR, (2.44) tends to reach a minimum for some value of n_θ. This value indicates that the model complexity becomes more relevant than its goodness of fit and, therefore, such a procedure can be terminated. An important point to be considered is the fact that the use of an information criterion provides models that are optimal in a statistical sense, which does not guarantee that such models are the best in dynamic terms, i.e. those that best mimic the dynamical features of the investigated system. Furthermore, when it

comes to identifying nonlinear systems, the rule to stop the inclusion of regressors in the model is not exact due to the possibility of local minima for different values of n_θ, which makes the stopping rule not evident. However, the use of information criteria has proved to be a useful way to guide and limit the search space for the best model structure (Gooijer et al., 1985; Aguirre, 1994; Martins et al., 2013). In practical terms, one can search around the first local minimum.

Remark 2.6. The term-by-term choice procedure, according to its importance, has some advantages related to the fact that, in general, few terms are really necessary and, therefore, this procedure tends to provide simple parsimonious models capable of accurately predicting the system behavior. This is usually done using the ERR (2.42) together with AIC criterion (2.44). Not only that, if the system is linear, such a procedure will tend to select only linear terms to compose an adequate model to describe it (Billings, 2013).

Another type of technique that is also used in the structure selection stage aims to eliminate insignificant terms, so that the initial set of candidate regressors can be reduced, and thereby facilitating the identification of an adequate model (Kadtke et al., 1993). In this sense, an interesting procedure grounded on the concepts of term clusters and cluster coefficients (Definition 2.2) has proved to be a powerful aid for structure selection (Aguirre and Billings, 1995b; Billings, 2013; Martins and Aguirre, 2016). Briefly, this procedure starts with the use of ERR (2.42) to rank the most significant regressors hierarchically. Whereas these regressors are included one at a time in the model, following such a classification, the cluster coefficients of each term cluster are monitored so that spurious clusters can be detected and discarded from the pool of candidate regressors. It is noteworthy that the presence of spurious terms in the model is prone to affect its global dynamics, since such terms explain nonlinear behaviors that, in principle, are not present in the collected data (Aguirre and Billings, 1995a). Therefore, as mentioned above, when discarding all regressors belonging to the spurious clusters of the set of candidate regressors by means of this procedure, we have a reduction in the initial set of candidate terms that leads to subsequently identifying models with improved dynamics. Based on this new set of candidate terms, the model can be identified using, for example, the ERR together with AIC criterion, as discussed above.

Finally, some of the main properties and tips on how to detect spurious clusters using the present procedure are: i) models composed of effective cluster terms are more likely to mimic the dynamics of the original system fairly, ii) greater robustness for data noise and for overparametrization issues in the estimated model when spurious terms are avoided are advantages achieved with this procedure, iii) if the inclusion of a certain cluster in the model is late, this suggests that it is a spurious cluster, furthermore, iv) cluster coefficients with an absolute value much smaller than the parameters of the corresponding cluster, and v) coefficients with oscillatory values. More details on this procedure can be found in (Aguirre and Billings, 1995b; Billings, 2013).

2.3.5 Parameter Estimation

Once the structure of the NARX polynomial model (2.12) has been determined, the next step concerns some techniques that are developed to estimate the parameters that weigh each of the regressors that compose it. It should be emphasized that, as such a polynomial model is linear-in-the-parameters, it can be represented in linear regression form as shown in (2.39). Hence, from the least squares family algorithms, both batch and recursive estimation techniques can be used to estimate the values of the parameter vector (Ljung, 1999; Isermann and Münchhof, 2011). In short, it can be argued that batch estimation techniques fall into the category of algorithms commonly associated with time-invariant systems, for which it is assumed that invariant models (with *constant parameters*) are capable of accurately describing the system behavior. On the other hand, recursive estimation is commonly used to adapt models in order to capture time-variant and nonlinear behavior of the investigated system, which is usually done by updating the model parameters at each sampling time (Pröll and Karim, 1994; Nelles, 2001; Isermann and Münchhof, 2011; Keesman, 2011).

A data set $Z^N=\{y_k, u_k, \phi_{i,k}\}_{k=1}^N$ is assumed available. Usually y_k and u_k are measured, and the additional regressors $\phi_{i,k}$ can be readily computed from the measurements. Evaluating the regression model (2.39) along this data set, the resulting set of equations can be expressed in matrix form as:

$$\boldsymbol{y} = \Psi\hat{\boldsymbol{\theta}} + \boldsymbol{\xi}, \tag{2.45}$$

where $\Psi \triangleq [\boldsymbol{\psi}_1 \ \boldsymbol{\psi}_2 \ \cdots \ \boldsymbol{\psi}_{n_\theta}] \in \mathbb{R}^{N\times n_\theta}$ is the regressor matrix composed by the measurement vectors $\boldsymbol{\psi}_l \triangleq [\psi_{l,1} \ \psi_{l,2} \ \cdots \ \psi_{l,N}]^T \in \mathbb{R}^N$ of the l-th regressor $\psi_{l,k-1}$ defined above for (2.39), while $\boldsymbol{y}$ and $\boldsymbol{\xi}$ are the same defined in (2.41). From expression (2.45), it is possible to estimate the parameter vector using the unconstrained least squares (LS) batch estimator, given by:

$$\hat{\boldsymbol{\theta}}_{\text{LS}} = (\Psi^T\Psi)^{-1}\Psi^T\boldsymbol{y}, \tag{2.46}$$

which yields an estimate of the model parameters by minimizing the squared Euclidean norm of the residual vector (Ljung, 1999), i.e. $\hat{\boldsymbol{\theta}}_{\text{LS}} = \arg_{\boldsymbol{\theta}} \min(\boldsymbol{\xi}^T\boldsymbol{\xi})$. A more refined alternative to parameter estimation, which will be useful in Chapters 4 and 5, is the constrained least squares (CLS) batch estimator. For this estimator, it is assumed that there is a linear set of equality constraints on the parameter vector to be satisfied, which can be written as $\boldsymbol{c} = S\boldsymbol{\theta}$, where $\boldsymbol{c} \in \mathbb{R}^{n_c}$ and $S \in \mathbb{R}^{n_c\times n_\theta}$ are known constants. Then, the constrained least squares estimation problem is:

$$\hat{\boldsymbol{\theta}}_{\text{CLS}} = \underset{\boldsymbol{\theta}\,:\,\boldsymbol{c}=S\boldsymbol{\theta}}{\arg\min}\left(\boldsymbol{\xi}^T\boldsymbol{\xi}\right), \tag{2.47}$$

whose solution is (Draper and Smith, 1998):

$$\hat{\boldsymbol{\theta}}_{\text{CLS}} = \hat{\boldsymbol{\theta}}_{\text{LS}} - (\Psi^T\Psi)^{-1}S^T[S(\Psi^T\Psi)^{-1}S^T]^{-1}(S\hat{\boldsymbol{\theta}}_{\text{LS}} - \boldsymbol{c}). \tag{2.48}$$

Other algorithms that have proved to be useful for batch estimation of parameters, i.e. when the data set is processed all at once, and that deal with more subtle aspects related to their statistical properties are presented in (Young, 1970; Ljung, 1999; Billings, 2013).

In contrast to batch estimators, recursive algorithms provide an update of the model parameter estimates at run time as the data is collected and made available sequentially. For this purpose, one can find in the literature a variety of algorithms, commonly derived based on the LS estimator, so that the parameter vector in (2.39) can be updated recursively, e.g. using the recursive least squares (RLS) algorithm (Ljung, 1999). Note that, in this case, (2.39) becomes:

$$y_k = \boldsymbol{\psi}_{k-1}^T \hat{\boldsymbol{\theta}}_k + \xi_k = \sum_{l=1}^{n_\theta} \hat{\theta}_{l,k} \psi_{l,k-1} + \xi_k, \tag{2.49}$$

where $\hat{\boldsymbol{\theta}}_k$ indicates the parameter vector estimated at an instant k, and the other terms are the same as defined in (2.39). Therefore, considering that the aim is to update the parameters of this dynamic model at each sampling time, one can define the class of RLS algorithms with variable forgetting factor (FF), whose general formulation is:

$$K_k = \frac{P_{k-1}\boldsymbol{\psi}_{k-1}}{\boldsymbol{\psi}_{k-1}^T P_{k-1}\boldsymbol{\psi}_{k-1} + \lambda_k}, \tag{2.50}$$

$$\hat{\boldsymbol{\theta}}_k = \hat{\boldsymbol{\theta}}_{k-1} + K_k[y_k - \boldsymbol{\psi}_{k-1}^T \hat{\boldsymbol{\theta}}_{k-1}], \tag{2.51}$$

$$P_k = \frac{1}{\lambda_k}\left(P_{k-1} - \frac{P_{k-1}\boldsymbol{\psi}_{k-1}\boldsymbol{\psi}_{k-1}^T P_{k-1}}{\boldsymbol{\psi}_{k-1}^T P_{k-1}\boldsymbol{\psi}_{k-1} + \lambda_k}\right), \tag{2.52}$$

in which $0 \ll \lambda_k < 1$ is the FF, K_k is called the Kalman gain, and P_k is the covariance matrix. For the standard RLS, λ_k is constant for all k (Nelles, 2001). In practice one can first obtain the parameter vector using the batch LS estimator over a window of data and then update it with an RLS algorithm.

Based on the RLS algorithm (2.50)–(2.52), many works in the literature have been developed in order to deal with, for example, issues related to time-varying dynamics and lack of persistence of excitation in the input signal, as well as to propose methods that aim to provide an adequate update of predictive models through the adaptation of the FF value, λ_k (Paleologu et al., 2008; Keesman, 2011; Beza and Bongiorno, 2014; Abreu et al., 2016a,b; Abreu et al., 2021).

2.3.6 Model Validation

The last step in system identification corresponds to the validation of the identified model, in which such a model is evaluated in relation to its predictive capacity. According to Aguirre (2019), some of the natural questions that arise and should be answered at this step are: *What is the intended use for the model?* and *Is the model valid?*

In terms of gray-box identification, the former usually arises from a desired goal to be achieved (e.g. mimicking a specific behavior), whose answer becomes a kind of auxiliary information that should be used during the identification procedure. Thus, when dealing with the validation of the identified model, the assessment should be made to verify if the required features are incorporated into it, since an absolute answer is something unattainable.

In order to check the quality of the identified models, one can find in the literature a variety of tools, which are commonly divided into *qualitative* and *statistical* methods (Billings, 2013). Concerning the qualitative validation, the main objective is to verify if the identified model is able to describe behaviors that are commonly used to characterize or that are assumed to be invariant characteristics of the investigated system. One of the most used and simple methods aims to graphically compare the estimated and measured temporal responses, in which special attention is focused on the differences in their fluctuations, gains and phases, among other features present in them. Looking at these features tends to provide some indication of how well the identified models fit the system data. For instance, in the scope of hysteretic systems, not only their temporal responses but also an input-output graph have been widely assumed to be adequate ways to validate the identified models, since a characteristic loop behavior displayed on this plane is recognized as an intrinsic feature of such systems. More sophisticated qualitative methods commonly used to bring out invariant dynamic characteristics can be found in (Haynes and Billings, 1992; Aguirre and Billings, 1994, 1995a; Billings and Zheng, 1999; Letellier et al., 2002).

In the context of statistical validation, the core idea is to quantify the similarities between data measured from the system and those estimated from identified models. A common type of criterion used for this purpose is based on the calculation of indices related to the estimation error which, besides quantifying the accuracy of the identified models to mimic the system, makes it possible to compare them. Some more specific criteria that were developed to somehow verify if the identified model incorporates the relevant dynamic information contained in the data set can be found in (Billings and Voon, 1986; Billings and Tao, 1991). Interesting recommendations and tips related to basic rules to be followed in the model validation step are discussed in (Billings, 2013; Aguirre, 2019).

2.3.7 Overview of Works on Hysteresis

Here the aim is to focus mainly on some ways and insights that have been raised to enable NARX polynomial models to describe subtle aspects of hysteretic systems. Nevertheless, some early works that were developed following a black-box perspective and those that used some gray-box approach without much concern about *why* to use it (e.g. the use of a class of regressors $\phi_{i,k}$ without apparent reason), hereby called *weakly gray-box approaches*, are also briefly discussed below.

2.3.7.1 Black-Box approaches

From the point of view of black-box modeling, there are few works that compare techniques in the identification of hysteretic systems (Parlitz et al., 2004; Mohammadzaheri et al., 2012). In this context, the use of NARX models has been considered a convenient choice due to their ability to predict a wide class of nonlinear behaviors. Nevertheless, very few works consider NARX models, especially in polynomial form, in the representation of hysteresis, and in most cases the approach is black-box and structure selection is mostly *ad hoc*. Interesting works that fall in this category are (Parlitz et al., 2004), where the estimated model has 32 terms and (Worden et al., 2007) where a model with no less than 84 terms was estimated. Although these models can predict the temporal response of the hysteretic system, no critical analysis with respect to their ability to describe behaviors that are commonly used to characterize such systems, e.g. hysteresis loop, was done. Likewise, Karami et al. (2021) proposed a decoupling algorithm for NARX polynomial models that was used to identify a hysteretic system, which led to an estimated model with 196 terms. Zhang et al. (2017a), in turn, proposed a new truncation condition to be assumed during the structure selection step, whose models were estimated with about 11 terms. However, the possible occurrence of singularity problems when the model output is equal to zero was found by the authors and, although a hysteresis loop is shown, model validation is not very exacting.

Related work was performed by Masri and co-workers using continuous-time polynomials in a black-box fashion (Masri et al., 2004). As with the previous papers, the authors set off with a large model either 22 or 42 terms, but in a second stage, they prune the model by eliminating those terms with small coefficients. This procedure is known to lack robustness with respect to noise (Aguirre, 1994), as was confirmed by the authors in (Masri et al., 2004). The need for a more careful structure selection procedure was also acknowledged by them. In a similar vein, apart from continuous-time monomials the authors in (Brewick et al., 2016) use Chebyshev polynomials and point out that very compact models were possible to be obtained at the cost of some performance, but still presenting some important aspects of hysteresis. It should be emphasized that black-box modeling does not rely on prior knowledge about the system, since the works in this field are only intended to build models that closely fit the collected data set (Chan et al., 2015; Ayala et al., 2015; Fu et al., 2016). Consequently, relevant features that should be present in a model to reproduce hysteresis and even an appropriate structure for designing compensators, a subject that will be covered in Chapter 3, are not ensured by black-box techniques. Hence, the search for models that have specific features, that are accurate and that have a suitable structure for designing compensators remains an open problem. Results in the field of neural networks can be found in (Zhang et al., 2010; Wang and Song, 2014; Wang et al., 2020).

2.3.7.2 Weakly Gray-Box approaches

As discussed earlier in Section 2.3.1, a particular advantage of models obtained using gray-box techniques is that they can be tailored to reproduce specific relevant features and/or to meet possible constraints on the structure and parameters to make them suitable for a model-based control or compensation scheme (Pearson, 1999; Aguirre, 2019). Furthermore, it was argued the reasons why some works in the literature deal with the NARX model represented as (2.12) and some ways to determine promising candidate regressors $\phi_{i,k}$ to be included in this model (see Example 2.3). However, although these additional regressors tend to play an important role in the predictive capacity of the identified models, some interesting works apparently adopted them without knowing/explaining why, or simply because their main focus was not on identifying a hysteretic model, which is used as a mere example.

In this sense, Leva and Piroddi (2002) proposed an identification algorithm in order to build simple and accurate NARX polynomial models, which could be directly employed in the design of controllers. In order to assess the validity of the proposed algorithm, the authors used a phenomenological model of a magneto-rheological damper as a benchmark system, which exhibits hysteretic behavior. Although the main focus of this paper is an algorithm for a general class of systems and not dedicated to characterizing the hysteresis nonlinearity, a glance over the identified hysteretic model might be interesting. So rewriting this model following the notation adopted here, we have:

$$y_k = \theta_1 y_{k-1} + \theta_2 \phi_{2,k-1} \phi_{1,k-1}^2 + \theta_3 \phi_{2,k} \phi_{1,k}^2 u_{1,k} + \theta_4 \phi_{1,k}^3 y_{k-1} + \theta_5 \phi_{2,k} \phi_{1,k}^{10} + \theta_6 \phi_{2,k} \phi_{1,k} u_{1,k}, \quad (2.53)$$

for which y_k refers to hysteretic force, $u_{1,k}$ and $u_{2,k}$ are, respectively, the sampled inputs of the control voltage and displacement, while the additional specific functions $\phi_{i,k}$ were determined as:

$$\begin{cases} \phi_{1,k} = |v_k|^{0.2}, \\ \phi_{2,k} = \text{sign}(v_k), \end{cases} \quad (2.54)$$

where v_k is the velocity, which is sampled from the time derivative of the displacement signal, i.e. $v(t) = \frac{du_2(t)}{dt}$. It is noteworthy that the final model identified by the proposed algorithm had 13 terms, however, after a more careful analysis the authors chose to prune this original model to produce the compact model in (2.53).

Some points that deserve attention in relation to model (2.53) refer to its high value of the degree of nonlinearity, which is $\ell = 11$, and the complexity of its additional terms (2.54). The former tends to lead to a considerable increase in the number of candidate regressors and thus hinders the structure selection procedure, as discussed in Section 2.3.4. In the latter case, the authors did not clarify *how* such functions were chosen. In addition, note that if we adopt the way to extract information described in Example 2.3 **A)** for the phenomenological model used as a benchmark system, we

will notice the presence of the sign function, but not fractional powers as $\phi_{1,k}$ (2.54). Perhaps, this could be an indication that these fractional powers terms may not be an adequate choice as a class of candidate regressors to represent such a system.

In a different way, Worden and Barthorpe (2012) presented an approach for building a NARX model to a discrete version of a Bouc-Wen hysteresis model, i.e. with a fixed structure, giving rise to the so-called NARX Bouc-Wen model. Due to the presence of problems related to highly nonlinear terms, nonlinearity in the parameters, and unmeasured states in such continuous-time Bouc-Wen model, many of these are reflected in its discrete form by the need for strong approximations. It was pointed out by the authors that the minimal NARX Bouc-Wen model achieved has 10 terms with 8 parameters that appear in a nonlinear way and for which an evolutionary optimization scheme was adopted to estimate them. Furthermore, they raised many issues that were observed during the estimation of these parameters, which require further investigation, such as stability properties, noise sensitivity, and the blow-up effect of the evolutionary algorithm. Also, an alternative was presented to make the model linear-in-the-parameters, so that classical algorithms like those described in Sections 2.3.4 and 2.3.5 could be used, at the cost of some more approximations and, consequently, less performance. Finally, the authors stated that, for this case, polynomial terms up to fifth order will be needed to represent the minimal NARX Bouc-Wen model, which generates a search space for candidate polynomial terms large enough to make the structure selection algorithm prohibitively expensive.

Given both directions covered above, i.e. the black-box and weakly gray-box approaches, we will now revisit in more detail two works that take a different look at enabling NARX polynomials to deal with some subtle aspects of hysteresis nonlinearity.

2.3.7.3 Hysteretic operator

As far as we know and as stated by Deng and Tan (2009), their work is probably the first in the literature on gray-box modeling of hysteretic systems using NARX polynomials, where specific actions to capture the basic behavior or the change tendency of the hysteresis nonlinearity were made. A key point of this work was the proposal of a hysteretic operator to be used as an additional regressor $\phi_{i,k}$ of a NARX model (2.12). Some details follow.

Remark 2.7. The action of adding new inputs $\phi_{i,k}$ to the model (2.12) has been addressed by Deng and Tan (2009) as a kind of an expanded input space approach that transforms the multi-valued mapping of hysteresis into a one-to-one mapping so that NARX models can be employed to describe the hysteresis behavior.

In order to extract the change tendency of hysteresis, which should be used as a new input $\phi_{1,k}$, the following hysteretic operator was proposed (Deng and Tan, 2009):

$$h_k \triangleq h(u_k) = \Big|\arctan(u_k - u_{\text{ext},k})\Big|[u_k - u_{\text{ext},k}] + h(u_{\text{ext},k}), \tag{2.55}$$

where $h_k \in \mathbb{R}$ is the output of the operator, $u_k \in \mathbb{R}$ is the current input, $u_{\text{ext},k}$ refers to the dominant extremum adjacent to u_k, and $h(u_{\text{ext},k})$ is the output of the operator when the input is $u_{\text{ext},k}$. Both $u_{\text{ext},k}$ and $h(u_{\text{ext},k})$ can be initialized to null values.

Remark 2.8. It should be noted that $u_{\text{ext},k}$ and $h(u_{\text{ext},k})$ can be seen as variables that act as a *buffer*. More specifically, given that u_k reaches an extremum value, it should be stored in $u_{\text{ext},k}$ and the corresponding value of h_k in $h(u_{\text{ext},k})$, which are referred to as the dominant extremum adjacent to u_k and whose values are held constant until u_k reaches a new extremum. In the case of u_k moving to different input extrema, such a process is repeated, while for the case where it arrives an extremum already reached at a previous time, its corresponding stored value can be used.

Remark 2.9. The operator has a simple mathematical description based on the basic function, i.e. $h_k = \left|\arctan(u_k)\right|u_k$, that can roughly describe the variation information of hysteresis. Furthermore, the introduction of previous extremum coordinates $u_{\text{ext},k}$ and $h(u_{\text{ext},k})$ reflects the characteristic memory effect of hysteresis, as done in (2.55).

Theorem 2.1. [(Deng and Tan, 2009)]. *For an arbitrary hysteresis with the input u_k being a bounded continuous function, e.g. $u_k = \sin(\omega k)$, assume the hysteresis forms a closed loop $\mathcal{H}_k(\omega)$ in the input-output plane when the input travels between two extrema. Then, there exists a continuous one-to-one mapping $\Gamma : \mathbb{R}^2 \mapsto \mathbb{R}$, such that $y(u_k) = \Gamma(u_k, h_k)$, where $y(u_k)$ and h_k are the outputs of hysteresis and hysteretic operator, respectively.*

Proof. See (Deng and Tan, 2009) and, for some more details, see also (Deng et al., 2014; Tan and Deng, 2014). ■

Remark 2.10. In addition to having proven that adding new inputs to the model can decompose the multi-valued mapping of hysteresis into a one-to-one mapping (this is also discussed in (Mohammadzaheri et al., 2012)), it has also been shown that the hysteretic operator (2.55) is able to describe some subtle features found in hysteretic systems, such as the ascending, turning and descending behavior that give rise to the hysteresis loop displayed on the input-output plane.

Example 2.8. Hysteretic Operator and its Hysteresis Loop.

For illustration purposes, the hysteretic operator (2.55) is fed with the input signal $u_k = 2.5\sin(1.5k) + 4\sin(0.5k)$, for which the sampling time is $T_s = 0.02\,\text{s}$ and the data set is 14 s long ($N = 700$) (Deng and Tan, 2009). Such an input signal and its corresponding hysteresis loop displayed on the $u \times h$ plane are shown in Figure 2.10.

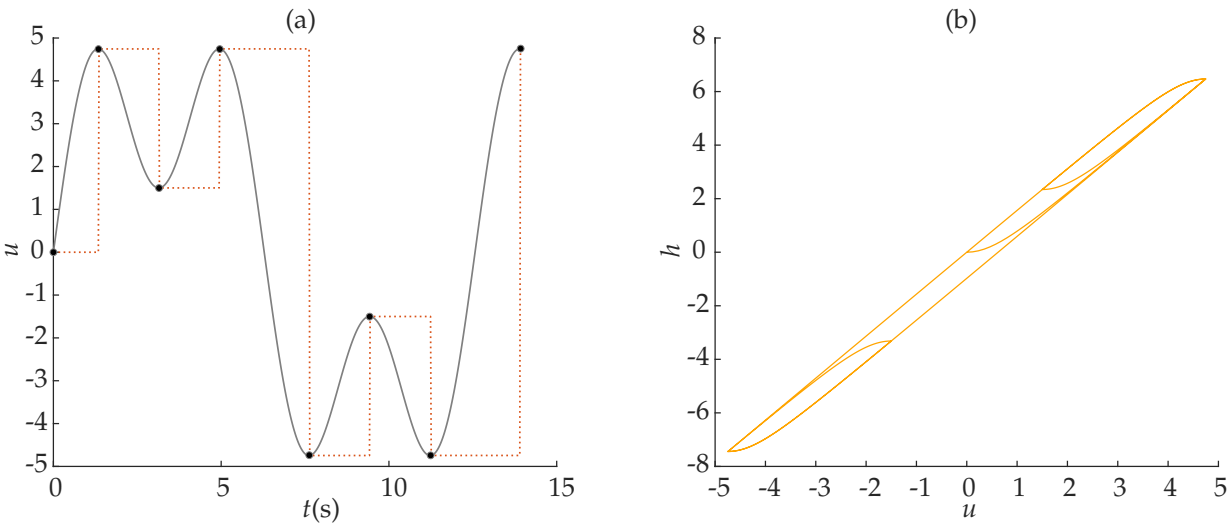

Figure 2.10: A simulation of the hysteretic operator (2.55). (a) input u_k=2.5 sin(1.5k)+4 sin(0.5k) and in (b) the hysteresis loop $\mathcal{H}_k(\omega)$. (—) refers to the input, while (•) indicates each dominant extremum value u_{ext} adjacent to u_k and (···) shows its value over time (see Remark 2.8).

In (Deng and Tan, 2009), the behavior of the hysteresis loop in Figure 2.10(b) is compared with one obtained from a hysteretic model fed with the same input signal u_k shown in Figure 2.10(a), from which the similarity between them was highlighted. Based on these results, the authors suggest that the proposed operator (2.55) might provide useful information about the change feature of hysteresis and, therefore, might improve the predictive power of a NARX model (2.12) with its inclusion in the set of candidate regressors. As a side note, the difference between the hysteresis loop shown in Figure 2.10(b) and the one in (Deng and Tan, 2009) – see Figure 2 therein – is due to some type of normalization used there, for the current example, which was not explained and therefore we do not use it here. △

In order to state the following two definitions, based on Theorem 2.1, it is assumed that a hysteretic system, represented by a closed loop $\mathcal{H}_k(\omega)$ in the input-output plane, is fed with a periodic input signal u_k with frequency ω.

Definition 2.6. [Rate-independent Hysteresis (Morris, 2011)]. *If the shape of the hysteresis loop $\mathcal{H}_k(\omega)$ in the input-output plane is not affected by changes in the input frequency ω, i.e. it only depends on the input values, such loop behavior is called* rate-independent hysteresis *or* static hysteresis.

Definition 2.7. [Rate-dependent Hysteresis (Morris, 2011)]. *If the shape of the hysteresis loop $\mathcal{H}_k(\omega)$ in the input-output plane is affected by changes in the input frequency ω, such loop behavior is called* rate-dependent hysteresis *or* dynamic hysteresis.

Remark 2.11. In fact, one of the typical features inherent in hysteretic systems is the rate-independent hysteresis loop displayed on the input-output plane; see Definition 2.6. However, this loop behavior is a dominant feature when such systems are under a low-frequency input signal so that other dynamic effects do not interfere (Visintin, 1994; Mayergoyz, 2003; Ikhouane and Rodellar, 2007; Morris, 2011; Cao et al., 2013). For this reason, hysteretic systems are commonly known to have an input-output loop behavior that does not disappear when the input frequency approaches zero (Bernstein, 2007). In other words, it can be treated as a persistent phase delay, which is not seen in other types of linear or nonlinear systems.

Remark 2.12. According to Mayergoyz (2003) and Morris (2011), if the input frequency ω is increased to become comparable to the system dynamics, Definition 2.6 may fail and an apparent rate-dependent hysteresis loop in the input-output plane will be observed. Therefore, when dealing with real systems and processes that have rate-independent hysteretic behavior, it is reasonable to expect that such behavior is valid for a given limited range of frequencies and becomes rate-dependent at higher frequencies.

Based on the features described in Definitions 2.6 and 2.7, Deng and Tan (2009) used different models to identify these hysteresis behaviors. In terms of rate-independent hysteresis, the model used consists of a special case of the NARX model (2.12), in which the autoregressive terms are removed from the set of candidate regressors. In the literature, this type of model is also called *Finite Impulse Response* (FIR) model. To model the rate-dependent hysteresis behavior, the gray-box NARX model (2.12) is adopted by them. It should be remembered that, for both cases, the hysteretic operator (2.55) is included as a candidate regressor $\phi_{1,k}$ during the identification procedure, in which some approach should be used to decide which specific regressors will compose the final model.

In contrast to classical approaches, Deng and Tan (2009) assume that all candidate terms (2.38) are used to compose the model, which could lead to problems such as those pointed out in Section 2.3.4 and Remark 2.2. The structure selection procedure proposed by them consists of two steps. First, through a brute force search, different combinations of meta-parameters values, within a predefined range, are used to build models, and those whose estimates fit the measured data in terms of model error are selected. Then, the selected models are evaluated using a modified version of AIC (2.44), which will indicate the appropriate model. To estimate the model parameters, a recursive least squares algorithm, similar to (2.50)–(2.52), is used.

In order to validate the proposed modeling approach, the authors applied it to an experimental piezoelectric actuator, where the estimated model, for the static case, has 34 terms and, for the dynamic case, 55 terms. As expected, both estimated models have a large number of terms, which is probably due to the structure selection procedure adopted. This type of model tends to hinder its use in control or compensation schemes, as well as in a more careful analysis with respect to its ability to describe more subtle

hysteresis behavior. In terms of hysteretic systems, one of the characteristics commonly associated with such systems is the existence of several fixed points (Morris, 2011). However, to the best of our knowledge, there is only one work in the literature of NARX polynomials that took the first steps towards exploring this feature (Martins and Aguirre, 2016), which is revisited in Section 2.3.7.4. In Chapter 4, a more general framework is developed to explain how hysteresis occurs in NARX polynomials.

2.3.7.4 The use of equilibria

An important step in modeling hysteresis nonlinearity was advanced in (Martins and Aguirre, 2016), where specific actions on the structure selection of polynomial models lead to sufficient conditions for such models to be able to display a hysteresis loop when subject to a certain class of input signals. A key feature of such a proposal was the explicit use of equilibria. Some details follow.

Definition 2.8. [Loading-unloading signal (Martins and Aguirre, 2016)]. *A periodic signal u_k with period $N = (k_{f_2} - k_{i_1} + 1)$ and frequency $\omega = 2\pi/N$ is called a loading-unloading signal if u_k increases monotonically from $u_{\min}$ to $u_{\max}$, for $k_{i_1} \leq k \leq k_{f_1}$* (loading regime) *and decreases monotonically from $u_{\max}$ to $u_{\min}$, for $k_{i_2} \leq k \leq k_{f_2}$* (unloading regime)*; see Figure 2.11(a).*

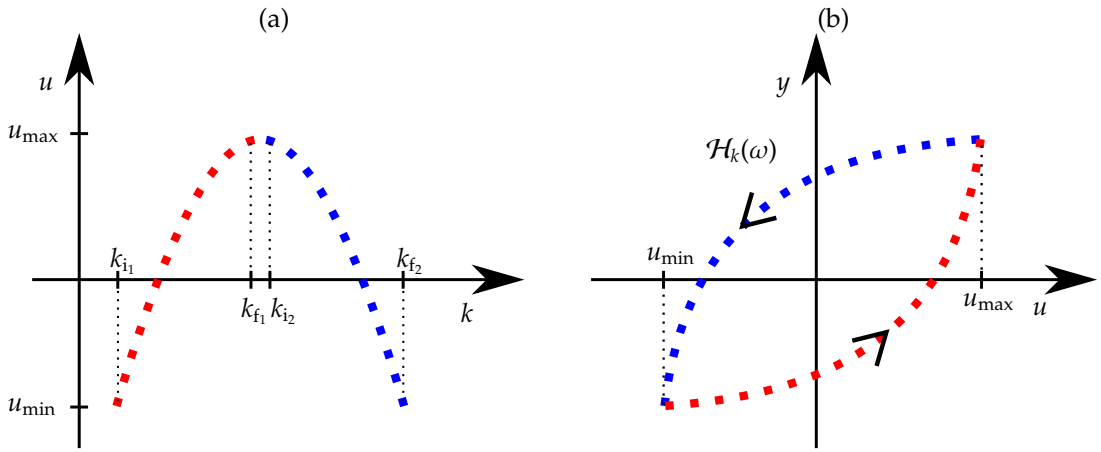

Figure 2.11: A loading-unloading signal in (a), and its corresponding hysteresis loop in (b).

Remark 2.13. It should be emphasized that the purpose of assuming that a loading-unloading excitation signal is periodic is due to a characteristic loop behavior displayed in the input-output plane (see Figure 2.11(b)), which is present in hysteretic systems, is readily observed using such a signal. If this signal is not periodic, this behavior will not be easily seen.

Definition 2.9. [Quasi-static signal (Martins and Aguirre, 2016)]. *If a loading-unloading signal changes with $\omega \to \epsilon$, $0 < \epsilon \ll f_s/2$, where f_s is the sampling frequency, the signal is also called a quasi-static signal.*

A mathematical function that plays an important role in the work revisited here, and is adopted as a candidate regressor $\phi_{i,k}$ to be included in model (2.12), is defined below.

Definition 2.10. [Multi-valued functions (Martins and Aguirre, 2016)]. $\Phi(u_k) : \mathbb{R} \to \mathbb{R}$ *is a multi-valued function, also called a piecewise-defined function, if:*

$$\Phi(u_k) = \begin{cases} \Phi_1, & \text{if } u_k > \epsilon; \\ \Phi_2, & \text{if } u_k < \epsilon; \\ \Phi_3, & \text{if } u_k = 0, \end{cases} \tag{2.56}$$

where Φ_1, Φ_2 *and* Φ_3 *are arbitrary functions, and* $\epsilon \in \mathbb{R}$.

A commonly used multi-valued function (Definition 2.10) is the sign function (Definition 2.1).

Property 2.2. [(Martins and Aguirre, 2016)]. *Consider a model excited by a loading-unloading quasi-static input (Definition 2.9). If such a model has at least one real and stable fixed point for input values corresponding to the loading regime, and likewise for the unloading regime (the equilibria depend on the history of the input), the model will display a hysteresis loop* $\mathcal{H}_k(\omega)$*; see Figure 2.11(b).*

Theorem 2.2. [(Martins and Aguirre, 2016)]. *Given a single-input single-output (SISO) autoregressive stable model:*

$$y_k = \sum_{\tau_p=1}^{n_y} c_y(\tau_p) y_{k-\tau_p} + \sum_{\tau_{q_2}=1}^{n_{\phi_2}} c_{\phi_2}(\tau_{q_2}) \phi_{2,k-\tau_{q_2}}, \tag{2.57}$$

where $c_y(\tau_p)$ *and* $c_{\phi_2}(\tau_{q_2})$ *are constant parameters and* $\phi_{2,k}$ *is a multi-valued function; see Definition 2.10. If* $\phi_{1,k} = u_k - u_{k-1}$ *and* $\phi_{2,k} = \text{sign}(\phi_{1,k})$*, for which* u_k *is a loading-unloading quasi-static input signal of frequency* ω *(Definition 2.9), then there will be a rate-dependent hysteresis loop* $\mathcal{H}_k(\omega)$ *in the* $u \times y$ *plane confined by the bounding structure* $\mathcal{H}$ *defined by the model equilibria.*

Proof. See (Martins and Aguirre, 2016). ■

Remark 2.14. The bounding structure $\mathcal{H}$ confines the hysteresis loop $\mathcal{H}_k(\omega)$. As the frequency of the loading-unloading input signal becomes smaller ($\omega \to \epsilon, 0 < \epsilon \ll f_s/2$), the hysteresis loop $\mathcal{H}_k(\omega)$ converges to the bounding structure $\mathcal{H}$, i.e. $\mathcal{H} = \lim_{\omega \to 0} \mathcal{H}_k(\omega)$, and therefore the hysteresis loop depends on the input frequency; see Definition 2.7.

Remark 2.15. As the input u_k should be assumed as a loading-unloading quasi-static signal in order to comply with Property 2.2, then its first difference $\phi_{1,k}$ will satisfy:

$$\phi_{1,k} = \begin{cases} > \ 0, & \text{if} \quad k_{i_1} \le k \le k_{f_1} \quad \text{(loading)}; \\ < \ 0, & \text{if} \quad k_{i_2} \le k \le k_{f_2} \quad \text{(unloading)}; \end{cases} \tag{2.58}$$

see Figure 2.11(a). Due to $\phi_{1,k} \neq 0 \ \ \forall k$, the regressor $\phi_{2,k} = \text{sign}(\phi_{1,k})$ has a constant value $\bar{\phi}_2$ that depends on the sign/condition of $\phi_{1,k}$ such as (2.58). Therefore, according to (2.58) and Definition 2.1, $\bar{\phi}_2 = 1$ for the input u_k in loading regime, while $\bar{\phi}_2 = -1$ in unloading regime; see Definition 2.8.

Remark 2.16. A reasonable assumption has been considered by Martins and Aguirre (2016) in order to calculate the equilibria (see Definition 2.3) of the identified polynomial models and hence the bounding structure through an *approximate steady-state analysis*. Such an assumption consists in considering that: $y_k \approx \bar{y}, \forall k$, $u_k \approx \bar{u}, \forall k$, $\phi_{1,k} \approx \bar{\phi}_1, \forall k$ and $\phi_{2,k} \approx \bar{\phi}_2, \forall k$, and from these approximations, the "model equilibria" (i.e. $\bar{y}$) is calculated. These approximations are a direct consequence of the features described in Remark 2.15.

The framework proposed in (Martins and Aguirre, 2016) considers that the bounding structure $\mathcal{H}$ is formed by sets of equilibria that are determined when the model is subject to a loading-unloading quasi-static input signal. As a consequence, the approximations stated in Remark 2.16 should be assumed which leads to a kind of *approximate steady-state analysis*. By definition, the equilibria or fixed points are defined when the model is subject to a constant input signal using the steady-state analysis (Definition 2.3), such that: $y_k = \bar{y}, \forall k$, $u_k = \bar{u}, \forall k$ and, consequently, $\phi_{1,k} = u_k - u_{k-1} = 0$ and $\phi_{2,k} = \text{sign}(\phi_{1,k}) = 0, \forall k$. In (Martins and Aguirre, 2016), the solution(s) $\bar{y}$ of the identified polynomial model, considering the assumption indicated in Remark 2.16, are also called equilibria. A more general framework to explain how the hysteresis loop results from an interplay of *attracting* and *repelling* regions in the input-output plane, by means of a *quasi-static analysis*, is developed in Chapter 4.

Remark 2.17. If the input u_k becomes constant, then $\phi_{1,k} = u_k - u_{k-1} = 0$ and $\phi_{2,k} = 0$. Hence (2.57) becomes a purely autoregressive model with fixed point (Definition 2.3) at $\bar{y} = 0$. Therefore, the model output will *generally not* remain on the hysteresis loop for constant inputs. This problem can be overcome as discussed in Chapter 4.

Example 2.9. Bounding Structure and Hysteresis Loop.

Consider the following autoregressive model (Martins and Aguirre, 2016):

$$y_k = c_y(1) y_{k-1} + c_{\phi_2}(1) \phi_{2,k-1}, \tag{2.59}$$

for which $c_y(1) = 0.9$, $c_{\phi_2}(1) = 0.5$, $\phi_{2,k} = \text{sign}(\phi_{1,k})$, $\phi_{1,k} = u_k - u_{k-1}$, and $u_k = \sin(\omega k)$. From Definition 2.2, the term clusters and cluster coefficients of model (2.59) are trivially defined as: Ω_y with coefficient $\Sigma_y = c_y(1) = 0.9$ and Ω_{ϕ_2} with $\Sigma_{\phi_2} = c_{\phi_2}(1) = 0.5$, respectively. Hence, for model (2.59) represented in terms of clustering and from Remark 2.16, the equilibria are given by:

$$\bar{y}(\phi_2) \approx \begin{cases} \dfrac{\Sigma_{\phi_2}}{1 - \Sigma_y} = 5, & \text{for } \bar{\phi}_2 = 1 \text{ (loading);} \\ \dfrac{-\Sigma_{\phi_2}}{1 - \Sigma_y} = -5, & \text{for } \bar{\phi}_2 = -1 \text{ (unloading),} \end{cases} \tag{2.60}$$

which are the bounding structure $\mathcal{H}$ that confines the hysteresis loop, according to Theorem 2.2. In Figure 2.12, it may be notice how the input frequency influences $\mathcal{H}_k(\omega)$ but not the bounding structure, as pointed out in Remark 2.14.

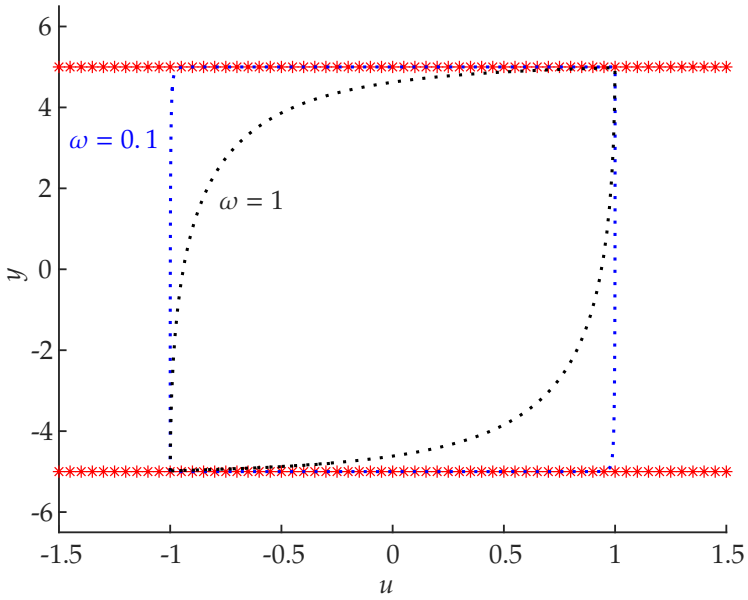

Figure 2.12: The black and blue dots are on $\mathcal{H}_k(\omega)$ (see Remark 2.14) for model (2.59). The bounding structure $\mathcal{H}$ (2.60) in red (*) will always confine $\mathcal{H}_k(\omega)$. The top limit corresponds to a loading situation, whereas the bottom limit, to unloading.

△

Remark 2.18. As can be seen in Figure 2.12, the hysteresis loop $\mathcal{H}_k(\omega)$ will tend to become indistinguishable from a given value of the input frequency ω, which indicates that, for very low-frequency values, a rate-independent hysteresis loop (Definition 2.6) will be observed. For this case, it would be possible to define a limited range of frequencies for which such behavior is found, e.g. $0 < \omega < 0.1$; see Remark 2.12.

Remark 2.19. Polynomial autoregressive model structure typically does not carry information about reversal (extremum) points and therefore are models with local memory.

In view of Property 2.2, terms from the cluster Ω_{y^p} for $p > 1$ will be automatically excluded from the following analysis. Also, as $\phi_{2,k}$ is defined here as a sign function (see Definition 2.1), terms from the cluster $\Omega_{\phi_2^{q_2}}$ for $q_2 > 1$ will also be excluded because such terms are likely to lose their fundamental properties to higher powers. For instance, in the context described in Remark 2.15, if $\phi_{2,k}^2$ is selected as a regressor of the identified model, then $\bar{\phi^2}_2$ will be equal to 1 regardless of whether the input u_k is in a loading or unloading regime. The following theorem is an extension of Theorem 2.2 for the nonlinear case, referring here to NARX models (2.12).

Theorem 2.3. [(Martins and Aguirre, 2016)]. *Given a particular SISO nonlinear autoregressive stable model:*

$$y_k = \Sigma_0 + \sum_{\tau_p=1}^{n_y} c_y(\tau_p) y_{k-\tau_p} + \sum_{\tau_{q_2}=1}^{n_{\phi_2}} c_{\phi_2}(\tau_{q_2}) \phi_{2,k-\tau_{q_2}} + \sum_{\tau_p=1}^{n_y} \sum_{\tau_{q_2}=1}^{n_{\phi_2}} c_{y\phi_2}(\tau_p, \tau_{q_2}) y_{k-\tau_p} \phi_{2,k-\tau_{q_2}}, \quad (2.61)$$

where Σ_0, $c_y(\tau_p)$, $c_{\phi_2}(\tau_{q_2})$ *and* $c_{y\phi_2}(\tau_p, \tau_{q_2})$ *are constant parameters. If* $\phi_{1,k} = u_k - u_{k-1}$ *and* $\phi_{2,k} = \text{sign}(\phi_{1,k})$, *where* u_k *is a loading-unloading quasi-static input signal of frequency* ω *(Definition 2.9), then there will be a hysteresis loop* $\mathcal{H}_k(\omega)$ *in the* $u \times y$ *plane confined by the bounding structure* $\mathcal{H}$ *defined by the model equilibria.*

Proof. See (Martins and Aguirre, 2016). ∎

Similar to what was done in Example 2.9, from Definition 2.2 and Remark 2.16, the equilibria of model (2.61) can be expressed as:

$$\bar{y}(\phi_2) \approx \begin{cases} \dfrac{\Sigma_{\phi_2} + \Sigma_0}{1 - \Sigma_y - \Sigma_{y\phi_2}}, & \text{for } \bar{\phi}_2 = \ 1 \ \text{(loading)}; \\ \dfrac{-\Sigma_{\phi_2} + \Sigma_0}{1 - \Sigma_y + \Sigma_{y\phi_2}}, & \text{for } \bar{\phi}_2 = -1 \ \text{(unloading)}, \end{cases} \quad (2.62)$$

which are the bounding structure $\mathcal{H}$ and must be stable to ensure that the identified model is able to reproduce the hysteresis loop; see Theorem 2.3. When the model is composed of unit-delayed regressors, which is a common choice in the case of systems with hysteresis (Leva and Piroddi, 2002; Du et al., 2006), the Jacobian matrix of model (2.61) is $D = \frac{\partial F^\ell}{\partial y_{k-1}} = \Sigma_y + \Sigma_{y\phi_2}\phi_{2,k-1}$, and the condition for stability is $-1 < \Sigma_y + \Sigma_{y\phi_2}\bar{\phi}_2 < 1$; see Definition 2.4. Therefore, the domain of validity for the hysteresis loop is:

$$\begin{cases} -1 \ < \ \Sigma_y + \Sigma_{y\phi_2} \ < \ 1, & \text{for } \bar{\phi}_2 = \ 1 \ \text{(loading)}; \\ -1 \ < \ \Sigma_y - \Sigma_{y\phi_2} \ < \ 1, & \text{for } \bar{\phi}_2 = -1 \ \text{(unloading)}. \end{cases} \quad (2.63)$$

As shown in (Martins and Aguirre, 2016), assuming that the model is composed of adequate terms, the term clusters in the nonlinear model will affect the shape of the hysteresis loop, but will not interfere on its occurrence as long as the conditions established in Theorem 2.3 are met.

In order to validate the proposals, Martins and Aguirre (2016) used as a benchmark system the same phenomenological model of the magneto-rheological damper studied by Leva and Piroddi (2002), which was briefly detailed in Section 2.3.7.2. Aiming at the model structure selection, they adopted the procedure based on the concepts of term clusters and cluster coefficients to eliminate spurious clusters from the set of candidate regressors and, thus, used the ERR together with AIC criterion to build the final model. Such procedure was described in Section 2.3.4. The model parameters are estimated

using the *Extended Least Squares* (ELS) method (Ljung, 1999; Billings, 2013), which is a modification of the classic LS estimator (2.46) to deal with noise effects. An appealing feature of this work is the performance and generality achieved with a simple model of 4 terms, which is promising for designing compensators. Such identified model can be rewritten, adapting its notation, as:

$$y_k = \theta_1 y_{k-1} + \theta_2 \phi_{2,k-1} + \theta_3 \phi_{1,k-1} u_{1,k-1} + \theta_4 \phi_{2,k-1} \phi_{1,k-1} y_{k-1}, \tag{2.64}$$

with:

$$\begin{cases} \phi_{1,k} = v_k, \\ \phi_{2,k} = \text{sign}(u_{2,k} - u_{2,k-1}), \end{cases} \tag{2.65}$$

where the variables y_k, $u_{1,k}$, $u_{2,k}$ and v_k are the same as defined in (2.53). As both models (2.53) and (2.64) were identified to predict the same system, a brief comparison between them can be made. As for the degree of nonlinearity, note that for model (2.53) it is $\ell = 11$ while for model (2.64) it is $\ell = 3$, which indicates that the latter has a simpler structure than the former. With regard to additional terms (2.65), both can be found if a discrete version of the phenomenological model used by them is computed, which suggests that such choices are adequate to describe the evolution rule of this system.

It should be noted that, as $\phi_{2,k}$ (2.65) is a multi-valued function (Definition 2.10) of the first difference of the input $u_{2,k}$, model (2.64) will reproduce a hysteresis loop in the input-output plane as long as the equilibria are stable; see Theorem 2.3. The results of stability analysis and simulation that confirm the ability of such a model to mimic the hysteresis loop are presented in more detail in (Martins and Aguirre, 2016).

It is interesting to note that $\phi_{1,k}$ (2.65) was defined, for the current numerical example, as the velocity, which can be rewritten as: $\phi_{1,k} = v_k \approx \frac{u_{2,kT_s} - u_{2,[k-1]T_s}}{T_s}$. As stated by Mohammadzaheri et al. (2012), when it comes to real-time applications, the inclusion of additional terms $\phi_{i,k}$ that involve a derivative operation to calculate the input or output rate, e.g. as $\phi_{1,k}$ (2.65), is very sensitive to measurement noise, which might become impractical in such applications, particularly with respect to the output rate. Therefore, to alleviate this kind of issue, we suggest replacing the derivative by the first difference when T_s has a value less than 1, which is very common in practice. Note that this is not a problem, as the relevant information about the change tendency or rate of the signal of interest that is provided by its derivative is also present in its first difference, except for a gain difference due to T_s, which will be automatically offset during the parameter estimation step (Section 2.3.5). This recommendation is also directed to the additional term (2.16), which was proposed to capture varying dynamics in a pH process, as addressed in Example 2.3 **B)**.

In terms of comprehensiveness, it is noteworthy that the sufficient conditions proposed by Martins and Aguirre (2016) cover only the dynamical features of the hysteresis nonlinearity, while its static behavior is neglected, which is evident since such condi-

tions are guaranteed only for a class of time-varying input signals; see Theorems 2.2 and 2.3. Also, the concept of bounding structure $\mathcal{H}$ is limited to cases in which the sets of equilibria that form this structure are stable; see Remark 2.14. Therefore, for more general cases, this concept and conditions need to be adapted. For instance, such conditions are not sufficient to ensure the existence of multiple fixed points at steady-state (see Remark 2.17), which is a very important feature for hysteretic systems (Bernstein, 2007; Morris, 2011). Despite this, to the best of the authors knowledge, there are no works in the literature of NARX polynomial models that guarantee such a feature. In Chapters 4 and 5, special attention is devoted to dealing with the static behavior of the hysteresis nonlinearity (see Definition 2.5), so that the identified NARX models are able to describe both its static and dynamic features.

2.3.8 Guidelines for Future Work

As discussed so far and in line with the identification philosophy, a model is only able to describe more subtle aspects of a system if such a feature is incorporated into it, either through the inclusion of a certain class of regressors $\phi_{i,k}$, adoption of constraints on its structure and/or parameters, or by updating the model parameters over time, among others. Therefore, since in the literature on NARX models there are only a handful of works devoted to characterizing the hysteresis nonlinearity (see Section 2.3.7), a number of features and properties related to it are still subject to study. Thus, in this section, we investigate some interesting properties of hysteretic systems and briefly discuss alternative ways to achieve them using gray-box NARX models.

2.3.8.1 Local and non-local memory

According to Mayergoyz (2003), *non-local memory* is a property found in some hysteretic systems in which the future value of the output depends not only on the current value of the output and input, but also on past extremum values of the input. Thus, a striking feature of such systems is the existence of more than one distinct trajectory for any reachable state in the input-output plane (see Figure 2.13(b)), and which one the state will follow depends on a particular sequence of past extremum values of input (de Almeida et al., 2003; Merola et al., 2015). In addition, some works in the literature also associate non-local memory with the existence of crossing and partially coincident *minor loops* in the input-output plane (see Figure 2.13(c)), since such facts suggest that the states of the hysteretic system are not uniquely determined by their inputs and outputs (Mayergoyz, 2003; Berenyi et al., 2005; Drincic and Bernstein, 2009; Liu and Yang, 2015; Jankowski et al., 2017). Conversely, hysteretic systems with *local memory* have their future output value dependent only on the current output and input value, without being influenced by past extremum values. For this type of hysteresis nonlinearity, a common feature is that: for any reachable state in the input-output plane, its

next values will be reached through only one trajectory for increasing the input value and one for decreasing it; Figure 2.13(a).

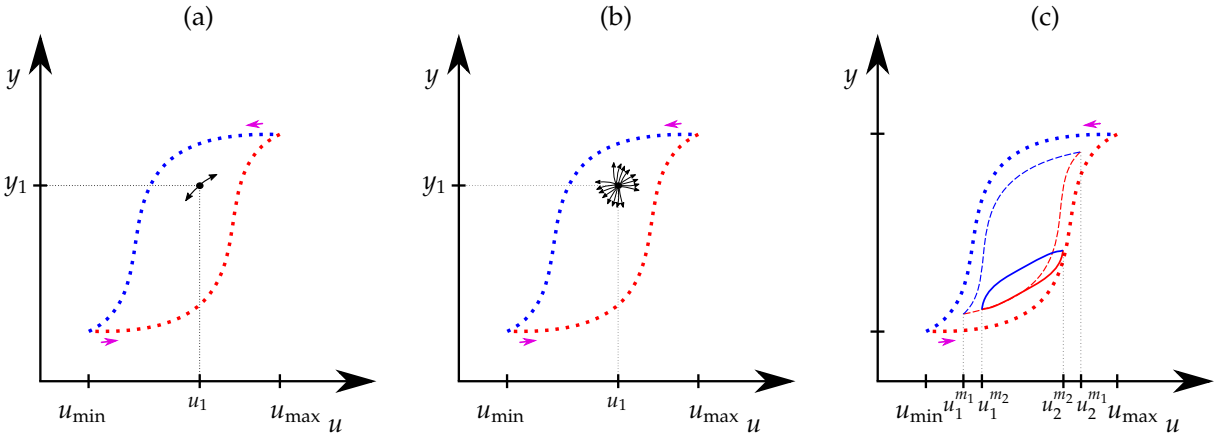

Figure 2.13: Illustration of features related to hysteretic systems with local and non-local memory displayed in the input-output plane. (a) local memory, in (b) non-local memory, and (c) evidence of non-local memory. (·····) refers to the hysteresis loop, also called *major loop* with extremum input value being $\{u_{\min}, u_{\max}\}$, (– – –) represents a *minor loop* with extremum values $\{u_1^{m_1}, u_2^{m_1}\}$, while (—) is another one with extremum values $\{u_1^{m_2}, u_2^{m_2}\}$. (→) indicates the orientation of the hysteresis loop, while (→) illustrates possible trajectories for a state $\{u_1, y_1\}$.

Based on these two properties, a primary question that is somewhat controversial in the literature concerns which of them is more consistent with real experimental systems, where some authors have stated that there is a lack of evidence for non-local memory, while others for local memory (Mayergoyz, 2003; de Almeida et al., 2003). Despite such controversy, many works have used and developed models to represent hysteretic systems in which local or non-local memory is assumed. For instance, considering the phenomenological models (Section 2.2), those based on differential equations, such as the Bouc-Wen model, the Duhem model, the Dahl and the LuGre model, have commonly been related to hysteresis with local memory, while those based on operators, such as the Preisach and the Prandtl-Ishlinskii models, have been shown to be able to capture the property of non-local memory.

In the case of hysteretic systems with non-local memory, it is essential that the models used to describe these systems incorporate in their structure ways to detect and store input extremum values, such as the Preisach model (Ge and Jouaneh, 1996; Al-Bender et al., 2004). For the case of NARX models, Martins and Aguirre (2016) mentioned that due to the fact that this information about extremum values of the input signal is commonly disregarded during the identification procedure (see Remark 2.19), NARX models are generally unable to capture the non-local memory effect and, therefore, a more careful investigation is needed to make them capable of handling this feature. Although not mentioned by Deng and Tan (2009), it is interesting to note that the use of extremum values of the input in the proposed hysteretic operator (2.55) might be a

promising way to indirectly incorporate non-local memory in NARX models. In this sense, some interesting questions to be investigated follow below.

As aforementioned, non-local memory might lead to more than one distinct trajectory (see Figure 2.13(b)) that will depend on a particular sequence of past extremum values. So, the following question arises: *How to enable NARX models to choose the proper trajectory considering the sequence of extremum values stored so far?* In addition, issues related to the need to store extremum values by *dynamic allocation* and *how many extremum values are really useful and feasible to capture the non-local memory effect*, appear in this context (de Almeida et al., 2003; Al-Bender et al., 2004; Jankowski et al., 2017). Another point that deserves attention and still needs answers concerns which benefits would be achieved in terms of predictive and compensation performance if the model had non-local memory. Some additional discussions that might be helpful in dealing with these issues can be found in (Swevers et al., 2000; Bashash and Jalili, 2006; Liu and Yang, 2015).

2.3.8.2 Asymmetric loops

As mentioned throughout the review, one of the main features adopted in the literature to characterize hysteretic systems refers to a persistent loop behavior displayed on the input-output plane, which has led many works to focus on understanding how it arises. For instance, considering smart materials-based actuators, such a behavior has been associated with a strong nonlinear dependence on the type of materials, magnitude and rate of the input signal (Al Janaideh et al., 2008a; Rakotondrabe, 2013). In this context, two important properties of the hysteresis loop have been studied for a class of time-varying input signals. The first one refers to the symmetry property of the hysteresis loop, which has commonly been attributed to the type of material used for the design of the actuator. As an example, many piezoceramic actuators are known to generally produce symmetric hysteresis loops (Yu et al., 2001; Cao et al., 2019). It should be mentioned that the phenomenological models reviewed in Section 2.2 were developed to describe symmetric hysteresis. On the other hand, the second property is related to the asymmetric hysteresis loop, which has been cited in the literature as a feature commonly found in shape memory alloys and magnetostrictive actuators (Kuhnen, 2003; Shakiba et al., 2018). In this case, many works have proposed ways to incorporate into classical phenomenological models (Section 2.2) the ability to describe asymmetric hysteresis (Ge and Jouaneh, 1995; Gu et al., 2014; Wei et al., 2014).

In terms of NARX models, both approaches reviewed in Sections 2.3.7.3 and 2.3.7.4 identify models that tend to reproduce symmetric hysteresis loops, e.g. see the hysteresis loop in Figure 2.12. Based on the approach discussed in Section 2.3.7.4 and the Remark 2.14, Martins (2016) highlighted the fact that the format of the bounding structure $\mathcal{H}$ is directly related to the shape of the hysteresis loop $\mathcal{H}_k(\omega)$ and, therefore, the use of different structures $\mathcal{H}$ leads to different shapes of $\mathcal{H}_k(\omega)$. Also, it was shown that the

use of asymmetric multi-valued functions (Definition 2.10) could be an alternative way to obtain asymmetric hysteresis loop, which is illustrated in the following example.

Example 2.10. Asymmetry in the Bounding Structure and its Hysteresis Loop.

For model (2.59) in Example 2.9, it is assumed that the regressor $\phi_{2,k} = \text{sign}(\phi_{1,k})$ with $\phi_{1,k} = u_k - u_{k-1}$ (Definition 2.1), which is symmetric, is replaced by an asymmetric multi-valued function, given by (Martins, 2016):

$$\phi_{2,k} = \begin{cases} u_k, & \text{if } \phi_{1,k} > 0; \\ -1, & \text{if } \phi_{1,k} < 0; \\ 0, & \text{if } \phi_{1,k} = 0. \end{cases} \tag{2.66}$$

Considering the input frequency as $\omega = 1$, the bounding structure $\mathcal{H}$ and its resulting asymmetric hysteresis loop $\mathcal{H}_k(\omega)$ are shown in Figure 2.14.

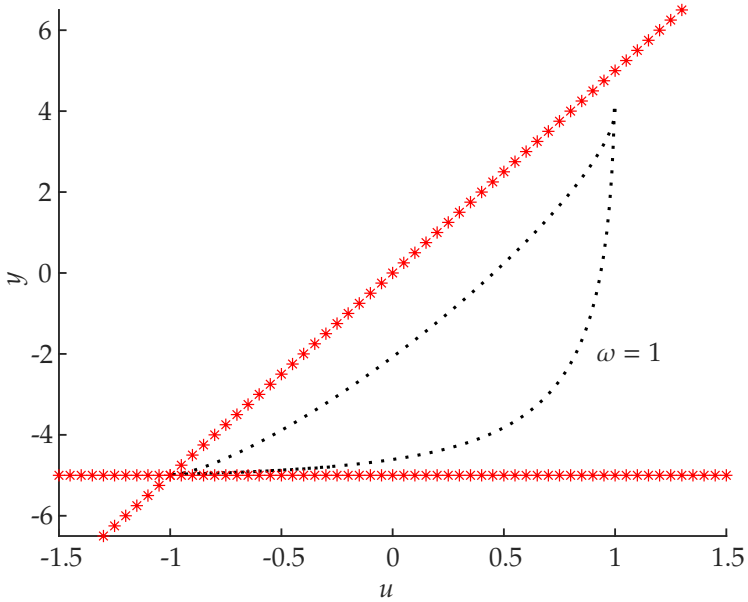

Figure 2.14: The black dots are on $\mathcal{H}_k(\omega)$ (see Remark 2.14) for model (2.59) with regressor (2.66). The bounding structure $\mathcal{H}$ in red (*) will always confine $\mathcal{H}_k(\omega)$. The top limit corresponds to a loading situation, whereas the bottom limit, to unloading.

△

As can be seen in Figure 2.14, the use of an asymmetric multi-valued function might become an effective way for gray-box NARX models to reproduce asymmetric hysteresis (Martins, 2016). However, there are some relevant questions that have not yet been answered and require further investigation. In short, two fundamental questions arise: *How to determine an appropriate asymmetric multi-valued function to be used?* and *How will this function affect the number, location, and stability of the fixed points?*

In order to achieve this goal, it is suggested to use a regression method (e.g. polynomial) to model the relationship between the output (dependent variable) and the input

signal (independent variable) in two different contexts. Basically, the idea would be to collect a data set using a loading-unloading quasi-static input signal (Definition 2.9) and its corresponding output, so that a regression model is fitted for the loading regime (i.e. for $k_{i_1} \leq k \leq k_{f_1}$) and another for the unloading regime (i.e. for $k_{i_2} \leq k \leq k_{f_2}$) of the data; see Figure 2.11(a). Then, in (2.66), u_k and -1 would be replaced by the regression model fitted for the loading and unloading regime, respectively. Therefore, assuming (2.66) with these modifications, we believe that it would be possible to indirectly capture relevant information about the behavior of the hysteresis loop, be it symmetric or asymmetric, and thus use it as a candidate regressor during the identification procedure. This is a possible way that still needs to be unraveled.

2.3.8.3 Lack of validation

As exhaustively mentioned here and in the literature on hysteretic systems, the persistent loop behavior exhibited in the input-output plane has been widely accepted by the scientific community as the hallmark of such systems. As a result, an invaluable amount of scientific papers developed to model hysteretic systems has focused only on the description of their hysteresis loop, as well as their temporal response, when such systems are subject to a time-varying input signal (Ni et al., 1998; Smyth et al., 2002; Hu and Ben Mrad, 2003; Oh and Bernstein, 2005; Al Janaideh et al., 2008b; Zakerzadeh et al., 2011; Domínguez-González et al., 2014; Zhang et al., 2017a). Therefore, a fundamental question arises: *Is this feature the only one or sufficient to be assumed to, for example, assess whether an identified hysteretic model is really representative?* or rather, *What is hysteresis?*

Faced with this question, Bernstein (2007) and Morris (2011) provided an extremely rich and detailed discussion that goes far beyond the simple fact that hysteretic systems have a characteristic loop, but somehow analyzes the reason that cause it in different contexts. Based on the valuable insight they provide about hysteresis nonlinearity, we raised Definition 2.5 (in Section 2.3.3), so that an important feature that is expected in hysteretic models can be considered, in addition to the hysteresis loop, when it comes to modeling such systems. It should be highlighted that Definition 2.5 describes a feature commonly present in the static response, i.e. in steady-state, of a hysteretic system. We do not find in the literature studies that impose this feature during the identification procedure or that show the performance of the identified NARX models in the steady-state, e.g. see (Leva and Piroddi, 2002; Parlitz et al., 2004; Worden et al., 2007; Deng and Tan, 2009; Worden and Barthorpe, 2012; Martins and Aguirre, 2016; Zhang et al., 2017a; Lacerda Júnior et al., 2019). Therefore, in Chapters 4 and 5, we explore this feature during the identification procedure in order to provide identified NARX models with the ability to predict dynamical and static features of the hysteresis nonlinearity.

2.4 Concluding Remarks

This chapter reviewed some features found in hysteretic models. In terms of classical hysteretic models, a brief contextualization of phenomenological models was presented, with emphasis on the Bouc-Wen model and the Prandtl-Ishlinskii model. For the case where a more comprehensive model is considered, not limited to describing only the hysteresis nonlinearity, some of the main concepts, definitions and tools formulated based on the NARX philosophy, which corresponds to a black-box approach, were addressed. However, as the black-box approach does not allow to obtain models that reproduce more subtle aspects of the system dynamics, such as the hysteretic behavior, a gray-box modeling approach was revisited. In this case, all necessary extensions in the formulation and definitions to cover the black-box and gray-box techniques have been made, and also some interesting tips and fair contributions are duly shared throughout the chapter. The next chapter reviews strategies for controlling and compensating hysteretic systems when the models discussed here are used.

Chapter 3

Control Approaches for Hysteretic Systems

3.1 Introduction

This chapter addresses some approaches used to design controllers and compensators for hysteretic systems found in the literature. These approaches are related to some contributions and proposals developed in this work, which will be detailed in Chapter 4. For the development of these control and compensation schemes, it is assumed that such systems are represented as a cascaded model structure (Peng and Chen, 2013; Gu et al., 2016b).

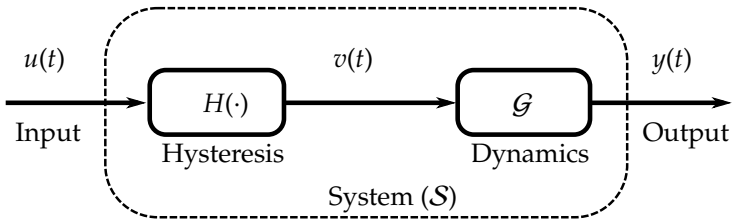

Figure 3.1: Block diagram of the cascaded model structure used to represent hysteretic systems $\mathcal{S}$. The output $v(t)$ of the hysteresis model $H(\cdot)$ is the input of the dynamic model $\mathcal{G}$.

As can be seen in Figure 3.1, a way to represent hysteretic systems consists of a cascade structure, which is composed of a dynamic model $\mathcal{G}$ that describes the linear behavior of the system $\mathcal{S}$, preceded by a model $H(\cdot)$ that describes the hysteretic behavior (Liu et al., 2010; Gu et al., 2016a). It is noteworthy that this type of representation is similar to that of Hammerstein models, in which model $\mathcal{G}$ refers to linear dynamics and model $H(\cdot)$ is a static nonlinearity. However, when dealing with hysteretic systems, it should be clear that model $H(\cdot)$ describes the nonlinear dynamic behavior of hysteresis. Some works in the literature have called the cascade between $\mathcal{G}$ and $H(\cdot)$ for hysteretic systems as a pseudo-Hammerstein model (Cao and Chen, 2012; Deng et al., 2014). This representation can be used to describe hysteretic systems modeled either from phenomenological models, such as the Bouc-Wen and the Prandtl-Ishlinskii models, or from gray-box NARX models (see Chapter 2). For the use of NARX representation, we will assume that both process and hysteresis dynamics are described by a single model.

The approaches commonly adopted to design controllers and compensators for hysteretic systems can be classified into three categories: (i) compensation approaches, (ii) feedback control, and (iii) combination of compensation and feedback control approaches. Among the controllers and compensators obtained through these approaches, it is noteworthy that they differ mainly in relation to the type of hysteresis model that is used during their design, since there is still no proposal for a general model capable of fully representing this behavior (Gu et al., 2016b). Therefore, in order to provide a better performance when dealing with regulation or tracking problems in hysteretic systems, new approaches to control and compensation have been proposed.

As the control and compensation schemes proposed in the literature are formulated to deal with the hysteretic behavior modeled by a given structure, we will emphasize those developed for the classes of models presented in Chapter 2. Therefore, the purpose of this chapter is to present the control challenges that remain open and some of the limitations that are found in existing approaches.

This chapter is organized as follows. Section 3.2 reviews some approaches for designing compensators based on: the inversion of a predictive model and the identification of a model that estimates the inverse behavior of the hysteretic system under investigation. Section 3.3 addresses the problem of designing feedback controllers for hysteretic systems. Finally, Section 3.4 presents some works that deal with the combination of both compensation and feedback control approaches.

3.2 Compensation Approaches

Compensation-based approaches aim to design a compensation input that mitigates undesirable behaviors, e.g. nonlinearities, exhibited by the system so that it becomes more amenable for control. In the context of hysteretic systems, the designed compensator is cascaded with the system in an open-loop scheme to attenuate the hysteretic behavior; see Figure 3.2.

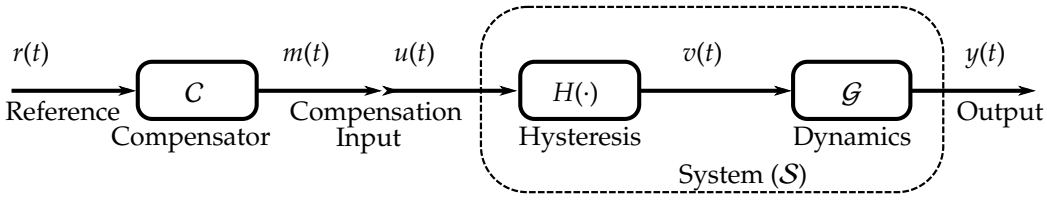

Figure 3.2: Block diagram of the compensation approach C for a hysteretic system $\mathcal{S}$, which is represented by a linear dynamic model $\mathcal{G}$ preceded by the hysteresis model $H(\cdot)$.

According to Gu et al. (2016b), there exist two steps that are commonly used to design compensators to mitigate the hysteretic behavior. The first one aims to identify a model capable of predicting the hysteresis behavior. The second uses this model

to design a compensator C. In what follows, two different compensation approaches found in the literature are presented.

3.2.1 Model-Based Compensation

One of the approaches to design the compensator C is through the construction of an inverse function $H^{-1}(\cdot)$ of the hysteresis model $H(\cdot)$, which will provide a compensation input m to mitigate the hysteresis present in the system $\mathcal{S}$; see Figure 3.2. According to Rakotondrabe (2013), due to the lack of methods to analytically obtain the inverse of hysteretic models based on differential equations, such models have not been viable to be used for designing compensators when the construction of the *complete inverse function* of these models is considered. Therefore, based on the models reviewed in Chapter 2, it is worth mentioning that although the Bouc-Wen hysteresis model is of great relevance in the academic community, due to its ability to predict a wide class of real hysteretic systems, this model is inapplicable in this compensation approach. Faced with this problem, Rakotondrabe (2011) proposed an alternative approach that considers the restructuring of the Bouc-Wen model in an *inverse multiplicative scheme* for the compensation of hysteresis in smart materials, so that the inversion of complex terms (or non-invertible) that make up the model is not required. Thus, this approach tends to be easy to implement and has a lower computational cost, since a complete inversion of the model is not required (Wang et al., 2011; Zhou et al., 2012; Hassani et al., 2014). It should be mentioned that such an approach requires that the input signal appears explicitly expressed in the models.

Regarding the phenomenological models of hysteresis based on operators, it is noteworthy that these models have been widely used for compensation since their inverse can be determined by different methods (Peng and Chen, 2013). For the case of the Preisach model, which is one of the most popular operators, it should be mentioned that it is not analytically invertible, but its inverse can be approximated by numerical methods (Song et al., 2005; Visone, 2008; Ruderman and Bertram, 2010). On the other hand, the Prandtl-Ishlinskii hysteresis model has the advantage of being analytically invertible and, consequently, is more suitable for practical applications as it provides better accuracy and lower computational cost when compared to the inverse Preisach model (Krejci and Kuhnen, 2001). For this reason, many works have used this model to design compensators based on its inverse model (Kuhnen and Janocha, 2001; Mokaberi and Requicha, 2008; Rakotondrabe et al., 2010; Al Janaideh et al., 2011, 2016a). Although operator-based models are invertible, compensation schemes without the need for complete inversion of such hysteresis models, based on the inverse multiplicative scheme mentioned above, have also been proposed (Rakotondrabe, 2012; Li et al., 2014; Aljanaideh et al., 2017). Some works have reported that the use of such a compensation scheme compared to the construction of the complete inverse function provided improvements with regard to the simplicity of implementation and the fact that there

is no extra computational cost for compensation, since the same parameters and structure of the identified model are maintained. Although the Prandtl-Ishlinskii model has interesting features for designing compensators using an inverse model, its accuracy for predicting the hysteretic behavior depends on the number of operators that make up the model. As a result, the computation time increases with the desired accuracy for the model, since this model is based on the weighted sum of hysteresis operators (see Section 2.2.2). Therefore, from a practical point of view, one must consider the existing trade-off between accuracy and computational time based on this type of model.

It should be emphasized that the compensation approaches reviewed so far have been proposed assuming the use of some specific phenomenological hysteresis model, such as the Bouc-Wen and the Prandtl-Ishlinskii models (Rakotondrabe, 2011; Gu et al., 2012). However, not every hysteretic system is represented by such models. Also, there are some challenges related to the estimation of their parameters that might appear nonlinearly in the equation, and their structural complexity that represents an additional difficulty in the design of compensators (Peng and Chen, 2013; Hassani et al., 2014). On the other hand, as discussed in Section 2.3, a promising alternative to predict the hysteresis nonlinearity is using NARX models, which can be tailored, in a gray-box scheme, to reproduce specific features and to meet possible constraints on the structure and parameters to make them suitable for use in a compensation scheme. However, the literature on the use of NARX models in the compensation of hysteresis is still scarce (Dong and Tan, 2014; Lacerda Júnior et al., 2019). One of the very few papers that is concerned with obtaining structurally simple NARX models that are particularly suitable for model-based control was proposed by Leva and Piroddi (2002) and discussed in Section 2.3.7.2. Although the authors identified the compact model (2.53) for a hysteretic system, they have not used this model in any control or compensation scheme. It is also important to note that the methodology proposed by them does not guarantee that the identified models are suitable for designing compensators. This can be verified by manipulating (2.53) so that its inverse function $H^{-1}(\cdot)$ is obtained. Thus, isolating the input signal $u_{1,k}$ to construct its inverse model, i.e. compensator, the following resulting equation is obtained:

$$u_{1,k}=\frac{1}{\theta_3\phi_{2,k}\phi_{1,k}^2+\theta_6\phi_{2,k}\phi_{1,k}}\Big[y_k-\theta_1 y_{k-1}-\theta_2\phi_{2,k-1}\phi_{1,k-1}^2-\theta_4\phi_{1,k}^3 y_{k-1}-\theta_5\phi_{2,k}\phi_{1,k}^{10}\Big]. \quad (3.1)$$

As a result, it can be seen that the compensator (3.1) would have a singularity when the velocity variable is equal to zero or when the sum of its denominator is equal to zero, which makes this compensator invalid in these cases.

Recently, Lacerda Júnior et al. (2019) presented a case study in which the identification proposals made in (Martins and Aguirre, 2016), and reviewed in Section 2.3.7.4, are used to identify a NARX model for an experimental electronic circuit with hysteresis, and this model is used to construct the compensator C based on its inversion. As with the previous paper, the proposed methodology for obtaining a compensator is subject

to failure, i.e. singularity issues in their compensators, since there is no guarantee that the identified models are suitable for designing compensators. For example, considering the model (2.64) identified in (Martins and Aguirre, 2016), and isolating the input $u_{1,k}$ as done in (3.1) to construct the inverse function, we have:

$$u_{1,k-1}=\frac{1}{\theta_3\phi_{1,k-1}}\Big[y_k-\theta_1 y_{k-1}-\theta_2\phi_{2,k-1}-\theta_4\phi_{2,k-1}\phi_{1,k-1}y_{k-1}\Big], \tag{3.2}$$

which is the same as shown in equation (12) in (Lacerda Júnior et al., 2019), except for a difference in its notation. Again, in cases where the velocity has a value equal to zero, the compensator (3.2) is not defined. Therefore, these results allow us to conclude that there is a lack of systematic methods in the literature to ensure that the identified NARX models are suitable for designing compensators. In Chapter 4, effective systematic methodologies are provided for designing compensators.

3.2.2 Compensation Based on Compensator Identification

An alternative approach aims to identify the compensator C directly from a set of data collected from the hysteretic system $\mathcal{S}$ under investigation. Therefore, this approach has the advantage of obtaining the inverse model in a single step, without the need to first identify a model to predict the hysteretic behavior and only then construct its inverse function using this predictive model, which was presented in Section 3.2.1. Conversely, according to Gu et al. (2016b), only an approximate compensation can be expected when using this approach. For hysteretic systems in which the hysteresis behavior is modeled by differential equations, no work was found in the literature.

In terms of operator-based hysteresis models, such as the Preisach and the Prandtl-Ishlinskii models, there are some works that have addressed this type of compensation approach (Croft et al., 1999; Gu et al., 2012; Qin et al., 2013). Basically, its core idea revolves around modifications that are carried out in the model, such as structure specifications, changes in the input mapping function of the inverse model, among others, in order to benefit the identification of the inverse features.

As for the use of NARX models for this type of compensation, very little has been done. During the research, the only work found that addresses the identification of NARX polynomial models to predict the inverse hysteresis behavior was proposed in (Dong and Tan, 2014). In that work, the authors defined an operator similar to the one discussed in Section 2.3.7.3, which was proposed by Deng and Tan (2009) to capture the change tendency of the hysteresis behavior, but now with the aim of mapping the inverse hysteresis behavior. Thus, the output of this inverse hysteretic operator is used as an additional candidate regressor $\phi_{i,k}$ for identifying a NARX model (2.12) that estimates the input $\hat{u}_k$ rather than the output signal y_k of the hysteretic system. Hence, according to Dong and Tan (2014), it is possible to develop the compensator based on an inverse gray-box NARX model to attenuate the hysteresis effect in order to obtain

a more linear relationship between the input and output of the hysteretic system. It should be mentioned that the structure selection step used by them is the same as in (Deng and Tan, 2009) and, therefore, the problems discussed in Section 2.3.7.3 could happen when identifying this compensator. As a side note, the degree of nonlinearity used to obtain the compensator was not mentioned, which makes some additional information about it inaccessible, such as the number of regressors required to obtain the compensator identified by them. Also, nothing was mentioned about the potential problem of causality, which might happen in this type of compensation approach. In order to overcome this shortcoming, a procedure is developed in Chapter 4. For the case of NARX neural models, Li and Chen (2013) proposed the design of a nonlinear adaptive compensator that is adjusted online to mitigate the hysteresis nonlinearity in a piezoelectric actuator.

Although the compensation approaches provide advantages in terms of mitigating hysteretic behavior, easy implementation and simplicity, these approaches are highly sensitive to unknown effects (Peng and Chen, 2013). More specifically, the performance of these open-loop schemes might be significantly degraded by parametric uncertainties, unmodeled dynamics and external disturbances, as well as changes in system dynamics over time. For this type of scenario, the feedback control approaches correspond to an appropriate option and are presented in what follows.

3.3 Feedback Control Approaches

Feedback control approaches have interesting features due to their ability to deal with the presence of effects arising from model uncertainties, disturbances and nonlinearities in the system to be controlled. For the case of hysteretic systems, the feedback controller is inserted in the closed-loop branch so that, in addition to suppressing the effects mentioned above, an efficient attenuation of the hysteretic behavior might be achieved. Figure 3.3 shows the block diagram for this control approach.

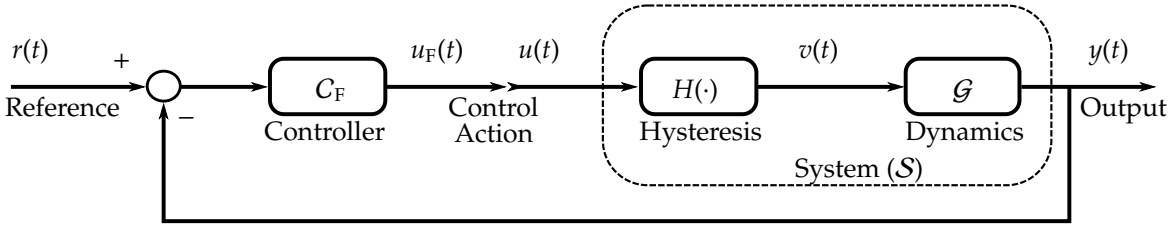

Figure 3.3: Block diagram of the feedback control approach C_F for a hysteretic system $\mathcal{S}$, which is represented by a linear dynamic model $\mathcal{G}$ preceded by the hysteresis model $H(\cdot)$.

In the literature, there are many feedback control approaches that have been developed based on linear and nonlinear control techniques to deal with hysteretic systems (Zhou et al., 2004; Ikhouane and Rodellar, 2006; Payam et al., 2009; Riccardi et al., 2013,

2014; Cheng et al., 2015). The choice of which control technique to use depends on the purpose and how the control problem is formulated. When it is desired to handle both transient and steady-state responses, the Proportional-Integral-Derivative (PID) control technique is one of the most used and accepted options in both academic and industrial fields (Ang et al., 2005). Due to this recognition, works have investigated methodologies that enable the compensation of the hysteretic behavior through the proper tuning of this control law (Ikhouane and Rodellar, 2006; Riccardi et al., 2012, 2013, 2014). In the case where it is desired to obtain robust feedback controllers to model uncertainties and external disturbances in the system, linear techniques based on $\mathcal{H}_2$ and $\mathcal{H}_\infty$ norms comprise an interesting option to be considered (Doyle et al., 1989). The use of these techniques to mitigate hysteresis can be found in (Salapaka et al., 2002; Chuang and Petersen, 2013; Ahmad et al., 2017). This approach commonly considers the hysteresis as a bounded disturbance in the nominal model of the system and adjusts the control law by optimizing an objective function that minimizes the $\mathcal{H}_2$ or $\mathcal{H}_\infty$ norm. In Figure 3.3, the nominal model for hysteretic systems corresponds to the linear dynamic model $\mathcal{G}$, while the hysteresis behavior $H(\cdot)$ can be treated as a disturbance or uncertainty (Gu et al., 2016b).

In the context of nonlinear techniques for designing feedback controllers to handle hysteretic systems, when it comes to tracking and stabilization problems, the *back-stepping* technique is an interesting tool to be studied (Payam et al., 2009). With this technique, the control law and the Lyapunov function to ensure stability are constructed systematically (Khalil, 2002). Sliding mode control technique has the characteristic of providing controllers that are robust to uncertainties and disturbances (Edwards and Spurgeon, 1998). Its use to attenuate hysteresis can be found in (Liaw et al., 2007; Xu and Li, 2009). Other control techniques, such as those based on neural networks (Liaw and Shirinzadeh, 2009) and adaptive control (Chen et al., 2008), have also been applied to the feedback control of these systems. Furthermore, a large number of modifications and combinations of these techniques to control hysteretic systems have been proposed, such as adaptive backstepping (Zhou et al., 2004; Feng et al., 2005; Ikhouane et al., 2005; Zhou and Wen, 2008; Zhang et al., 2017b) and adaptive sliding mode (Chen and Hisayama, 2008; Zheng et al., 2014; Mansourfar and Baradarannia, 2018).

A common goal that is pursued in this research field is to adapt existing techniques or propose new control approaches that are promising to control hysteretic systems. From the methodological point of view, most of the aforementioned techniques aim to design controllers that meet and provide improvements in some performance requirement of the closed-loop system. Since stability corresponds to the minimum performance expected by a control system, ensuring this requirement during controller design has been of fundamental importance. In order to apply the stability analysis to nonlinear dynamical systems, two frequently used methods are based on linearization and Lyapunov theory. Linearization-based methods are commonly used due to the wide range of tools available to analyze linear systems (Chen, 1999). For this type of

approach, the system is linearized around a fixed point and the analyzes developed in the linearized model provide estimates of the local behavior of the nonlinear system.

An alternative to these linearization methods is based on Lyapunov theory which, in turn, makes it possible to analyze the stability of the fixed points directly from the nonlinear representation of the system. In this way, it is avoided that complex dynamic characteristics of the hysteresis, such as strong nonlinear dependencies on its variables, are neglected when the dynamic model is linearized (Rakotondrabe, 2013). For this reason, stability analysis in the Lyapunov sense is commonly used to design controllers. Some important definitions, theorems, and their proofs about the stability in the sense of Lyapunov are detailed and found in (Khalil, 2002). It is interesting to mention that, considering the use of Lyapunov theory, two works were developed. In one work, an adaptation of the backstepping controller developed in (Payam et al., 2009) through the inclusion of an integral action into the problem formulation was proposed, aiming to improve the closed-loop performance with robustness against parametric uncertainties and constant disturbances; see (Abreu et al., 2018b). In the second work, as far as we know, the first methodology to design a PID controller via LMIs to deal with the combination of hysteresis and time-delay was proposed, which are effects often found in real applications; see (Abreu et al., 2018a).

According to Peng and Chen (2013), although feedback control approaches offer advantages that are superior to compensation, the presence of uncertainties together with hard nonlinearities might degrade the performance of such controllers. Therefore, it is possible to combine the compensation and feedback control approaches so that the results achieved present better accuracy when compared to those obtained using only one of these approaches. The combination of the compensation and feedback control approaches is discussed in the next section.

3.4 Compensation with Feedback Control Approaches

The last approach deals with the design of control laws that combine the advantages coming from the use of compensators and feedback controllers. Thus, when it comes to controlling hysteretic systems, one of the compensation approaches presented in Section 3.2 can be used to construct an *inverse hysteresis model*, i.e. compensator, that is cascaded with the system to make the relationship between its input and output signals more linear. Thereafter, a feedback controller (Section 3.3) is designed and used to compose the closed-loop scheme so that compensation errors due to imprecision in the identified inverse hysteresis model and the remaining dynamics of the system might be mitigated. Figure 3.4 shows the block diagram that illustrates this control approach.

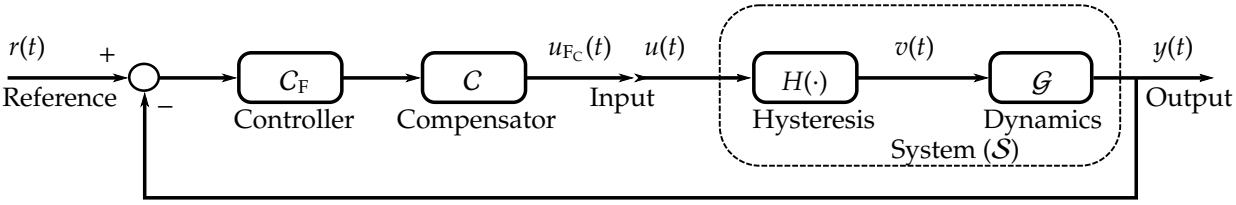

Figure 3.4: Block diagram of the compensator C combined with feedback controller C_F for a hysteretic system $\mathcal{S}$, which is represented by a linear dynamic model $\mathcal{G}$ preceded by the hysteresis model $H(\cdot)$.

Due to the different models used to design compensators and the different feedback control techniques existing in the literature, many works have dealt with the combination of these approaches (Ge and Jouaneh, 1996; Song et al., 2005; Shen et al., 2008; Peng and Chen, 2010; Cao et al., 2013; Schindele and Aschemann, 2013; Liu et al., 2014). In the field of linear control, studies regarding the use of compensator with linear techniques, such as PID and $\mathcal{H}_2$, have reported a considerable increase in control performance (Ge and Jouaneh, 1996; Peng and Chen, 2010). Some works highlight the improvement achieved in the maximum tracking error that was reduced by about 50% when comparing the case where the approaches are combined with the case where they are treated separately (Song et al., 2005). In a similar way, controllers based on nonlinear techniques, such as sliding mode control and backstepping, are combined with the use of compensators to handle hysteretic systems (Shen et al., 2008; Schindele and Aschemann, 2013).

Despite the advantages that have been presented by works in the literature about these combined approaches, some challenges related to the stability analysis of these control schemes remain an open problem. According to Gu et al. (2016b), the main challenge when using this approach is to demonstrate the stability of the closed-loop system when considering the errors generated by the designed compensator, since obtaining their analytical expressions is not a trivial task.

3.5 Concluding Remarks

This chapter discussed some approaches developed in the literature for designing control laws for hysteretic systems. The revised approaches were divided into three categories that address the design of compensators, feedback controllers, and combining compensators with feedback controllers. Some control challenges that remain open were presented, as well as some advantages and limitations found in existing control approaches in the literature to deal with hysteresis modeled by the Bouc-Wen, the Prandtl-Ishlinskii and the NARX models, which were reviewed in Chapter 2.

The next chapter develops some systematic methodologies for designing compensators using NARX models so that the gaps discussed in Section 3.2 are overcome.

These proposed methodologies are not limited to hysteresis and can be used to deal with other nonlinearities. In addition, advances in the identification of hysteretic system are presented, in which some subtle features of this nonlinearity are now adopted during the identification procedure and, thus, enabling NARX models to predict it.

Chapter 4

Hysteresis Identification and Compensator Design via NARX Models

4.1 Introduction

This chapter addresses the problem of identification and nonlinearity compensation in dynamical systems using NARX polynomial models. As mentioned in Section 2.3, our analysis gives special attention to the use of NARX models to deal with hysteresis, since there are few works in the literature dedicated to this subject. Also, a lack of more critical analyzes with respect to the ability of these models to characterize more subtle aspects of hysteretic systems, such as the hysteresis loop and a continuum of steady-state solutions (Definition 2.5), has been observed. Indeed, to the best of our knowledge, there are no works in the literature that impose the feature of a continuum of steady-state solutions during the identification procedure or that show the performance of the identified NARX models in steady-state. In order to achieve this, based on gray-box identification techniques, some constraints on the structure and parameters of NARX models are proposed to ensure that the identified models have the ability to predict both dynamical and static features of the hysteresis nonlinearity. In addition, we provide a more general framework to explain how hysteresis occurs in such models. In terms of hysteresis compensation, the lack of NARX-based methods can arguably be explained by the modeling problems that could not be solved in the context of black-box techniques. Based on gray-box models, our work has been advanced by proposing three systematic procedures to ensure that the identified NARX models are suitable for designing compensators. The compensation procedures are formulated to deal with hysteresis and other nonlinearities modeled by NARX models.

The chapter is organized as follows. Section 4.2 discusses a constraint to ensure hysteresis in the identified models and a framework for understanding how the hysteresis loop is formed. Based on NARX models, preliminary information about their use to design compensators, which will be combined in an open-loop scheme with the investigated system, is presented in Section 4.3. Compensation procedures are formulated from Section 4.4 to Section 4.6, where each section details one of the proposed approaches. Section 4.7 presents the concluding remarks.

The content of this chapter is similar to that published in (Abreu et al., 2020), with a richer and more detailed discussion of the proposals, as well as some of the content that

we published in (Tavares et al., 2022), with a more concise presentation of the dynamic compensation approach based on the roots of an algebraic polynomial.

4.2 Identification of Hysteretic Systems

The scientific community has investigated which relevant features must be present in a model to reproduce hysteresis. Some of these features are: a characteristic loop behavior displayed on the input-output plane (Bernstein, 2007), several stable fixed points (Morris, 2011), and multi-valued mapping (Deng and Tan, 2009). However, as discussed in Chapter 2, which and how these features can be used in the identification procedure remains an open problem.

As proposed by Martins and Aguirre (2016), and reviewed in Section 2.3.7.4, the inclusion of a regressor $\phi_{i,k}$ given by a multi-valued function (Definition 2.10), such as the sign function (Definition 2.1) of the first difference of the input, in addition to polynomial terms of the gray-box NARX model (2.12) is a sufficient condition to reproduce a hysteresis loop; see Theorem 2.3. Therefore, in this work, the models adopted are of the type:

$$y_k = F^{\ell}\Big(y_{k-1}, \cdots, y_{k-n_y}, u_{k-\tau_d}, \cdots, u_{k-n_u}, \phi_{1,k-\tau_d}, \cdots, \phi_{1,k-n_{\phi_1}}, \phi_{2,k-\tau_d}, \cdots, \phi_{2,k-n_{\phi_2}}\Big), \tag{4.1}$$

where:

$$\begin{cases} \phi_{1,k} = u_k - u_{k-1}, \\ \phi_{2,k} = \text{sign}(\phi_{1,k}), \end{cases} \tag{4.2}$$

and the other variables are the same as defined in (2.12). It is interesting to note that the addition of the regressors $\phi_{1,k}$ and $\phi_{2,k}$ does not affect the number, location and stability of fixed points (Definition 2.3) (Aguirre and Mendes, 1996).

In what follows, a constraint is proposed to ensure a key-feature of hysteresis. Also, it is shown how the hysteresis loop can be seen as an interplay of *attracting* and *repelling* regions in the input-output plane of certain models. Then, in the sequel the resulting models will be used to design compensators. We start with a property that summarizes a feature commonly expected in models identified to represent hysteretic systems, i.e. the existence of more than one fixed point in steady-state, as discussed in (Bernstein, 2007; Morris, 2011; Martins and Aguirre, 2016).

Property 4.1. *An identified hysteretic model, under a constant input, has two or more real non-diverging equilibria.*

In (Martins and Aguirre, 2016), Property 4.1 was attained by ensuring that the model had at least one fixed point under loading-unloading quasi-static inputs (Definition 2.9), with different values for the loading and unloading regime, in which the additional term

$\phi_{2,k}$ in (4.2) becomes $\bar{\phi}_2$=1 and $\bar{\phi}_2$= − 1, respectively (see Remark 2.15). Undoubtedly, this enables NARX models to describe the dynamical features of hysteretic systems, i.e. mimic their hysteresis loop and temporal response. However, as discussed throughout the review in Chapter 2, hysteresis is a nonlinear behavior that also appears in the *static response* and, despite being a relevant feature of such systems, not many works in the literature have highlighted this fact (Bernstein, 2007; Morris, 2011). In some works, this nonlinearity is classified as *quasi-static* because the analyses are performed when the system is excited by a periodic signal that is very slow compared to the system dynamics (Ikhouane and Rodellar, 2007).

Based on a static analysis of NARX models (4.1), we will show that an additional constraint needs to be considered in the identification procedure in order for Property 4.1 to be satisfied. Thereafter, a quasi-static analysis will be used to describe how hysteresis happens in these models and an illustrative example will be presented.

4.2.1 Static Analysis

By means of static analysis it is possible to determine the fixed points of a model, as described in Definition 2.3. In what follows, the notation of term clusters and cluster coefficients presented in Definition 2.2 is used.

Assumption 4.1. [Systems with hysteresis]. *In order to comply with Property 4.1, following recommendations of the literature, the identified models should not have regressors from the following term clusters:*

(i) Ω_{y^p}, $\Omega_{y^p\phi_1^{q_1}}$ *and* $\Omega_{y^p\phi_2^{q_2}}$ *for* $p > 1$ *and* $\forall q_1, q_2$ *(Aguirre and Mendes, 1996),*

(ii) $\Omega_{\phi_2^{q_2}}$ *for* $q_2 > 1$ *(Martins and Aguirre, 2016),*

as will be shown in this thesis, the following regressors should also be removed:

(iii) $\Omega_{y^p u^m}$ *and* Ω_{u^m} $\forall p, m$.

The steady-state analysis (Remark 2.5) is done by taking $y_k = \bar{y}, \forall k$, $u_k = \bar{u}, \forall k$ and, consequently, $\phi_{1,k} = u_k - u_{k-1} = 0$ and $\phi_{2,k} = \text{sign}(\phi_{1,k}) = 0, \forall k$. For a model that complies with Assumption 4.1, we get $\bar{y} = \Sigma_y \bar{y}$, where Σ_y is the sum of all parameters of all linear output regressors; see Definition 2.2. For the sake of clarity, we discuss the most common case, in which the hysteretic model has only one linear output term: $\hat{\theta}_1 y_{k-1}$ (Martins and Aguirre, 2016; Lacerda Júnior et al., 2019). Hence, the model has only one fixed point for which stability analysis yields the following: if $|\hat{\theta}_1| < 1$ ($|\hat{\theta}_1| > 1$), then $\bar{y} = 0$ is a single asymptotically stable (diverging) equilibria and, as a result, Property 4.1 is not satisfied. To overcome this problem, with Definition 2.5 in mind, the following lemma is stated.

Lemma 4.1. *Given that Assumption 4.1 holds, if* $\hat{\theta}_1 = 1$, *then the identified model has a continuum of solutions at steady-state.*

Proof. The steady-state analysis of a model that satisfies Assumption 4.1 and Lemma 4.1 yields $\bar{y} = \bar{y}$ which is trivially true for any value $\bar{y}$. Hence, the model has a non-hyperbolic fixed point and will display a *continuum of steady-state solutions* which will play the role required by Property 4.1. ■

It is worth mentioning that if the regressors of the term clusters in Assumption 4.1 are not removed, the steady-state analysis and Lemma 4.1 presented above are not assured to the identified models and, consequently, a continuum of steady-state solutions is not achieved by them.

Remark 4.1. Lemma 4.1 guarantees that the model fixed point (Definition 2.3) is non-hyperbolic and in that way it will be able to guarantee multiple steady-state solutions. However, the case of a non-hyperbolic fixed point is known to be structurally unstable. Hence, unless the constraint in Lemma 4.1 is used, the probability of estimating a model with a non-hyperbolic fixed-point is zero. If the model has more than one linear output term, the constraint in Lemma 4.1 becomes $\Sigma_y = 1$ and this will guarantee that the Jacobian matrix has one eigenvalue at 1. In order for the model to have a continuum of steady-state solutions all the remaining eigenvalues of the Jacobian matrix evaluated at the fixed point (Definition 2.4) must have modulus less than one.

4.2.2 Quasi-static Analysis

The core idea of the framework proposed in (Martins and Aguirre, 2016) to identify models with a hysteresis loop is to build a bounding structure $\mathcal{H}$ made of sets of equilibria *and* to ensure that one set is stable during loading and the other one, during unloading; see Property 2.2 and Theorem 2.3. Such a scenario is effective, but it does not help to understand models with more complicated structures and with both attracting and repelling regions in the $u \times y$ plane. This section aims at enlarging the scenario developed in (Martins and Aguirre, 2016).

In quasi-static analysis, it is assumed that the input u_k is a loading-unloading quasi-static signal (Definition 2.9) that is much slower than the system dynamics to the point that, at a given time k, the system will be in a certain *attracting* region, avoiding any possible *repelling* regions. Also, such regions depend on u_k, $\phi_{1,k}$ and $\phi_{2,k}$. More specifically, there will be one or two sets of regions during loading and the same number of sets during unloading. We discuss the case where there will be two sets of regions, since the occurrence of only one set is a special case of it.

For quasi-static analysis, we assume that $y_k \approx y_{k-j} = \tilde{y}$, $j = 1, 2, \ldots, n_y$, such that (4.1) is given by:

$$\tilde{y} \approx F^{\ell}\Big(\tilde{y}, u_{k-\tau_d}, \cdots, u_{k-n_u}, \phi_{1,k-\tau_d}, \cdots, \phi_{1,k-n_{\phi_1}}, \phi_{2,k-\tau_d}, \cdots, \phi_{2,k-n_{\phi_2}}\Big), \tag{4.3}$$

which can be usually solved for $\tilde{y}$, especially if higher powers of the output, i.e. Ω_{y^p} for $p > 1$, are not in $F^{\ell}(\cdot)$ (Aguirre and Mendes, 1996). This is achieved in practice by

removing such term clusters from the set of candidates as done in Assumption 4.1. If the inputs are all constant, then $\tilde{y}$ will depend on such values.

Given a quasi-static input, if $\tilde{y}$ is in an attractive region, then the model output moves towards an attracting solution. In what follows, $\tilde{y}^{\mathrm{a}}_{\mathrm{L}}$ and $\tilde{y}^{\mathrm{a}}_{\mathrm{U}}$ are, respectively, the solutions to (4.3) in attracting regions under loading and unloading; $\tilde{y}^{\mathrm{r}}_{\mathrm{L}}$ and $\tilde{y}^{\mathrm{r}}_{\mathrm{U}}$ are the counterparts in repelling regions. The conditions for $\tilde{y}$ to be attracting is:

$$\left|\mathrm{eig}\left(\frac{\partial F^{\ell}\left(\mathbf{y}, u_{k-\tau_{\mathrm{d}}}, \cdots, u_{k-n_u}, \phi_{1,k-\tau_{\mathrm{d}}}, \cdots, \phi_{1,k-n_{\phi_1}}, \phi_{2,k-\tau_{\mathrm{d}}}, \cdots, \phi_{2,k-n_{\phi_2}}\right)}{\partial \mathbf{y}}\right)\right| < 1, \tag{4.4}$$

where $\mathbf{y} = [y_{k-1} \ \ldots \ y_{k-n_y}]^T$. This procedure resembles that of determining the stability of fixed points (Aguirre and Mendes, 1996). Here the Jacobian matrix is not evaluated at fixed points, as described in Definition 2.4. Hence, we do not speak in terms of stable and unstable fixed points.

To illustrate how this helps to understand the formation of a hysteresis loop, consider the schematic representation in Figure 4.1. The input is a loading-unloading signal such that $u_{\min} \leq u_k \leq u_{\max}$, $\forall k$. The sets $\tilde{y}^{\mathrm{a}}_{\mathrm{L}}$, $\tilde{y}^{\mathrm{a}}_{\mathrm{U}}$, $\tilde{y}^{\mathrm{r}}_{\mathrm{L}}$ and $\tilde{y}^{\mathrm{r}}_{\mathrm{U}}$ are shown. Consider the point A, which takes place under loading, hence only solutions $\tilde{y}^{\mathrm{r}}_{\mathrm{L}}$ and $\tilde{y}^{\mathrm{a}}_{\mathrm{L}}$ are active and should be considered. Given that the system is under the direct influence of $\tilde{y}^{\mathrm{r}}_{\mathrm{L}}$, which is responsible for pushing upwards (see vertical component y_{A}), and it is the loading regime, there is a horizontal component u_{A} (related to the input) that points to the right. The resulting effect is to pull the system along the loop in the NE direction. The same can be said for point B; however, at that point the vertical component is the result of the attracting action of $\tilde{y}^{\mathrm{a}}_{\mathrm{L}}$. A similar analysis can be readily done for the unloading regime, given by points D and E. At the turning points C and F, $\phi_{2,k}$ switches from 1 to -1 and from -1 to 1, respectively. Hence, the analysis also switches from using $\tilde{y}^{\mathrm{a}}_{\mathrm{L}}$ and $\tilde{y}^{\mathrm{r}}_{\mathrm{L}}$, to using $\tilde{y}^{\mathrm{a}}_{\mathrm{U}}$ and $\tilde{y}^{\mathrm{r}}_{\mathrm{U}}$. This analysis will be useful in Chapter 5 to understand the formation of hysteresis loops in identified models.

It is important to point out that the assumption that the set $\tilde{y}$ comes in two disjoint parts, either for loading or unloading, is a consequence of the solution of (4.3) being rational instead of polynomial. This is useful to analyze models with more general model structures. In addition, a NARX polynomial model, due to its simplicity, is typically unable to reproduce a number of aspects found in more sophisticated hysteretic models, as in the Preisach model (Ge and Jouaneh, 1996) and in the Masing model (Jayakumar, 1987) that present some more subtle aspects of hysteresis.

The constraint in Lemma 4.1 enables the model to "remember" its last state and remain there even when the input becomes constant (this was not the case in (Martins and Aguirre, 2016)). Also, since the hysteresis branches are here formed as a result of the position of fixed points, which depend on the model parameters which are fixed in this work, so is the hysteresis loop. In order to enable the model to follow other branches, as seen in the Preisach model, we would need some mechanism for updating

parameters recursively; see Section 2.3.5. This is not a concern in this work.

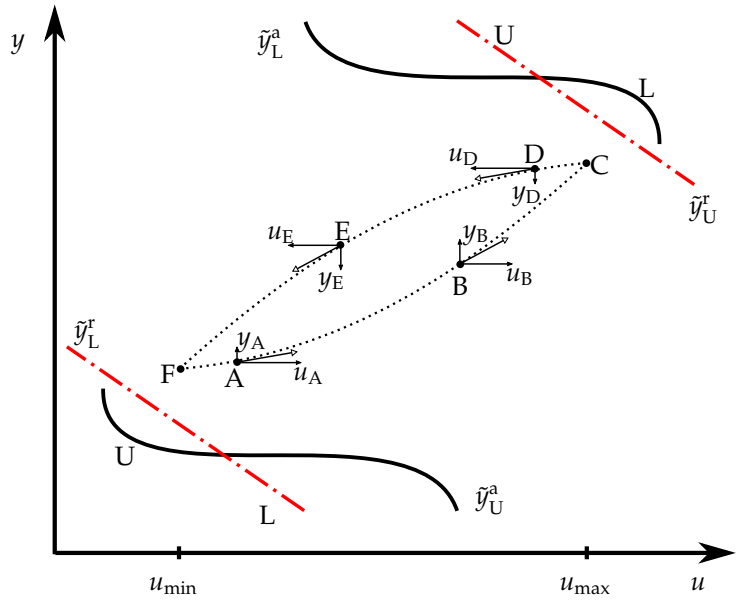

Figure 4.1: Schematic representation of hysteresis loop in the $u \times y$ plane. Attracting sets are shown in black continuous lines, whereas the repelling sets are indicated in red dash-dot. The hysteresis loop is indicated by dotted lines.

The following example illustrates the application of this analysis.

Example 4.1. Static and Quasi-static Analysis to Identify Hysteretic Models.

Consider the following NARX model that complies with Assumption 4.1:

$$\begin{aligned} y_k &= \hat{\theta}_1 y_{k-1} + \hat{\theta}_2 \phi_{1,k-1} + \hat{\theta}_3 \phi_{2,k-1}\phi_{1,k-1} u_{k-1} + \hat{\theta}_4 \phi_{2,k-1}\phi_{1,k-1} y_{k-1} + \hat{\theta}_5 \phi_{1,k-1} u^2_{k-1} \\ &\quad + \hat{\theta}_6 \phi_{1,k-1} u_{k-1} y_{k-1}. \end{aligned} \tag{4.5}$$

In order to ensure that such a model has a continuum of steady-state solutions, according to Lemma 4.1, the constraint $\hat{\theta}_1 = 1$ might be achieved using estimator (2.48) with $c = 1$ and $S = [1\ 0\ 0\ 0\ 0\ 0]$.

For a more complicated model structure, the constraint in Lemma 4.1 is still in the form $1 = S\boldsymbol{\theta}$ (2.47) but with S having more that one element equal to one, e.g. as shown in (Aguirre, 2014) to obtain NARX models able to reproduce dead-zone and in (Aguirre et al., 2004) for a quadratic nonlinearity.

The quasi-static analysis of model (4.5) is performed following the steps provided in Section 4.2.2. So rewriting this model as (4.3), we have:

$$\tilde{y} \approx \hat{\theta}_1 \tilde{y} + \hat{\theta}_2 \phi_{1,k-1} + \hat{\theta}_3 \phi_{2,k-1}\phi_{1,k-1} u_{k-1} + \hat{\theta}_4 \phi_{2,k-1}\phi_{1,k-1} \tilde{y} + \hat{\theta}_5 \phi_{1,k-1} u^2_{k-1} + \hat{\theta}_6 \phi_{1,k-1} u_{k-1} \tilde{y},$$

which can be described by:

$$\tilde{y}(u,\phi_1,\phi_2) \approx \begin{cases} \dfrac{\hat{\theta}_2\phi_1 + \hat{\theta}_3\phi_1 u + \hat{\theta}_5\phi_1 u^2}{1 - \hat{\theta}_1 - \hat{\theta}_4\phi_1 - \hat{\theta}_6\phi_1 u}, & \text{for } \phi_2 = 1; \\ \dfrac{\hat{\theta}_2\phi_1 - \hat{\theta}_3\phi_1 u + \hat{\theta}_5\phi_1 u^2}{1 - \hat{\theta}_1 + \hat{\theta}_4\phi_1 - \hat{\theta}_6\phi_1 u}, & \text{for } \phi_2 = -1, \end{cases} \tag{4.6}$$

where the time indices have been omitted for simplicity. Therefore, the solution given at the top in (4.6) represents the set $\tilde{y}_\mathrm{L}$, while the bottom is the set $\tilde{y}_\mathrm{U}$.

To define whether the solutions to (4.6) are in the attracting or repelling regions, (4.4) should be computed for model (4.5). This yields:

$$\begin{aligned} -1 < \quad & \hat{\theta}_1 + \hat{\theta}_4\phi_{2,k-1}\phi_{1,k-1} + \hat{\theta}_6\phi_{1,k-1}u_{k-1} \quad < 1, \\ \frac{-1 - \hat{\theta}_1 - \hat{\theta}_4\phi_{2,k-1}\phi_{1,k-1}}{\hat{\theta}_6\phi_{1,k-1}} < \quad & u_{k-1} \quad < \frac{1 - \hat{\theta}_1 - \hat{\theta}_4\phi_{2,k-1}\phi_{1,k-1}}{\hat{\theta}_6\phi_{1,k-1}}. \end{aligned} \tag{4.7}$$

Since it is assumed that the input u_k is a loading-unloading signal, the conditions (4.7) to ensure that the solutions (4.6) are in attracting regions can be readily verified numerically. For illustration purposes, consider model (4.5) with parameters: $\hat{\theta}_1$=1.00, $\hat{\theta}_2$=0.77, $\hat{\theta}_3$=1.42×10^{-2}, $\hat{\theta}_4$=-9.60×10^{-3}, $\hat{\theta}_5$=3.16×10^{-4}, and $\hat{\theta}_6$=-2.47×10^{-4}. Also, suppose that the input signal is u_k=70 sin($2\pi k$) with a sampling time of T_s = 0.001 s. Based on these assumptions, Figure 4.2 shows the hysteresis loop obtained with model (4.5) and some additional points in this loop, similar to those in Figure 4.1, used to highlight the influence of the attracting and repelling regions.

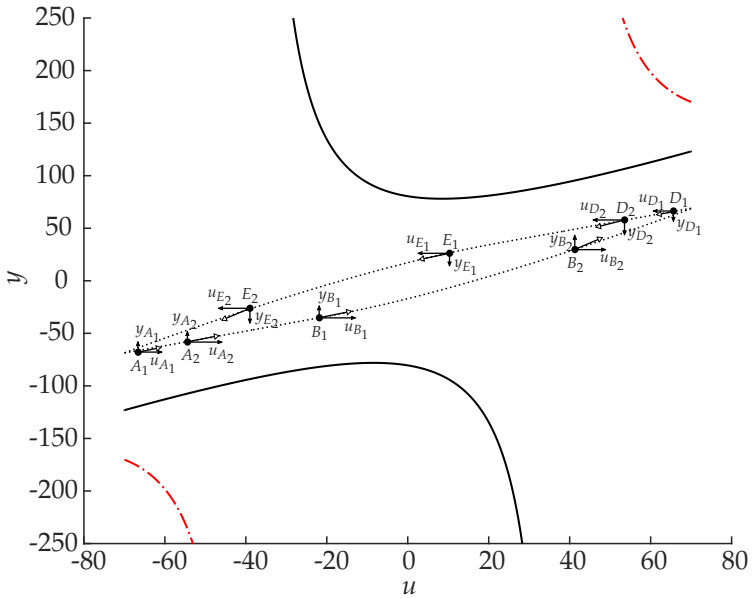

Figure 4.2: Quasi-static analysis for model (4.5). The hysteresis loop indicated with (···) is a result of the interaction of (—) attracting ($\tilde{y}^\mathrm{a}_\mathrm{L}$, $\tilde{y}^\mathrm{a}_\mathrm{U}$) and (-·-) repelling ($\tilde{y}^\mathrm{r}_\mathrm{L}$, $\tilde{y}^\mathrm{r}_\mathrm{U}$) sets, calculated from (4.6) and (4.7), with the input signal u. Compare to Figure 4.1.

Figure 4.3 shows a more detailed picture, compared to Figure 4.2, of how the solutions (4.6), which are responsible for attracting (∗) and repelling (□) the output (•) of

model (4.5), influence the formation of the hysteresis loop $(\cdots)$ for this model. It is noteworthy that from Figure 4.3(a) to Figure 4.3(e) are presented the results obtained with the input signal under the loading regime, while from Figure 4.3(f) to Figure 4.3(j) are those for the unloading regime. Note that the calculated results are given for two specific input values (see left side of Figure 4.3), for the range of input values that produce only regions of attracting or repelling (see middle column of Figure 4.3), and for the case where both regions are combined (see right side of Figure 4.3). Also, note that Figure 4.2 is the combination of the results presented in Figures 4.3(e) and 4.3(j).

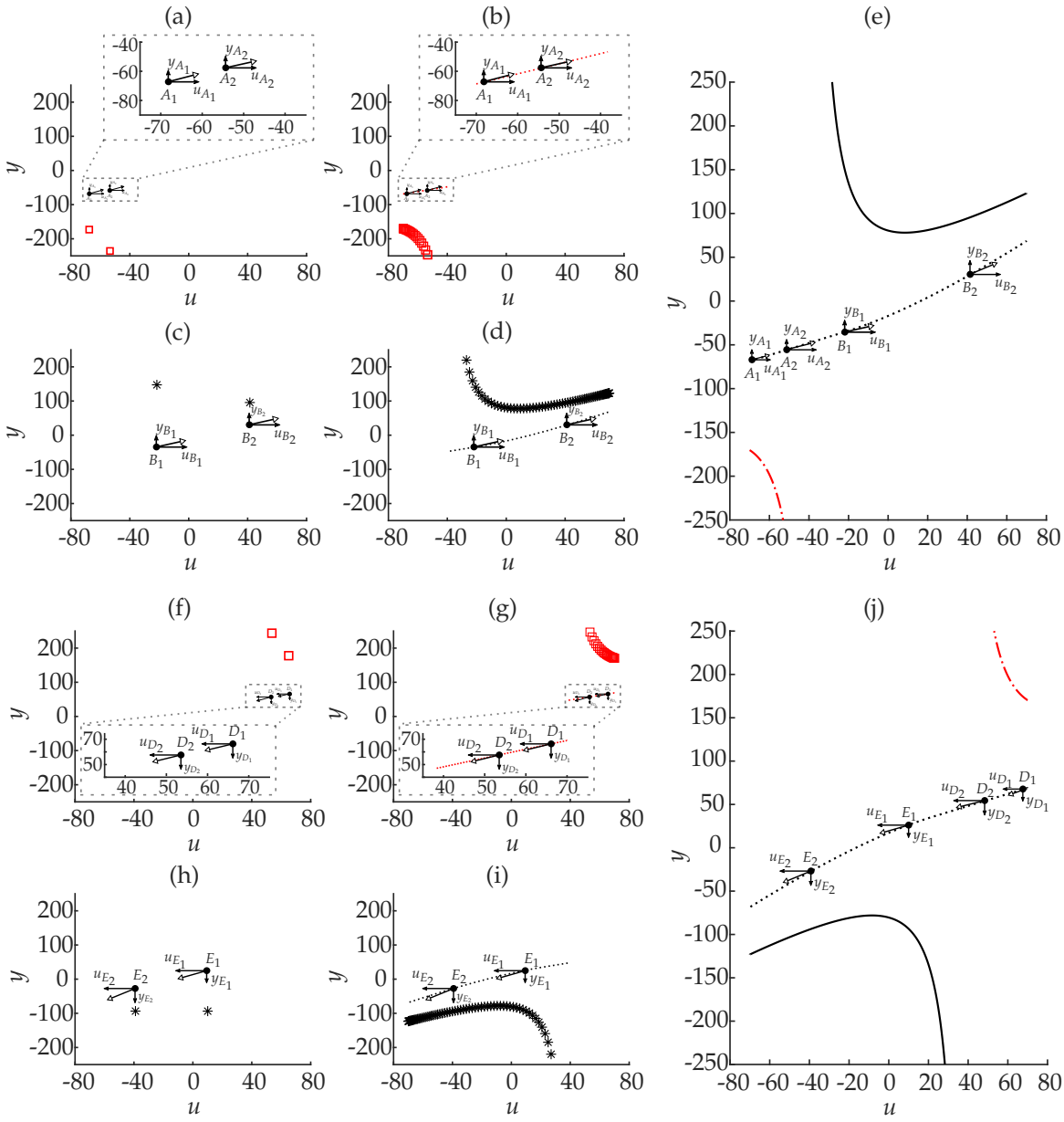

Figure 4.3: A more detailed view of the results shown in Figure 4.2. (•) refers to some specific output values calculated from a given input value u_k under loading, in (a)-(e), or unloading, in(f)-(j), for which the corresponding solutions of (4.6) attract (∗) or repel (□) the output $(\cdots)$. (—) refers to the set formed by the solutions that attract, while (- - -) by the solutions that repel.

It should be remembered that, as mentioned earlier, there will be one or two sets of regions during loading and unloading, and that the framework raised in Section 4.2.2 does not change regardless of the number of sets of regions. In the present example, the hysteresis loop for model (4.5) is the result of the interaction of two sets of regions that appear for loading and another two sets for unloading, with one set referring to an attracting region and the other to a repelling one; see Figures 4.2 and 4.3. In order to illustrate a case where there is only one set of regions during loading and unloading, assume that model (4.5) is composed only of the first *five* terms and their corresponding parameter values that were defined above. After performing the quasi-static analysis in this new model, similar to what was done above for model (4.5), it is possible to obtain the results shown in Figure 4.4.

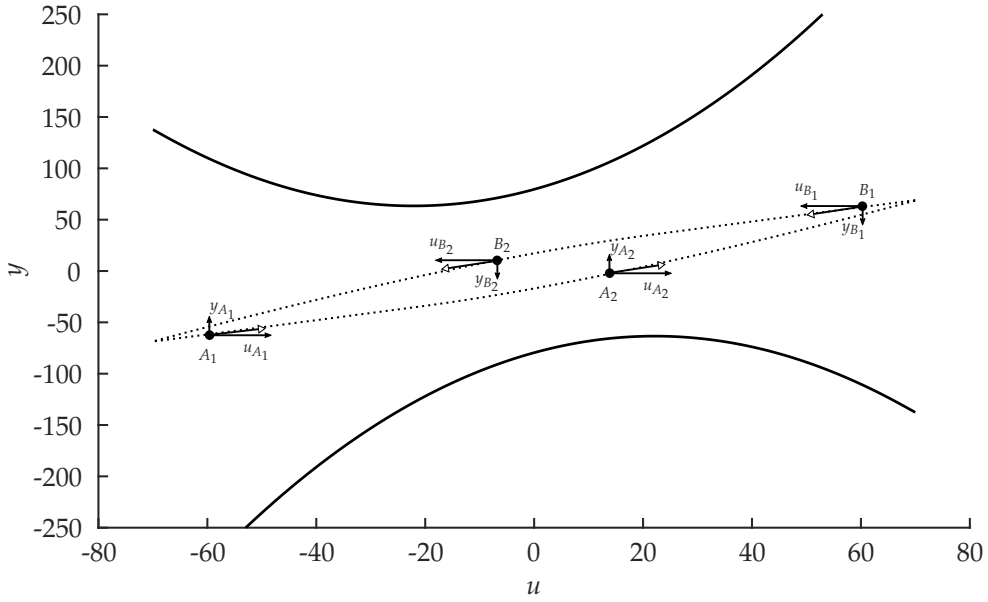

Figure 4.4: Quasi-static analysis for a model composed of the first five terms of model (4.5) with input u_k=70 sin($2\pi k$). For meaning of line patterns refer to captions of Figures 4.1 and 4.2.

As can be seen in Figure 4.4, the hysteresis loop obtained with the investigated model is the result of the interaction of attracting sets with the input signal, which also helps to explain how such models are able to describe hysteresis.

In Chapter 5, the static and quasi-static analysis will be performed for the identified models. △

4.3 Preliminary Statements for Compensator Design

Given a dynamical nonlinear system $\mathcal{S}$, the first step is to obtain representative models for $\mathcal{S}$; Figure 4.5(a). In the second step, the identified model is used to design a compensator C that yields the compensation signal m_k for a given reference r_k. Thus, the aim is that the use of the designed compensator C in cascade with the system $\mathcal{S}$,

in an open-loop scheme as shown in Figure 4.5(b), leads to a system with more linear dynamic behavior (i.e. $y_k \approx r_k$) and, therefore, more amenable for control as previously discussed in Section 3.2.

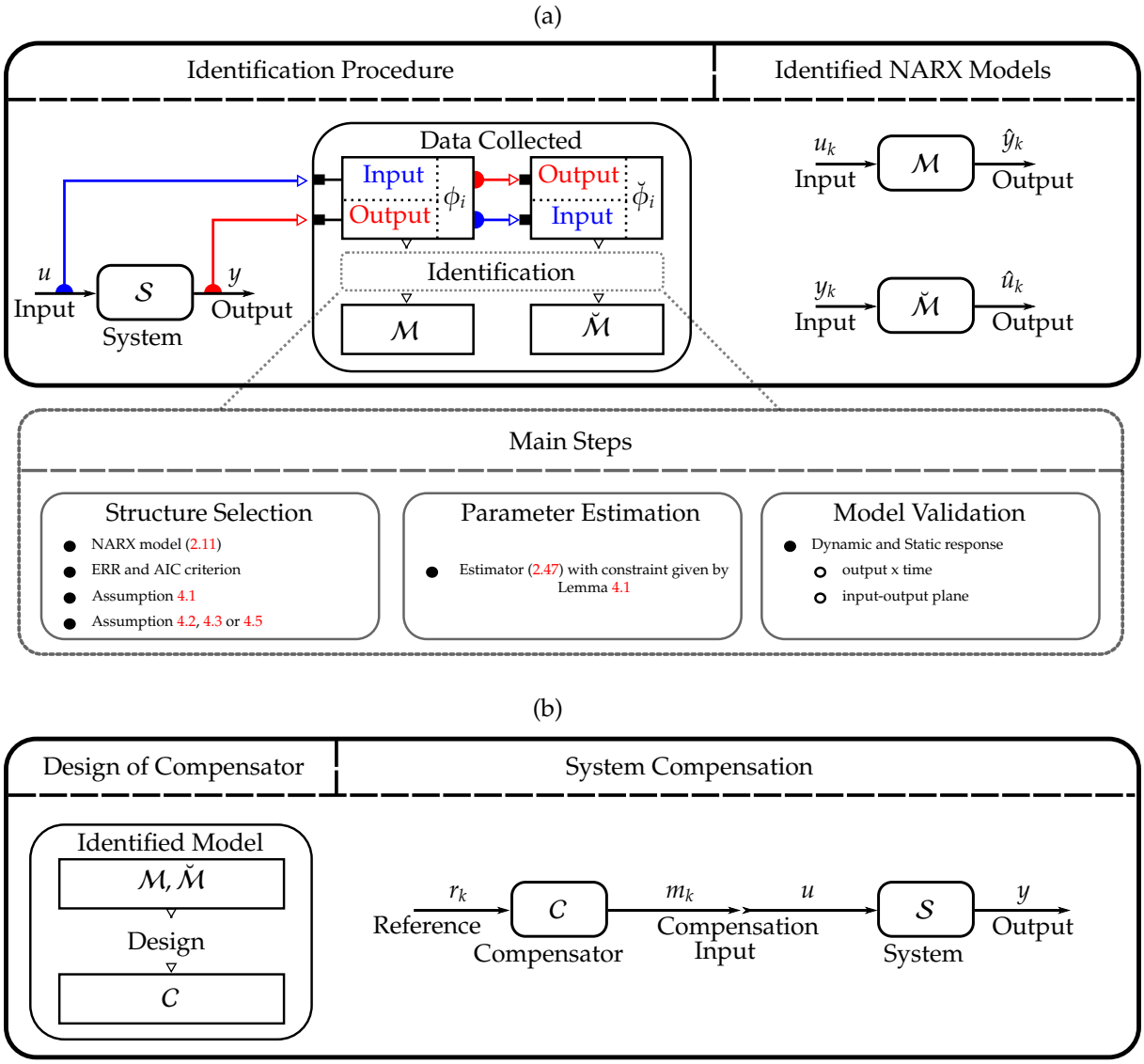

Figure 4.5: Schematic representation of the steps adopted for the design of compensators based on identified NARX models. (a) Model identification, and (b) compensator design based on identified models. $\mathcal{M}$ and $\check{\mathcal{M}}$ are models built to estimate, respectively, the output y and input u signal of the system $\mathcal{S}$.

In this context, three approaches are proposed. The first two design a compensator from a model $\mathcal{M}$ identified from u, y and, optionally, additional regressors ϕ_i, with output $\hat{y}_k$; see Figure 4.5(a). It should be remembered that u and y are assumed to be collected from a system $\mathcal{S}$, while regressors ϕ_i can be readily calculated from these measurements. These two approaches follow a philosophy similar to that reviewed in Section 3.2.1, which intends to design a compensator C through the construction of an

inverse function for model $\mathcal{M}$, so that the compensation input m_k can be obtained by solving such compensator dynamically. Specifically, the first one aims at rewriting $\mathcal{M}$ as an algebraic polynomial with the unknown variable being m_k and thus the polynomial roots correspond to possible compensation input values at a time k; see Section 4.4. The second approach consists of assigning constraints during the structure selection step (Section 2.3.4) of the model $\mathcal{M}$ so that the compensation input m_k can be isolated when such model is rewritten as a compensator; see Section 4.5. Finally, following a philosophy similar to that reviewed in Section 3.2.2, the third proposed approach is based on a model of the inverse relationship, in which case a model $\breve{\mathcal{M}}$ is obtained to yield $\hat{u}_k$; see Figure 4.5(a) and Section 4.6. Some of the algorithms and considerations adopted in the three main steps of system identification are also outlined in Figure 4.5(a).

In this thesis, the following remark and subsequent assumptions are made for NARX polynomial models (2.12).

Remark 4.2. For design, in models $\mathcal{M}$ and $\breve{\mathcal{M}}$, y_k is replaced by r_k, and u_k by m_k, respectively. The motivation behind this is that y_k should ideally be equal to r_k under compensation, that is, when m_k is used as the input to the dynamical system.

4.4 Roots of an Algebraic Polynomial

In this approach, the main idea is to algebraically manipulate an identified model $\mathcal{M}_{\mathrm{R}}$ in such way that it yields a polynomial in which the unknown variable is m_k. From Remark 4.2 and omitting the additional term $\phi_{i,k}$, $\mathcal{M}_{\mathrm{R}}$ (2.12) can be written as:

$$r_{k+\tau_{\mathrm{d}}} = F^{\ell}\Big(r_{k+\tau_{\mathrm{d}}-1}, \cdots, r_{k+\tau_{\mathrm{d}}-n_y}, m_k, \cdots, m_{k+\tau_{\mathrm{d}}-n_u}\Big), \tag{4.8}$$

which, for convenience, has been written τ_{d} instants of time ahead, i.e. $k \to k+\tau_{\mathrm{d}}$ – meaning that k is replaced by $k+\tau_{\mathrm{d}}$.

Remark 4.3. The methodologies for the three compensation approaches proposed in this chapter will not change with the inclusion of $\phi_{i,k}$, since they might be easily adapted when this regressor is defined a priori, e.g. $\phi_{1,k} = u_k - u_{k-1}$. In such cases, only a proper mathematical manipulation of the predefined additional regressor $\phi_{i,k}$ is needed during compensator design, and so we choose to omit it for simplicity.

As aforementioned, the aim is to find m_k that will drive the system to the desired target r_k, i.e. $y_k \approx r_k$. For this purpose, (4.8) is expressed in terms of a polynomial in the unknown variable m_k as:

$$c_{\ell_m,k} m_k^{\ell_m} + c_{\ell_m-1,k} m_k^{\ell_m-1} + \cdots + c_{1,k} m_k + c_{0,k} = 0 \tag{4.9}$$

where $1 \leq \ell_m \leq \ell$ is the degree of the dynamic compensator C (4.9), whose time-varying coefficients ($c_{j_c,k}$ for $j_c = 0, 1, \ldots, \ell_m$) can depend on past values of m up to time $k-1$,

and on past and future values of r up to time $k+\tau_d$. Hence, the following assumption is needed.

Assumption 4.2. *It is assumed that: (i) the compensation signal m_k is known up to time $k-1$; and (ii) the reference r_k is known up to time $k+\tau_d$.*

The following example illustrates this procedure.

Example 4.2. Design of a Polynomial Compensator.
Consider the following NARX model $\mathcal{M}_R$:

$$y_k=\hat{\theta}_1 y_{k-1} + \hat{\theta}_2 u_{k-1} + \hat{\theta}_3 u_{k-1}u_{k-2} + \hat{\theta}_4 u_{k-1}^2 + \hat{\theta}_5 u_{k-1}^3, \tag{4.10}$$

for which τ_d=1, n_y=1, n_u=2, and ℓ=3. From Remark 4.2, this model is rewritten as:

$$r_{k+1}=\hat{\theta}_1 r_k + \hat{\theta}_2 m_k + \hat{\theta}_3 m_k m_{k-1} + \hat{\theta}_4 m_k^2 + \hat{\theta}_5 m_k^3,$$

which is in the form (4.8) and, therefore, can be expressed in the format of (4.9) as:

$$\underbrace{[\hat{\theta}_5]}_{c_{3,k}} m_k^3 + \underbrace{[\hat{\theta}_4]}_{c_{2,k}} m_k^2 + \underbrace{[\hat{\theta}_2 + \hat{\theta}_3 m_{k-1}]}_{c_{1,k}} m_k + \underbrace{[\hat{\theta}_1 r_k - r_{k+1}]}_{c_{0,k}} = 0, \tag{4.11}$$

where, because Assumption 4.2 is satisfied, all values of r and all past values of m are known. Hence, at each time step k the solutions to (4.11), i.e. the three values of m_k, are the potential compensation inputs. A practical problem is to decide which of the three roots in this example should be used. If there is only one real root, then it is chosen as the compensation input. However, if there are three real roots, a more general decision-making process is required. △

It is important to note that, although the ℓ_m values of m_k are solutions/roots of the compensator (4.9), not all m_k are appropriate to be used in practice. Therefore, assuming that the investigated system $\mathcal{S}$ can only be excited by input signals u_k whose amplitudes are within the range of $u_{min} \leq u_k \leq u_{max}$, $\forall k$, the following property must be considered.

Property 4.2. *A viable root, in practical terms, has a real value that is consistent with the amplitude range of the investigated system.*

Note that Property 4.2 removes possible complex roots and real ones outside the range of the investigated system. In this way, the proposed decision-making process to determine the root to be used as the compensation input m_k is defined below.

Definition 4.1. [The decision-making process]. *Let* $\boldsymbol{m}_k \triangleq [m_{1,k} \ \cdots \ m_{\ell_m,k}]^T$ *be the set of roots of (4.9). If only one element of* $\boldsymbol{m}_k$ *satisfies Property 4.2, then this element will be the compensation input at time k, otherwise we choose the root according to:*

$$m_k = \underset{m_{j,k},\ \forall j\in\{1,\ldots,\ell_m\}}{\arg\min} \Big(|m_{j,k} - m_{k-1}|\Big), \tag{4.12}$$

$$\text{subject to}: \begin{cases} m_{j,k} \in \mathbb{R}, \\ u_{\min} \leq m_{j,k} \leq u_{\max}. \end{cases}$$

If $\boldsymbol{m}_k$ *is composed only of complex conjugate values, which can happen when* ℓ_m *is even, or of roots that do not satisfy the above constraints, then* m_k=m_{k-1} *will be used. The use of (4.12) selects the solution* $m_{j,k}$ *that is closest to the compensation value used in the previous time step, i.e.* m_{k-1}*. This simple criterion results in smoother signals* m_k *and, consequently, in less compensation effort.*

It is interesting to note that the decision-making process (Definition 4.1) may present a singularity when none of the possible roots $\boldsymbol{m}_k$ satisfies the constraints of (4.12), in which case m_k=m_{k-1} is considered. However, as pointed out in (Tavares et al., 2022), the appearance of such a singularity in this compensation approach tends not to happen when the identified process model is able to accurately describe the system, as seen for the systems investigated in it. On the other hand, when considering the methodologies proposed in (Leva and Piroddi, 2002; Lacerda Júnior et al., 2019) to construct an inverse function of the identified models (i.e. compensators), such as those shown in (3.1) and (3.2), the simple fact that the input signal becomes constant would lead to a singularity. Therefore, although there is a kind of singularity in the decision-making process proposed above, its occurrence is less likely than that discussed in Section 3.2.1 for compensators (3.1) and (3.2) (Leva and Piroddi, 2002; Lacerda Júnior et al., 2019).

Compensation of Hysteretic Systems

As stated in Remark 4.3, when it comes to designing compensators using identified NARX models that have some predefined additional regressor $\phi_{i,k}$, a proper mathematical manipulation of such a regressor is needed. Therefore, in order to design compensators using hysteretic models (4.1), which are also symbolized as $\mathcal{M}_{\mathrm{R}}$ in this approach, some recommendations and adaptations that should be considered in the present methodology are provided here.

First, it should be noted that the additional regressors (4.2) only become available for non-constant inputs, since for any constant input given by $u_k = \bar{u}, \forall k$, then $\phi_{1,k} = u_k - u_{k-1} = 0$ and $\phi_{2,k} = \text{sign}(\phi_{1,k}) = 0, \forall k$. Therefore, it is considered that the hysteretic models are under loading-unloading inputs and, thus, $\phi_{1,k} > 0$ and $\phi_{2,k} = 1$ for the loading regime, while $\phi_{1,k} < 0$ and $\phi_{2,k} = -1$ for the unloading regime; see Remark 2.15. With this in mind, the compensator C can be developed by following the *steps* below:

1. Rewrite the identified model (4.1) so that it explicitly shows the additional regressors (4.2), i.e. *replace* $\phi_{1,k}$ *with* $[u_k - u_{k-1}]$ *and* $\phi_{2,k}$ *with* $\text{sign}(u_k - u_{k-1})$;

2. From Remark 4.2 and performing the time-shift $k \to k + \tau_\text{d}$, rewrite this equation in the form (4.8);

3. To express this equation in the format of (4.9), assume that $\text{sign}(m_k - m_{k-1}) = 1$ for m_k in loading regime, while $\text{sign}(m_k - m_{k-1}) = -1$ for m_k in unloading regime, i.e. *the only term that prevents the unknown variable* m_k *from being made explicit is properly transformed*, thus yielding:

$$\begin{cases} c^{\text{L}}_{\ell_m,k} m_k^{\ell_m} + c^{\text{L}}_{\ell_m-1,k} m_k^{\ell_m-1} + \cdots + c^{\text{L}}_{1,k} m_k + c^{\text{L}}_{0,k} = 0, & \text{for} \quad m_k > m_{k-1} \quad \text{(loading)}, \quad (4.13) \\ c^{\text{U}}_{\ell_m,k} m_k^{\ell_m} + c^{\text{U}}_{\ell_m-1,k} m_k^{\ell_m-1} + \cdots + c^{\text{U}}_{1,k} m_k + c^{\text{U}}_{0,k} = 0, & \text{for} \quad m_k < m_{k-1} \quad \text{(unloading)}, \quad (4.14) \end{cases}$$

where the superscripts L and U refer to loading and unloading regimes, respectively. Because now the system is hysteretic, (4.9) has two counterparts: one for loading (4.13), and one for unloading (4.14). In this case, the compensation input m_k will be a feasible root of (4.13) or (4.14). Before detailing the decision-making process, the previous steps are illustrated in the following example.

Example 4.3. Design of a Polynomial Hysteretic Compensator.

Consider the same hysteretic model (4.5) that was used in Example 4.1. Following step 1, (4.5) is rewritten as:

$$\begin{aligned} y_k = &\hat{\theta}_1 y_{k-1} + \hat{\theta}_2 \text{sign}(u_{k-1} - u_{k-2}) + \hat{\theta}_3 [u_{k-1} - u_{k-2}] u_{k-1} + \hat{\theta}_4 \text{sign}(u_{k-1} - u_{k-2}) [u_{k-1} - u_{k-2}] y_{k-1} \\ &+ \hat{\theta}_5 [u_{k-1} - u_{k-2}]. \end{aligned}$$

Applying step 2 in this model, we get (remember that $\tau_\text{d} = 1$):

$$\begin{aligned} r_{k+1} = &\hat{\theta}_1 r_k + \hat{\theta}_2 \text{sign}(m_k - m_{k-1}) + \hat{\theta}_3 [m_k - m_{k-1}] m_k + \hat{\theta}_4 \text{sign}(m_k - m_{k-1}) [m_k - m_{k-1}] r_k \\ &+ \hat{\theta}_5 [m_k - m_{k-1}], \end{aligned}$$

which can be split into two polynomials using step 3, i.e. replace $\text{sign}(m_k - m_{k-1})$ with 1 or with -1 by assuming m_k in the loading or unloading regime, respectively, so that:

$$\underbrace{[\hat{\theta}_3]}_{c^{\text{L}}_{2,k}} m_k^2 + \underbrace{[\hat{\theta}_5 + \hat{\theta}_4 r_k - \hat{\theta}_3 m_{k-1}]}_{c^{\text{L}}_{1,k}} m_k + \underbrace{[\hat{\theta}_1 r_k - r_{k+1} + \hat{\theta}_2 - \hat{\theta}_4 r_k m_{k-1} - \hat{\theta}_5 m_{k-1}]}_{c^{\text{L}}_{0,k}} = 0, \quad \text{for} \quad m_k > m_{k-1}, \quad (4.15)$$

$$\underbrace{[\hat{\theta}_3]}_{c^{\text{U}}_{2,k}} m_k^2 + \underbrace{[\hat{\theta}_5 - \hat{\theta}_4 r_k - \hat{\theta}_3 m_{k-1}]}_{c^{\text{U}}_{1,k}} m_k + \underbrace{[\hat{\theta}_1 r_k - r_{k+1} - \hat{\theta}_2 + \hat{\theta}_4 r_k m_{k-1} - \hat{\theta}_5 m_{k-1}]}_{c^{\text{U}}_{0,k}} = 0, \quad \text{for} \quad m_k < m_{k-1}. \quad (4.16)$$

Here, (4.15) refers to loading regime similar to form (4.13), while (4.16) refers to unloading regime in form (4.14). Therefore, because Assumption 4.2 is satisfied, the roots of these two polynomials can be computed. △

In terms of the decision-making process for choosing the root to be used as the compensation input m_k for hysteretic systems, some adaptations are made in Definition 4.1 in order to adequately deal with the two existing compensators (4.13) and (4.14), which must be used if m_k is in the loading or unloading regime, respectively. For this purpose, the following process is defined.

Definition 4.2. [The decision-making process for hysteretic systems]. *Let the set of roots be arranged as* $\boldsymbol{m}_k \triangleq \left[m^{\mathrm{L}}_{1,k} \ \cdots \ m^{\mathrm{L}}_{\ell_m,k} \ m^{\mathrm{U}}_{\ell_m+1,k} \ \cdots \ m^{\mathrm{U}}_{2\ell_m,k}\right]^T$, *in which the j-th root* $m^{(\bullet)}_{j,k}$ *is one of its first* ℓ_m *roots* $m^{\mathrm{L}}_{j,k}$ *calculated from (4.13), for the loading regime, or one of its last* ℓ_m *roots* $m^{\mathrm{U}}_{j,k}$ *calculated from (4.14), for the unloading regime. In order to choose the appropriate root to be used as the compensation input* m_k *at a time k, the following optimization problem is specified:*

$$m_k = \underset{m^{(\bullet)}_{j,k},\ \forall j\in\{1,\ldots,2\ell_m\}}{\arg\min} \left(|m^{(\bullet)}_{j,k} - m_{k-1}|\right), \tag{4.17}$$

$$\text{subject to}: \begin{cases} m^{(\bullet)}_{j,k} \in \mathbb{R}, \\ u_{\min} \leq m^{(\bullet)}_{j,k} \leq u_{\max}, \\ \begin{cases} m^{\mathrm{L}}_{j,k} > m_{k-1}, & \text{for} \quad j \in \{1,\cdots,\ell_m\}, \quad \text{OR} \\ m^{\mathrm{U}}_{j,k} < m_{k-1}, & \text{for} \quad j \in \{\ell_m+1,\cdots,2\ell_m\}. \end{cases} \end{cases}$$

If $\boldsymbol{m}_k$ *is composed only of complex conjugate values, which can happen when* ℓ_m *is even, or of roots that do not satisfy the above constraints, then* $m_k{=}m_{k-1}$ *will be used. The first two constraints are necessary to comply with Property 4.2, while the last two ensure that the root is consistent with the regime for which it was calculated. The use of (4.17) selects the solution* $m^{(\bullet)}_{j,k}$ *that is closest to the compensation value used in the previous time step, i.e.* m_{k-1}. *This simple criterion results in smoother signals* m_k *and, consequently, in less compensation effort.*

A more detailed analysis of this compensation approach with some tips on the initial compensator conditions, as well as the formulation of this approach to deal with the compensation of static nonlinearities, are provided in (Tavares, 2020; Tavares et al., 2022). These references provide some additional results from our collaborative efforts in terms of developing compensation approaches.

4.5 Isolating the Compensation Input

In what follows, the main idea is to specify a general model structure for $\mathcal{M}_{\mathrm{I}}$ to determine the compensation input m_k. The following assumption is needed.

Assumption 4.3. [The general case]. *It is assumed that: (i) the only regressor involving $u_{k-\tau_d}$ is linear; (ii) $n_u > \tau_d$; (iii) the compensation signal m_k is known up to time $k-1$; and (iv) the reference r_k is known up to time $k+\tau_d$.*

Assumption 4.3 imposes conditions on the selection of the model structure; Figure 4.5(a). Note that (i) ensures that $u_{k-\tau_d}$ can be isolated; (ii) allows having as regressors input terms with a delay greater than τ_d; and the other constraints guarantee that the control action can be computed from known values. Therefore, the model $\mathcal{M}_I$ is rewritten as:

$$A(q)y_k = B(q)u_k + f\Big(y_{k-1}, \cdots, y_{k-n_y}, u_{k-\tau_d-1}, \cdots, u_{k-n_u}\Big), \tag{4.18}$$

where q^{-1} is the backward time-shift operator such that $q^{-1}u_k = u_{k-1}$, and the linear regressors are grouped in $A(q)y_k$ and $B(q)u_k$ with:

$$A(q) = 1 - a_1 q^{-1} - a_2 q^{-2} - \cdots - a_{n_y} q^{-n_y}, \tag{4.19}$$

$$B(q) = b_{\tau_d} q^{-\tau_d} + \underbrace{b_{\tau_d+1} q^{-\tau_d-1} + \cdots + b_{n_u} q^{-n_u}}_{B^*(q)}, \tag{4.20}$$

and $f(\cdot)$ includes all the nonlinear terms and possibly the constant term of the NARX model (2.12). As before, the additional term $\phi_{i,k}$ has been omitted for simplicity (see Remark 4.3). Using (4.20), model (4.18) can be rewritten as:

$$A(q)y_k = b_{\tau_d}u_{k-\tau_d} + B^*(q)u_k + f\Big(y_{k-1}, \cdots, y_{k-n_y}, u_{k-\tau_d-1}, \cdots, u_{k-n_u}\Big). \tag{4.21}$$

From Remark 4.2, we have:

$$A(q)r_{k+\tau_d} = b_{\tau_d}m_k + B^*(q)m_{k+\tau_d} + f\Big(r_{k+\tau_d-1}, \cdots, r_{k+\tau_d-n_y}, m_{k-1}, \cdots, m_{k+\tau_d-n_u}\Big), \tag{4.22}$$

which, for convenience, has been written τ_d instants of time ahead, i.e. $k \to k + \tau_d$. From Assumption 4.3, the compensation input can be obtained from (4.22) as:

$$m_k = \frac{1}{b_{\tau_d}}\Big[A(q)r_{k+\tau_d} - B^*(q)m_{k+\tau_d} - f\Big(r_{k+\tau_d-1}, \cdots, r_{k+\tau_d-n_y}, m_{k-1}, \cdots, m_{k+\tau_d-n_u}\Big)\Big]. \tag{4.23}$$

Assumption 4.4. *In the case of systems with hysteresis, it should be remembered that according to Assumption 4.1-(iii) regressors from the cluster Ω_{u^m} $\forall m$ are removed. Therefore, Assumptions 4.3-(i) and 4.3-(ii) should read: the only regressor involving $\phi_{1,k-\tau_d}$ is linear, and let $n_{\phi_1} > \tau_d$, $n_{\phi_2} > \tau_d$ and $n_u > \tau_d$, respectively, while the other items are maintained.*

This is illustrated in the following example.

Example 4.4. Design of a Compensator from a model $\mathcal{M}_{\mathrm{I}}$.

Consider the NARX model that complies with Assumptions 4.1 and 4.4 described by:

$$y_k = \hat{\theta}_1 y_{k-1}+\hat{\theta}_2\phi_{2,k-2}+\hat{\theta}_3\phi_{1,k-2}u_{k-2}+\hat{\theta}_4\phi_{2,k-2}\phi_{1,k-2}y_{k-1}+\hat{\theta}_5\phi_{1,k-1}, \tag{4.24}$$

for which τ_{d}=1. Since $\phi_{1,k}$=$u_k - u_{k-1}$ and $\phi_{2,k}$=sign($\phi_{1,k}$), we have:

$$\begin{aligned} y_k =&\hat{\theta}_1 y_{k-1}+\hat{\theta}_2\mathrm{sign}(u_{k-2}-u_{k-3})+\hat{\theta}_3[u_{k-2}-u_{k-3}]u_{k-2}+\hat{\theta}_4\mathrm{sign}(u_{k-2}-u_{k-3})[u_{k-2}-u_{k-3}]y_{k-1} \\ &+ \hat{\theta}_5[u_{k-1}-u_{k-2}], \end{aligned}$$

which is in the form (4.18) and, therefore,

$$A(q)y_k = B(q)u_k+f\Big(y_{k-1},u_{k-2},u_{k-3},\mathrm{sign}(u_{k-2} - u_{k-3})\Big), \tag{4.25}$$

where $A(q) = 1 - \hat{\theta}_1 q^{-1}$, $B(q) = \hat{\theta}_5 q^{-1} - \hat{\theta}_5 q^{-2}$, and

$$f(\cdot) = \hat{\theta}_2\mathrm{sign}(u_{k-2} - u_{k-3})+\hat{\theta}_3[u_{k-2} - u_{k-3}]u_{k-2}+\hat{\theta}_4\mathrm{sign}(u_{k-2} - u_{k-3})[u_{k-2} - u_{k-3}]y_{k-1}.$$

From Remark 4.2, the model (4.25) is recast as:

$$A(q)r_{k+1} = \hat{\theta}_5 m_k-\hat{\theta}_5 m_{k-1}+f\Big(r_k,m_{k-1},m_{k-2},\mathrm{sign}(m_{k-1} - m_{k-2})\Big), \tag{4.26}$$

and, because Assumption 4.4 is satisfied, we have:

$$\begin{aligned} m_k &= \frac{1}{\hat{\theta}_5}\Big[A(q)r_{k+1}+\hat{\theta}_5 m_{k-1} - f\Big(r_k,m_{k-1},m_{k-2},\mathrm{sign}(m_{k-1}-m_{k-2})\Big)\Big], \\ &= \frac{1}{\hat{\theta}_5}\Big[r_{k+1} - \hat{\theta}_1 r_k+\hat{\theta}_5 m_{k-1} - \hat{\theta}_2\mathrm{sign}(m_{k-1}-m_{k-2}) - \hat{\theta}_3[m_{k-1}-m_{k-2}]m_{k-1} \\ &\qquad -\hat{\theta}_4\mathrm{sign}(m_{k-1}-m_{k-2})[m_{k-1}-m_{k-2}]r_k\Big]. \end{aligned} \tag{4.27}$$

△

4.6 Compensation Based on Compensator Identification

Here, the strategy is to identify NARX models $\check{\mathcal{M}}$ that describe the inverse relationship between u and y of $\mathcal{S}$. The advantage is that the compensator C is obtained directly from $\check{\mathcal{M}}$ (see Remark 4.2). However, some issues related to the identification procedure of these models need to be addressed. For simplicity, in this section, we assume that $\tau_{\mathrm{d}} = 1$ and, as aforementioned, the additional term $\phi_{i,k}$ has been omitted for simplicity (see Remark 4.3).

For the inverse model $\check{\mathcal{M}}$, the output $\hat{u}_k$ depends on y_k. Hence in order to avoid the lack of causality, y_k should be delayed by τ_{s} time steps with respect to u_k, yielding (Xia,

2003):

$$\hat{u}_k = \breve{F}\left(\hat{u}_{k-1}, \cdots, \hat{u}_{k-n_u}, y_{k-1+\tau_s}, \cdots, y_{k-n_y+\tau_s}\right), \tag{4.28}$$

where $\breve{F}(\cdot)$ is the inverse nonlinear function and $\hat{u}_k \in \mathbb{R}$ and $y_k \in \mathbb{R}$ are related as shown in Figure 4.5(a). It should be noted that $\tau_s \geq \tau_d + 1$, where usually the equality is preferred. Similar ways to avoid noncausal models can be found in the literature (Rakotondrabe, 2011; Lacerda Júnior et al., 2019).

Assumption 4.5. *It is assumed that: (i) there is at least one regressor of the output* $(y_k)^j$ *for* $j \geq 1$*; (ii) the compensation signal* m_k *is known up to time* $k-1$*; and (iii) the reference* r_k *is known up to time* $k-1+\tau_s$*.*

Assumption 4.5 should be observed during the structure selection of the inverse model $\breve{\mathcal{M}}$. Note that (i) ensures that there is at least one input signal y_k in the identified models; (ii) and (iii) ensure that m_k to be computed at time k is the only unknown variable. Given Assumption 4.5 and Remark 4.2, the compensation signal m_k can be obtained directly from $\breve{\mathcal{M}}$ as:

$$m_k = \breve{F}\left(m_{k-1}, \cdots, m_{k-n_u}, r_{k-1+\tau_s}, \cdots, r_{k-n_y+\tau_s}\right). \tag{4.29}$$

When dealing with hysteretic models, it is important to keep in mind that the additional terms (4.2) should also be properly adapted to this inverse context. As the regressors (4.2) are functions of the model input u_k, which is now given by the system output y_k, then these additional inverse terms to be included as candidate regressors in model (4.28) become $\breve{\phi}_{1,k} = y_k - y_{k-1}$ and $\breve{\phi}_{2,k} = \text{sign}(\breve{\phi}_{1,k})$; Figure 4.5(a).

4.7 Concluding Remarks

This chapter addressed the problems of identification and compensation of hysteretic systems. In the context of *system identification*, the contribution is twofold. First, we build models with regressors that use the sign function of the first difference of the input, as proposed by (Martins and Aguirre, 2016), and present an additional condition in order to guarantee a *continuum of steady-state solutions*, which is an important ingredient for hysteresis (Bernstein, 2007; Morris, 2011). To this aim, a particular constraint on the parameters is presented in Lemma 4.1. As a consequence, the identified models are able to describe both dynamical and static features of the hysteresis nonlinearity, whose comparison with other identified models that do not use Lemma 4.1 will be provided in Chapter 5. Second, following a *quasi-static analysis* of these models, a schematic framework is proposed to explain how the hysteresis loop occurs on the input-output plane; see Figure 4.1.

In the field of identification there are promising approaches based on computational intelligence, such as those reviewed in (Quaranta et al., 2020). However, this thesis uses

NARX polynomials due to the structural simplicity and fair generality. Such features allow: (i) using constraints such that simple models display hysteresis and (ii) using such models in compensator design by simple manipulations.

In the context of *hysteresis compensation*, this thesis proposes three approaches to design compensators. In one approach, the compensation law can be obtained for dynamical systems with or without the use of constraints during model identification. In the second approach, it is shown how to restrict the pool of candidate regressors in order to solve the compensation problem, so that the compensation law can be obtained through simple algebraic manipulations performed on the identified models. In the last approach, it is shown how some issues related to the identification procedure of inverse models should be addressed to overcome potential causality problems, so that the compensation law can be directly identified from the data. Such approaches are not limited to hysteresis and can be extended to other nonlinearities, or even to linear systems using ARX models.

The next chapter presents the effectiveness of the identification and compensation proposals through simulated and experimental tests. Initially, it employs the appropriate constraints to identify models that are suitable for designing compensators, according to the approach to be used, and that may predict both the dynamic and static features of the hysteretic system adopted in the numerical and experimental case. Then, the compensators designed with these identified models are placed in an open-loop scheme with the system in order to improve its tracking performance compared to the uncompensated one.

Chapter 5

Numerical and Experimental Results

5.1 Introduction

This chapter builds NARX models using the procedures addressed in Chapter 4 in order to predict the dynamic and static behavior of hysteretic systems from a simulated and an experimental data set, as well as to mitigate the nonlinearity of such systems. Some peculiarities of each of the proposed compensation approaches, such as the influence of some structural constraints on the predictive performance of the identified NARX models, are discussed.

The chapter is organized as follows. The numerical and experimental results for the model identification and the compensator design are, respectively, given in Sections 5.2 and 5.3. Section 5.4 presents the concluding remarks.

The contents of this chapter are similar to those published in (Abreu et al., 2020) and part of those in (Tavares et al., 2022).

5.2 Numerical Results

This section builds models to predict the behavior of a hysteretic system from simulated data, and evaluates the performance of these models in predicting its dynamic and static features, as well as in compensating the nonlinearity of the simulated system.

5.2.1 Identification of a Bench Test System

Consider the piezoelectric actuator with hysteretic nonlinearity modeled by the Bouc-Wen model (Wen, 1976), reviewed in Section 2.2.1, and whose mathematical model is given by (Rakotondrabe, 2011):

$$\begin{cases} \dot{h}(t) = A\dot{u}(t) - \beta|\dot{u}(t)|h(t) - \gamma\dot{u}(t)|h(t)|, \\ y(t) = d_{\mathrm{p}}u(t) - h(t), \end{cases} \tag{5.1}$$

where $y(t)$ is the displacement, $u(t)$ is the voltage applied to the actuator within the range $-80\,\mathrm{V} \leq u(t) \leq 80\,\mathrm{V}$, $d_{\mathrm{p}} = 1.6\,\frac{\mu\mathrm{m}}{\mathrm{V}}$ is the piezoelectric coefficient, $h(t)$ is the hysteretic

nonlinear term and $A = 0.9\,\frac{\mu m}{V}$, $\beta = 0.008\,V^{-1}$ and $\gamma = 0.008\,V^{-1}$ are parameters that determine the shape and scale of the hysteresis loop.

Model (5.1) was integrated numerically using a fourth-order Runge-Kutta method with integration step $\delta t = 0.001$ s. In this work, the sampling time is set to $T_s = \delta t = 0.001$ s and a sinusoidal input with frequency of 1 Hz is chosen to validate the identified models (Rakotondrabe, 2011). The excitation input signal was generated using the algorithm (2.22)–(2.25), which was revisited and discussed in Section 2.3.2 to design a Pseudo Random Filtered Signal (PRFS); see Figure 5.1(a). The setup coefficients used to design it were: $n_f = 1$, $f_1 = 1$ Hz, $v = 1$, $o_1 = 0$, $G_1 = 80$, and $N = N_1 = 50000$. The data sets are 50 s long ($N = 50000$). The identification data are shown in Figure 5.1. The meta-parameters are $\ell = 3$, $n_y = 1$ and $n_u = n_{\phi_1} = n_{\phi_2} = 1$. This choice is based on the discussion in (Martins and Aguirre, 2016; Lacerda Júnior et al., 2019).

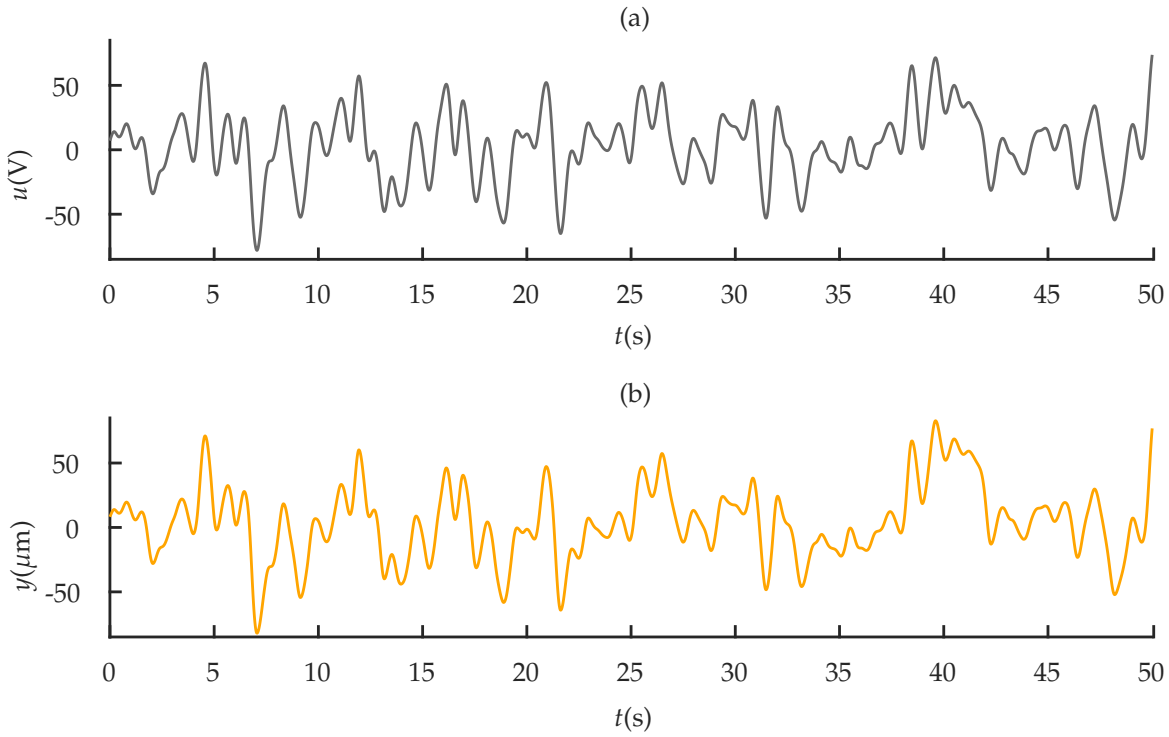

Figure 5.1: Identification data obtained from (5.1). (a) excitation as a PRFS, and (b) output.

5.2.1.1 Estimating direct $\mathcal{M}$ models – $\mathcal{M}_R$ and $\mathcal{M}_I$

In this example, the particularities of the first two compensation approaches proposed in Chapter 4, whose models $\mathcal{M}$ are based on the direct relationship between u and y (see Figure 4.5), are adopted during the identification procedure. Therefore, one NARX model $\mathcal{M}_R$ is identified to fulfill the assumptions that allow using it to design compensators according to the approach proposed in Section 4.4, and another $\mathcal{M}_I$ for the approach in Section 4.5.

Model $\mathcal{M}_{\mathrm{R}}$

For the model $\mathcal{M}_{\mathrm{R}}$, there is no need to specify constraints on the model structure in order to make it suitable for designing compensators, as discussed in Section 4.4. Therefore, using the meta-parameters values defined above, the data shown in Figure 5.1, Assumption 4.1 and the ERR criterion (2.42), the n_θ (2.38) candidate regressors to compose the hysteretic model are ranked according to their importance. Then, following this order, one regressor is included at a time and the trade-off between the model complexity and its goodness of fit to the identification data is evaluated using the AIC index (2.44). It is worth remembering that, when it comes to identifying nonlinear systems, the AIC tends to reach local minima for different values of n_θ, which makes the stopping rule for the inclusion of regressors in the model, i.e. the choice of the size of the final model, not evident, as stated in Section 2.3.4. Furthermore, as this criterion is statistical, there is no guarantee that the model indicated as optimal, which is commonly defined as one whose number of n_θ provides the first minimum of the AIC, is actually the best in dynamic terms. Therefore, whenever possible, some additional steps using the AIC index would be interesting to choose a more appropriate model. As an alternative procedure, the steps below are recommended:

1. Following the order determined with ERR (2.42), include one regressor at a time to compose a candidate model and calculate its corresponding AIC(n_{θ_j}) index (2.44), for which n_{θ_j} refers to the number of regressors in the model, such that $n_{\theta_j} = j$ for $j = 1, 2, \cdots, n_{\theta_{\max}}$, with $1 \ll n_{\theta_{\max}} \leq n_\theta$.

   - It is interesting to define a maximum limit of terms $n_{\theta_{\max}}$ to be analyzed, since the number of candidate regressors n_θ (2.38) tends to be too high.
   - In this example, in order to identify model $\mathcal{M}_{\mathrm{R}}$, it was assumed $n_{\theta_{\max}}$=20, where the corresponding AIC(n_{θ_j}) values are illustrated in Figure 5.2.

2. From the $n_{\theta_{\max}}$ computed AIC(n_{θ_j}) values, select those that are local minima $n^*_{\theta_j}$.

   - It does not necessarily have to be a minimum. If a subset of regressors n_{θ_j} (within the range of j=1, 2, $\cdots$, $n_{\theta_{\max}}$) does not provide a significant improvement in terms of AIC(n_{θ_j}) index when included in the model, i.e. $\left|\mathrm{AIC}(n_{\theta_j}) - \mathrm{AIC}(n_{\theta_{j-1}})\right| \approx 0$ starting with j=2, then it can be assumed that the first number of terms n_{θ_j} within this subset is a local minimum $n^*_{\theta_j}$, and should be selected.
   - This scenario can be seen in Figure 5.2, for the subset composed of n_{θ_9}, $n_{\theta_{10}}$ and $n_{\theta_{11}}$, where $n^*_{\theta_9}$ is a local minimum. Note that even if n_{θ_9} was not a local minimum, it would be selected as one, as suggested above, because the inclusion of $n_{\theta_{10}}$ and $n_{\theta_{11}}$-th regressor in the model does not significantly change the value of AIC(n_{θ_j}) compared to that obtained with n_{θ_9}, i.e. $\mathrm{AIC}(n_{\theta_9}) \approx \mathrm{AIC}(n_{\theta_{10}}) \approx \mathrm{AIC}(n_{\theta_{11}})$.
   - For the present example, the local minima were reached when the model is composed of 9, 12, and 17 regressors. These minima are represented as a (•) in Figure 5.2.

3. Determine a search interval $\Delta_{n^*_\theta}$ around the first selected local minima, i.e. $n^*_{\theta_j} \pm \Delta_{n^*_\theta}$.

   - Although the selected $n^*_{\theta_j}$ indicate the number of regressors that lead to optimal models in the statistical sense, whenever possible, some additional search around these number of terms is beneficial to help choose a more appropriate model, in a dynamic sense. In the literature, it is usually found that the model indicated as optimal using a statistical criterion, such as AIC(n_{θ_j}), is close to the dynamic optimal.
   - A search around the first two local minima has been empirically proven enough.
   - Considering the first two local minima (i.e. $n^*_{\theta_9}$ and $n^*_{\theta_{12}}$ shown in Figure 5.2) and the search interval being $\Delta_{n^*_\theta} = 2$, the models to be investigated are those composed of 7, 8, 9, 10, 11, 12, 13 and 14 regressors.

4. Calculate a predictive performance index for each model in the search space.

   - Evaluate the models that make up the search space determined in step 3 using a dynamic criterion.
   - For this case, some criteria related to estimation error can be used to quantify the accuracy between the data measured from the system and those estimated from the free-run simulation of each identified model.
   - It is suggested that preference be given to models with fewer regressors, unless a significant improvement in predictive performance is achieved in a model with many regressors.
   - After evaluating the structures that make up the search space determined in step 3, the one composed of 9 regressors was selected as the model $\mathcal{M}_{\mathrm{R}}$, for the present example.

Remark 5.1. Note that, as the search space for the best model structure might be limited by an interval $\Delta_{n^*_\theta}$ of regressors around the first two local minima $n^*_{\theta_j}$, this procedure could be done iteratively.

So, following the recommended procedure above, the identified model $\mathcal{M}_{\mathrm{R}}$ is:

$$\begin{aligned} y_k &= \hat{\theta}_1 y_{k-1} + \hat{\theta}_2 \phi_{1,k-1} + \hat{\theta}_3 \phi_{2,k-1}\phi_{1,k-1}u_{k-1} + \hat{\theta}_4 \phi_{2,k-1}\phi_{1,k-1}y_{k-1} + \hat{\theta}_5 \phi_{1,k-1}u^2_{k-1} \\ &\quad + \hat{\theta}_6 \phi_{1,k-1}u_{k-1}y_{k-1} + \hat{\theta}_7 \phi_{2,k-1}y_{k-1} + \hat{\theta}_8 \phi_{2,k-1}\phi^2_{1,k-1} + \hat{\theta}_9 \phi_{2,k-1}u_{k-1}, \end{aligned}$$

where its free prediction representation is given by:

$$\begin{aligned} \hat{y}_k &= \hat{\theta}_1 \hat{y}_{k-1} + \hat{\theta}_2 \phi_{1,k-1} + \hat{\theta}_3 \phi_{2,k-1}\phi_{1,k-1}u_{k-1} + \hat{\theta}_4 \phi_{2,k-1}\phi_{1,k-1}\hat{y}_{k-1} + \hat{\theta}_5 \phi_{1,k-1}u^2_{k-1} \\ &\quad + \hat{\theta}_6 \phi_{1,k-1}u_{k-1}\hat{y}_{k-1} + \hat{\theta}_7 \phi_{2,k-1}\hat{y}_{k-1} + \hat{\theta}_8 \phi_{2,k-1}\phi^2_{1,k-1} + \hat{\theta}_9 \phi_{2,k-1}u_{k-1}. \end{aligned} \tag{5.2}$$

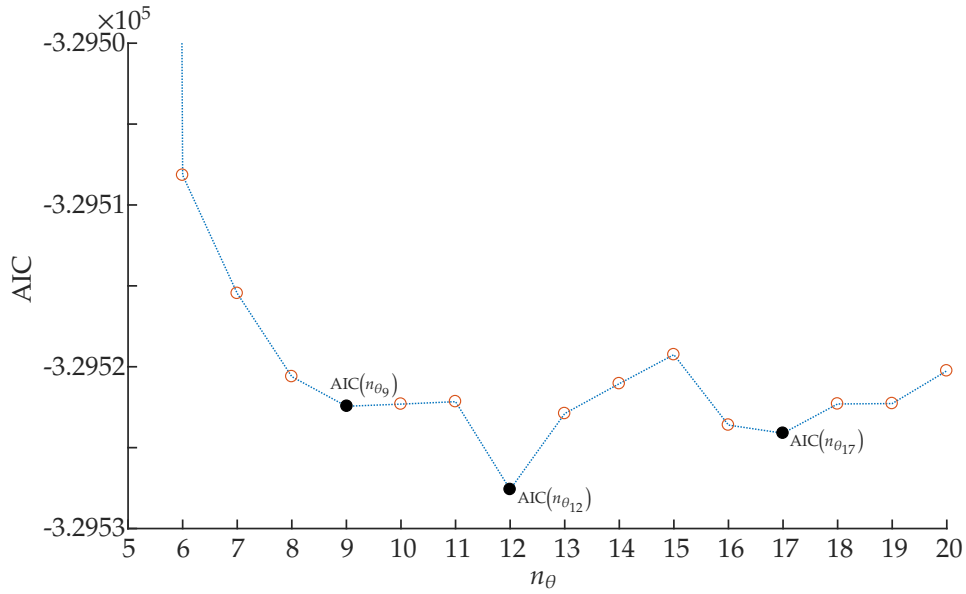

Figure 5.2: Akaike's Information Criterion (AIC) calculated to help choose the number of regressors to be included in the model $\mathcal{M}_{\mathrm{R}}$. (∘) refers to the AIC values, (•) indicates the local minima, and (· · ·) is illustrative only.

Based on Lemma 4.1 and Example 4.1, for model (5.2) to fulfill Property 4.1, the constraint $\hat{\theta}_1 = 1$ should be imposed. This can be done using (2.48) with the constraint written as:

$$c = 1; \qquad S = [1 \;\; 0 \;\; 0 \;\; 0 \;\; 0 \;\; 0 \;\; 0 \;\; 0 \;\; 0]. \tag{5.3}$$

Hence, the parameter values estimated by the constrained least squares (CLS) estimator (2.48) are shown in Table 5.1.

Table 5.1: Model parameters obtained with (2.48) and (5.3).

Model	Values		
$\mathcal{M}_{\mathrm{R}}$ (5.2)	$\hat{\theta}_1$=1.0000	$\hat{\theta}_2$=0.7785	$\hat{\theta}_3$=0.0144
	$\hat{\theta}_4$= − 0.0098	$\hat{\theta}_5$=3.2660×10^{-4}	$\hat{\theta}_6$= -2.5767×10^{-4}
	$\hat{\theta}_7$=4.9204×10^{-5}	$\hat{\theta}_8$= − 0.0844	$\hat{\theta}_9$= -3.5147×10^{-5}
$\mathcal{M}_{\mathrm{I}}$ (5.6)	$\hat{\theta}_1$=1.0000	$\hat{\theta}_2$= − 0.2310	$\hat{\theta}_3$=0.0146
	$\hat{\theta}_4$= − 0.0099	$\hat{\theta}_5$=3.2333×10^{-4}	$\hat{\theta}_6$= -2.5494×10^{-4}
	$\hat{\theta}_7$=1.7891×10^{-5}	$\hat{\theta}_8$=1.0080	$\hat{\theta}_9$= − 0.0604
$\breve{\mathcal{M}}$ (5.9)	$\hat{\theta}_1$=1.0000	$\hat{\theta}_2$=1.2705	$\hat{\theta}_3$= − 0.0160
	$\hat{\theta}_4$=0.0100	$\hat{\theta}_5$= -9.9216×10^{-6}	$\hat{\theta}_6$=7.3525×10^{-6}
	$\hat{\theta}_7$= − 0.0468	$\hat{\theta}_8$=0.0344	$\hat{\theta}_9$=1.1025

A quasi-static analysis is performed (see Section 4.2.2 and Example 4.1). First, we write for (5.2) the corresponding to (4.3) as:

$$\begin{aligned}\tilde{\hat{y}} \;\approx\; & \hat{\theta}_1\tilde{\hat{y}} + \hat{\theta}_2\phi_{1,k-1} + \hat{\theta}_3\phi_{2,k-1}\phi_{1,k-1}u_{k-1} + \hat{\theta}_4\phi_{2,k-1}\phi_{1,k-1}\tilde{\hat{y}} + \hat{\theta}_5\phi_{1,k-1}u_{k-1}^2 \\ & + \hat{\theta}_6\phi_{1,k-1}u_{k-1}\tilde{\hat{y}} + \hat{\theta}_7\phi_{2,k-1}\tilde{\hat{y}} + \hat{\theta}_8\phi_{2,k-1}\phi_{1,k-1}^2 + \hat{\theta}_9\phi_{2,k-1}u_{k-1},\end{aligned}$$

yielding:

$$\tilde{\hat{y}}(u,\phi_1,\phi_2) \approx \begin{cases} \dfrac{\hat{\theta}_2\phi_1 + \hat{\theta}_3\phi_1 u + \hat{\theta}_5\phi_1 u^2 + \hat{\theta}_8\phi_1^2 + \hat{\theta}_9 u}{1 - \hat{\theta}_1 - \hat{\theta}_4\phi_1 - \hat{\theta}_6\phi_1 u - \hat{\theta}_7}, & \text{for } \phi_2 = \;\; 1; \\ \dfrac{\hat{\theta}_2\phi_1 - \hat{\theta}_3\phi_1 u + \hat{\theta}_5\phi_1 u^2 - \hat{\theta}_8\phi_1^2 - \hat{\theta}_9 u}{1 - \hat{\theta}_1 + \hat{\theta}_4\phi_1 - \hat{\theta}_6\phi_1 u + \hat{\theta}_7}, & \text{for } \phi_2 = -1, \end{cases} \tag{5.4}$$

where the time indices have been omitted for brevity.

The top expression in (5.4) gives the set $\tilde{y}_{\mathrm{L}}$, while the bottom one, $\tilde{y}_{\mathrm{U}}$. Computing the derivative of (5.2) with respect to $\hat{y}_{k-1}$ and using (4.4), we obtain:

$$\begin{aligned} -1 < \;\; & \hat{\theta}_1 + \hat{\theta}_4\phi_{2,k-1}\phi_{1,k-1} + \hat{\theta}_6\phi_{1,k-1}u_{k-1} + \hat{\theta}_7\phi_{2,k-1} \;\; < 1, \\ \frac{-1-\hat{\theta}_1-\hat{\theta}_4\phi_{2,k-1}\phi_{1,k-1}-\hat{\theta}_7\phi_{2,k-1}}{\hat{\theta}_6\phi_{1,k-1}} < u_{k-1} < & \frac{1-\hat{\theta}_1-\hat{\theta}_4\phi_{2,k-1}\phi_{1,k-1}-\hat{\theta}_7\phi_{2,k-1}}{\hat{\theta}_6\phi_{1,k-1}}. \end{aligned} \tag{5.5}$$

Taking $\phi_{2,k-1} = 1$ or $\phi_{2,k-1} = -1$, the conditions for attracting regions under load or unloading, respectively, are obtained. Considering the parameter values presented in Table 5.1 and a loading-unloading input signal, the points (5.4) and their attraction conditions (5.5) are computed numerically and shown in Figure 5.3. Hence, in this way it is possible to see how model (5.2) is able to describe the hysteresis nonlinearity.

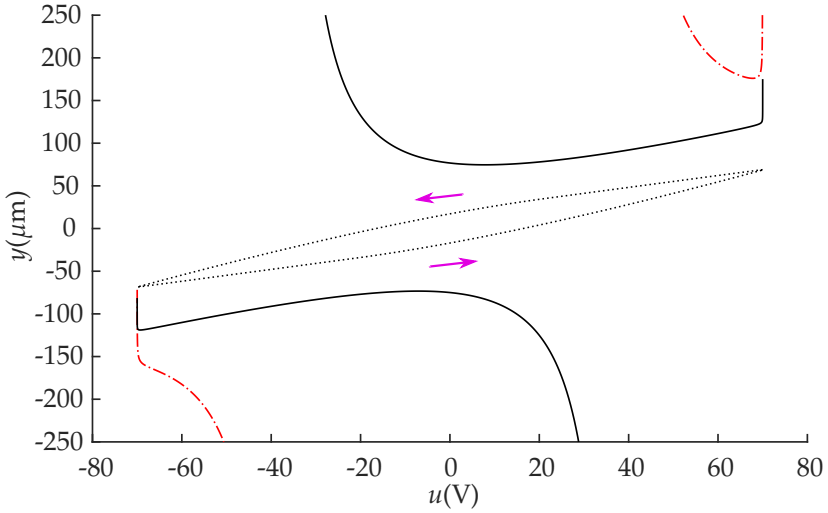

Figure 5.3: Results of quasi-static analysis for model (5.2) with input u_k=70 sin(2πk) V. The hysteresis loop indicated with (⋯) is a result of the interaction of (—) attracting ($\tilde{y}_{\mathrm{L}}^{\mathrm{a}}$, $\tilde{y}_{\mathrm{U}}^{\mathrm{a}}$) and (-·-) repelling ($\tilde{y}_{\mathrm{L}}^{\mathrm{r}}$, $\tilde{y}_{\mathrm{U}}^{\mathrm{r}}$) sets. (→) indicates the orientation of the hysteresis loop. Compare to Figure 4.1.

Model $\mathcal{M}_{\mathrm{I}}$

In order to identify model $\mathcal{M}_{\mathrm{I}}$, we take $n_u = n_{\phi_1} = n_{\phi_2} = 2$ which is the smallest value that complies with Assumption 4.3-(ii), following the mention made in Assumption 4.4 for the approach described in Section 4.5, while n_y and ℓ were chosen as detailed above. Using the data shown in Figure 5.1, Assumption 4.1 and the ERR together with AIC, as recommended above through steps 1 to 4, the final number of chosen regressors produces the model:

$$\begin{aligned}\hat{y}_k \;=\; & \hat{\theta}_1\hat{y}_{k-1} + \hat{\theta}_2\phi_{1,k-2} + \hat{\theta}_3\phi_{2,k-2}\phi_{1,k-2}u_{k-2} + \hat{\theta}_4\phi_{2,k-2}\phi_{1,k-2}\hat{y}_{k-1} + \hat{\theta}_5\phi_{1,k-2}u_{k-2}^2 \\ & + \hat{\theta}_6\phi_{1,k-2}u_{k-2}\hat{y}_{k-1} + \hat{\theta}_7\phi_{2,k-2}\hat{y}_{k-1} + \hat{\theta}_8\phi_{1,k-1} + \hat{\theta}_9\phi_{2,k-2}\phi_{1,k-2}^2,\end{aligned} \tag{5.6}$$

whose parameters values estimated by the CLS (2.48) estimator with constraints (5.3) are shown in Table 5.1.

It is interesting to note that the regressors selected to compose models (5.2) and (5.6) are practically the same and, roughly, we could point out that the main difference is related to their delays, where the nonlinear regressors that are functions of the input signal have a delay of $k-1$ in model (5.2), and of $k-2$ in model (5.6). Such similarity highlights the importance of these regressors to describe the investigated system, which were automatically chosen by the ERR algorithm. In addition, the difference in the delay of these regressors is the result of the constraints raised for the approach described in Section 4.5, which are reflected in the different values of meta-parameters used and, therefore, in the set of candidate regressors.

Performing the quasi-static analysis to model (5.6), we get:

$$\tilde{\hat{y}}(u,\phi_1,\phi_2) \approx \begin{cases} \dfrac{\hat{\theta}_2\phi_1 + \hat{\theta}_3\phi_1 u + \hat{\theta}_5\phi_1 u^2 + \hat{\theta}_8\phi_1 + \hat{\theta}_9\phi_1^2}{1 - \hat{\theta}_1 - \hat{\theta}_4\phi_1 - \hat{\theta}_6\phi_1 u - \hat{\theta}_7}, & \text{for } \phi_2 = \;\; 1; \\ \dfrac{\hat{\theta}_2\phi_1 - \hat{\theta}_3\phi_1 u + \hat{\theta}_5\phi_1 u^2 + \hat{\theta}_8\phi_1 - \hat{\theta}_9\phi_1^2}{1 - \hat{\theta}_1 + \hat{\theta}_4\phi_1 - \hat{\theta}_6\phi_1 u + \hat{\theta}_7}, & \text{for } \phi_2 = -1, \end{cases} \tag{5.7}$$

where the time indices have been omitted for simplicity, and whose solutions are in the attracting region if the following condition is satisfied:

$$\begin{aligned} -1 < \;\; & \hat{\theta}_1 + \hat{\theta}_4\phi_{2,k-2}\phi_{1,k-2} + \hat{\theta}_6\phi_{1,k-2}u_{k-2} + \hat{\theta}_7\phi_{2,k-2} \;\; < 1, \\ \frac{-1-\hat{\theta}_1-\hat{\theta}_4\phi_{2,k-2}\phi_{1,k-2}-\hat{\theta}_7\phi_{2,k-2}}{\hat{\theta}_6\phi_{1,k-2}} < u_{k-2} < & \frac{1-\hat{\theta}_1-\hat{\theta}_4\phi_{2,k-2}\phi_{1,k-2}-\hat{\theta}_7\phi_{2,k-2}}{\hat{\theta}_6\phi_{1,k-2}}. \end{aligned} \tag{5.8}$$

As before, it is possible to numerically calculate the solutions (5.7) and their attracting conditions (5.8), which helps explain how the hysteresis loop occurs in model (5.6). Figure 5.4 shows this result.

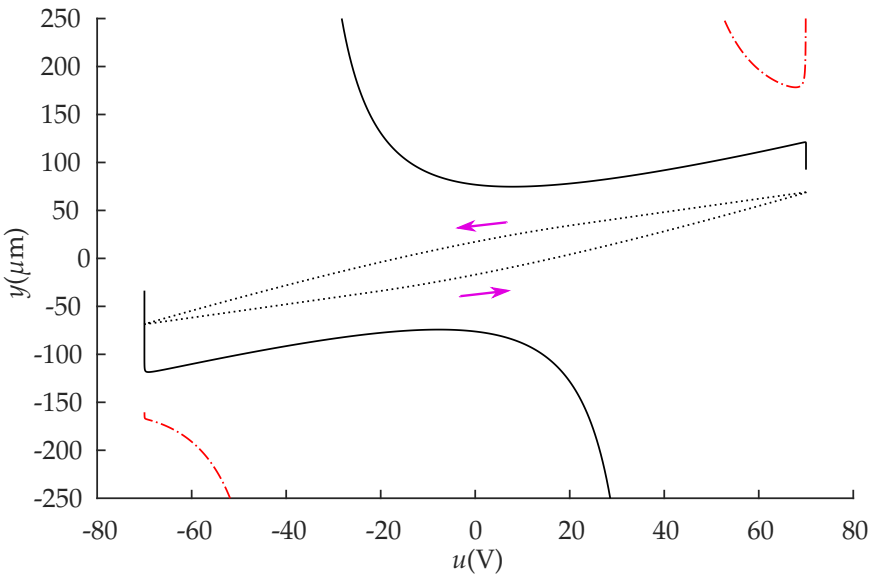

Figure 5.4: Results of quasi-static analysis for model (5.6) with input u_k=70 sin(2πk) V. For meaning of line patterns refer to captions of Figures 4.1 and 5.3.

Models $\mathcal{M}_{\mathrm{R}}$ (5.2) and $\mathcal{M}_{\mathrm{I}}$ (5.6) are simulated with a loading-unloading input (see left side of Figure 5.5) and, in cases where the input becomes constant, either during loading or unloading (see right side of Figure 5.5), *the system remains at the corresponding point of the hysteresis loop.* This is a direct consequence of using Lemma 4.1. This feature is not generally present in identified models found in the literature.

An interesting point to be considered is the fact that models $\mathcal{M}_{\mathrm{R}}$ and $\mathcal{M}_{\mathrm{I}}$ estimate the system with a certain accuracy and, therefore, *steady-state errors* are expected when time-varying inputs become constant; see Figure 5.5(d). For comparison purposes, consider the errors highlighted in the enlarged part of Figure 5.5(d), which occur when the input becomes constant during the loading and unloading regime. In this case, model $\mathcal{M}_{\mathrm{R}}$ provides a steady-state error of approximately 0.16 μm and 0.18 μm, while $\mathcal{M}_{\mathrm{I}}$ presents an error of about 0.23 μm and 0.29 μm for the loading and unloading regime, respectively. In addition, one should emphasize a subtle behavior found in the results obtained with model $\mathcal{M}_{\mathrm{I}}$ during the transition to steady-state, where a sudden change in the estimated output value led to a larger steady-state error; see Figure 5.5(d). This sudden change is related to the fact that during the transition to steady-state, only the input regressors $\phi_{i,k}$ with delay k−1 are immediately canceled. Therefore, as model $\mathcal{M}_{\mathrm{I}}$ has regressors that depend on the instant k−3, e.g. $\phi_{1,k-2}$=u_{k-2}−u_{k-3}, such terms produce sudden changes during transition, giving rise to a larger error in the steady-state. It is noteworthy that such regressors appear in model $\mathcal{M}_{\mathrm{I}}$ due to the need to fulfill Assumption 4.3-(ii), so that the input regressor can be explicit to apply the compensation approach presented in Section 4.5. As the general conclusions that can be drawn from the results achieved when the input becomes constant during the loading and unloading regime are the same, from now on we will only discuss the case for the unloading regime.

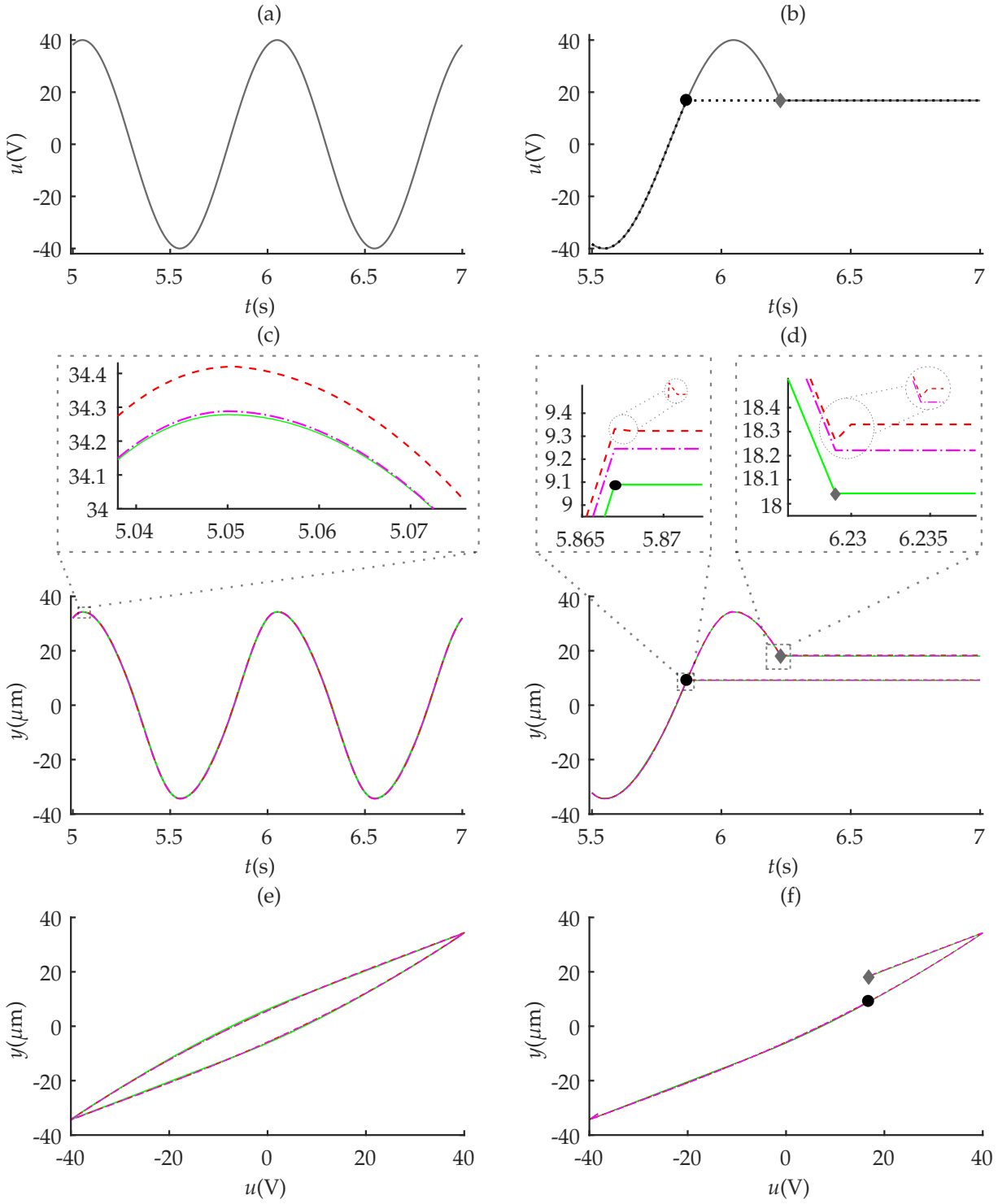

Figure 5.5: Free-run simulation of models (5.2) and (5.6). (a) sinusoidal input of voltage u_k=40 sin($2\pi k$) V and in (b) the case where this input becomes constant during loading (•) and unloading (⧫) with final value 16.8 V, temporal responses are in (c) and (d) while the hysteresis loops are in (e) and (f), respectively. (—) original data, (- · -) and (- -) are, respectively, the estimated output of models $\mathcal{M}_{\mathrm{R}}$ (5.2) and $\mathcal{M}_{\mathrm{I}}$ (5.6).

The improvement due to using Lemma 4.1 is shown in Figure 5.6. Despite different initial conditions, all models tend to the behavior of the dynamical system after a transient. The main difference is the ability of models (5.2) and (5.6) to predict the hysteretic behavior even when the input becomes constant. On the other hand, models estimated using black-box techniques and the model identified without using Lemma 4.1 (Martins and Aguirre, 2016) may diverge over time or converge to a single final value, either during loading or unloading regimes. Note that, as discussed before, the hysteretic behavior leads to different values for the output when the input becomes constant during loading and unloading with the same final value; see Figure 5.5(d). Most works in the literature (Leva and Piroddi, 2002; Parlitz et al., 2004; Worden et al., 2007; Deng and Tan, 2009; Worden and Barthorpe, 2012; Lacerda Júnior et al., 2019) do not test for this feature which in this work is guaranteed by Lemma 4.1.

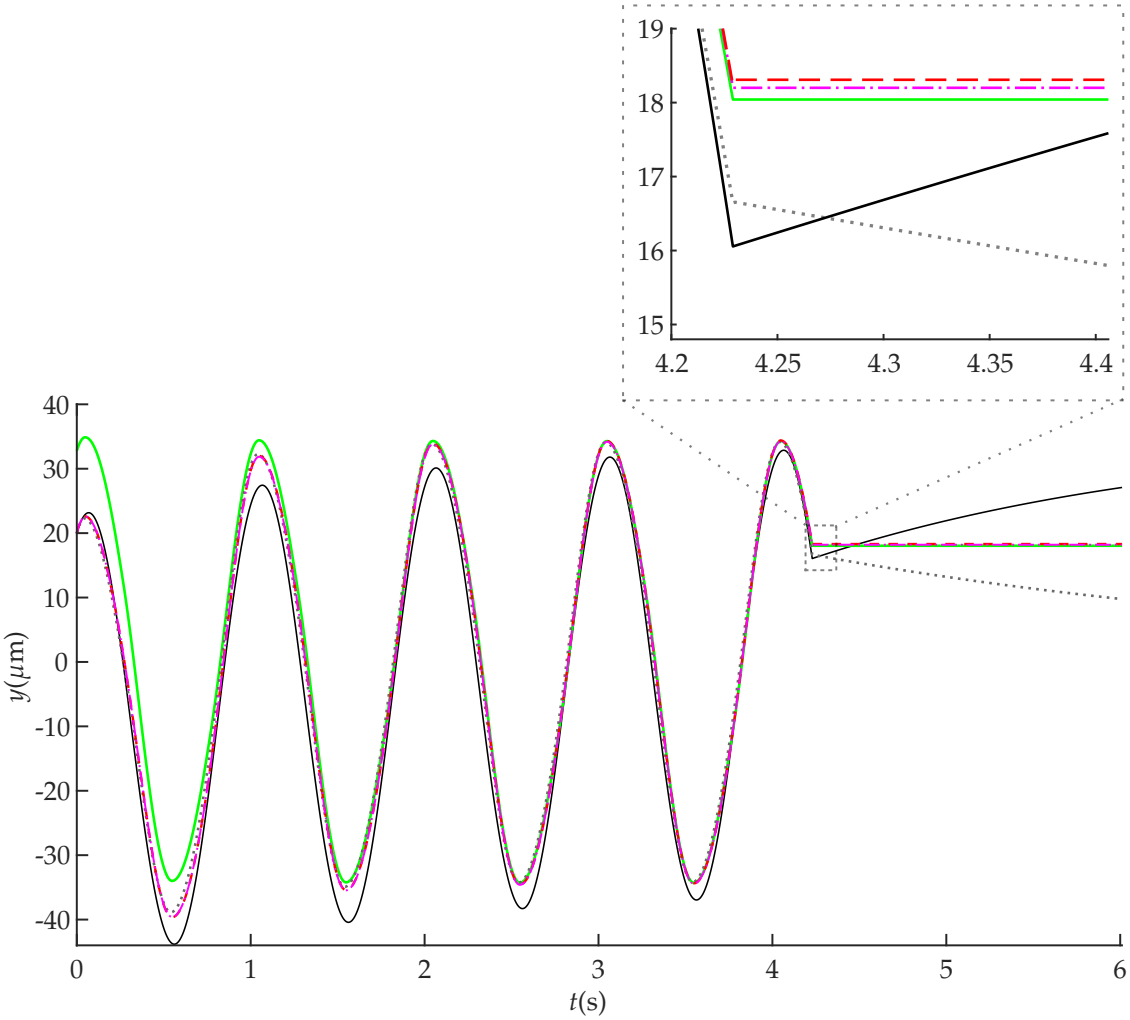

Figure 5.6: Model outputs to an input which is u_k=40 sin(2πk) V up to a certain point and then remains constant. (—) the original output, (-··-) and (- -) are, respectively, models $\mathcal{M}_R$ (5.2) and $\mathcal{M}_I$ (5.6), that use Lemma 4.1, (—) a black-box model, (···) a gray-box model but without considering Lemma 4.1 (Martins and Aguirre, 2016).

5.2.1.2 Estimating inverse $\breve{\mathcal{M}}$ model

The identified model that complies with Assumptions 4.1 and 4.5 is given by:

$$\begin{aligned}\hat{u}_k &= \hat{\theta}_1\hat{u}_{k-1} + \hat{\theta}_2\breve{\phi}_{1,k-1} + \hat{\theta}_3\breve{\phi}_{2,k-1}\breve{\phi}_{1,k-1}\hat{u}_{k-1} + \hat{\theta}_4\breve{\phi}_{2,k-1}\breve{\phi}_{1,k-1}y_{k-1} + \hat{\theta}_5\breve{\phi}_{2,k-1}y_{k-1}\hat{u}_{k-1} \\ &\quad +\hat{\theta}_6\breve{\phi}_{2,k-1}y_{k-1}^2 + \hat{\theta}_7\breve{\phi}_{1,k-1}^2u_{k-1} + \hat{\theta}_8\breve{\phi}_{1,k-1}^2y_{k-1} + \hat{\theta}_9\breve{\phi}_{1,k-1}^3, \end{aligned} \tag{5.9}$$

where $\breve{\phi}_{1,k} = y_k - y_{k-1}$, $\breve{\phi}_{2,k} = \text{sign}(\breve{\phi}_{1,k})$, $\hat{u}_k$ is the estimated input (model output), and y_k is the output of system (5.1) (model input).

Note that the regressors of (5.6) and of (5.9) are different. In both cases, the regressors are automatically chosen from the pool of candidates using the ERR criterion. Nevertheless, also for (5.9), the steady-state analysis yields $\bar{\hat{u}}=\theta_1\bar{\hat{u}}$, which is similar to the result found for model (5.6). Proceeding as before, the constrained least squares estimated parameters are shown in Table 5.1.

The formation of the hysteresis loop for this model (5.9) is shown in Figure 5.7. The different orientation of the hysteresis loop has been discussed in (Gu et al., 2012).

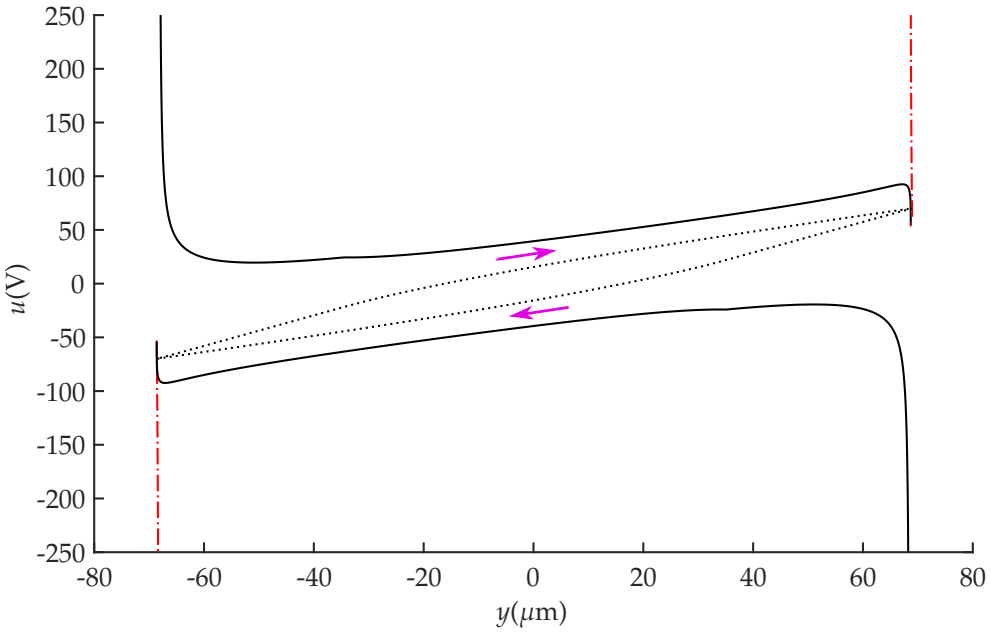

Figure 5.7: Results of quasi-static analysis for model (5.9). For meaning of line patterns refer to captions of Figures 4.1 and 5.3.

Considering the same input and output signal used to simulate models $\mathcal{M}_\text{R}$ and $\mathcal{M}_\text{I}$ (see Figure 5.5), but now in an inverse context with model $\breve{\mathcal{M}}$ (5.9), we obtain the results shown in Figure 5.8. It should be noted that, as $\breve{\mathcal{M}}$ is an inverse model, which predicts the input instead of the output signal, a direct comparison of its predictive performance with that of models $\mathcal{M}_\text{R}$ and $\mathcal{M}_\text{I}$ is not adequate. Model $\breve{\mathcal{M}}$ is also able to remain at its last output value when the input becomes constant, due to the use of Lemma 4.1. This model produces an error of about 0.55 V during the unloading regime; Figure 5.8(d).

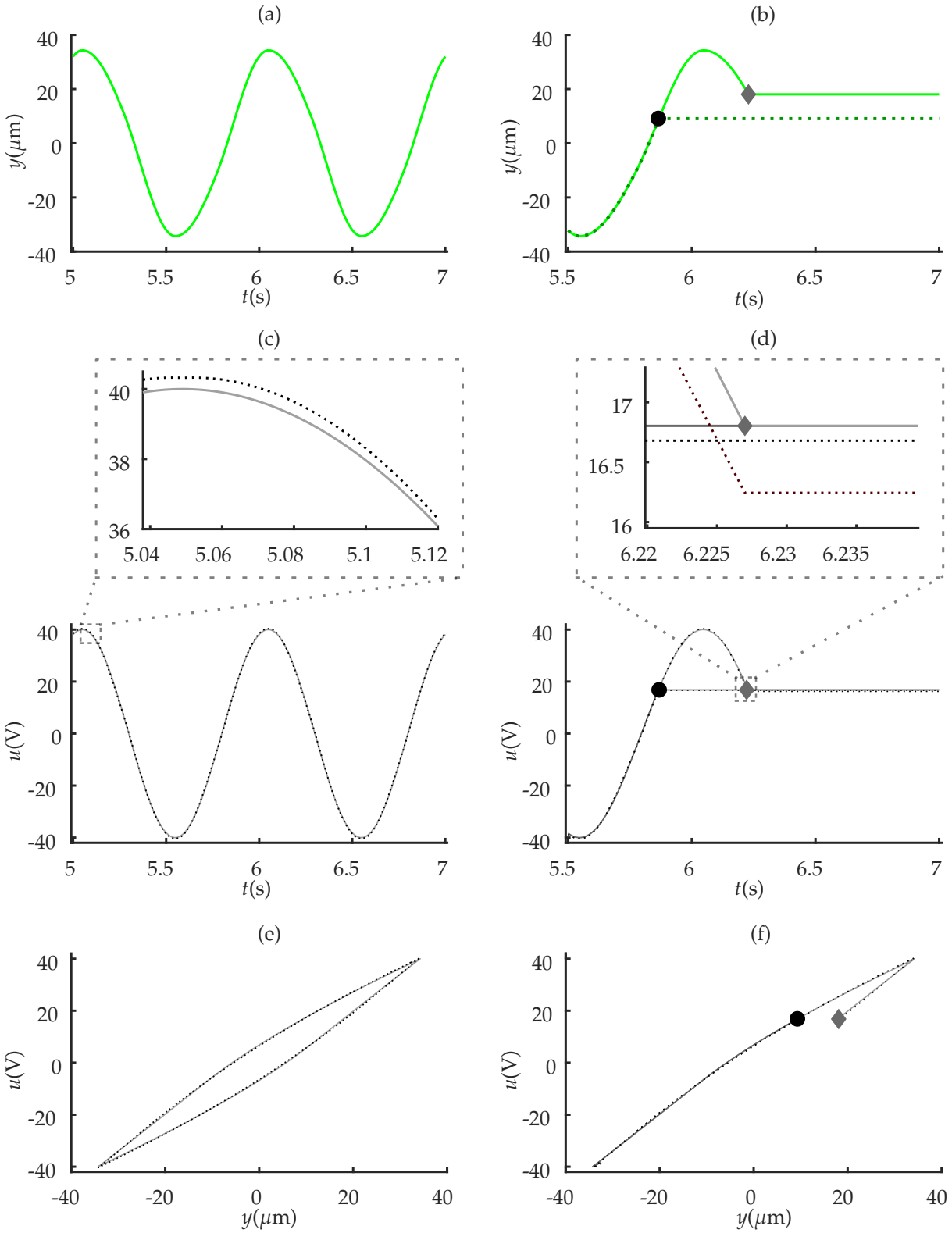

Figure 5.8: Free-run simulation of the inverse model (5.9). (a) and (b) the measured output data (—) y which are the input of the inverse model; (c) and (d) their corresponding voltage inputs (—), to be predicted, and in (e) and (f) the hysteresis loops. ($\cdots$) the estimated output of model $\breve{\mathcal{M}}$ (5.9). For more details of line patterns and voltage inputs refer to caption of Figure 5.5.

The mean absolute percentage error (MAPE):

$$\text{MAPE} = \frac{100 \sum_{k=1}^{N} |y_k - \hat{y}_k|}{N|\max(\boldsymbol{y}) - \min(\boldsymbol{y})|}, \tag{5.10}$$

was computed for models (5.2), (5.6), (5.9) and a black-box NARX polynomial model for sinusoidal input (Table 5.2). It should be remembered that the results obtained for (5.9) are not comparable to the others, and its MAPE accuracy is provided only as a reference index of its predictive performance. The results obtained suggest that models identified using gray-box techniques outperform those built using black-box.

Table 5.2: Model performance.

Context	**Model**	MAPE
Section 4.4	$\mathcal{M}_{\text{R}}$ (5.2)	0.2309
Section 4.5	$\mathcal{M}_{\text{I}}$ (5.6)	0.2523
Black-box	not shown	1.494
Section 4.6	$\check{\mathcal{M}}$ (5.9)	0.3753

5.2.2 Compensation of a Bench Test System

Next, the models identified in the previous section are used to design compensators using the procedure illustrated in Figure 4.5(b).

5.2.2.1 Design of the compensation input signals

Applying the steps described in Section 4.4 to model $\mathcal{M}_{\text{R}}$ (5.2), the following compensator, which corresponds to two cubic polynomials, is obtained:

$$\begin{aligned} &\underbrace{[\hat{\theta}_5]}_{c^{\text{L}}_{3,k}} m_k^3 + \underbrace{[\hat{\theta}_3 - \hat{\theta}_5 m_{k-1} + \hat{\theta}_6 r_k + \hat{\theta}_8]}_{c^{\text{L}}_{2,k}} m_k^2 + \underbrace{[\hat{\theta}_2 - \hat{\theta}_3 m_{k-1} + \hat{\theta}_4 r_k - \hat{\theta}_6 r_k m_{k-1} - 2\hat{\theta}_8 m_{k-1} + \hat{\theta}_9]}_{c^{\text{L}}_{1,k}} m_k \\ &\quad + \underbrace{[\hat{\theta}_1 r_k - r_{k+1} - \hat{\theta}_2 m_{k-1} - \hat{\theta}_4 r_k m_{k-1} + \hat{\theta}_7 r_k + \hat{\theta}_8 m_{k-1}^2]}_{c^{\text{L}}_{0,k}} = 0, \quad \text{for} \quad m_k > m_{k-1}, \end{aligned} \tag{5.11}$$

$$\begin{aligned} &\underbrace{[\hat{\theta}_5]}_{c^{\text{U}}_{3,k}} m_k^3 + \underbrace{[-\hat{\theta}_3 - \hat{\theta}_5 m_{k-1} + \hat{\theta}_6 r_k - \hat{\theta}_8]}_{c^{\text{U}}_{2,k}} m_k^2 + \underbrace{[\hat{\theta}_2 + \hat{\theta}_3 m_{k-1} - \hat{\theta}_4 r_k - \hat{\theta}_6 r_k m_{k-1} + 2\hat{\theta}_8 m_{k-1} - \hat{\theta}_9]}_{c^{\text{U}}_{1,k}} m_k \\ &\quad + \underbrace{[\hat{\theta}_1 r_k - r_{k+1} - \hat{\theta}_2 m_{k-1} + \hat{\theta}_4 r_k m_{k-1} - \hat{\theta}_7 r_k - \hat{\theta}_8 m_{k-1}^2]}_{c^{\text{U}}_{0,k}} = 0, \quad \text{for} \quad m_k < m_{k-1}, \end{aligned} \tag{5.12}$$

whose root to be used as the compensation input is chosen as described in Definition 4.2.

From model $\mathcal{M}_{\mathrm{I}}$ (5.6), according to Section 4.5, the following compensation input is obtained:

$$\begin{aligned} m_k &= \frac{1}{\hat{\theta}_8}\Big[r_{k+1}-\hat{\theta}_1 r_k+\hat{\theta}_8 m_{k-1}-\Big[\hat{\theta}_3 m_{k-1}+\hat{\theta}_4 r_k+\hat{\theta}_9[m_{k-1}-m_{k-2}]\Big]\mathrm{sign}(m_{k-1}-m_{k-2})[m_{k-1}-m_{k-2}] \\ &\quad -[\hat{\theta}_2+\hat{\theta}_5 m_{k-1}^2+\hat{\theta}_6 m_{k-1} r_k][m_{k-1}-m_{k-2}]-\hat{\theta}_7\mathrm{sign}(m_{k-1}-m_{k-2})r_k\Big]. \end{aligned} \tag{5.13}$$

Similarly, following Section 4.6, after the change of variables in $\check{\mathcal{M}}$ (5.9) the following compensator is obtained:

$$\begin{aligned} \check{m}_k &= \hat{\theta}_1\check{m}_{k-1}+\hat{\theta}_2[r_{k+1}-r_k]+[\theta_3\check{m}_{k-1}+\theta_4 r_{k+1}]\mathrm{sign}(r_{k+1}-r_k)[r_{k+1}-r_k] \\ &\quad +[\theta_5 r_{k+1}\check{m}_{k-1}+\theta_6 r_{k+1}^2]\mathrm{sign}(r_{k+1}-r_k)+[\hat{\theta}_7\check{m}_{k-1}+\hat{\theta}_8 r_{k+1}][r_{k+1}-r_k]^2 \\ &\quad +\hat{\theta}_9[r_{k+1}-r_k]^3. \end{aligned} \tag{5.14}$$

The parameters of compensators C_{R} (5.11)-(5.12), C_{I} (5.13) and $\check{C}$ (5.14) are given in Table 5.1.

5.2.2.2 Compensation performance

The designed compensators were applied to the piezoelectric actuator (5.1) with results summarized in Figure 5.9. From the hysteresis loops, Figure 5.9(c), it is clear that a practically linear relation between the reference and the compensated output was achieved. This would greatly facilitate the design and increase the performance of a feedback controller. For the uncompensated system, the input is the reference r_k.

The accuracy achieved by each compensator was quantified by the MAPE index (5.10). In order to quantify how much more effort must be made to achieve compensation, the normalized sum of the absolute variation of the input (NSAVI):

$$\mathrm{NSAVI} = \sum_{k=1}^{N-1}\frac{\left|m_{k+1}-m_k\right|}{\left|r_{k+1}-r_k\right|}, \tag{5.15}$$

is calculated. These indices are shown in Table 5.3.

Table 5.3: Compensator performance.

Design Approach	**Compensator**	MAPE	NSAVI
Section 4.4	C_{R} (5.11)-(5.12)	0.1486	1.1377
Section 4.5	C_{I} (5.13)	0.1516	1.1363
Section 4.6	$\check{C}$ (5.14)	0.5443	1.1487
Black-box	not shown	1.8194	1.1542
no compensation		6.5363	1.0000

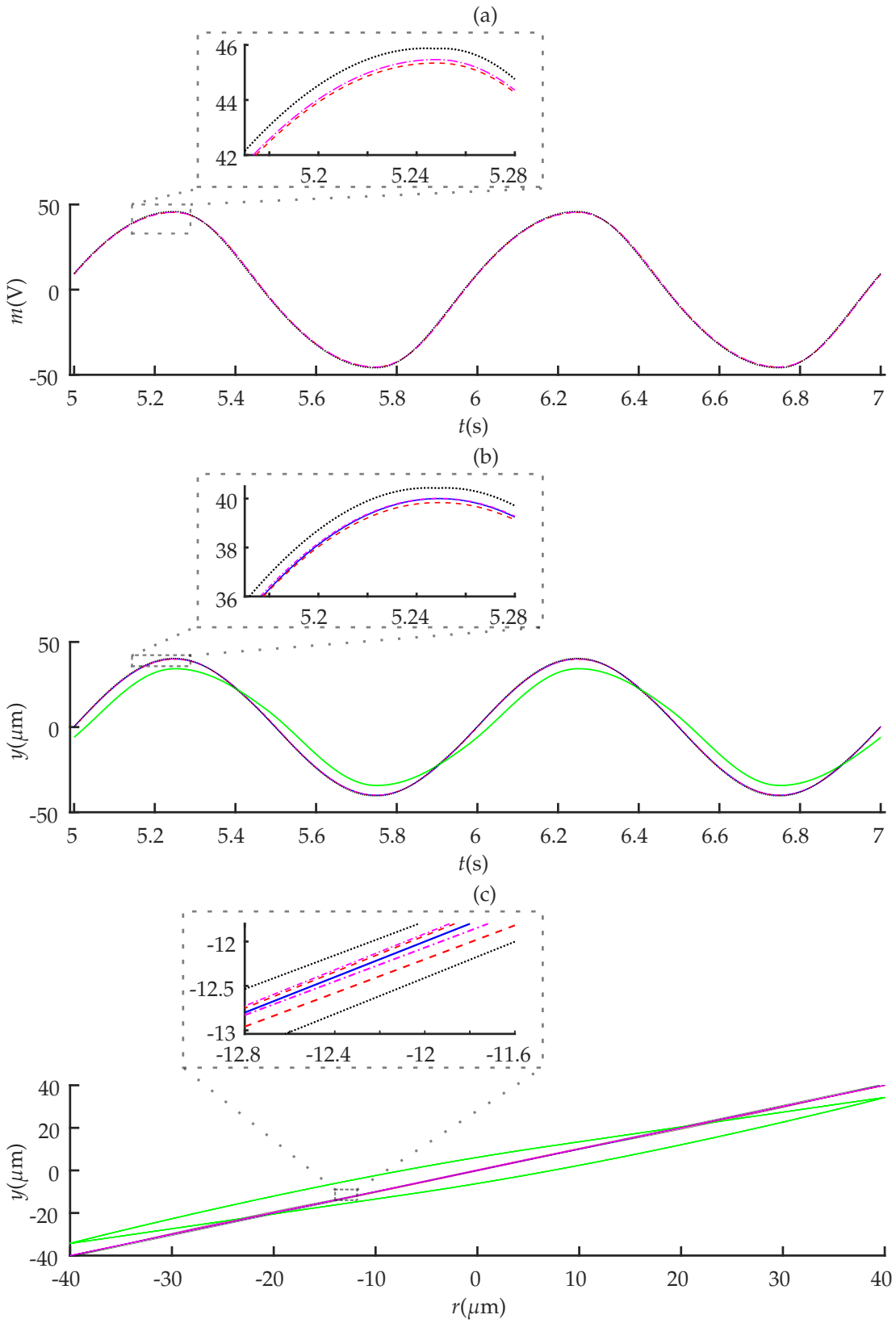

Figure 5.9: Hysteresis compensation for the piezoelectric actuator (5.1). (a) Compensation inputs, (b) outputs and in (c) hysteresis loops. (- · -) results obtained with compensator C_{R} (5.11)-(5.12), (- -) results with compensator C_{I} (5.13), ($\cdots$) results with compensator $\check{C}$ (5.14), (—) uncompensated system output and (—) reference $r = 40\sin(2\pi t)\ \mu$m.

The results shown in Figure 5.9 and Table 5.3 indicate that the compensators may provide a significant improvement in the tracking performance of system (5.1). The improvement achieved in the tracking error, due to the use of compensators C_{R} and C_{I}, was about 97.7% at the cost of an approximately 13.7% increase in the compensation effort when compared to the uncompensated system. Although these two compensation approaches produce similar results, the design approach of Section 4.4 does not need to impose constraints during the identification procedure and therefore can handle more general model structures to design compensators. On the other hand, to obtain the compensation input m_k at each iteration, it is necessary to calculate the roots of a polynomial compensator C_{R} and then solve the optimization problem proposed in Definition 4.2, whereas for compensator C_{I} only a single algebraic equation is calculated. For compensator $\check{C}$, which also provides the compensation input by solving a single algebraic equation, the tracking error was reduced by about 91.6% at the cost of a 14.8% increase in the compensation effort. Therefore, despite the particularities of each compensation approach, a general conclusion that can be drawn from these results is that either approach significantly reduces tracking error compared to not using one.

To further characterize the performance of the proposed designs, the influence of the sampling time T_{s} was also investigated. In Figure 5.10, it can be seen that the model accuracy somewhat deteriorates as T_{s} is increased. It should be noted that even the largest values of T_{s} in Figure 5.10 are still comfortably small in terms of the sampling theorem. However, since one of the regressors is the first difference of the input, then the identification of systems with hysteresis seems to be particularly sensitive to the sampling time (Lacerda Júnior et al., 2017). Another conclusion that can be drawn from Figure 5.10 is that, for all three design approaches, the compensation performance is correlated to the model accuracy, and that the approach in Section 4.4 is somewhat less sensitive to such accuracy; see Figure 5.10(a).

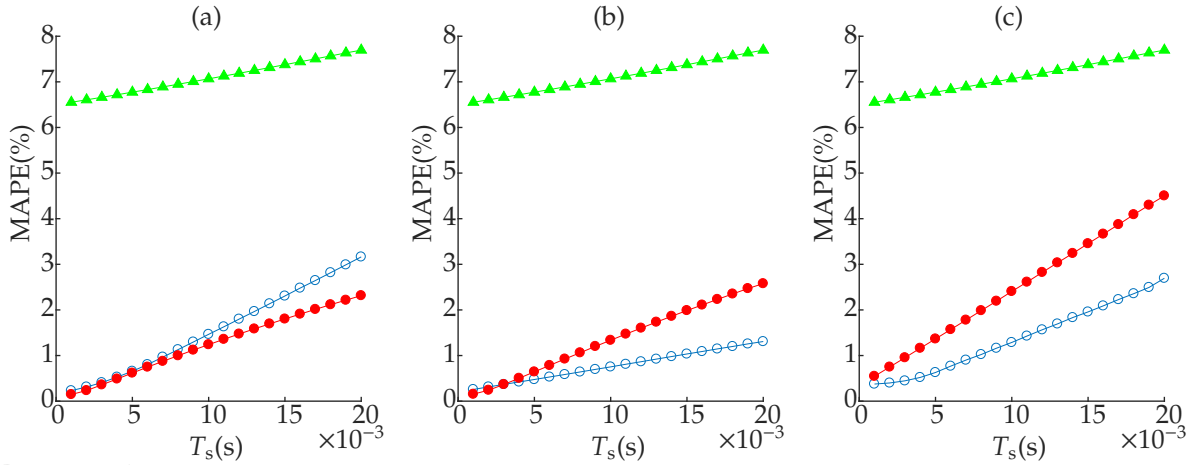

Figure 5.10: MAPE index (5.10) computed for the models and compensators described, respectively, by equations (a) $\mathcal{M}_{\mathrm{R}}$ (5.2) and C_{R} (5.11)-(5.12); (b) $\mathcal{M}_{\mathrm{I}}$ (5.6) and C_{I} (5.13); (c) $\check{\mathcal{M}}$ (5.9) and $\check{C}$ (5.14). (○) model and (●) tracking accuracies. (▲) accuracy of uncompensated system.

Finally, the same analysis was carried out for situations with different shapes of the hysteresis loop varying β in the range $0.004 \leq \beta \leq 0.1$ with increments of $\Delta = 0.002$; see Figure 5.11. The results are quite similar to the ones described so far and are not shown.

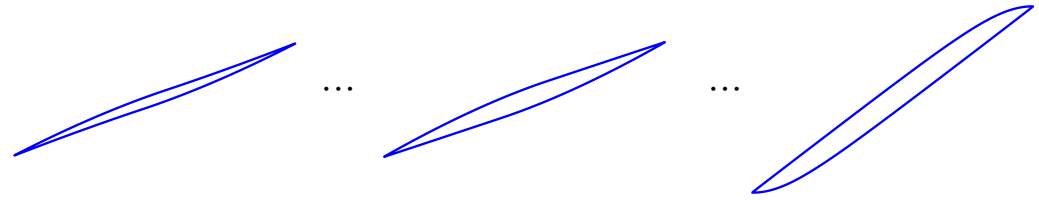

Figure 5.11: Bouc-Wen hysteresis loops.

5.3 Experimental Results

Both identification and compensation approaches are now applied to an experimental pneumatic control valve. This type of actuator is widely used in industrial processes, for which control performance can degrade significantly due to valve problems caused by nonlinearities (Srinivasan and Rengaswamy, 2005) such as friction (Romano and Garcia, 2011; Baeza and Garcia, 2018), dead-zone, dead-band and hysteresis (Choudhury et al., 2008). Hence, in this section we aim at compensation hysteresis using the developed techniques.

To illustrate the experimental setup adopted to identify models and design compensators for the pneumatic valve under study, which is the actuator of a level pilot plant, consider the schematic representation in Figure 5.12 (Tavares, 2020). The experimental setup can be summarized as follows. Using MATLAB® software installed on a microcomputer, the voltage input signal to be applied to the valve is digitally encoded and sent to a data acquisition board that performs the Digital/Analog (D/A) conversion. Such a voltage input is converted into a current signal through an auxiliary circuit, i.e. V/I conversion, and then sent to the pilot plant. In the pilot plant, this current signal, after passing I/P conversion, becomes a pressure signal applied to the valve. The measured output is the stem position of the pneumatic valve, which is converted into a voltage signal via a potentiometer. Such a voltage signal is sent to the data acquisition board that performs the Analog/Digital (A/D) conversion so that this digital signal can be read by the microcomputer.

The output and input voltage signals are measured with a sampling time of T_s=0.01 s. For model identification, the input signal is set as a PRFS (2.22)–(2.25), for which the following setup coefficients were used: n_f=1, f_1=0.1 Hz, v=1, o_1=3 V, G_1=0.8 V, and N=N_1=20000. The identification data are shown in Figure 5.13. For model validation, the input is a sinusoid with frequency 0.1 Hz. Both data sets are 200 s long (N=20000).

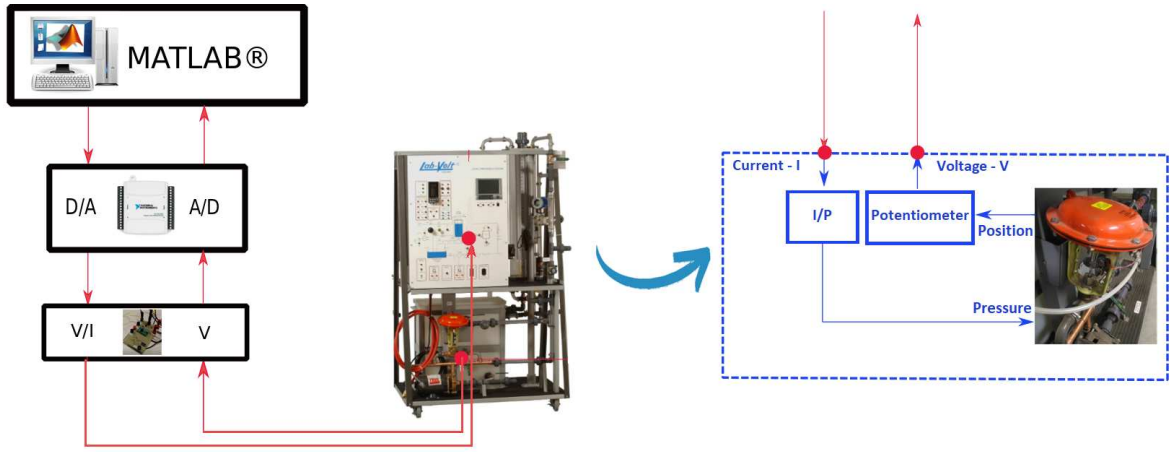

Figure 5.12: Schematic representation of the experimental setup involving the pneumatic valve under study. Adapted from (Tavares, 2020).

The identification of the direct $\mathcal{M}$ and inverse $\check{\mathcal{M}}$ models was performed as in Section 5.2. The pool of candidate terms is generated with ℓ=3, n_y=1 and n_u=n_{ϕ_1}=n_{ϕ_2}=2. The model parameters are estimated using (2.48) in order to comply with Lemma 4.1.

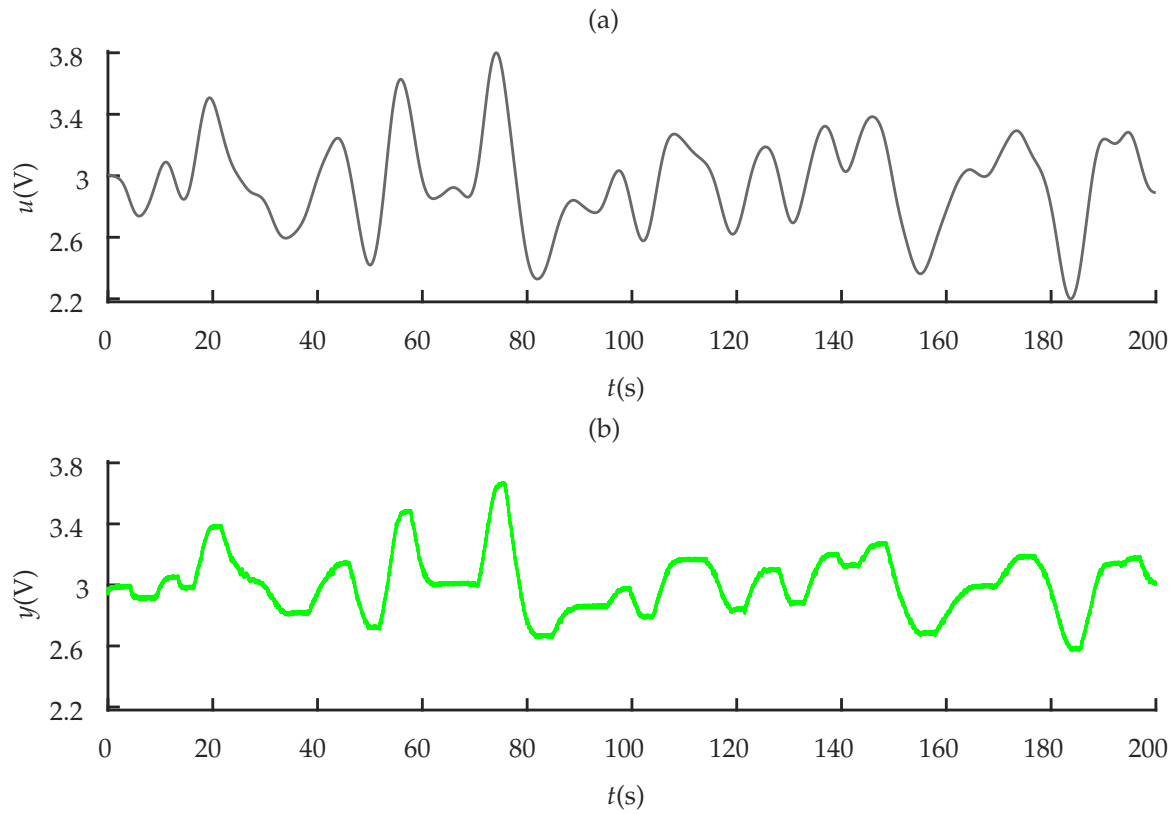

Figure 5.13: Identification data collected from pneumatic control valve. (a) excitation input as a PRFS, and (b) measured output.

An interesting point to be emphasized concerns the identification of the direct model $\mathcal{M}_{\mathrm{R}}$, which is identified to design compensators using the approach described in Section 4.4, for the valve under study. For this model, the meta-parameters used were: ℓ=3, n_y=2 and n_u=n_{ϕ_1}=n_{ϕ_2}=1, whereas for models $\mathcal{M}_{\mathrm{I}}$ and $\breve{\mathcal{M}}$ the values previously defined were adopted. This difference between meta-parameters values and some more details are discussed in (Tavares, 2020; Tavares et al., 2021, 2022). In what follows, the three identified models and the respective compensators designed from them are presented, as well as the results achieved with each one of them so that comparisons can be made.

The estimated model $\mathcal{M}_{\mathrm{R}}$ is:

$$\hat{y}_k=0.976\hat{y}_{k-1}+0.024\hat{y}_{k-2}+0.119\phi_{1,k-1}+3.76\phi_{2,k-1}\phi_{1,k-1}u_{k-1}-4.73\phi_{2,k-1}\phi_{1,k-1}\hat{y}_{k-2}. \quad (5.16)$$

Note that, as the first two terms of this model are linear output regressors, the constraint used to fulfill Lemma 4.1 became to ensure that the sum of the parameters of these two regressors was equal to 1, which can be verified as $\Sigma_y = 0.976 + 0.024 = 1$. Following the design approach of Section 4.5, model $\mathcal{M}_{\mathrm{I}}$ is identified as:

$$\hat{y}_k=\hat{y}_{k-1} - 19.76\phi_{1,k-2} + 19.32\phi_{1,k-1}+9.44\phi_{2,k-2}\phi_{1,k-2}u_{k-2}-12.61\phi_{2,k-2}\phi_{1,k-2}\hat{y}_{k-1}, \quad (5.17)$$

and the inverse model $\breve{\mathcal{M}}$ (Section 4.6) is:

$$\begin{aligned}\hat{u}_k \;=\; & \hat{u}_{k-1}+86.67\breve{\phi}_{1,k-1}-85.02\breve{\phi}_{1,k-2}-0.98\breve{\phi}_{1,k-1}y_{k-2}+1.72\breve{\phi}_{2,k-2}\breve{\phi}_{1,k-2}y_{k-2} \\ & -1.13\breve{\phi}_{2,k-2}\breve{\phi}_{1,k-2}\hat{u}_{k-1}, \end{aligned} \quad (5.18)$$

which was estimated from a smoothed version of y_k obtained by quadratic regression. This is done only to estimate $\breve{\mathcal{M}}$ to avoid the error-in-the-variables problem, since y_k serves as the input for $\breve{\mathcal{M}}$. Each model performance is given in Figure 5.14 and Table 5.4.

Table 5.4: Experimental model performance.

Context	**Model**	MAPE
Section 4.4	$\mathcal{M}_{\mathrm{R}}$ (5.16)	3.4072
Section 4.5	$\mathcal{M}_{\mathrm{I}}$ (5.17)	3.9267
Section 4.6	$\breve{\mathcal{M}}$ (5.18)	2.3746

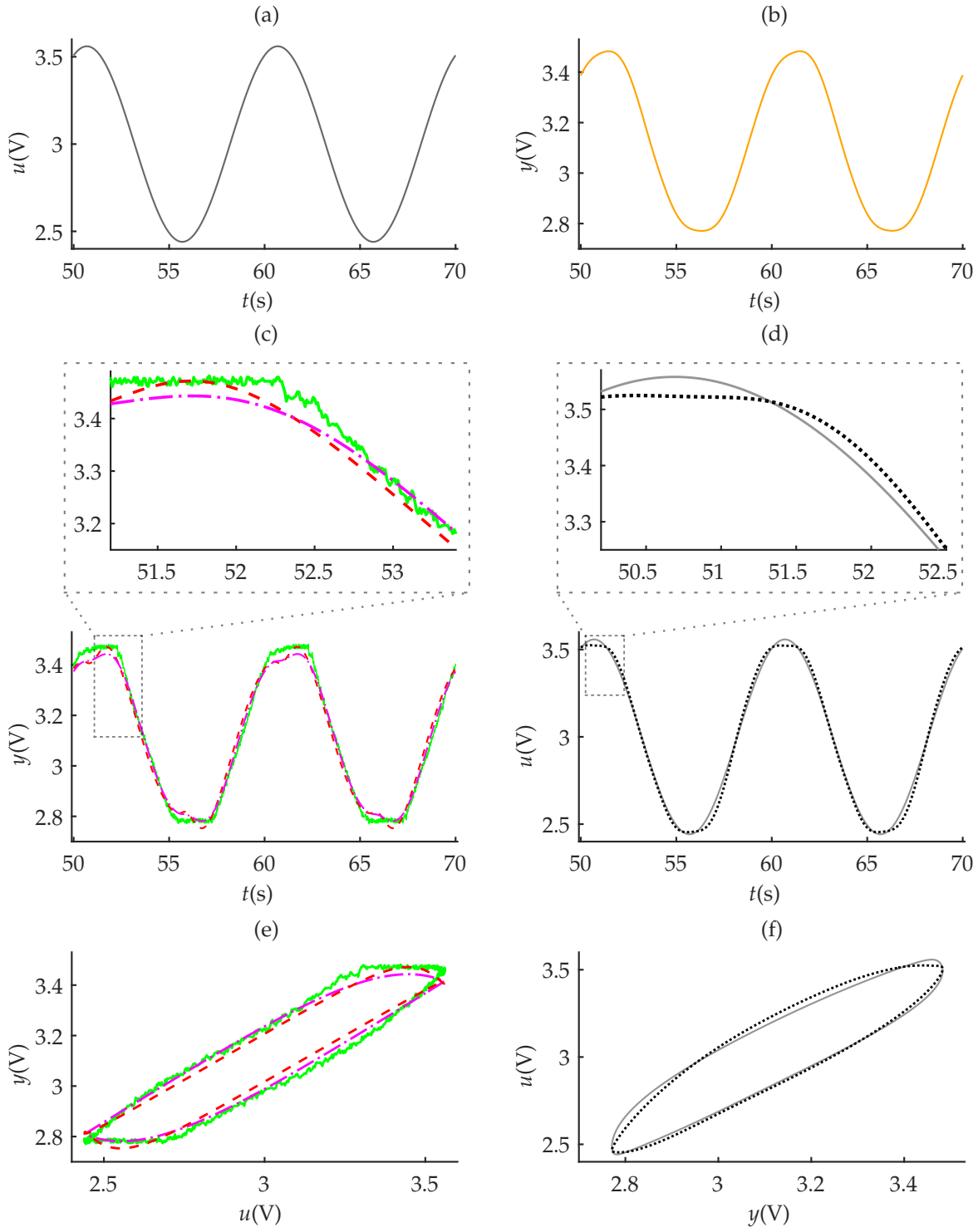

Figure 5.14: Left column refers to the direct models $\mathcal{M}_R$ (5.16) and $\mathcal{M}_I$ (5.17) and right column to the inverse model $\breve{\mathcal{M}}$ (5.18). (a) input u_k=0.56 sin(0.2πk) + 3 V and (c) the corresponding measured output (—) y and free-run simulation of models $\mathcal{M}_R$ (- · -) and $\mathcal{M}_I$ (- -); (b) smoothed version of y in (c); (d) the corresponding output which is u_k in (a) and free-run simulation of model $\breve{\mathcal{M}}$ (· · ·). (e) and (f) show the same data as (c) and (d), respectively.

As discussed earlier, the use of Lemma 4.1 provides a way to incorporate into a model the ability to mimic the feature of hysteretic systems in reaching different output values when subjected to an input that becomes constant during loading and unloading with the same final value, as shown in Figures 5.5, 5.6 and 5.8 for the numerical example. In the same line, such tests were performed for the experimental valve under study, whose results are shown in Figure 5.15.

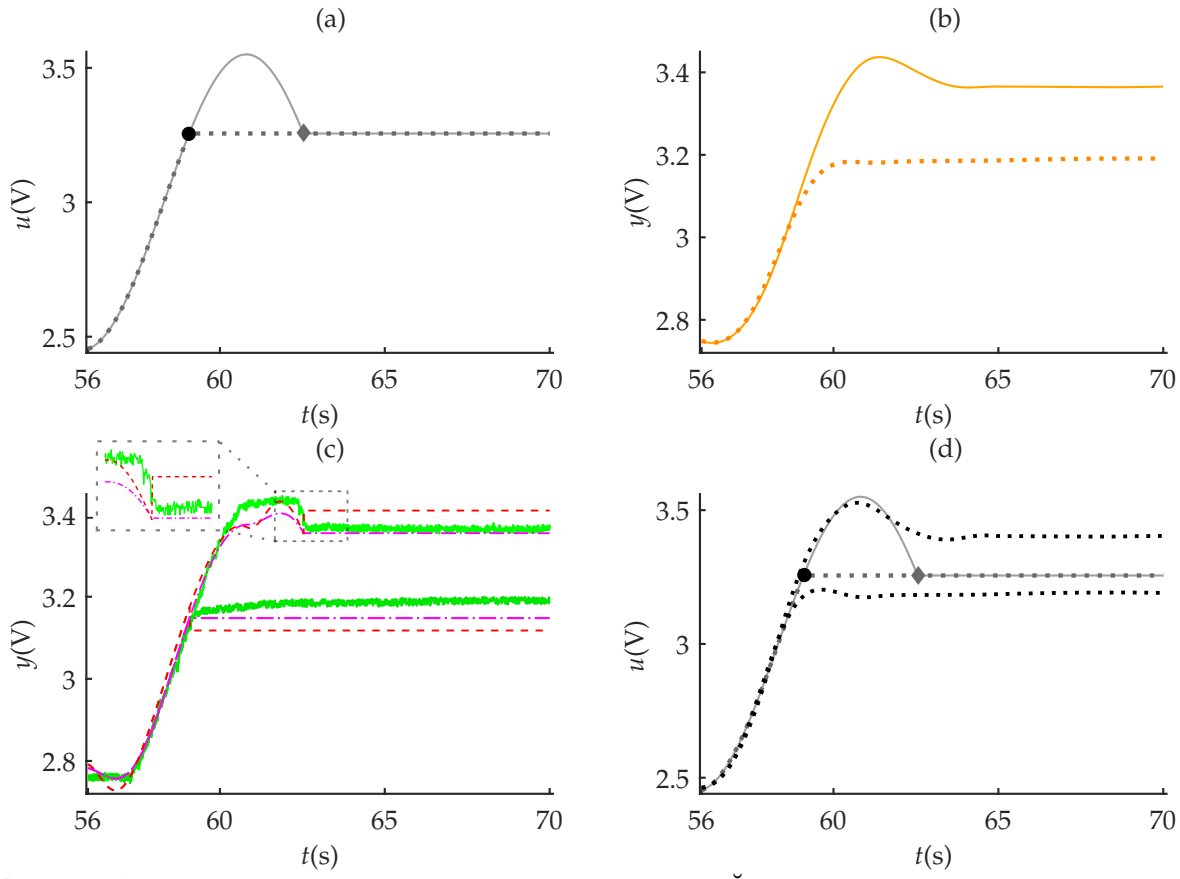

Figure 5.15: Results of models $\mathcal{M}_R$ (5.16), $\mathcal{M}_I$ (5.17) and $\breve{\mathcal{M}}$ (5.18) for a time-varying input that becomes constant. (a) sinusoidal input of voltage u_k=0.55 sin(0.2πk)+3 V that becomes constant during loading (•) and unloading (⧫) with final value 3.256 V and (c) the corresponding output of valve (—) y and models $\mathcal{M}_R$ (- · -) and $\mathcal{M}_I$ (- -); (b) smoothed version of y for loading (—) and unloading (· · ·) in (c) which is the input of the inverse model, whose output which is u in (a) and model $\breve{\mathcal{M}}$ (· · ·) free-run simulation are in (d).

It should be noted that, in terms of the identified direct models $\mathcal{M}_R$ and $\mathcal{M}_I$, the same peculiarities found in the results obtained in the numerical example shown in Figure 5.5 occur in the experimental results; see left side of Figure 5.15. Considering the case where the time-varying input becomes constant during the unloading regime, which is highlighted in the enlarged part of Figure 5.15(c), models $\mathcal{M}_R$ and $\mathcal{M}_I$ present steady-state errors of about 0.009 V and 0.046 V, respectively. In this case, it is interesting to note that when the measured output reaches the constant value plateau, the estimated output of model $\mathcal{M}_I$ has a value similar to that of model $\mathcal{M}_R$, however, it undergoes

a sudden change resulting in a considerable increase in its steady-state error; see Figure 5.15(c). It is worth remembering that, as explained for the results in Figure 5.5, this sudden behavior is related to the fact that only the input regressors $\phi_{i,k}$ with delay $k-1$ are immediately canceled. Therefore, as model $\mathcal{M}_{\mathrm{R}}$ has higher-delay input regressors, which are multiplied by high magnitude parameters, such terms produce an underlying dynamic during the transition to steady-state, resulting in such considerable errors. In terms of the inverse model $\check{\mathcal{M}}$, the steady-state error produced is about $0.145\,\mathrm{V}$. In this context, an interesting point refers to the fact that the input of the inverse model is the measured output, which, as it is a noisy signal, requires pre-processing to avoid the error-in-the-variables problem. For this reason, note that the smoothed version of the measured output, shown in Figure 5.15(b), exhibits some fluctuation rather than being constant and, consequently, this behavior can also be observed in the estimated output of the inverse model; see Figure 5.15(d).

Models $\mathcal{M}_{\mathrm{R}}$ (5.16), $\mathcal{M}_{\mathrm{I}}$ (5.17) and $\check{\mathcal{M}}$ (5.18) are used to implement the approaches described in Sections 4.4, 4.5 and 4.6, thus yielding, respectively, the three compensators presented below. The designed compensator C_{R} is:

$$\underbrace{3.76}_{c^{\mathrm{L}}_{2,k}}\, m_k^2 + \underbrace{\left[0.119-3.76m_{k-1}-4.73r_{k-1}\right]}_{c^{\mathrm{L}}_{1,k}}\, m_k + \underbrace{\left[0.976r_k+0.024r_{k-1}-r_{k+1}+[4.73r_{k-1}-0.119]m_{k-1}\right]}_{c^{\mathrm{L}}_{0,k}} = 0, \quad \text{for} \quad m_k > m_{k-1}, \tag{5.19}$$

$$\underbrace{-3.76}_{c^{\mathrm{U}}_{2,k}}\, m_k^2 + \underbrace{\left[0.119+3.76m_{k-1}+4.73r_{k-1}\right]}_{c^{\mathrm{U}}_{1,k}}\, m_k + \underbrace{\left[0.976r_k+0.024r_{k-1}-r_{k+1}-[4.73r_{k-1}+0.119]m_{k-1}\right]}_{c^{\mathrm{U}}_{0,k}} = 0, \quad \text{for} \quad m_k < m_{k-1}, \tag{5.20}$$

whose root to be used as the compensation input is chosen as described in Definition 4.2. Compensators C_{I} and $\check{C}$ are, respectively, given by:

$$\begin{aligned} m_k \;=\; \frac{1}{19.32}\Big[& r_{k+1}-r_k+19.32m_{k-1}+19.76[m_{k-1}-m_{k-2}]-9.44\,\mathrm{sign}(m_{k-1}-m_{k-2})[m_{k-1}-m_{k-2}]m_{k-1} \\ & +12.61\,\mathrm{sign}(m_{k-1}-m_{k-2})[m_{k-1}-m_{k-2}]r_k\Big], \end{aligned} \tag{5.21}$$

and

$$\begin{aligned} \check{m}_k \;=\; & \check{m}_{k-1}+86.67[r_{k+1}-r_k]-85.02[r_k-r_{k-1}]-0.98[r_{k+1}-r_k]r_k+1.72\,\mathrm{sign}(r_k-r_{k-1})[r_k-r_{k-1}]r_k \\ & -1.13\,\mathrm{sign}(r_k-r_{k-1})[r_k-r_{k-1}]\check{m}_{k-1}. \end{aligned} \tag{5.22}$$

Experimental compensation results are shown in Figure 5.16 and assessed in Table 5.5. Note that the three approaches significantly reduce the tracking error. As a side note, it is worth mentioning that the performance of these three compensators was com-

pared with one designed from the approach proposed in (Rakotondrabe, 2011), which is based on the Bouc-Wen model, whose detailed discussion is provided in (Tavares et al., 2022). It was found that all compensators can achieve nonlinearity compensation for the valve and that they are competitive. In what follows, for brevity and to keep the focus on the characteristics of each of the compensation approaches proposed here, the compensator from (Rakotondrabe, 2011) is not addressed, however, we provide a detailed discussion and comparison of it in (Tavares et al., 2022).

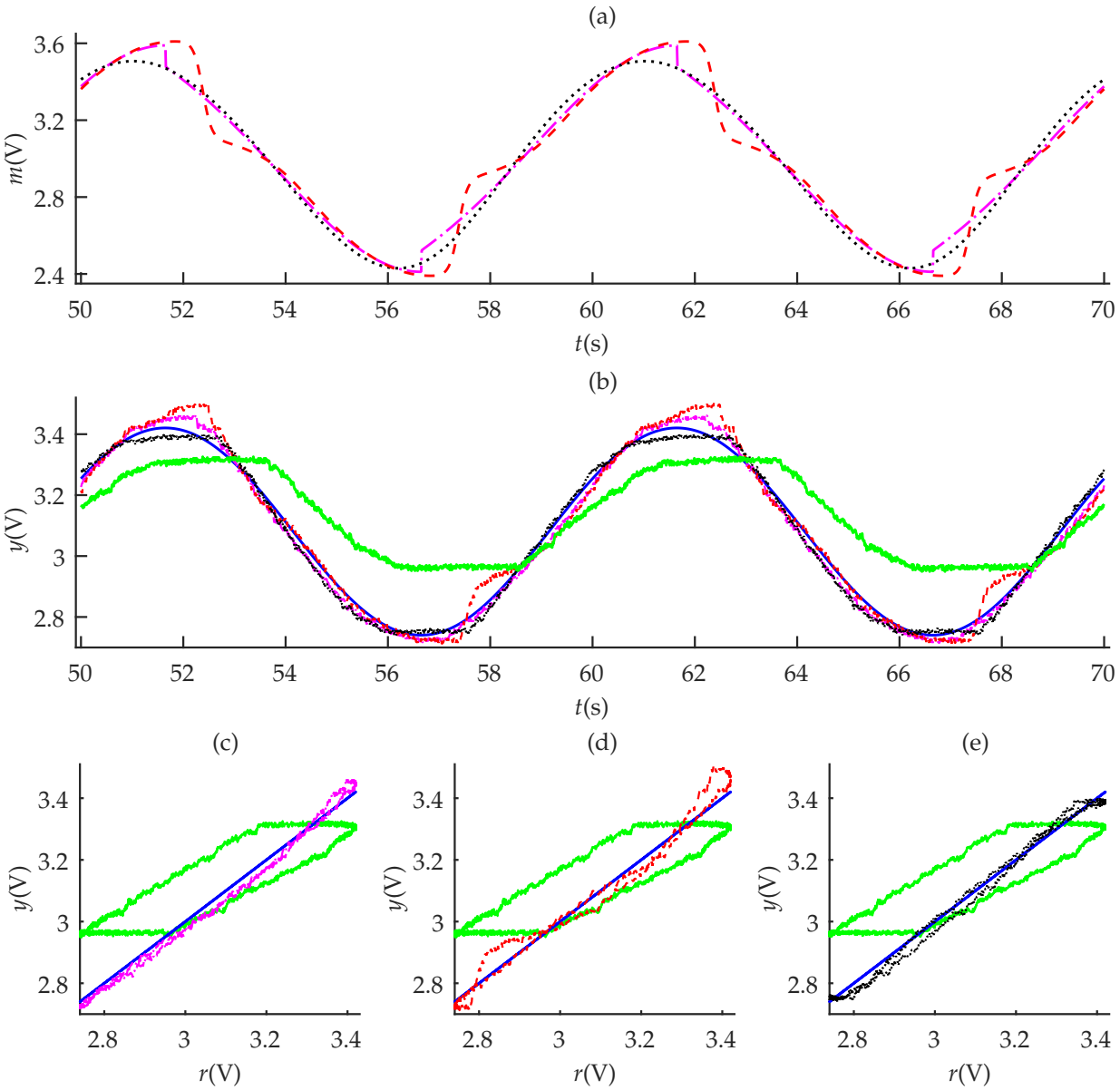

Figure 5.16: Hysteresis compensation for the pneumatic valve. (a) Compensation inputs, (b) its temporal responses and in (c), (d) and (e) the hysteresis loops. (- · -) refers to results obtained with compensator C_{R} (5.19)-(5.20), (- -) illustrates the results obtained with compensator C_{I} (5.21), (· · ·) refers to the results by using compensator $\check{C}$ (5.22), (—) the system output without compensation, and (—) the reference r=0. 34 sin(0. 2πt)+3. 08 V.

Table 5.5: Performance of the compensation step. Experimental results.

Design Approach	**Compensator**	MAPE	NSAVI
Section 4.4	C_{R} (5.19)-(5.20)	3.2636	1.7321
Section 4.5	C_{I} (5.21)	4.3228	1.7913
Section 4.6	$\check{C}$ (5.22)	2.9166	1.6140
no compensation		18.1308	1.0000

The compensation produced by $\check{C}$ (5.22) is smoother than the one obtained with C_{R} (5.19)-(5.20) and with C_{I} (5.21); see Figure 5.16(a). This occurs because, for the compensator $\check{C}$, the argument of the sign function depends on the difference of the reference signal, while, for the compensator C_{I}, it depends on the difference of the autoregressive variable which usually produces stronger oscillations and sudden changes; see Figure 5.16(a), e.g. in the range of 51−53 s. A similar but somewhat smooth change in the compensation signal also occurs when using the compensator C_{R}, since during the transition from loading to unloading regime this compensator switches from using (5.19) to using (5.20) to compute m_k; see Figure 5.16(a), e.g. around 52 s. As a result, larger compensation effort is required when using compensators C_{R} and C_{I} as quantified by NSAVI (5.15) in Table 5.5. Such results corroborate the effectiveness that any of the proposed compensation approaches in mitigating the nonlinearity present in the investigated valve.

It should be mentioned that, although $\check{C}$ requires less compensation effort, a priori, a careful pre-processing of the data will be necessary during the identification of the inverse model $\check{\mathcal{M}}$ if the measured output is a noisy signal. In terms of compensator C_{I}, special care is required during the structure selection of model $\mathcal{M}_{\mathrm{I}}$ so that the compensation input m_k can be explicitly calculated, as discussed before. On the one hand, this compensation law tends to be easier to calculate than the one obtained with the compensator C_{R}. On the other hand, it tends to produce a compensation input with more abrupt changes and, consequently, leading to a greater compensation effort, as discussed above for the results in Figure 5.16. When it comes to compensator C_{R}, there is no need for special treatment during the identification of model $\mathcal{M}_{\mathrm{R}}$ and therefore more general model structures can be used to design such a compensator. However, for cases where model $\mathcal{M}_{\mathrm{R}}$ leads to a compensator C_{R} (Section 4.4) with a degree of nonlinearity greater than 3, which, although not common in practice, but could happen, numerical solvers would be necessary to find its solutions/roots, besides the need to solve the optimization problem proposed in Definition 4.2 for choosing which root to use. In this case, this compensator can become a problem for more demanding online applications. Fortunately, many systems can be represented by models $\mathcal{M}_{\mathrm{R}}$ that, when subjected to the steps described in Section 4.4, produce compensators C_{R} up to 3rd degree of nonlinearity, for which the roots can be found with analytic expressions, as pointed out in (Tavares et al., 2022).

As extensively discussed earlier, the use of Lemma 4.1 enables to the identified model to "remember" its last state and remain there even when the time-varying input becomes constant. For the experimental valve under analysis, such feature was verified in the identified models $\mathcal{M}_{\mathrm{R}}$, $\mathcal{M}_{\mathrm{I}}$ and $\check{\mathcal{M}}$, whose results were shown in Figure 5.15. A natural question that may arise is: *Is this feature also observed in compensators designed even from models that comply with Lemma 4.1?* Basically, the answer to this question is that for compensator $\check{C}$ this feature is guaranteed, while for compensators C_{R} and C_{I} there is no guarantee. However, a more careful investigation of some subtle features, like the one mentioned above, which are found in the compensators designed using the three approaches proposed in Chapter 4 refer to topics to be pursued in the future.

For illustrative purposes, the experimental compensation results, when the time-varying reference becomes constant, are shown in Figure 5.17.

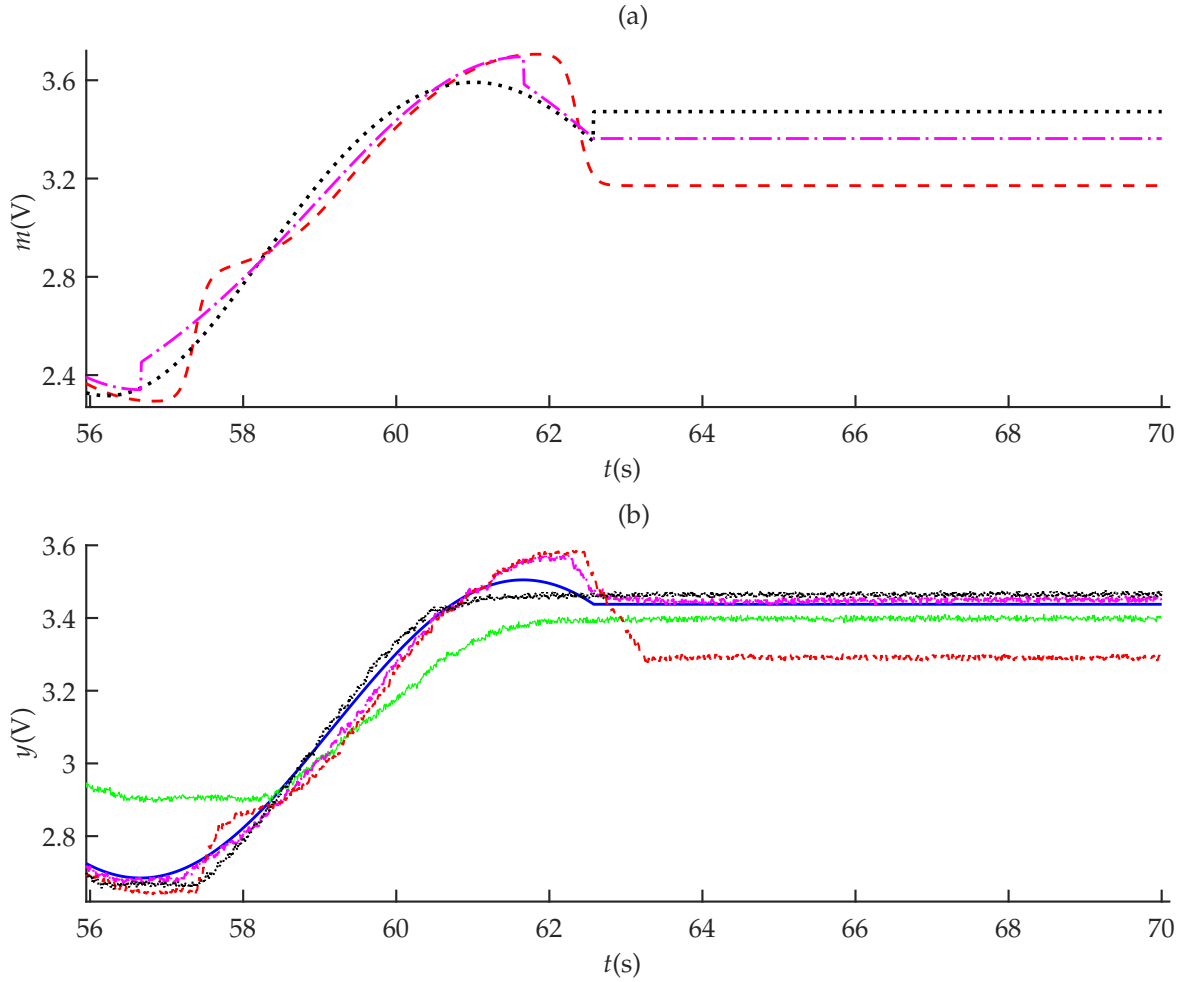

Figure 5.17: Results of compensators C_{R} (5.19)-(5.20),C_{I} (5.21) and $\check{C}$ (5.22) for a time-varying reference signal that becomes constant. (a) Compensation inputs, and (b) its temporal responses. (-·-) refers to results obtained with compensator C_{R}, (- -) illustrates the results obtained with compensator C_{I}, (···) refers to the results by using compensator $\check{C}$, (—) the system output without compensation, and (—) the reference r=0. 41 sin(0. 2πt)+3. 09 V that becomes constant with final value 3. 438 V.

As can be seen in Figure 5.17, the results indicate that all compensators were able to provide constant input values when the reference becomes constant and that some steady-state errors are found, which is expected since the compensation methods work in open-loop. Note that such compensation errors could be overcome if a feedback controller was combined with the compensation approach. This is a matter to be investigated in the future.

5.4 Concluding Remarks

This chapter presented the numerical and experimental results achieved with the identification and compensation proposals raised in Chapter 4. In terms of hysteresis identification, it has been shown that the use of the proposed constraints on the structure (Assumption 4.1) and on the parameters (Lemma 4.1) provide NARX models that are able to describe both dynamical and static features of such systems, whose comparison with other identified models that do not use these constraints is provided in Figure 5.6. In addition, performing the quasi-static analysis in such models, which was put forward in Section 4.2.2, it is possible to see how the hysteresis loop occurs on the input-output plane; see Figures 4.1, 5.3, 5.4 and 5.7.

In the context of hysteresis compensation, this thesis proposes three approaches to design compensators. An important aspect of such procedures is that they show how a model-based compensator can be designed with or without the need to enforce some structural specifications during the identification procedure in such way that the identified NARX model can be effectively used to mitigate the hysteresis nonlinearity. Details of each compensation approach are given in Chapter 4. Such approaches are not limited to hysteresis and can be extended to other nonlinearities. In addition, compensators designed by all proposed approaches can be readily employed in online compensation schemes.

The effectiveness of the compensation schemes is illustrated by means of a simulated hysteretic system (Section 5.2) and an experimental pneumatic valve (Section 5.3). All compensators provided nonlinearity compensation for both systems. Some peculiarities found in each approach were discussed.

Based on both numerical and experimental results, it has been observed that the quality of the achieved compensation is correlated with the accuracy of the identified model; compare Table 5.2 with Table 5.3 and Table 5.4 with Table 5.5. Also, our results suggest that the compensation effort tends to be lower and more effective whenever the identified models are more accurate. In particular, compensators based on gray-box models clearly outperformed those based on black-box models.

Finally, as a general remark, we noticed that the identified models have a discontinuity due to the sign function used in some regressors. When the model has many such terms, it sometimes happens that the compensation signal presents abrupt transitions. The use of smoother functions in place of the sign function, in order to alleviate this

problem, will be investigated in the future. In addition, as the designed compensators were able to cancel most of the nonlinearity of the investigated systems, the design of linear feedback controllers would be promising to implement a closed-loop scheme together with these compensators. This would allow compensation errors, both dynamic and steady-state, to be reduced and thus improve tracking and regulation performance. Also, a more analytical study of the compensators designed with each of the proposed approaches also correspond to interesting topics to be pursued in the future.

Chapter 6

Conclusions

6.1 Final Considerations

This thesis detailed three systematic methodologies for designing compensators, via identified NARX models, and put forward a new look at the process of identification and validation of hysteretic systems. In terms of compensation, the goal is that the use of the designed compensator in cascade with the system under investigation, in an open-loop scheme (Figure 4.5(b)), makes the relationship between a reference signal and the resulting output more linear and, therefore, more amenable for control. For the case of identification and validation of hysteretic systems, some constraints on the structure and parameters of NARX models are proposed in order to enable such models to describe not only the dynamic behavior, but also the static response which, although being a very important feature for hysteretic systems, has been neglected by many works in the literature. Some more detailed descriptions of the content and considerations of this thesis are given below.

Chapter 1 introduced and motivated the use of auxiliary information when identifying systems in order to build models suitable to be used for some specific purpose, such as predicting subtle dynamic behaviors or using them to design compensators. Also, it punctuated the contributions of this thesis.

Chapter 2 presented the literature review on modeling of hysteretic systems. Some of the classic phenomenological models of hysteresis, already established in the literature, were briefly contextualized, with emphasis on the Bouc-Wen model (Section 2.2.1) and the Prandtl-Ishlinskii operator (Section 2.2.2). Aiming at a more comprehensive model, not limited to describing only the hysteresis nonlinearity, some of the main concepts, definitions and tools formulated based on the NARX philosophy, which corresponds to a black-box approach, were addressed. However, as the black-box approach does not allow to obtain models that reproduce more subtle aspects of the system dynamics, such as the hysteretic behavior, a gray-box modeling approach was revisited. In this case, all necessary extensions in the formulation and definitions to cover the black-box and gray-box techniques have been made, and also some interesting tips and fair contributions were duly shared, such as the proposed procedures to generate excitation input signals suitable for nonlinear identification; see Section 2.3.2. Some works that use NARX models for hysteretic systems were reviewed, adopting a critical posture on their pros and cons to represent some features of such systems

(Section 2.3.7). Also, some properties of hysteretic systems, as well as alternative ways and guidelines for achieving them using gray-box NARX models, which correspond to interesting topics to be pursued in the future, were discussed in Section 2.3.8.

Chapter 3 reviewed some commonly used approaches to designing compensators and controllers for hysteretic systems. As the control and compensation schemes proposed in the literature are formulated to deal with the hysteretic behavior modeled by a given structure, those developed for the Bouc-Wen, the Prandtl-Ishlinskii and the NARX models presented in Chapter 2, were addressed. The revised approaches were divided into three categories that address the design of compensators, feedback controllers, and combining compensators with feedback controllers. Some control challenges that remain open were presented, as well as some advantages and limitations found in existing control approaches in the literature to deal with hysteresis.

Chapter 4 introduced the proposals developed in this thesis to deal with the problems of identification and compensation of nonlinearities in dynamical systems using NARX polynomial models. In order to build more appropriate models to describe hysteretic systems, we addressed some more subtle properties related to features commonly present in the static response of such systems (Section 2.3.8.3). By establishing a continuum of steady-state solutions (Definition 2.5) as an important feature in hysteretic models when subjected to constant inputs, we raised an additional condition to be considered during the identification procedure and also to be evaluated in models built to predict hysteresis. To guarantee this feature, we proposed some constraints on the structure (Assumption 4.1) and a particular one on the parameters (Lemma 4.1) of NARX models. In addition, a more general framework, based on a quasi-static analysis, was developed to explain how the hysteresis loop occurs in such models as an interplay of attracting and repelling regions in the input-output plane (Section 4.2.2). In the context of compensation, three approaches to design compensators were formulated for general dynamical systems and also for hysteretic systems. All proposed approaches have overcome singularity problems, such as those found in literature when the velocity variable is equal to zero (Section 3.2), since these problems were avoided during the design procedure. An important aspect of such procedures is that they show how a model-based compensator can be designed with or without the need to impose some structural specifications during the identification procedure, such that the identified NARX model can be effectively used to mitigate nonlinearities and, thus, make the behavior of the system more linear and therefore more amenable for control. Such approaches are not limited to nonlinear systems and can be extended to deal with linear systems using ARX models.

Chapter 5 presented the effectiveness of the identification and compensation proposals, made in Chapter 4, by means of a simulated piezoelectric actuator (Section 5.2) and an experimental pneumatic control valve (Section 5.3). As a first step, we employed both the proposed constraints to obtain models suitable for designing compensators and those to ensure that such models are also able to describe the static and dynamic

features of the hysteretic systems under study. In terms of hysteresis identification, a comparison of these models with other identified models that do not use the proposed constraints showed the improvement achieved by the constrained models in describing such hysteretic systems when a time-varying input becomes constant; e.g. see Figure 5.6. Also, some more detailed analyzes of how constraints coming from each compensation approach affect the predictive performance of the identified NARX models were presented. An interesting feature found in such analyzes refers to the case where the identified models, which comply with the constraints of the compensation approach described in Section 4.5, are subjected to time-varying input signals that become constant. For these models, a sudden change in the estimated output value, observed during the transition from time-varying input to steady-state, produces larger steady-state errors than those obtained from models built to meet the compensation approach described in Section 4.4, in which there is no need to impose structural constraints during the identification procedure. It was found that this sudden change in the estimated output value is directly related to the necessary constraints for the use of such models in the design of compensators following the approach of Section 4.5, as explained in Section 5.2. As a second step, the compensators designed with these identified models were placed in an open-loop scheme with the investigated system in order to improve its tracking performance. Both numerical and experimental results demonstrated that, despite the particularities of each compensation approach, either approach significantly reduces the tracking error compared to the uncompensated system. In terms of compensation quality, it was found that compensation performance is correlated with the accuracy of the identified model and that the compensation effort tends to be lower and more effective whenever the identified models are more accurate. In particular, compensators based on gray-box models outperform those based on models identified using black-box techniques. Some more detailed analyzes addressing particularities found in each compensator design approach, such as the possible need for careful data processing, adoption of constraints on the model structure and/or the use of numerical solvers, were also discussed.

6.2 Future Work

This section summarizes some possible guidelines for future work already discussed throughout this thesis and presents some more suggestions.

- As NARX models are not able to describe the property of non-local memory (Remark 2.19), it is suggested to investigate ways to incorporate this property in such models during the identification procedure; see Section 2.3.8.1.

- As some hysteretic systems can produce a symmetric or asymmetric hysteresis loop on the input-output plane, the development of a methodology that allows to

incorporate in NARX models the ability to describe asymmetric hysteresis is an interesting future work; see Section 2.3.8.2. For this case, it is suggested to look for ways to determine an appropriate asymmetric multi-valued function to be used as a candidate regressor and to investigate how this function will affect the number, location and stability of fixed points of the resulting models. Note that the symmetric hysteresis loop is already possible to be achieved with the NARX models built here.

- The presence of the sign function of the first difference of the input in some regressors of the identified NARX models generates discontinuity during the input signal transition from loading to unloading regime and vice-versa. When the model has many of these regressors, the compensator designed with such a model tends to produce a compensation input with abrupt transitions. Therefore, future works include investigating the use of smoother functions in place of the sign function during the identification procedure, and evaluating whether this change will result in compensators that provide smoother and more efficient compensation signals.

- As the designed compensators were able to cancel most of the nonlinearity of the investigated systems, a natural next step concerns the design of linear feedback controllers to be implemented in a closed-loop scheme together with these compensators. The objective is to compare the efficiency of the control system when the compensator is used together with the feedback controller and when these are used separately.

- Finally, a more analytical study of the compensators designed with each of the proposed approaches is a relevant topic. In this case, attention should be paid to compensators designed from the approaches provided in Sections 4.4 and 4.5, since there is no guarantee that features, such as stability, of the identified models are maintained when such models are used to design these compensators.

Bibliography

Abdullah, N. H. S., Karsiti, M. N., and Ibrahim, R. (2012). A review of pH neutralization process control. In *4th International Conference on Intelligent and Advanced Systems (ICIAS)*, volume 2, pages 594–598, Kuala Lumpur, Malaysia.

Abreu, P. E. O. G. B., Castro, H. C., Barbosa, B. H. G., and Aguirre, L. A. (2022). Identification and control of nonlinear systems: concepts and tools. *To be submitted*.

Abreu, P. E. O. G. B., Dreke, V. D. R., Aguirre, L. A., and Garcia, C. (2021). Enabling Invariant Models to Describe Time-Varying Dynamics: A Case Study. *IFAC-PapersOnLine*, 54(14):1–6. 3rd IFAC Conference on Modelling, Identification and Control of Nonlinear Systems, Tokyo, Japan.

Abreu, P. E. O. G. B., Souza, F. O., Teixeira, B. O. S., and Aguirre, L. A. (2018a). Projeto de Controlador PID via LMIs para Sistemas de Posicionamento Sujeitos a Histerese e Retardo de Tempo. In *Anais do XXII Congresso Brasileiro de Automática*, João Pessoa, Brasil.

Abreu, P. E. O. G. B., Tavares, L. A., Teixeira, B. O. S., and Aguirre, L. A. (2020). Identification and nonlinearity compensation of hysteresis using NARX models. *Nonlinear Dynamics*, 102(1):285–301.

Abreu, P. E. O. G. B., Teixeira, B. O. S., and Aguirre, L. A. (2018b). Projeto de Controlador *Backstepping* Robusto para Sistemas de Posicionamento Acionados por um Atuador Piezoelétrico. In *Anais do XXII Congresso Brasileiro de Automática*, João Pessoa, Brasil.

Abreu, P. E. O. G. B., Teixeira, B. O. S., and Mesquita, A. R. (2016a). Abordagens para atualização de parâmetros no contexto de estimação dual de estados e parâmetros. In *Anais do XXI Congresso Brasileiro de Automática*, Vitória, Brasil.

Abreu, P. E. O. G. B., Teixeira, B. O. S., and Mesquita, A. R. (2016b). Estimação recursiva de parâmetros variantes no tempo para sistemas com sinal de entrada com excitação intermitente. In *Anais do XXI Congresso Brasileiro de Automática*, Vitória, Brasil.

Aguirre, L. (1997). On the structure of nonlinear polynomial models: higher order correlation functions, spectra, and term clusters. *IEEE Transactions on Circuits and Systems I: Fundamental Theory and Applications*, 44(5):450–453.

Aguirre, L., Corrêa, M., and Cassini, C. (2002). Nonlinearities in NARX polynomial models: representation and estimation. *IEE Proceedings - Control Theory and Applications*, 149(4):343–348.

Aguirre, L. A. (1994). Some remarks on structure selection for nonlinear models. *International Journal of Bifurcation and Chaos*, 4(6):1707–1714.

Aguirre, L. A. (2014). Identification of smooth nonlinear dynamical systems with non-smooth steady-state features. *Automatica*, 50(4):1160–1166.

Aguirre, L. A. (2015). *Introdução à Identificação de Sistemas: Técnicas Lineares e Não Lineares Aplicadas a Sistemas Reais*. Editora UFMG, Belo Horizonte, 4 edition.

Aguirre, L. A. (2019). A Bird's Eye View of Nonlinear System Identification. *arXiv:1907.06803 [eess.SY]*.

Aguirre, L. A., Barroso, M. F. S., Saldanha, R. R., and Mendes, E. M. A. M. (2004). Imposing steady-state performance on identified nonlinear polynomial models by means of constrained parameter estimation. *IEE Proceedings - Control Theory and Applications*, 151(2):174–179.

Aguirre, L. A. and Billings, S. A. (1994). Validating identified nonlinear models with chaotic dynamics. *International Journal of Bifurcation and Chaos*, 04(01):109–125.

Aguirre, L. A. and Billings, S. A. (1995a). Dynamical effects of overparametrization in nonlinear models. *Physica D: Nonlinear Phenomena*, 80(1):26–40.

Aguirre, L. A. and Billings, S. A. (1995b). Improved structure selection for nonlinear models based on term clustering. *International Journal of Control*, 62(3):569–587.

Aguirre, L. A. and Mendes, E. M. A. M. (1996). Global Nonlinear Polynomial Models: Structure, Term Clusters and Fixed Points. *International Journal of Bifurcation and Chaos*, 6(2):279–294.

Ahmad, I. (2018). Two Degree-of-Freedom Robust Digital Controller Design With Bouc-Wen Hysteresis Compensator for Piezoelectric Positioning Stage. *IEEE Access*, 6:17275–17283.

Ahmad, I., Abdurraqeeb, A. M., and Ahmad, W. (2017). Modern H-Infinity Control Design for Ultra-Precise Micro/Nanopositioning with Hysteresis Compensation. In *9th IEEE-GCC Conference and Exhibition (GCCCE)*, pages 1–6, Manama, Bahrain.

Akaike, H. (1974). A New Look at the Statistical Model Identification. *IEEE Transactions on Automatic Control*, 19(6):716–723.

Al-Bender, F., Symens, W., Swevers, J., and Van Brussel, H. (2004). Theoretical analysis of the dynamic behavior of hysteresis elements in mechanical systems. *International journal of non-linear mechanics*, 39(10):1721–1735.

Al Janaideh, M., Rakheja, S., and Su, C.-Y. (2008a). Modelling rate-dependent symmetric and asymmetric hysteresis loops of smart actuators. *International Journal of Advanced Mechatronic Systems*, 1(1):32–43.

Al Janaideh, M., Rakheja, S., and Su, C.-Y. (2011). An Analytical Generalized Prandtl-Ishlinskii Model Inversion for Hysteresis Compensation in Micropositioning Control. *IEEE/ASME Transactions on Mechatronics*, 16(4):734–744.

Al Janaideh, M., Rakotondrabe, M., and Aljanaideh, O. (2016a). Further Results on Hysteresis Compensation of Smart Micropositioning Systems with the Inverse Prandtl-Ishlinskii Compensator. *IEEE Transactions on Control Systems Technology*, 24(2):428–439.

Al Janaideh, M., Rakotondrabe, M., and Tan, X. (2016b). Guest editorial focused section on hysteresis in smart mechatronic systems: Modeling, identification, and control. *IEEE/ASME Transactions on Mechatronics*, 21(1):1–3.

Al Janaideh, M., Su, C.-Y., and Rakheja, S. (2008b). Development of the rate-dependent Prandtl-Ishlinskii model for smart actuators. *Smart Materials and Structures*, 17(3):035026.

Aljanaideh, O., Rakotondrabe, M., Al-Darabsah, I., Aljanaideh, K. F., and Al Janaideh, M. (2017). A Model-Based Feedforward Hysteresis Compensator for Micropositioning Control. In *American Control Conference (ACC)*, pages 3506–3511, Seattle, WA, USA.

Ang, K. H., Chong, G., and Li, Y. (2005). PID Control System Analysis, Design, and Technology. *IEEE Transactions on Control Systems Technology*, 13(4):559–576.

Araújo, I. B. Q., Guimarães, J. P. F., Fontes, A. I. R., Linhares, L. L. S., Martins, A. M., and Araújo, F. M. U. (2019). NARX Model Identification Using Correntropy Criterion in the Presence of Non-Gaussian Noise. *Journal of Control, Automation and Electrical Systems*, 30(4):453–464.

Ayala, H. V. H., Habineza, D., Rakotondrabe, M., Klein, C. E., and Coelho, L. S. (2015). Nonlinear black-box system identification through neural networks of a hysteretic piezoelectric robotic micromanipulator. *IFAC-PapersOnLine*, 48(28):409–414.

Baeza, J. R. and Garcia, C. (2018). Friction compensation in pneumatic control valves through feedback linearization. *Journal of Control, Automation and Electrical Systems*, 29(3):303–317.

Baldacchino, T., Anderson, S. R., and Kadirkamanathan, V. (2013). Computational system identification for bayesian narmax modelling. *Automatica*, 49(9):2641–2651.

Banks, H. T., Kurdila, A. J., and Webb, G. (1997). Identification of hysteretic control influence operators representing smart actuators part I: Formulation. *Mathematical Problems in Engineering*, 3(4):287–328.

Bashash, S. and Jalili, N. (2006). Underlying memory-dominant nature of hysteresis in piezoelectric materials. *Journal of Applied Physics*, 100(1):014103.

Bequette, B. W. (1991). Nonlinear control of chemical processes: a review. *Industrial & Engineering Chemistry Research*, 30(7):1391–1413.

Berenyi, P., Horvath, G., Lampaert, V., and Swevers, J. (2005). Nonlocal hysteresis function identification and compensation with neural networks. *IEEE Transactions on Instrumentation and Measurement*, 54(6):2227–2238.

Bernstein, D. S. (2007). Ivory Ghost [Ask The Experts]. *IEEE Control Systems Magazine*, 27(5):16–17.

Beza, M. and Bongiorno, M. (2014). Application of recursive least squares algorithm with variable forgetting factor for frequency component estimation in a generic input signal. *IEEE Transactions on Industry Applications*, 50(2):1168–1176.

Bhadra, S., Panda, A., and Bhowmick, P. (2019a). A nonlinear model-based control scheme for benchmark industrial processes. In *International Conference on Opto-Electronics and Applied Optics (Optronix)*, pages 1–5, Kolkata, India.

Bhadra, S., Panda, A., and Bhowmick, P. (2019b). Model-based adaptive control scheme for benchmark pH-neutralisation process. In *International Conference on Ubiquitous and Emerging Concepts on Sensors and Transducers (UEMCOS)*, pages 1–6, Kolkata, India.

Biagiola, S. I., Agamennoni, O. E., and Figueroa, J. L. (2016). Robust control of wiener systems: Application to a ph neutralization process. *Brazilian Journal of Chemical Engineering*, 33(1):145–153.

Billings, S. A. (2013). *Nonlinear system identification: NARMAX methods in the time, frequency, and spatio-temporal domains*. John Wiley & Sons.

Billings, S. A. and Aguirre, L. A. (1995). Effects of the sampling time on the dynamics and identification of nonlinear models. *International Journal of Bifurcation and Chaos*, 05(06):1541–1556.

Billings, S. A. and Chen, S. (1989). Extended Model Set, Global Data and Threshold Model Identification of Severely Non-Linear Systems. *International Journal of Control*, 50(5):1897–1923.

Billings, S. A., Chen, S., and Korenberg, M. J. (1989). Identification of MIMO non-linear systems using a forward-regression orthogonal estimator. *International Journal of Control*, 49(6):2157–2189.

Billings, S. A. and Tao, Q. H. (1991). Model validity tests for non-linear signal processing applications. *International Journal of Control*, 54(1):157–194.

Billings, S. A. and Voon, W. S. F. (1986). Correlation based model validity tests for non-linear models. *International Journal of Control*, 44(1):235–244.

Billings, S. A. and Zheng, G. L. (1999). Qualitative validation of radial basis function networks. *Mechanical Systems and Signal Processing*, 13(2):335–349.

Bomberger, J. D. and Seborg, D. E. (1998). Determination of model order for NARX models directly from input-output data. *Journal of Process Control*, 8(5-6):459–468.

Bouc, R. (1971). Modèle Mathématique d'hystérésis (A mathematical model for hysteresis). *Acustica*, 21(1):16–25.

Brewick, P. T., Masri, S. F., Carboni, B., and Lacarbonara, W. (2016). Data-based nonlinear identification and constitutive modeling of hysteresis in NiTiNOL and steel strands. *Journal of Engineering Mechanics*, 142(12):04016107.

Brokate, M. and Sprekels, J. (1996). *Hysteresis and Phase Transitions*. Springer-Verlag, New York.

Cao, K., Li, R., Du, H., and Ma, J. (2019). Modeling and compensation of symmetric hysteresis in piezoceramic actuators. *Results in Physics*, 13:102095.

Cao, Y. and Chen, X. B. (2012). A Novel Discrete ARMA-Based Model for Piezoelectric Actuator Hysteresis. *IEEE/ASME Transactions on Mechatronics*, 17(4):737–744.

Cao, Y., Cheng, L., Chen, X. B., and Peng, J. Y. (2013). An inversion-based model predictive control with an integral-of-error state variable for piezoelectric actuators. *IEEE/ASME Transactions on Mechatronics*, 18(3):895–904.

Carboni, B., Lacarbonara, W., Brewick, P. T., and Masri, S. F. (2018). Dynamical response identificaiton of a class of nonlinear hysteretic systems. *Journal of Intelligent Material Systems and Structures*, 29(13):1–16.

Chan, R. W. K., Yuen, J. K. K., Lee, E. W. M., and Arashpour, M. (2015). Application of Nonlinear-Autoregressive-Exogenous model to predict the hysteretic behaviour of passive control systems. *Engineering Structures*, 85:1–10.

Chaoui, H. and Gualous, H. (2016). Adaptive Control of Piezoelectric Actuators with Hysteresis and Disturbance Compensation. *Journal of Control, Automation and Electrical Systems*, 27(6):579–586.

Charalampakis, A. E. (2010). Parameters of bouc-wen hysteretic model revisited. In *Proceedings of the 9th HSTAM International Congress on Mechanics*, pages 1–8, Limassol, Cyprus.

Chen, C.-T. (1999). *Linear System Theory and Design*. Oxford University Press, Inc., New York.

Chen, S. and Billings, S. A. (1989). Representations of non-linear systems: the NARMAX model. *International Journal of Control*, 49(3):1013–1032.

Chen, S., Billings, S. A., and Luo, W. (1989). Orthogonal Least Squares Methods and their Application to Non-Linear System Identification. *International Journal of Control*, 50(5):1873–1896.

Chen, X. and Hisayama, T. (2008). Adaptive Sliding-Mode Position Control for Piezo-Actuated Stage. *IEEE Transactions on Industrial Electronics*, 55(11):3927–3934.

Chen, X., Su, C.-Y., and Fukuda, T. (2008). Adaptive Control for the Systems Preceded by Hysteresis. *IEEE Transactions on Automatic Control*, 53(4):1019–1025.

Cheng, L., Liu, W., Hou, Z.-G., Yu, J., and Tan, M. (2015). Neural-Network-Based Nonlinear Model Predictive Control for Piezoelectric Actuators. *IEEE Transactions on Industrial Electronics*, 62(12):7717–7727.

Choudhury, M. A. A. S., Shah, S. L., and Thornhill, N. F. (2008). *Diagnosis of Process Nonlinearities and Valve Stiction: Data Driven Approaches*. Springer, Berlin Heidelberg.

Chuang, N. and Petersen, I. R. (2013). Robust H^{∞} Control of Hysteresis in a Piezoelectric Stack Actuator. *Journal of Dynamic Systems, Measurement, and Control*, 135(6):064501.

Coelho, A. A. R. and dos Santos Coelho, L. (2016). *Identificação de sistemas dinâmicos lineares*. Editora da UFSC, Florianópolis, 2 edition.

Croft, D., Shed, G., and Devasia, S. (1999). Creep, Hysteresis, and Vibration Compensation for Piezoactuators: Atomic Force Microscopy Application. *Journal of Dynamic Systems, Measurement, and Control*, 123(1):35–43.

de Almeida, L. A. L., Deep, G. S., Lima, A. M. N., and Neff, H. (2003). Limiting loop proximity hysteresis model. *IEEE Transactions on Magnetics*, 39(1):523–528.

Deng, L. and Tan, Y. (2009). Modeling Hysteresis in Piezoelectric Actuators Using NARMAX Models. *Sensors and Actuators A: Physical*, 149(1):106–112.

Deng, L., Yang, P., Xue, Y., and Lv, X. (2014). NARMAX model based pseudo-Hammerstein identification for rate-dependent hysteresis. In *Fifth International Conference on Intelligent Control and Information Processing*, pages 155–162, Dalian, China.

Domínguez-González, A., Stiharu, I., and Sedaghati, R. (2014). Practical Hysteresis Model for Magnetorheological Dampers. *Journal of Intelligent Material Systems and Structures*, 25(8):967–979.

Dong, R. and Tan, Y. (2014). Inverse Hysteresis Modeling and Nonlinear Compensation of Ionic Polymer Metal Composite Sensors. In *Proceeding of the 11th World Congress on Intelligent Control and Automation*, pages 2121–2125, Shenyang, China.

Doyle, J., Glover, K., Khargonekar, P., and Francis, B. (1989). State-Space Solutions to Standard $\mathcal{H}_2$ and $\mathcal{H}_\infty$ Control Problems. *IEEE Transactions on Automatic Control*, 34(8):831–847.

Draper, N. R. and Smith, H. (1998). *Applied regression analysis*. John Wiley & Sons, New York, 3 edition.

Drincic, B. and Bernstein, D. S. (2009). A multiplay model for rate-independent and rate-dependent hysteresis with nonlocal memory. In *Proceedings of the 48h IEEE Conference on Decision and Control (CDC)*, pages 8381–8386, Shenyang, China.

Du, H., Lam, J., and Zhang, N. (2006). Modelling of a magneto-rheological damper by evolving radial basis function networks. *Engineering Applications of Artificial Intelligence*, 19(8):869âĂŞ881.

Edwards, C. and Spurgeon, S. (1998). *Sliding mode control: theory and applications*. Crc Press, London, 1 edition.

Esbrook, A., Tan, X., and Khalil, H. K. (2013). Control of systems with hysteresis via servocompensation and its application to nanopositioning. *IEEE Transactions on Control Systems Technology*, 21(3):725–738.

Esbrook, A., Tan, X., and Khalil, H. K. (2014). Inversion-Free Stabilization and Regulation of Systems with Hysteresis via Integral Action. *Automatica*, 50(4):1017–1025.

Eskinat, E., Johnson, S. H., and Luyben, W. L. (1993). Use of auxiliary information in system identification. *Industrial & engineering chemistry research*, 32(9):1981–1992.

Falsone, A., Piroddi, L., and Prandini, M. (2015). A randomized algorithm for nonlinear model structure selection. *Automatica*, 60:227–238.

Feng, Y., Wu, Y.-X., Hu, Y.-M., and Su (2005). Adaptive backstepping control of a class of uncertain nonlinear systems with prandtl-ishlinskii hysteresis. In *International Conference on Machine Learning and Cybernetics*, volume 2, pages 697–701.

Fu, J., Liao, G., Yu, M., Li, P., and Lai, J. (2016). NARX neural network modeling and robustness analysis of magnetorheological elastomer isolator. *Smart Materials and Structures*, 25(12):125019.

Fujii, F., Tatebatake, K., Morita, K., and Shiinoki, T. (2018). A Bouc-Wen Model-Based Compensation of the Frequency-Dependent Hysteresis of a Piezoelectric Actuator Exhibiting Odd Harmonic Oscillation. *Actuators*, 7(3):37.

Ge, P. and Jouaneh, M. (1995). Modeling hysteresis in piezoceramic actuators. *Precision Engineering*, 17(3):211–221.

Ge, P. and Jouaneh, M. (1996). Tracking Control of a Piezoceramic Actuator. *IEEE Transactions on Control Systems Technology*, 4(3):209–216.

Gebraad, P. M. O., van Wingerden, J., Fleming, P. A., and Wright, A. D. (2013). LPV identification of wind turbine rotor vibrational dynamics using periodic disturbance basis functions. *IEEE Transactions on Control Systems Technology*, 21(4):1183–1190.

Gomez, J. C. (2015). Comparison of nonlinear identification techniques on a benchmark pH neutralization process. In *Conference on Electrical, Electronics Engineering, Information and Communication Technologies (CHILECON)*, pages 153–158, Santiago, Chile.

Gooijer, J. G., Abraham, B., Gould, A., and Robinson, L. (1985). Methods for Determining the Order of an Autoregressive-Moving Average Process: A Survey. *International Statistical Review*, 53(3):301–329.

Gu, G.-Y., Li, C.-X., Zhu, L.-M., and Su, C.-Y. (2016a). Modeling and Identification of Piezoelectric-Actuated Stages Cascading Hysteresis Nonlinearity With Linear Dynamics. *IEEE/ASME Transactions on Mechatronics*, 21(3):1792–1797.

Gu, G. Y., Yang, M. J., and Zhu, L. M. (2012). Real-Time Inverse Hysteresis Compensation of Piezoelectric Actuators with a Modified Prandtl-Ishlinskii Model. *Review of Scientific Instruments*, 83(6):065106.

Gu, G.-Y., Zhu, L.-M., and Su, C.-Y. (2014). Modeling and Compensation of Asymmetric Hysteresis Nonlinearity for Piezoceramic Actuators With a Modified Prandtl-Ishlinskii Model. *IEEE Transactions on Industrial Electronics*, 61(3):1583–1595.

Gu, G.-Y., Zhu, L.-M., Su, C.-Y., Ding, H., and Fatikow, S. (2016b). Modeling and Control of Piezo-Actuated Nanopositioning Stages: A Survey. *IEEE Transactions on Automation Science and Engineering*, 13(1):313–332.

Ha, J.-L., Fung, R.-F., and Yang, C.-S. (2005). Hysteresis Identification and Dynamic Responses of the Impact Drive Mechanism. *Journal of Sound and Vibration*, 283(3-5):943–956.

Hassani, V., Tjahjowidodo, T., and Do, T. N. (2014). A survey on hysteresis modeling, identification and control. *Mechanical Systems and Signal Processing*, 49(1-2):209–233.

Hatipoglu, C. and Ozguner, U. (1998). Robust control of systems involving non-smooth nonlinearities using modified sliding manifolds. In *Proceedings of American Control Conference (ACC)*, volume 4, pages 2133–2137, Philadelphia, USA.

Haynes, B. R. and Billings, S. A. (1992). Method for the global analysis of non-linear parametrized systems. *International Journal of Control*, 55(2):457–482.

Hermansson, A. W. and Syafiie, S. (2015). Model predictive control of pH neutralization processes: A review. *Control Engineering Practice*, 45:98–109.

Hernández, E. and Arkun, Y. (1993). Control of nonlinear systems using polynomial ARMA models. *AIChE Journal*, 39(3):446–460.

Hong, T., Morris, A. J., Karim, M. N., Zhang, J., and Luo, W. (1996). Nonlinear control of a wastewater pH neutralisation process using adaptive NARX models. In *International Conference on Systems, Man and Cybernetics. Information Intelligence and Systems*, volume 2, pages 911–916, Beijing, China.

Householder, A. S. (1958). Unitary triangularization of a nonsymmetric matrix. *Journal of the ACM (JACM)*, 5(4):339–342.

Hu, H. and Ben Mrad, R. (2003). On the Classical Preisach Model for Hysteresis in Piezoceramic Actuators. *Mechatronics*, 13(2):85–94.

Ikhouane, F., Mañosa, V., and Rodellar, J. (2005). Adaptive Control of a Hysteretic Structural System. *Automatica*, 41(2):225–231.

Ikhouane, F. and Rodellar, J. (2006). A Linear Controller for Hysteretic Systems. *IEEE Transactions on Automatic Control*, 51(2):340–344.

Ikhouane, F. and Rodellar, J. (2007). *Systems with Hysteresis: Analysis, Identification and Control Using the Bouc-Wen Model*. John Wiley & Sons.

Isermann, R. and Münchhof, M. (2011). *Identification of Dynamic Systems: An Introduction with Applications*. Springer-Verlag Berlin Heidelberg, New York, 1 edition.

Ismail, M., Ikhouane, F., and Rodellar, J. (2009). The Hysteresis Bouc-Wen Model, a Survey. *Archives of Computational Methods in Engineering*, 16(2):161–188.

Jankowski, K., Marszal, M., and Stefański, A. (2017). Formulation of presliding domain non-local memory hysteretic loops based upon modified maxwell slip model. *Tribology Letters*, 65(2):56.

Jayakumar, P. (1987). *Modeling and identification in structural dynamics*. Technical Report EERL-87-01, California Institute of Technology, Pasadena, CA.

Kadtke, J. B., Brush, J., and Holzfuss, J. (1993). Global dynamical equations and lyapunov exponents from noisy chaotic time series. *International Journal of Bifurcation and Chaos*, 03(03):607–616.

Karami, K., Westwick, D., and Schoukens, J. (2021). Applying polynomial decoupling methods to the polynomial NARX model. *Mechanical Systems and Signal Processing*, 148:107134.

Kay, S. (2006). *Intuitive probability and random processes using MATLAB®*. Springer Science & Business Media, New York, 1 edition.

Keesman, K. J. (2011). *System Identification: An Introduction*. Springer-Verlag London, New York, 1 edition.

Khalid, M., Yusof, R., Joshani, M., Selamat, H., and Joshani, M. (2014). Nonlinear identification of a magneto-rheological damper based on dynamic neural networks. *Computer-Aided Civil and Infrastructure Engineering*, 29(3):221–233.

Khalil, H. K. (2002). *Nonlinear Systems*. Prentice-Hall, Upper Sadlle River, New Jersey, 3 edition.

Koo, T.-K. J. (1995). Model reference adaptive fuzzy control of robot manipulator. In *IEEE International Conference on Systems, Man and Cybernetics. Intelligent Systems for the 21st Century*, volume 1, pages 424–429, Vancouver, Canada.

Korenberg, M., Billings, S. A., Liu, Y. P., and McILroy, P. J. (1988). Orthogonal Parameter Estimation Algorithm for Non-Linear Stochastic Systems. *International Journal of Control*, 48(1):193–210.

Krejci, P. and Kuhnen, K. (2001). Inverse Control of Systems with Hysteresis and Creep. *IEE Proceedings - Control Theory and Applications*, 148(3):185–192.

Kuhnen, K. (2003). Modeling, Identification and Compensation of Complex Hysteretic Nonlinearities: A Modified Prandtl-Ishlinskii Approach. *European Journal of Control*, 9(4):407–418.

Kuhnen, K. and Janocha, H. (2001). Inverse Feedforward Controller for Complex Hysteretic Nonlinearities in Smart-material Systems. *Control and Intelligent Systems*, 29(3):74–83.

Kyprianou, A., Worden, K., and Panet, M. (2001). Identification of hysteretic systems using the differential evolution algorithm. *Journal of Sound and Vibration*, 248(2):289–314.

Lacerda Júnior, W. R., Martins, S. A. M., and Nepomuceno, E. G. (2017). Influence of Sampling Rate and Discretization Methods in the Parameter Identification of Systems with Hysteresis. *Journal of Applied Nonlinear Dynamics*, 6(4):509–520.

Lacerda Júnior, W. R., Martins, S. A. M., Nepomuceno, E. G., and Lacerda, M. J. (2019). Control of Hysteretic Systems Through an Analytical Inverse Compensation based on a NARX model. *IEEE Access*, 7:98228–98237.

Larico, E. R. E. and Garcia, C. (2019). Predictive Controller Applied to a pH Neutralization Process. *IFAC-PapersOnLine*, 52(1):202–206.

Leontaritis, I. J. and Billings, S. A. (1985a). Input-Output Parametric Models for Non-Linear Systems Part I: Deterministic Non-Linear Systems. *International Journal of Control*, 41(2):303–328.

Leontaritis, I. J. and Billings, S. A. (1985b). Input-Output Parametric Models for Non-Linear Systems Part II: Stochastic Non-Linear Systems. *International Journal of Control*, 41(2):329–344.

Leontaritis, I. J. and Billings, S. A. (1987). Experimental design and identifiability for non-linear systems. *International Journal of Systems Science*, 18(1):189–202.

Letellier, C., Ménard, O., and Aguirre, L. A. (2002). Validation of selected global models. In Soofi, A. S. and Cao, L., editors, *Modelling and Forecasting Financial Data. Studies in Computational Finance*, volume 2, pages 283–302. Springer, Boston, MA.

Leva, A. and Piroddi, L. (2002). NARX-based Technique for the Modelling of Magneto-Rheological Damping Devices. *Smart Materials and Structures*, 11(1):79–88.

Li, W. and Chen, X. (2013). Compensation of Hysteresis in Piezoelectric Actuators without Dynamics Modeling. *Sensors and Actuators A: Physical*, 199:89–97.

Li, Z., Su, C.-Y., and Chai, T. (2014). Compensation of Hysteresis Nonlinearity in Magnetostrictive Actuators With Inverse Multiplicative Structure for Preisach Model. *IEEE Transactions on Automation Science and Engineering*, 11(2):613–619.

Liaw, H. C. and Shirinzadeh, B. (2009). Neural Network Motion Tracking Control of Piezo-Actuated Flexure-Based Mechanisms for Micro-/Nanomanipulation. *IEEE/ASME Transactions on Mechatronics*, 14(5):517–527.

Liaw, H. C., Shirinzadeh, B., and Smith, J. (2007). Enhanced Sliding Mode Motion Tracking Control of Piezoelectric Actuators. *Sensors and Actuators A: Physical*, 138(1):194–202.

Liu, L. and Yang, Y. (2015). *Modeling and precision control of systems with hysteresis*. Butterworth-Heinemann, 1 edition.

Liu, S., Su, C., and Li, Z. (2014). Robust Adaptive Inverse Control of a Class of Nonlinear Systems With Prandtl-Ishlinskii Hysteresis Model. *IEEE Transactions on Automatic Control*, 59(8):2170–2175.

Liu, Y.-T., Chang, K.-M., and Li, W.-Z. (2010). Model Reference Adaptive Control for a Piezo-Positioning System. *Precision Engineering*, 34(1):62–69.

Ljung, L. (1999). *System Identification: Theory for the User*. Prentice Hall, New Jersey, 2 edition.

Mansourfar, S. and Baradarannia, M. (2018). Adaptive Sliding Mode Control of a System with Bouc-Wen Model. In *11th International Symposium on Mechatronics and its Applications (ISMA)*, number 1, pages 1–5, Sharjah, United Arab Emirates.

Marques, F. G. (2015). *Modelagem Fenomenológica e Controle de uma Planta Piloto de Neutralização de pH*. Dissertação de Mestrado em Ciências, Escola Politécnica da Universidade de São Paulo, São Paulo.

Martins, S. A. M. (2016). *Modelos Auto regressivos para Representação de Sistemas com Histerese*. Ph.D. thesis, Escola de Engenharia, Universidade Federal de Minas Gerais, Belo Horizonte.

Martins, S. A. M. and Aguirre, L. A. (2016). Sufficient Conditions for Rate-Independent Hysteresis in Autoregressive Identified Models. *Mechanical Systems and Signal Processing*, 75:607–617.

Martins, S. A. M., Nepomuceno, E. G., and Barroso, M. F. S. (2013). Improved Structure Detection For Polynomial NARX Models Using a Multiobjective Error Reduction Ratio. *Journal of Control, Automation and Electrical Systems*, 24(6):764–772.

Masri, S. F., Caffrey, J. P., Caughey, T. K., Smyth, A. W., and Chassiakos, A. G. (2004). Identification of the state equation in complex non-linear systems. *International Journal of Non-Linear Mechanics*, 39(7):1111–1127.

Mayergoyz, I. D. (2003). *Mathematical Models of Hysteresis and Their Applications*. Elsevier Science, New York.

McMillan, G. and Cameron, R. (2004). *Advanced PH Measurement and Control*. ISA, 3 edition.

Mendes, E. M. A. M. and Billings, S. A. (2001). An alternative solution to the model structure selection problem. *IEEE Transactions on Systems, Man, and Cybernetics - Part A: Systems and Humans*, 31(6):597–608.

Merola, A., Colacino, D., Cosentino, C., and Amato, F. (2015). A parsimonious friction model for efficient identification and compensation of hysteresis with non-local memory. *International Journal of Modelling, Identification and Control*, 23(1):85–91.

Mohammadzaheri, M., Grainger, S., and Bazghaleh, M. (2012). A comparative study on the use of black box modelling for piezoelectric actuators. *The International Journal of Advanced Manufacturing Technology*, 63(9-12):1247–1255.

Mokaberi, B. and Requicha, A. (2008). Compensation of Scanner Creep and Hysteresis for AFM Nanomanipulation. *IEEE Transactions on Automation Science and Engineering*, 5(2):197–206.

Morris, K. A. (2011). What is Hysteresis? *Applied Mechanics Reviews*, 64(5):050801.

Nelles, O. (2001). *Nonlinear System Identification: From Classical Approaches to Neural Networks and Fuzzy Models*. Springer-Verlag Berlin Heidelberg.

Ni, Y. Q., Ko, J. M., and Wong, C. W. (1998). Identification of non-linear hysteretic isolators from periodic vibration tests. *Journal of Sound and Vibration*, 217(4):737–756.

Oh, J. and Bernstein, D. S. (2005). Semilinear Duhem model for rate-independent and rate-dependent hysteresis. *IEEE Transactions on Automatic Control*, 50(5):631–645.

Paleologu, C., Benesty, J., and Ciochina, S. (2008). A robust variable forgetting factor recursive least-squares algorithm for system identification. *IEEE Signal Processing Letters*, 15:597–600.

Parlitz, U., Hornstein, A., Engster, D., Al-Bender, F., Lampaert, V., Tjahjowidodo, T., Fassois, S. D., Rizos, D., Wong, C. X., Worden, K., and Manson, G. (2004). Identification of pre-sliding friction dynamics. *Chaos*, 14(2):420–430.

Payam, A. F., Fathipour, M., and Yazdanpanah, M. J. (2009). A Backstepping Controller for Piezoelectric Actuators with Hysteresis in Nanopositioning. In *4th IEEE International Conference on Nano/Micro Engineered and Molecular Systems*, pages 711–716, Shenzhen, China.

Pearson, R. K. (1999). *Discrete-Time Dynamic Models*. Oxford University Press, Oxford.

Peng, J. and Chen, X. (2010). H_2-optimal Digital Control of Piezoelectric Actuators. In *8th World Congress on Intelligent Control and Automation*, pages 3684–3690, Jinan, China.

Peng, J. and Chen, X. (2013). A Survey of Modeling and Control of Piezoelectric Actuators. *Modern Mechanical Engineering*, 3(1):1–20.

Peyton-Jones, J. C. and Billings, S. A. (1989). Recursive algorithm for computing the frequency response of a class of non-linear difference equation models. *International Journal of Control*, 50(5):1925–1940.

Piroddi, L. (2008). Simulation Error Minimisation Methods for NARX Model Identification. *International Journal of Modelling, Identification and Control*, 3(4):392–403.

Piroddi, L. and Spinelli, W. (2003). An identification algorithm for polynomial NARX models based on simulation error minimization. *International Journal of Control*, 76(17):1767–1781.

Pop, E., Ilcea, G., and Buzdugan, S. (2018). Use properties of distributions to model the systems with severe nonlinearities. In *CBU International Conference Proceedings*, volume 6, pages 1150–1157, Prague, Cezch Republic.

Popiołek, J. (1990). Some properties of functions modul and signum. *Formalized Mathematics*, 1(2):263–264.

Pröll, T. and Karim, M. N. (1994). Model-predictive ph control using real-time narx approach. *AIChE Journal*, 40(2):269–282.

Qin, Y., Tian, Y., Zhang, D., Shirinzadeh, B., and Fatikow, S. (2013). A Novel Direct Inverse Modeling Approach for Hysteresis Compensation of Piezoelectric Actuator in Feedforward Applications. *IEEE/ASME Transactions on Mechatronics*, 18(3):981–989.

Quaranta, G., Lacarbonara, W., and Masri, S. F. (2020). A review on computational intelligence for identification of nonlinear dynamical systems. *Nonlinear Dynamics*, 99:1709–1761.

Rakotondrabe, M. (2011). Bouc-Wen Modeling and Inverse Multiplicative Structure to Compensate Hysteresis Nonlinearity in Piezoelectric Actuators. *IEEE Transactions on Automation Science and Engineering*, 8(2):428–431.

Rakotondrabe, M. (2012). Classical Prandtl-Ishlinskii Modeling and Inverse Multiplicative Structure to Compensate Hysteresis in Piezoactuators. In *American Control Conference (ACC)*, pages 1646–1651, Montreal, QC, Canada.

Rakotondrabe, M. (2013). *Smart Materials-Based Actuators at the Micro/Nano-Scale: Characterization, Control and Applications*. Springer, New York.

Rakotondrabe, M., Clévy, C., and Lutz, P. (2010). Complete Open Loop Control of Hysteretic, Creeped, and Oscillating Piezoelectric Cantilevers. *IEEE Transactions on Automation Science and Engineering*, 7(3):440–450.

Retes, P. F. L. and Aguirre, L. A. (2019). NARMAX Model Identification Using a Randomised Approach. *International Journal of Modelling, Identification and Control*, 31(3):205–216.

Riccardi, L., Naso, D., Turchiano, B., and Janocha, H. (2013). LMI-Based Design of Linear Controllers for a Magnetic Shape Memory Push-Push Actuator. In *52nd IEEE Conference on Decision and Control*, pages 6634–6639, Florence, Italy.

Riccardi, L., Naso, D., Turchiano, B., and Janocha, H. (2014). Design of Linear Feedback Controllers for Dynamic Systems With Hysteresis. *IEEE Transactions on Control Systems Technology*, 22(4):1268–1280.

Riccardi, L., Naso, D., Turchiano, B., Janocha, H., and Schlueter, K. (2012). PID Control of Linear Systems with an Input Hysteresis Described by Prandtl-Ishlinskii Models. In *51st IEEE Conference on Decision and Control (CDC)*, pages 5158–5163, Maui, HI, USA.

Romano, R. A. and Garcia, C. (2011). Valve friction and nonlinear process model closed-loop identification. *Journal of Process Control*, 21(4):667–677.

Ruderman, M. and Bertram, T. (2010). Discrete Dynamic Preisach Model for Robust Inverse Control of Hysteresis Systems. In *49th IEEE Conference on Decision and Control*, pages 3463–3468, Atlanta, GA, USA.

Sain, P., Sain, M., Spencer, B., and Sain, J. (1998). The Bouc Hysteresis Model: An Initial Study of Qualitative Characteristics. In *Proceedings of the American Control Conference*, pages 2559–2563, Philadelphia, PA, USA.

Salapaka, S., Sebastian, A., Cleveland, J. P., and Salapaka, M. V. (2002). High Bandwidth Nano-Positioner: A Robust Control Approach. *Review of Scientific Instruments*, 73(9):3232–3241.

Schindele, D. and Aschemann, H. (2013). Comparison of Cascaded Backstepping Control Approaches with Hysteresis Compensation for a Linear Axis with Pneumatic Muscles. *IFAC Proceedings Volumes*, 46(23):773–778.

Schoukens, J. and Ljung, L. (2019). Nonlinear system identification: A user-oriented road map. *IEEE Control Systems Magazine*, 39(6):28–99.

Schoukens, J. and Pintelon, R. (1991). *Identification of linear systems: a practical guideline to accurate modeling*. Pergamon Press.

Shakiba, S., Zakerzadeh, M. R., and Ayati, M. (2018). Experimental characterization and control of a magnetic shape memory alloy actuator using the modified generalized rate-dependent Prandtl-Ishlinskii hysteresis model. *Proceedings of the Institution of Mechanical Engineers, Part I: Journal of Systems and Control Engineering*, 232(5):506–518.

Shannon, C. E. (1949). Communication in the Presence of Noise. *Proceedings of the Institute of Radio Engineers*, 37(1):10–21.

Shariff, H. M., Fazalul Rahiman, M. H., and Tajjudin, M. (2013). Nonlinear system identification: Comparison between prbs and random gaussian perturbation on steam distillation pilot plant. In *IEEE 3rd International Conference on System Engineering and Technology*, pages 269–274, Shah Alam, Malaysia.

Shen, J.-C., Jywe, W.-Y., Chiang, H.-K., and Shu, Y.-L. (2008). Precision Tracking Control of a Piezoelectric-Actuated System. *Precision Engineering*, 32(2):71–78.

Shi, Z.-K. and Wu, F.-X. (2013). Robust identification method for nonlinear model structures and its application to high-performance aircraft. *International Journal of Systems Science*, 44(6):1040–1051.

Sjöberg, J., Zhang, Q., Ljung, L., Benveniste, A., Delyon, B., Glorennec, P.-Y., Hjalmarsson, H., and Juditsky, A. (1995). Nonlinear black-box modeling in system identification: a unified overview. *Automatica*, 31(12):1691–1724.

Smyth, A. W., Masri, S. F., Kosmatopoulos, E. B., Chassiakos, A. G., and Caughey, T. K. (2002). Development of Adaptive Modeling Techniques for Non-linear Hysteretic Systems. *International Journal of Non-Linear Mechanics*, 37(8):1435–1451.

Song, G., Zhao, J., Zhou, X., and Abreu-Garcia, J. A. D. (2005). Tracking Control of a Piezoceramic Actuator with Hysteresis Compensation Using Inverse Preisach Model. *IEEE/ASME Transactions on Mechatronics*, 10(2):198–209.

Srinivasan, R. and Rengaswamy, R. (2005). Stiction Compensation in Process Control Loops: A Framework for Integrating Stiction Measure and Compensation. *Industrial & Engineering Chemistry Research*, 44(24):9164–9174.

Stebel, K. and Czeczot, J. (2009). Nonstationary modelling approaches of neutralization process for model-based control. *IFAC Proceedings Volumes*, 42(13):302–307.

Swevers, J., Al-Bender, F., Ganseman, C., and Projogo, T. (2000). An integrated friction model structure with improved presliding behavior for accurate friction compensation. *IEEE Transactions on Automatic Control*, 45(4):675–686.

Tan, Y. and Deng, L. (2014). Modeling the dynamic sandwich system with hysteresis using NARMAX model. *Mathematics and Computers in Simulation*, 97:162–188.

Tao, G. and Kokotovic, P. V. (1995). Adaptive Control of Plants with Unknown Hystereses. *IEEE Transactions on Automatic Control*, 40(2):200–212.

Tao, G. and Lewis, F. (2001). *Adaptive Control of Nonsmooth Dynamic Systems*. Springer London.

Tavares, L. A. (2020). *Compensação de Não Linearidades Via Modelos*. Dissertação de Mestrado em Engenharia Elétrica, Escola de Engenharia, Universidade Federal de Minas Gerais, Belo Horizonte.

Tavares, L. A., Abreu, P. E. O. G. B., and Aguirre, L. A. (2019). Estimação de Parâmetros de Modelos Bouc-Wen via Algoritmos Evolutivos para Compensação de Histerese. In *Anais do XIV Simpósio Brasileiro de Automação Inteligente*, Ouro Preto, Brasil.

Tavares, L. A., Abreu, P. E. O. G. B., and Aguirre, L. A. (2021). Input design and recommendations for the identification of hysteretic NARX models. In *Anais do XV Simpósio Brasileiro de Automação Inteligente*, Rio Grande, Brasil.

Tavares, L. A., Abreu, P. E. O. G. B., and Aguirre, L. A. (2022). Nonlinearity compensation based on identified NARX polynomials models. *Nonlinear Dynamics*, 107:709–725.

Visintin, A. (1994). *Differential Models of Hysteresis*. Springer, Berlin Heidelberg.

Visone, C. (2008). Hysteresis Modelling and Compensation for Smart Sensors and Actuators. *Journal of Physics: Conference Series*, 138(1):012028.

Wang, D. H. and Zhu, W. (2011). A Phenomenological Model for Pre-Stressed Piezoelectric Ceramic Stack Actuators. *Smart Materials and Structures*, 20(3):035018.

Wang, D. H., Zhu, W., and Yang, Q. (2011). Linearization of Stack Piezoelectric Ceramic Actuators Based on Bouc-Wen Model. *Journal of Intelligent Material Systems and Structures*, 22(5):401–413.

Wang, G., Yao, X., Cui, J., Yan, Y., Dai, J., and Zhao, W. (2020). A novel piezoelectric hysteresis modeling method combining lstm and narx neural networks. *Modern Physics Letters B*, 34(28):2050306.

Wang, H. and Song, G. (2014). Innovative NARX recurrent neural network model for ultra-thin shape memory alloy wire. *Neurocomputing*, 134:289–295.

Wei, Z., Xiang, B. L., and Ting, R. X. (2014). Online Parameter Identification of the Asymmetrical Bouc-Wen Model for Piezoelectric Actuators. *Precision Engineering*, 38(4):921–927.

Wen, Y. K. (1976). Method for Random Vibration of Hysteretic Systems. *Journal of the Engineering Mechanics Division*, 102(2):249–263.

Worden, K. and Barthorpe, R. J. (2012). Identification of hysteretic systems using NARX models, Part I: evolutionary identification. In Simmermacher, T., Cogan, S., Horta, L., and Barthorpe, R., editors, *Topics in Model Validation and Uncertainty Quantification*, volume 4, pages 49–56. Springer.

Worden, K. and Hensman, J. J. (2012). Parameter estimation and model selection for a class of hysteretic systems using Bayeisan inference. *Mechanical Systems and Signal Processing*, 32:153–169.

Worden, K., Wong, C. X., Parlitz, U., Hornstein, A., Engster, D., Tjahjowidodo, T., Al-Bender, F., Rizos, D. D., and Fassois, S. D. (2007). Identification of pre-sliding and sliding friction dynamics: Grey box and black-box models. *Mechanical Systems and Signal Processing*, 21(1):514–534.

Xia, P. Q. (2003). An Inverse Model of MR Damper using Optimal Neural Network and System Identification. *Journal of Sound and Vibration*, 266(5):1009–1023.

Xu, Q. and Li, Y. (2009). Dynamics Modeling and Sliding Mode Control of an XY Micropositioning Stage. In *The 9th International Symposium on Robot Control (SYROCO)*, pages 781–786, Nagaragawa Convention Center, Gifu, Japan.

Yi, S., Yang, B., and Meng, G. (2019). Ill-conditioned dynamic hysteresis compensation for a low-frequency magnetostrictive vibration shaker. *Nonlinear Dynamics*, 96(1):535–551.

Young, P. (1970). An instrumental variable method for real-time identification of a noisy process. *Automatica*, 6(2):271–287.

Yu, Y., Xiao, Z., Naganathan, N. G., and Dukkipati, R. V. (2001). Dynamic preisach modelling of hysteresis for the piezoceramic actuator system. *Proceedings of the Institution of Mechanical Engineers, Part C: Journal of Mechanical Engineering Science*, 215(5):511–521.

Zakerzadeh, M. R., Sayyaadi, H., and Zanjani, M. A. V. (2011). Characterizing Hysteresis Nonlinearity Behavior of SMA Actuators by Krasnosel'skii-Pokrovskii Model. *Applied Mathematics*, 1(1):28–38.

Zhang, W., Zhu, J., and Gu, D. (2017a). Identification of robotic systems with hysteresis using Nonlinear AutoRegressive eXogenous input models. *International Journal of Advanced Robotic Systems*, 14(3):1–10.

Zhang, X., Tan, Y., Su, M., and Xie, Y. (2010). Neural networks based identification and compensation of rate-dependent hysteresis in piezoelectric actuators. *Physica B: Condensed Matter*, 405(12):2687–2693.

Zhang, Y., Yan, P., and Zhang, Z. (2017b). Robust Adaptive Backstepping Control for Piezoelectric Nano-Manipulating Systems. *Mechanical Systems and Signal Processing*, 83:130–148.

Zheng, J., Wang, Q., and Li, Y. (2014). Adaptive Sliding Model Control for Linear Actuator with Hysteresis Using a Prandtl-Ishlinskii Model. In *IEEE International Conference on Robotics and Biomimetics (ROBIO 2014)*, pages 2553–2557, Bali, Indonesia.

Zhou, J. and Wen, C. (2008). *Adaptive Backstepping Control of Uncertain Systems: Nonsmooth Nonlinearities, Interactions or Time-Variations*. Springer, Berlin, Heidelberg.

Zhou, J., Wen, C., and Li, T. (2012). Adaptive Output Feedback Control of Uncertain Nonlinear Systems With Hysteresis Nonlinearity. *IEEE Transactions on Automatic Control*, 57(10):2627–2633.

Zhou, J., Wen, C., and Zhang, Y. (2004). Adaptive Backstepping Control of a Class of Uncertain Nonlinear Systems with Unknown Backlash-like Hysteresis. *IEEE Transactions on Automatic Control*, 49(10):1751–1759.